University of Iceland
Faculty of Engineering

The nitrogen discharge

A global (volume averaged) model study

by

Eyþór Gísli Þorsteinsson

A thesis submitted in partial satisfaction of the
requirements for the degree of Master of Science in
Electrical and Computer Engineering at the University of Iceland

Committee in charge:
Prof. Jón Tómas Guðmundsson, Chair
Dr. Halldór Guðfinnur Svavarsson
Dr. Ágúst Valfells

Reykjavík
October, 2008

Abstract

A global (volume averaged) model is developed for a nitrogen discharge for the pressure range 1-100 mTorr. A reaction set is created and the reaction rate coefficients reviewed and critically evaluated. The discharge is assumed to consist of 15 species of nitrogen; the seven lowest lying vibrational levels of the ground state nitrogen molecule $N_2(X^1\Sigma_g^+, v = 0-6)$, the metastable nitrogen molecule $N_2(A^3\Sigma_u^+)$, the ground state nitrogen atom $N(^4S)$, the metastable nitrogen atoms $N(^2D)$ and $N(^2P)$, and the ions N^+, N_2^+, N_3^+ and N_4^+. The electron energy distribution function is allowed to vary from Maxwellian to Druyvesteyn distribution. For a discharge in the steady state the plasma parameters, such as the particle densities and electron energy, are presented versus absorbed power, discharge pressure, gas flowrate, gas temperature, electron energy distribution function, wall recombination coefficient, wall quenching coefficient, and chamber dimensions. Furthermore, the global model is applied to investigate the reaction rates for the creation and loss of the discharge species as a function of discharge pressure. Additionally, for a pulsed power discharge the plasma parameters are presented versus time, frequency and duty ratio, and the reaction rates are investigated as a function of time. We find that the steady state calculations are in good agreement with measurements, with the exception of the dissociation fraction. We find that the discharge is essentially atomic at 1 mTorr, but highly molecular at 100 mTorr. Vibrationally excited nitrogen molecules are found to be important above 10 mTorr, but negligible at 1 mTorr. Furthermore, we predict that the N^+ density can be increased significantly by pulsing the power with low values of the modulation frequency and duty ratio, resulting in a higher electron density compared to the steady state calculations.

Contents

1 Introduction **3**

2 The global (volume averaged) model **5**

2.1 Basic discharge parameters 6

2.2 Effective area for particle loss 8

2.3 The electron energy distribution function 9

2.4 The collisional energy loss per ionization event 15

2.5 Detailed balancing 20

2.6 System of equations 23

2.6.1 Particle balance 23

2.6.2 Energy balance 27

3 Nitrogen specific parameters **29**

3.1 Electron impact dissociation 30

3.1.1 Electron impact dissociation of the nitrogen molecule 30

3.2 Electron impact ionization 34

3.2.1 Electron impact ionization of the nitrogen molecule 34

3.2.2 Electron impact ionization of the nitrogen atom 39

3.3 Electron impact excitation 41

3.3.1 Electron impact electronic excitation of the nitrogen molecule 41

3.3.2 Electron impact vibrational excitation of the ground state nitrogen molecule 47

3.3.3 Electron impact excitation of the nitrogen atom 53

3.4 Collisions of electrons with ions 56

3.4.1 Dissociative recombination of the N_2^+ ion 57

3.4.2 Dissociative excitation and ionization of the N_2^+ ion 59
3.4.3 Dissociative recombination of N_3^+ 63
3.4.4 Dissociative recombination of N_4^+ 64
3.5 Reactions of gaseous species 65
3.5.1 Charge transfer 65
3.5.2 Quenching by the nitrogen molecule 66
3.5.3 Quenching by the nitrogen atom 70
3.5.4 Transfer of excitation 72
3.5.5 Dissociation of ions 75
3.5.6 Rearrangement of chemical bonds 76
3.5.7 Three body association 77
3.5.8 Ionization 79
3.6 Optical emission of excited species 81
3.6.1 Emission from $N_2(A^3\Sigma_u^+)$ 82
3.6.2 Emission from $N(^2P)$ 83
3.6.3 Emission from $N(^2D)$ 83
3.7 Elastic electron scattering 84
3.7.1 Elastic scattering by the $N_2(X^1\Sigma_g^+, v = 0)$ molecule 84
3.7.2 Elastic scattering by the $N(^4S)$ atom 86
3.8 Wall interactions 88
3.8.1 Wall recombination coefficient 88
3.8.2 Wall quenching coefficients 90
3.8.3 Wall recombination of ions 93
3.9 Scattering cross sections 93
3.10 Gas temperature 95

4 The steady state discharge 101
4.1 Comparison with measurements 102
4.2 Densities and electron temperature 117
4.2.1 Absorbed power 118
4.2.2 Discharge pressure 120
4.2.3 Gas flow into the chamber 122
4.2.4 Electron energy distribution function 124
4.2.5 Gas temperature 126
4.2.6 Wall quenching coefficient 128

4.2.7 Wall recombination coefficient . . . 130
4.2.8 Chamber radius . . . 132
4.2.9 Chamber length . . . 134
4.3 Reaction Rates . . . 136

5 The pulsed-power discharge 155
5.1 Densities and electron temperature . . . 157
5.1.1 Time . . . 157
5.1.2 Frequency . . . 160
5.1.3 Duty ratio . . . 162
5.2 Reaction rates . . . 165

6 Conclusion 187

A The nitrogen reaction set 193

Chapter 1

Introduction

Low pressure nitrogen discharges have a wide range of applications, particularly within the semiconductor industry. They are used as an N atom source for the growth of III-V nitrides in plasma assisted molecular beam epitaxy (Czerwiec et al., 2005; Moustakas et al., 1993). The Ar/N_2 discharge is applied in reactive magnetron sputtering to grow TiN thin films (Tao et al., 2002). Nitridation processes are applied to form high quality oxynitride films that act as a boron diffusion barrier for the gate oxide (Niimi and Lucovsky, 1999). A mixture of N_2/H_2 is used to etch organic films with low dielectric constant (Ishikawa et al., 2006). Nitrogen discharges are also employed in surface post-processing of various metals and alloys. Plasma nitriding is used as an economical method to improve hardness, corrosion, wear resistance and surface quality of stainless steel (Wang et al., 2006; Shah et al., 2008). Additionally, plasma source ion implantation of nitrogen is used to substantially reduce the wear rate of various alloys (Conrad et al., 1987; Cho et al., 2001), commonly increasing the lifetime by $2-3$ orders of magnitude.

The volume averaged global model for high density discharges was developed

by Lieberman and Gottscho (1994) for noble gases and extended to molecular gases by Lee et al. (1994) and Lee and Lieberman (1995). A more elaborate volume averaged global model of O_2 (Patel, 1998; Gudmundsson et al., 2000, 2001) and Ar/O_2 mixture (Gudmundsson et al., 1999; Gudmundsson and Thorsteinsson, 2007a,b) has been developed and compared to Langmuir probe and mass spectrometer measurements (Gudmundsson and Lieberman, 1998; Gudmundsson et al., 1999, 2000). A time dependent global model was developed by Ashida et al. (1995) to describe a pulsed discharge and extended to include chlorine (Ashida and Lieberman, 1997) and oxygen discharge (Kim et al., 2006). The main idea of a global model is to neglect the complexity which arises when spatial variations are considered and to generate a model that encompasses large number of reactions in order to model a processing plasma with a limited computing power. Thus, the model does not describe spatial distribution but captures scalings of plasma parameters with control parameters. The model allows us to investigate various phenomena, such as the effects of excited species, negative ions and particular reactions on the overall discharge.

Here a global model of a nitrogen discharge is developed for the pressure regime $1 - 100$ mTorr. In the model presented here the electron energy distribution is allowed to vary from Maxwellian to Druyvesteyn distribution. Thus, for electron impact reactions a cross section is used to calculate the rate coefficient. The parameters of the global model, including the energy balance and particle balance, are defined in chapter 2. The reaction set is introduced in chapter 3. The steady state nitrogen discharge is discussed in chapter 4. The model calculations are compared to measured values before evaluating the production and loss mechanisms of each gas species. Similarly, the pulsed nitrogen discharge is discussed in chapter 5.

Chapter 2

The global (volume averaged) model

We assume a cylindrical stainless steel chamber of radius R and length L. A steady flow Q of neutral species is introduced through the inlet. The discharge pressure is maintained by concurrently pumping neutral species, radicals and positive ions out of the chamber. The operating pressure of the discharge is assumed to be in the regime 1 – 100 mTorr. The content of the chamber is assumed to be nearly spatially uniform and the power is assumed to be uniformly deposited into the plasma bulk. The ion densities are also assumed to have a uniform density profile except near the walls, where it drops sharply to the sheath-edge density, n_{is}. The sheath-edge density of negative ions is assumed to be zero. Energy losses due to collisions with ions and excited species are neglected because their density is small in comparison to the density of the ground state neutral species. Furthermore, for both positive and negative ions, only singly ionized species are considered, their density being much larger than of the multiple ionized species.

2.1 Basic discharge parameters

Plasma discharges are normally assumed to be quasi-neutral, that is

$$n_{\mathrm{e}} = \sum_{\mathrm{i}} Z_{\mathrm{i}} n_{\mathrm{i}} \tag{2.1}$$

where Z_{i} and n_{i} are the relative charge and density of ion i, respectively. The above expression is often called the plasma approximation and is one of the most basic principles in plasma discharge theory. The approximation is generally good throughout the discharge, except for the plasma sheath region, in which it is not accurate (Lieberman and Lichtenberg, 2005, p. 40).

Bohm (1949) found that in order for a stable sheath to be possible, the minimum kinetic energy of ions striking the sheath must be equal to half the electron energy. This relation is commonly known as the Bohm criterion, which results in an ion velocity exceeding the ion sound velocity in a collisionless sheath. The Bohm velocity for an ion i, when generalized for an electronegative plasma, is therefore given as (Lieberman and Lichtenberg, 2005, p. 347)

$$u_{\mathrm{B,i}} = \left[\frac{e\mathrm{T_e}(1+\alpha)}{m_{\mathrm{i}}(1+\alpha\gamma)}\right]^{1/2} \tag{2.2}$$

where $e = 1.6 \times 10^{-19}$ C is the electron charge, $\mathrm{T_e}$ is the effective electron temperature in volts, m_{i} is the mass of the corresponding ion, $\alpha = n_-/n_{\mathrm{e}}$ is the electronegativity in the discharge and $\gamma = \mathrm{T_e}/\mathrm{T_i}$ is the ratio of electron and ion temperatures.

In a discharge consisting of several gaseous species and free electrons, the diffusion constant for the species α is given by (Lieberman and Lichtenberg, 2005,

p. 134)

$$D^{(\alpha)} = \frac{e\mathrm{T_e}\lambda^{(\alpha)}}{m^{(\alpha)}\overline{v}^{(\alpha)}} \tag{2.3}$$

where $\overline{v}^{(\alpha)}$ is the mean velocity of the species α,

$$\overline{v}^{(\alpha)} = \left(\frac{8e\mathrm{T}^{(\alpha)}}{\pi m^{(\alpha)}}\right)^{1/2} \tag{2.4}$$

and $\lambda^{(\alpha)}$ is the mean free path of the species α,

$$\frac{1}{\lambda^{(\alpha)}} = \sum_j n_j \sigma_{\mathrm{sc}_j^{(\alpha)}} \tag{2.5}$$

where n_j is the density of the gas species j, and $\sigma_{\mathrm{sc}_j^{(\alpha)}}$ is the scattering cross section for the collision of the species α with the gas species j. The ambipolar diffusion coefficient, when generalized for an electronegative plasma, is given as (Lieberman and Lichtenberg, 2005, p. 346)

$$D_\mathrm{a} = D_\mathrm{i}\frac{1+\gamma+\gamma\alpha}{1+\gamma\alpha} \tag{2.6}$$

where D_i is the diffusion coefficient of ion i, given by equation (2.3).

The temperature of a species α, on the one hand in volts and on the other hand in Kelvin, has the relation

$$e\mathrm{T}^{(\alpha)}\ [\mathrm{volts}] = kT^{(\alpha)}\ [\mathrm{Kelvin}] \tag{2.7}$$

where $k = 1.38 \times 10^{-23}$ J/K is Boltzmann's constant. From this point forward the italic typeface T refers to a temperature value in Kelvin, whereas the roman typeface T refers to a temperature value in volts.

2.2 Effective area for particle loss

The effective area for ion loss in a cylindrical geometry of radius R and length L is given by Lieberman and Gottscho (1994) and Lieberman and Lichtenberg (2005) as

$$A_{\text{eff}} = 2\pi(R^2 h_L + 2\pi R L h_R) \tag{2.8}$$

where h_R and h_L are scaling factors that describe the ratios of sheath versus bulk density in the radial and axial directions, respectively. In the intermediate pressure regime, $(R, L) \geq \lambda_{\text{i}} \geq (\text{T}_{\text{i}}/\text{T}_{\text{e}})(R, L)$, Godyak (1986) joined the collisionless (low pressure) and collisional (intermediate pressure) solutions to the variable mobility diffusion model to give

$$h_L \equiv \frac{n_{\text{s}L}}{n_0} \simeq 0.86 \left(3 + \frac{L}{2\lambda_{\text{i}}}\right)^{-1/2} \tag{2.9}$$

$$h_R \equiv \frac{n_{\text{s}R}}{n_0} \simeq 0.8 \left(4 + \frac{R}{\lambda_{\text{i}}}\right)^{-1/2} \tag{2.10}$$

at the axial sheath edge and the radial sheath edge, respectively. These solutions are not valid at higher pressure where $\lambda_{\text{i}} \leq \text{T}_{\text{i}}/\text{T}_{\text{e}}(L, R)$ and a constant diffusion coefficient model is more appropriate. To include this regime Lee and Lieberman (1995) developed a heuristic equation, which, when generalized for an electronegative plasma, is given

$$h_L \simeq 0.86 \frac{1 + (3\alpha/\gamma)}{1 + \alpha} \left[3 + \frac{L}{2\lambda_{\text{i}}} + \left(\frac{0.86 L u_{\text{B}}}{\pi D_a}\right)^2\right]^{-1/2} \tag{2.11}$$

$$h_R \simeq 0.80 \frac{1 + (3\alpha/\gamma)}{1 + \alpha} \left[4 + \frac{R}{\lambda_{\text{i}}} + \left(\frac{0.80 R u_{\text{B}}}{\chi_{01} J_1(\chi_{01}) D_{\text{a}}}\right)^2\right]^{-1/2} \tag{2.12}$$

where $J_1(\chi)$ is the first order Bessel function, $\chi_{01} \simeq 2.405$ is the first zero of the zero order Bessel function J_0, $\alpha = n_-/n_e$ is the electronegativity of the discharge, $\gamma = T_e/T_i$ is the fraction of the electron and ion temperatures, D_a is the ambipolar diffusion coefficient, given by equation (2.6), and u_B is the Bohm velocity, given by equation (2.2).

As λ_i and T_i are allowed to vary from ion to ion, each ion is allowed to have different effective area for ion loss, $A_{eff}^{(\alpha)}$. The third term in the expressions for the scaling factors, equations (2.11) and (2.12), were added in this work and were not included in our previous model of the O_2/Ar discharge (Gudmundsson and Thorsteinsson, 2007b) to account for diffusion at higher pressures, approximately in the range $30 - 100$ mTorr. This addition is expected to decrease the effective area for ion loss compared to previous models since the scaling factors, h_L and h_R, decrease.

2.3 The electron energy distribution function

In the global model calculation we assume a particular electron energy distribution function for the discharge, the simplest being the Maxwellian-like distribution. In a capacitively coupled discharge the electron energy distribution function is commonly found to be bi-Maxwellian (Godyak et al., 1993). For a low pressure (< 30 mTorr) inductively coupled discharge, measurements have shown that the electron energy distribution is close to being Maxwellian-like in molecular gases, such as in N_2 and O_2 discharges (Gudmundsson et al., 1999; Singh and Graves, 2000a,b). For atomic gases, most commonly argon, the electron energy distribution is closer to being bi-Maxwellian, i.e. a sum of two Maxwellian distributions (Singh and Graves, 2000b; Ma and Pu, 2003). For higher pressure there are relatively fewer high energy electrons, and the electron energy distribution more resembles the so called

Druyvesteyn distribution, both for atomic (Li, 2006) and molecular gases (Singh and Graves, 2000b). Furthermore, the electron energy distribution of the nitrogen discharge has a strange anomaly; at low discharge power a hole is often observed at around 3 eV. This hole has been attributed to the strong vibrational loss property of nitrogen discharges (Singh and Graves, 2000b). Because of these variations in the electron energy distribution function it is important to evaluate the sensitivity of the results to the choice of electron energy distribution function. A suitable method would be to compare the results obtained when assuming a Maxwellian-like electron energy distribution to those obtained when assuming a Druyvesteyn-like electron energy distribution. A global model of an argon discharge has been developed where the electron energy distribution is allowed to vary from Maxwellian distribution to Druyvesteyn distribution (Gudmundsson, 2001). Furthermore, Kimura and Ohe (2001) proposed a global model for a two temperature electron energy distribution (bi-Maxwellian) in and argon discharge and compared the results to measurements with a satisfactory outcome. However, using a two temperature distribution is not as convenient as allowing the distribution function to vary from a Maxwellian distribution to Druyvesteyn electron energy distribution function. The reason for this lies in the strong resemblance of the Maxwellian and Druyvesteyn distributions, primarily in their mathematical expressions. A general equation for the electron energy distribution function, applying to both the Maxwellian and the Druyvesteyn distributions, is given by (Amemiya, 1997; Gudmundsson, 2001)

$$f(\mathcal{E}) = c_1 \mathcal{E}^{1/2} \exp(-c_2 \mathcal{E}^x) \tag{2.13}$$

where $x = 1$ corresponds to the Maxwellian distribution and $x = 2$ to the Druyvesteyn distribution. c_1 and c_2 are coefficients which depend on the energy $\mathcal{E}$ and the dis-

tribution parameter x, and are given as (Gudmundsson, 2001)

$$c_1 = \frac{x}{\langle \mathcal{E} \rangle^{3/2}} \frac{[\Gamma(\xi_2)]^{3/2}}{[\Gamma(\xi_1)]^{5/2}} \tag{2.14}$$

$$c_2 = \frac{1}{\langle \mathcal{E} \rangle^{x}} \left[\frac{\Gamma(\xi_2)}{\Gamma(\xi_1)} \right]^{x} \tag{2.15}$$

where $\langle \mathcal{E} \rangle$ is the average electron energy,

$$\langle \mathcal{E} \rangle = \frac{3}{2} e \mathrm{T_e} \tag{2.16}$$

and $\Gamma(\xi)$ is the solution to the gamma function with $\xi_1 = 3/2x$ and $\xi_2 = 5/2x$. When the electron energy distribution function changes there are several parameters that are affected. First and foremost are the rate coefficients of electron impact reactions that are found by averaging the corresponding cross section, $\sigma(\mathcal{E})$, over the assumed distribution function,

$$K(\mathrm{T_e}) = \langle \sigma(\mathcal{E})\, v_\mathrm{e} \rangle = \left(\frac{2\, e}{m_\mathrm{e}} \right)^{1/2} \int_0^\infty \sigma(\mathcal{E})\, \mathcal{E}^{1/2} f(\mathcal{E})\, \mathrm{d}\mathcal{E} \tag{2.17}$$

To obtain an analytical expression for the rate coefficients as a function of electron temperature we fit the result to the Arrhenius form,

$$K(\mathrm{T_e}) = A \times {\mathrm{T_e}}^{B} \times \exp\left(-C/{\mathrm{T_e}}^{x}\right) \tag{2.18}$$

For non-electron impact reaction the rate coefficients do not depend on the energy of electrons and are not affected by the choice of the electron energy distribution function. Previous models of molecular discharges (Lee et al., 1994; Lee and Lieberman, 1995; Patel, 1998; Gudmundsson et al., 2001; Kim et al., 2006; Gudmundsson and Thorsteinsson, 2007b) utilize a collection of reactions and rate

coefficients that have been averaged over the Maxwellian distribution function. Being able to change the distribution function therefore requires a set of reactions and their corresponding electron energy dependent cross sections instead of simply their rate coefficients. Changing the distribution function from a Maxwellian-like to a Druyvesteyn-like distribution results in lower rate coefficients for reactions that have high thresholds, such as ionization, but may increase rate coefficients for reactions with low thresholds, in particular elastic collisions.

Other parameters, that are normally simplified for an assumed Maxwellian-like distribution, need to be redefined for the more general distribution of (2.13). As the electron energy is proportional to the square of the electron velocity, changing the energy distribution function therefore changes the average electron velocity, now given by (Gudmundsson, 2001)

$$\overline{v}_{\mathrm{e}} = \langle \mathcal{E} \rangle^{1/2} \left(\frac{2\,e}{m_{\mathrm{e}}} \right)^{1/2} \frac{[\Gamma(\xi_4)]}{[\Gamma(\xi_1)\,\Gamma(\xi_2)]^{1/2}} \tag{2.19}$$

where $\xi_4 = 2/x$. Consequently the ion velocity changes, with the Bohm velocity now given as (Gudmundsson, 2001)

$$u_{\mathrm{B}} = \langle \mathcal{E} \rangle^{1/2} \left(\frac{2}{m_{\mathrm{i}}} \right)^{1/2} \frac{[\Gamma(\xi_1)]}{[\Gamma(\xi_2)\,\Gamma(\xi_3)]^{1/2}} \tag{2.20}$$

where $\xi_3 = 1/2x$. The sheath potential, V_{s}, can be determined by equating the ion and electron flux at the wall, $\Gamma_{\mathrm{e}} = \Gamma_{\mathrm{i}}$. That is (Gudmundsson, 2001)

$$\frac{1}{4} n_{\mathrm{e}} \overline{v}_{\mathrm{e}} c_1 \int_{V_{\mathrm{s}}}^{\infty} (\mathcal{E} - V_{\mathrm{s}})^{1/2} \exp(-c_2 \mathcal{E}^x)\, \mathrm{d}\mathcal{E} = n_{\mathrm{i}} u_{\mathrm{B}} \tag{2.21}$$

Solving for V_{s} yields an analytical solution when $x = 1$, for the Maxwellian-like distribution, but for other values of x the sheath potential has to be determined

numerically. To make that possible the integral needs to be rewritten so that the limits are finite. Start by rearranging and splitting the integral to two intervals,

$$\frac{4\,n_\mathrm{i}u_\mathrm{B}}{n_\mathrm{e}\overline{v}_\mathrm{e}c_1} = \int_{V_\mathrm{s}}^{V_\mathrm{s}+1} (\mathcal{E}-V_\mathrm{s})^{1/2}\,\exp\left(-c_2\,\mathcal{E}^x\right)\,\mathrm{d}\mathcal{E} + \int_{V_\mathrm{s}+1}^{\infty} (\mathcal{E}-V_\mathrm{s})^{1/2}\,\exp\left(-c_2\,\mathcal{E}^x\right)\,\mathrm{d}\mathcal{E} \tag{2.22}$$

then, after introducing the change of variables $u = \mathcal{E} - V_\mathrm{s}$ and $t = (\mathcal{E}-V_\mathrm{s})^{-1}$ for the left and right integrals, respectively, we arrive at

$$\frac{4\,n_\mathrm{i}u_\mathrm{B}}{n_\mathrm{e}\overline{v}_\mathrm{e}c_1} = \int_0^1 \underbrace{u^{1/2}\exp\left(-c_2\,[u+V_\mathrm{s}]^x\right)}_{f_1(u)}\,\mathrm{d}u + \int_0^1 \underbrace{t^{-5/2}\,\exp\left(-c_2\,[t^{-1}+V_\mathrm{s}]^x\right)}_{f_2(t)}\,\mathrm{d}t \tag{2.23}$$

where the singularity at $t = 0$ can be eliminated by observing that $\lim_{t\to 0} f_2(t) = 0$. It is now straightforward to integrate equation (2.23) numerically and obtain V_s with an iteration. However, since the solution depends on both the densities and the electron temperature, the calculation would need to be done in each iteration step. This proved to be extremely inefficient, the model calculations taking roughly 10 – 100 times longer to finish compared to when an analytical solution of V_s was used. The analytical solution for V_s for a Maxwellian-like electron energy distribution function, derived from equation (2.21), is

$$V_\mathrm{s} = -\mathrm{T_e}\ln\left(4\frac{n_\mathrm{i}u_\mathrm{B}}{n_\mathrm{e}\overline{v}_\mathrm{e}}\right) \tag{2.24}$$

For an argon discharge it has been shown that V_s decreases with an increasing x (Gudmundsson, 2001). In an attempt to find an approximate expression for the sheath potential, a heuristic solution was developed to account for its dependency

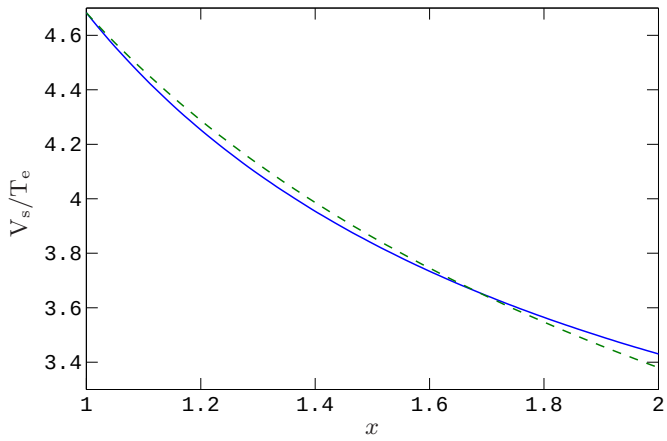

Figure 2.1: The normalized sheath potential, V_s/T_e, versus the parameter x. The heuristic solution for V_s, given by equation (2.25), (dashed line) compared to the numerically correct solution, given by equation (2.23), (solid line) in an argon discharge where $n_i = n_e$.

of the distribution parameter, x. By fitting the accurate solution of V_s in an argon discharge to a simple power law dependency of x, we arrive at

$$V_s = -T_e \ln\left(4\frac{n_i u_B}{n_e \overline{v}_e}\right) x^{-0.43} \tag{2.25}$$

By comparing equation (2.25) to the accurate numerical solution of (2.23) in an argon discharge, as in figure 2.1, we see that the error is sufficiently low in the range $1 < x < 2$.

The mean kinetic energy lost per ion lost, $\mathcal{E}_i$, is given by (Gudmundsson, 2001)

$$\mathcal{E}_i = \frac{[\Gamma(\xi_1)]^2}{\Gamma(\xi_2)\,\Gamma(\xi_3)}\langle\mathcal{E}\rangle + V_s \tag{2.26}$$

and the mean kinetic energy lost per electron lost, $\mathcal{E}_e$, is given by (Gudmundsson,

2001)

$$\mathcal{E}_{\mathrm{e}} = \frac{\Gamma(\xi_1)\,\Gamma(\xi_5)}{\Gamma(\xi_2)\,\Gamma(\xi_4)}\langle\mathcal{E}\rangle \tag{2.27}$$

where $\xi_5 = 3/x$. The total energy lost per electron-ion pair loss is

$$\mathcal{E}_{\mathrm{T}} = \mathcal{E}_{\mathrm{c}} + \mathcal{E}_{\mathrm{e}} + \mathcal{E}_{\mathrm{e}} \tag{2.28}$$

The collisional energy loss per electron-ion pair created, $\mathcal{E}_{\mathrm{c}}$, discussed in section 2.4 and given by equation (2.31), is normally the largest term in equation (2.28). It depends strongly on the rate coefficients of energy loss reactions and therefore any error in $\mathcal{E}_{\mathrm{T}}$ is mainly attributed to cross section errors, rather than errors in e.g. V_{s}. Furthermore, as x increases there is a steep increase in the collisional energy loss, $\mathcal{E}_{\mathrm{c}}$, as can be seen in figure 2.3. Thus, it has to be concluded that using the heuristic solution for the sheath potential V_{s}, given by equation (2.25), instead of the numerically correct solution, given by equation (2.23), is more than accurate enough, at least for the current study.

2.4 The collisional energy loss per ionization event

Collisional energy loss per electron-ion pair created, $\mathcal{E}_{\mathrm{c}}$, is an important parameter in our model since it represents a significant part of the total power loss included in the energy balance equation discussed in section 2.6.2. Before an electron-ion pair is created through ionization, the electron is likely to have lost a part of its energy to processes such as excitation or elastic scattering. Thus, assuming a single ionization process for each ion, the total collisional energy loss per electron-ion pair

created is given by (Lieberman and Lichtenberg, 2005, p. 81)

$$K_{\mathrm{iz}}\mathcal{E}_{\mathrm{c}} = K_{\mathrm{iz}}\mathcal{E}_{\mathrm{iz}} + K_{\mathrm{ex}}\mathcal{E}_{\mathrm{ex}} + K_{\mathrm{el}}\mathcal{E}_{\mathrm{el}} \tag{2.29}$$

where K and $\mathcal{E}$ refer to the rate coefficient and electron energy loss of the ionization, excitation and elastic scattering processes, and

$$\mathcal{E}_{\mathrm{el}} = \frac{3m_{\mathrm{e}}}{M} \tag{2.30}$$

is the mean electron energy loss of elastic scattering by a gaseous species with a mass M.

The collisional energy loss is usually found separately for each neutral species. As well as merging the terms on the right hand side, this yields a more convenient and general form of equation (2.29),

$$\mathcal{E}_{\mathrm{c}}^{(\alpha)} = \frac{1}{K_{\mathrm{iz},\alpha}} \sum_{\beta=1}^{N_{\beta,\alpha}} K_{\beta,\alpha}\mathcal{E}_{\beta,\alpha} \tag{2.31}$$

where $K_{\beta,\alpha}$ and $\mathcal{E}_{\beta,\alpha}$ are the rate coefficient and the electron energy loss of process β and species α, respectively. $N_{\beta,\alpha}$ is the total number of energy loss processes β due to collisions with species α. The processes in the sum over β should include all electron-neutral collisions, that is all rotational, vibrational and electronic excitation, dissociation, attachment and detachment processes, along with elastic collisions and ionization (Lee and Lieberman, 1995). Here, however, we will only include elastic, excitation, and basic ionization processes, as they are expected to dominate other processes. In any case, the resulting error should not be larger than errors arising from e.g. cross sections or the assumption of the electron energy distribution function. For a Maxwellian energy distribution for the electrons the

excitation processes are important and contribute significantly to $\mathcal{E}_c$ and thus have to be included. However, when assuming a Druyvesteyn energy distribution of electrons, even the excitation rate coefficients contribute little to $\mathcal{E}_c$, and it would be sufficient to only include elastic scattering and ionization processes in the calculation of the collisional energy loss. This has been confirmed by calculating the collisional energy loss with and without considering electron energy losses due to excitation. Although the excitation processes had a significant contribution for a Maxwellian electron energy distribution, their contribution to the total collisional energy loss was negligible for a Druyvesteyn electron energy distribution.

The collisional energy loss has been calculated for electron energy losses due to collisions with molecular nitrogen in the ground state, $N_2(X^1\Sigma_g^+, v = 0)$, on one hand, and with atomic nitrogen in the ground state, $N(^4S)$, on the other. The cross sections used to calculate the rate coefficients in equation (2.31) are discussed at length in chapter 3 (sections 3.2, 3.3 and 3.7 in particular). The rate coefficients and energy loss of each of the processes, calculated assuming a Maxwellian electron energy distribution, are summarized in tables A.7 and A.8. The collisional energy loss per electron-ion pair created is shown in figures 2.2 and 2.3. Figure 2.2(a) shows the collisional energy loss per electron-ion pair created for atomic nitrogen in the ground state, $N(^4S)$, and molecular nitrogen in the ground state, $N_2(X^1\Sigma_g^+, v = 0)$, calculated assuming a Maxwellian-like electron energy distribution. The collisional energy losses are very similar for the two species when the electron temperature is above 3 V, the collisional loss of the molecule increasing significantly faster when the electron temperature decreases any further. The collisional loss for the molecule is about 4.5×10^7 V and about 2×10^6 V for the atom when the electron temperature is 1 V, but are very similar at 100 V, or roughly 16 V and 18.8 V, respectively. Figure 2.2(b) shows the collisional loss of the molecular and atomic

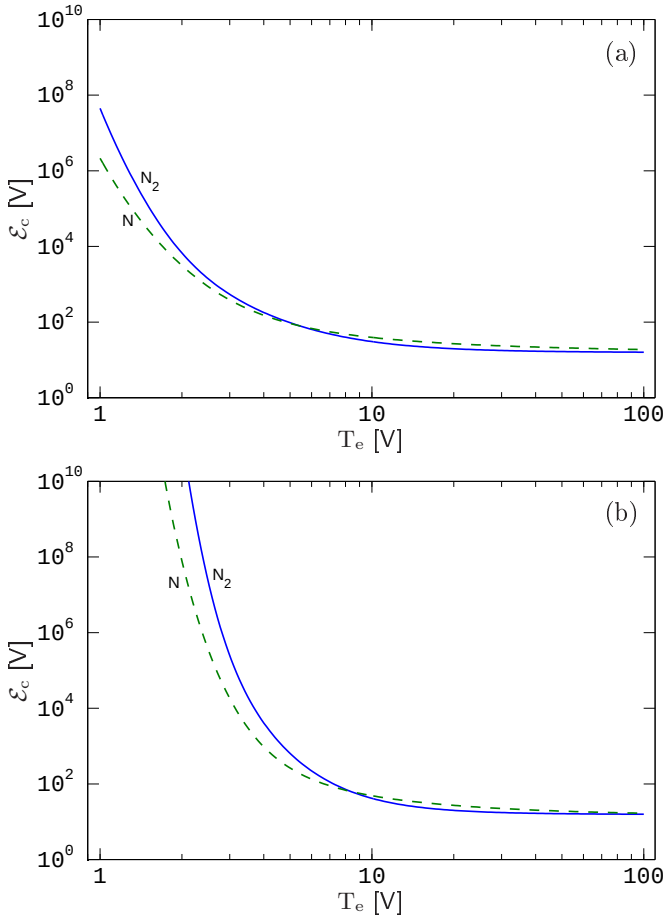

Figure 2.2: The collisional energy loss per electron-ion pair created, $\mathcal{E}_c$, as a function of the electron temperature for the ground state nitrogen molecule, $N_2(X^1\Sigma_g^+, v = 0)$, and the ground state nitrogen atom, $N(^4S)$, when assuming (a) a Maxwellian electron energy distribution and (b) a Druyvesteyn electron energy distribution.

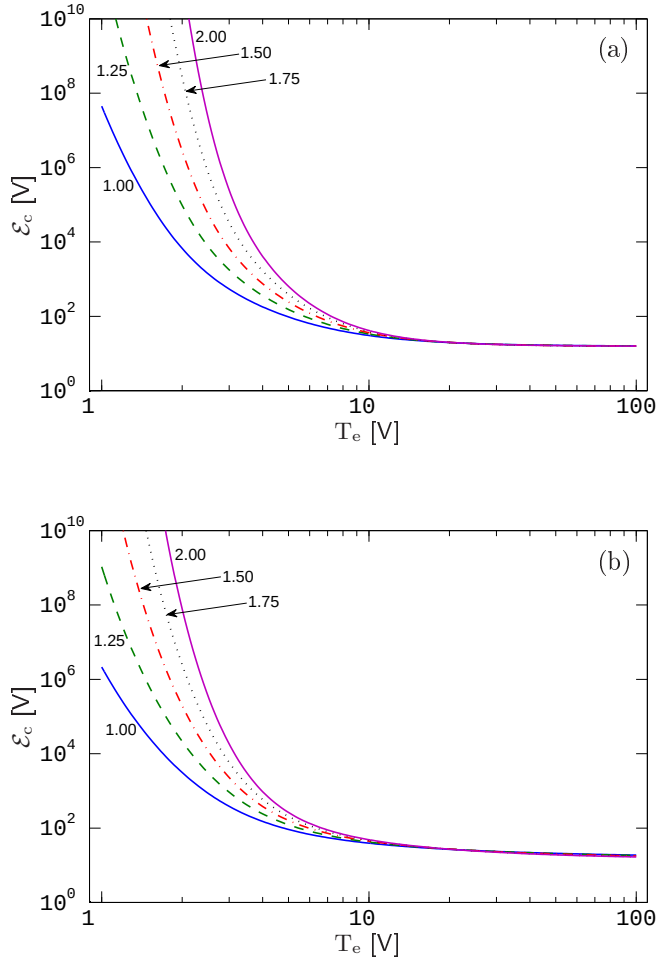

Figure 2.3: The collisional energy loss per electron-ion pair created, $\mathcal{E}_c$, as a function of the electron temperature for (a) the ground state nitrogen molecule, $N_2(X^1\Sigma_g^+, v = 0)$, and (b) the ground state nitrogen atom, $N(^4S)$. The electron energy distribution function is varied from being Maxwellian-like ($x = 1$) to Druyvesteyn-like ($x = 2$).

nitrogen calculated assuming a Druyvesteyn electron energy distribution. The collisional energy losses are very similar for the two species when the electron temperature is high, but unlike for the Maxwellian electron energy distribution case shown in figure 2.2(a), the collisional losses become different much sooner, or when the electron temperature is below roughly 7 V, and increase substantially more rapidly with decreasing electron temperature. The collisional loss is so large at 1 V electron temperature that we chose to omit parts of it that exceed 10^{10} V, being about 10^{42} V and 10^{26} V for the molecule and atom, respectively. When the electron temperature is 100 V the collisional losses are very similar, or 15.8 V and 16.8 V for the molecule and atom, respectively.

When changing the distribution function from Maxwellian to Druyvesteyn, i.e. $x = 1 \rightarrow 2$, as is done in figure 2.3, the energy loss increases exponentially, particularly at low electron temperatures. With its high threshold, the ionization rate coefficient decreases significantly when a Druyvesteyn distribution is assumed. This is normal as the tail of the Druyvesteyn distribution is noticeably smaller than that of the Maxwellian distribution. Furthermore, from comparison of figures 2.3(a) and (b) it can be seen that the collisional energy loss for the molecule has a significantly stronger dependence on x than the atom.

2.5 Detailed balancing

The reaction

$$A + B \longrightarrow C + D \tag{2.32}$$

is directly related to the inverse reaction

$$C + D \longrightarrow A + B \tag{2.33}$$

by detailed balancing (Lieberman and Lichtenberg, 2005, p. 267),

$$m_{\mathrm{R}}^2 g_A g_B v_{\mathrm{R}}^2 \sigma(v_{\mathrm{R}}) = {m'_{\mathrm{R}}}^2 g_C g_D {v'_{\mathrm{R}}}^2 \sigma'(v'_{\mathrm{R}}) \tag{2.34}$$

where m_{R} and m'_{R} are the reduced mass of the forward and inverse reactions,

$$m_{\mathrm{R}} = \frac{m_A m_B}{m_A + m_B} \qquad \text{and} \qquad m'_{\mathrm{R}} = \frac{m_C m_D}{m_C + m_D} \tag{2.35}$$

for the direct and inverse processes, respectively. Similarly the relative velocities are given by v_{R} and v'_{R}, and the cross sections by $\sigma(v_{\mathrm{R}})$ and $\sigma'(v'_{\mathrm{R}})$. Furthermore, the degeneracies of the particles A, B, C and D are given by g_A, g_B, g_C and g_D, respectively.

Our cross sections are given as a function of electron energy $\mathcal{E}$, and not the relative velocity v_{R}, as in equation (2.34). Kinetic energy and velocity of a particle are related by

$$\mathrm{e}\mathcal{E} = \frac{1}{2} m_{\mathrm{R}} v_{\mathrm{R}}^2 \tag{2.36}$$

and since $m_{\mathrm{R}} = m'_{\mathrm{R}}$ for electron impact excitation or de-excitation, equation (2.34) can be written

$$\mathcal{E} g_A g_B \sigma(\mathcal{E}) = \mathcal{E}' g_C g_D \sigma'(\mathcal{E}') \tag{2.37}$$

Using the relation

$$\frac{1}{2}m_{\mathrm{R}}v_{\mathrm{R}}^2 = \frac{1}{2}m'_{\mathrm{R}}{v'_{\mathrm{R}}}^2 + e\mathcal{E}_{\mathrm{a}} \tag{2.38}$$

along with equation (2.36), we find that

$$\mathcal{E} = \mathcal{E}' + \mathcal{E}_{\mathrm{a}} \tag{2.39}$$

Furthermore, $g_A = g_C$ for electron impact excitation or de-excitation and therefore we conclude that the cross section for the inverse process is related to the direct process by the equation

$$\sigma'(\mathcal{E}') = \left(1 + \frac{\mathcal{E}_{\mathrm{a}}}{\mathcal{E}'}\right)\frac{g_B}{g_D}\,\sigma(\mathcal{E}' + \mathcal{E}_{\mathrm{a}}) \tag{2.40}$$

for those processes. Dubé and Herzenberg (1979) calculated cross sections for both vibrational excitation and de-excitation, as well as stating that their calculations were consistent with the principle of detailed balancing. Using equation (2.40) on the $v = 1 \rightarrow 2$ cross section calculated by Dubé and Herzenberg, we found a near perfect fit to their $v = 2 \rightarrow 1$ cross section, giving us confidence in equation (2.40) and supporting their assessment that the calculations are consistent with the principle of detailed balancing. Furthermore, Mihajlov et al. (1999) gave an expression for the detailed balancing of a cross section which was consistent with equation (2.40).

By integrating equation (2.40) over the Maxwellian-like distribution, corresponding to $x = 1$ in equation (2.13), we obtain

$$K'(\mathrm{T_e}) = \frac{g_B}{g_D}\mathrm{e}^{\mathcal{E}_{\mathrm{a}}/\mathrm{T_e}}K(\mathrm{T_e}) \tag{2.41}$$

Equation (2.41) is actually never used in the model calculations to calculate inverse reaction rate coefficients since electron collision cross sections, and consequently equation (2.40), are utilized instead. The rate coefficient is obtained by averaging the cross section acquired with equation (2.40) over the electron energy distribution function. However, equation (2.41) is useful to manually check if the scaling of a given Maxwellian averaged inverse reaction rate coefficient is consistent with the principle of detailed balancing.

2.6 System of equations

The global (volume averaged) model is based on two types of balance equations to determine particle densities and electron temperature in the discharge. The system of equations consists of a set of non-linear particle balance equations, one for each discharge species, along with a single energy balance equation. Since the energy balance and particle balance equations are strongly coupled, the system of equations must be solved simultaneously. A numerical solver is the only viable choice for such a complex model.

2.6.1 Particle balance

The particle balance equation for a discharge species α is given as (Lieberman and Lichtenberg, 2005, p. 30),

$$\frac{\mathrm{d}n^{(\alpha)}}{\mathrm{d}t} + \nabla \cdot (n^{(\alpha)}\mathbf{u}^{(\alpha)}) = \mathrm{G}^{(\alpha)} - \mathrm{L}^{(\alpha)} \tag{2.42}$$

where $\mathrm{G}^{(\alpha)}$ and $\mathrm{L}^{(\alpha)}$ are the total rate of generation and loss of a species α, respectively.

Diffusion to the walls is included in the divergence term in equation (2.42).

However, it is possible to include any loss to the walls, including diffusion, in the loss term on the right hand side of equation (2.42). Furthermore, as the model is global, volume averaged, other spatial differentials are assumed to be zero and equation (2.42) reduces to

$$\frac{\mathrm{d}n^{(\alpha)}}{\mathrm{d}t} = \mathrm{G}^{(\alpha)} - \mathrm{L}^{(\alpha)} \tag{2.43}$$

Furthermore, for steady state calculations the left hand side is zero and the balance equation is further simplified, $\mathrm{G}^{(\alpha)} = \mathrm{L}^{(\alpha)}$, i.e. the generation of each species must be equal to its annihilation.

Loss and generation of a species can occur through various processes, but here we will consider loss and generation as a result of reactions of electrons with gaseous species, reactions of multiple gaseous species with each other, reactions on the wall, the flow of gas in and out of the chamber and the spontaneous optical emission of excited species.

Volume losses

For the reaction of two species,

$$A + B \xrightarrow{K} \text{products} \tag{2.44}$$

that involves the loss or generation of a species α the reaction rate is

$$R_{\mathrm{r}}^{(\alpha)} = n_A n_B K \tag{2.45}$$

For the spontaneous emission of an excited species A^*,

$$A^* \longrightarrow A + h\nu \tag{2.46}$$

involving the loss or generation of a species α (A^* or A, respectively), the reaction rate is given

$$R_{\text{rad}}^{(\alpha)} = n_{A^*} \frac{1}{\tau_{\text{rad},A^*}} \tag{2.47}$$

where τ_{rad,A^*} is the radiative lifetime of the excited species A^*.

Losses at walls

For the recombination of positive ions on the wall

$$A^+ + \text{wall} \longrightarrow A \tag{2.48}$$

that involves the loss or generation of a species α (A^+ or A, respectively), the reaction rate is

$$R_{\text{iw}}^{(\alpha)} = n_{A^+}\, u_{\text{B},A^+} \frac{A_{\text{eff}}}{V} \tag{2.49}$$

where V is the volume of the chamber, u_{B,A^+} is the Bohm velocity for the ion A^+, given by equation (2.2), and A_{eff} is the effective area for particle loss, as given by equation (2.8).

For the recombination of neutral atoms on the wall

$$B + \text{wall} \longrightarrow \frac{1}{2} B_2 \tag{2.50}$$

which involves the loss or generation of a species α (B or B_2, respectively), the reaction rate is (Booth and Sadeghi, 1991)

$$R_{\rm nwr}^{(\alpha)} = n_B \left[\frac{\Lambda_0^2}{D_B} + \frac{2V(2-\gamma_{{\rm rec},B})}{A\,\overline{v}_B\,\gamma_{{\rm rec},B}} \right]^{-1} \tag{2.51}$$

where $\gamma_{{\rm rec},B}$ is the wall recombination coefficient, $\overline{v}_B$ is the mean velocity given by equation (2.4), D_B is the diffusion coefficient of the neutral species B given by equation (2.3) and Λ_0 is the effective diffusion length, given by Chantry (1987) for a cylindrical chamber of length L and radius R,

$$\Lambda_0 = \left[\left(\frac{\pi}{L} \right)^2 + \left(\frac{2.405}{R} \right)^2 \right]^{-1/2} \tag{2.52}$$

For the quenching of excited particles B^* on the wall,

$$B^* + \text{wall} \longrightarrow B \tag{2.53}$$

which involves the loss or generation of a species α (B^* or B, respectively), the reaction rate has the same expression as for wall recombination, equation (2.51), but with a wall quenching coefficient $\gamma_{{\rm Q},B^*}$ instead of the wall recombination coefficient and the subscripts B replaced by B^*.

Pumping losses

The rate due to the flow of a species α into a chamber of volume V is

$$R_{\rm Qi}^{(\alpha)} = 4.48 \times 10^{17}\, \frac{Q_{\rm in}^{(\alpha)}}{V} \tag{2.54}$$

where $Q_{\rm in}^{(\alpha)}$ is the flow of the species α into the chamber in sccm and the factor 4.48×10^{17} converts sccm to particles/sec.

The rate due to the flow of a species α out of the chamber is

$$R_{\mathrm{Qo}}^{(\alpha)} = 1.27 \times 10^{-5} \frac{Q_{\mathrm{in}}^{\mathrm{T}}}{pV} n^{(\alpha)} \tag{2.55}$$

where $Q_{\mathrm{in}}^{\mathrm{T}}$ is the total flow of gas into the chamber in sccm, p is the outlet-flow pressure in Torr and the factor 1.27×10^{-5} converts sccm to Torr-m^3/sec.

Particle balance equations

By summing over processes β that involve the generation or loss of a particle α, β_{G} and β_{L}, respectively, the particle balance equation (2.43) for each species, α, can be written

$$\begin{aligned} \frac{\mathrm{d}n^{(\alpha)}}{\mathrm{d}t} = &\left[\sum_{\beta_{\mathrm{G}}} R_{\mathrm{r},\beta_{\mathrm{G}}}^{(\alpha)} + R_{\mathrm{iw,G}}^{(\alpha)} + R_{\mathrm{nw,G}}^{(\alpha)} + R_{\mathrm{Qi}}^{(\alpha)} + R_{\mathrm{rad,G}}^{(\alpha)} \right] \\ &- \left[\sum_{\beta_{\mathrm{L}}} R_{\mathrm{r},\beta_{\mathrm{L}}}^{(\alpha)} + R_{\mathrm{iw,L}}^{(\alpha)} + R_{\mathrm{nw,L}}^{(\alpha)} + R_{\mathrm{Qo}}^{(\alpha)} + R_{\mathrm{rad,L}}^{(\alpha)} \right] \end{aligned} \tag{2.56}$$

Since the discharge is quasi-neutral, according to equation (2.1), the electrons are balanced automatically due to the balance equations for the ions. We will therefore exclude the equation for the balance of electrons in the global model calculations and obtain the electron density from the ion densities with the help of equation (2.1). This will increase the efficiency of the global model calculations to some extent.

2.6.2 Energy balance

The total power absorbed in the plasma, P_{abs}, must be equal to the total power loss in the system due to the conservation of energy. The power balance equation,

given by Ashida et al. (1995), can be written

$$\frac{\mathrm{d}}{\mathrm{d}t}\left(\frac{3}{2}en_{\mathrm{e}}\mathrm{T_e}\right) = \frac{1}{V}\left[P_{\mathrm{abs}} - eVn_{\mathrm{e}}n_{\mathrm{g}}\sum_{\beta}K_{\beta,\alpha_{\mathrm{g}}}\mathcal{E}_{\beta,\alpha_{\mathrm{g}}} - eu_{\mathrm{B}}n_{\mathrm{i}}A_{\mathrm{eff}}(\mathcal{E}_{\mathrm{i}}+\mathcal{E}_{\mathrm{e}})\right] \quad (2.57)$$

where V is the volume of the discharge chamber, A_{eff} is the effective area for particle loss in the chamber given by equation (2.8) and u_{B} is the Bohm velocity given by equation (2.2). $\mathcal{E}_{\mathrm{i}}$ and $\mathcal{E}_{\mathrm{e}}$ are the mean kinetic energy lost per ion and electron lost, given by equations (2.26) and (2.27), respectively. The sum is over all collisional energy loss processes β, with rate coefficients $K_{\beta,\alpha}$ and energy loss $\mathcal{E}_{\beta,\alpha}$, for collisions with the species α. At last, n_{e}, n_{i} and n_{g} refer to the densities of electrons, ions and neutral species, respectively.

The second term on the right hand side of (2.57) represents the loss of power due to collisions of gaseous species, and the third term the power loss due to kinetic energy loss of ions and electrons as they bombard the chamber walls. The left hand side represents the time differential of the mean electron energy density, $\frac{3}{2}en_{\mathrm{e}}\mathrm{T_e} = \langle\mathcal{E}\rangle n_{\mathrm{e}}$. In steady state this term is zero, and the absorbed power must simply be equal to the sum of collisional and wall power losses.

Chapter 3

Nitrogen specific parameters

There are several parameters in a discharge that are specific to the type of gas being studied. Here we will discuss all the parameters specific to the nitrogen discharge. The nitrogen reaction set will be reviewed in sections 3.1 to 3.7. We will consider 15 species of nitrogen in the discharge; the seven lowest lying vibrational levels of the ground state nitrogen molecule $N_2(X^1\Sigma_g^+, v = 0-6)$, the metastable nitrogen molecule $N_2(A^3\Sigma_u^+)$, the ground state nitrogen atom $N(^4S)$, the metastable nitrogen atoms $N(^2D)$ and $N(^2P)$, and the ions N_2^+, N^+, N_3^+ and N_4^+. The most extensive collections of reaction rate coefficients in nitrogen are those by Kossyi et al. (1992) and Guerra et al. (2004). Unfortunately, the data set given by Kossyi et al. (1992) was developed for atmospheric research and thus for a lower electron energy than is expected in processing discharges. Additionally, Guerra et al. (2004) created the reaction set for modelling discharges in the pressure range $1-10$ Torr. As we allow the electron energy distribution function to vary, a set of electron impact cross sections is required. The most extensive collection of cross sections for electron collisions with nitrogen molecules can be found in the reviews by Itikawa (2006)

and Tabata et al. (2006). We will discuss the wall interaction processes in section 3.8. The available data for the wall recombination coefficient of neutral atoms will be reviewed, as well as the coefficients for the wall quenching of the various excited species in the discharge. The scattering cross sections for different particles in the discharge will be discussed in section 3.9. Furthermore, the gas temperature will be discussed in section 3.10.

3.1 Electron impact dissociation

Dissociation is a fundamental mechanism in molecular gas discharges. The dissociation energy of the ground state nitrogen molecule has been established to lie around 9.8 eV (Ren et al., 2005; Lofthus and Krupenie, 1977). The overall dissociation mechanism in nitrogen discharges is not qualitatively understood and the role of collisional dissociation or predissociation, the spontaneous dissociation of molecules excited to a high electronic or vibrational level, is not known. The dissociation mechanism is sometimes described by the sum of excitations to dissociative electronic and vibrational levels (Guerra and Loureiro, 1995, 1997; Guerra et al., 2004; Zipf and Mclaughlin, 1978; Phelps, 2008). In the current study, we will disregard predissociation and only assume that the dissociation is induced by collisions with electrons, which may in effect include the contribution of predissociation of highly excited species.

3.1.1 Electron impact dissociation of the nitrogen molecule

The mechanism of the electron impact dissociation of the nitrogen molecule is still not completely understood. There are several processes that contribute to the overall dissociation process. Aside from the predissociation of highly excited molecules,

electron impact dissociation of excited molecules, including electronically, vibrationally and rotationally excited molecules, is important as well. However, cross section data is only available for the general reaction

$$\mathrm{e} + \mathrm{N_2} \quad \longrightarrow \quad \mathrm{N} + \mathrm{N} + \mathrm{e} \tag{3.1}$$

where neither the state of the reactant or products is clearly specified.

Winters (1966) measured the total dissociation cross section by monitoring the pressure inside a constant volume chamber during electron-N_2 impact. The measured cross section has been suggested to be too large since it includes contribution from dissociative ionization (Itikawa et al., 1986). A cross section purely for reaction (3.1) can be extracted by subtracting the dissociative ionization cross section (section 3.2.1) from this total cross section. In a study of the predissociation of highly excited states of the nitrogen molecule, Zipf and Mclaughlin (1978) obtained a dissociation cross section that is in agreement with the total cross section measured by Winters (1966).

Cosby (1993) measured the cross section for reaction (3.1) using a crossed beams experiment. He estimated that the N_2 beam consisted of 90 % $N_2(X^1\Sigma_g^+, v = 0)$, but was also able to use a beam that he believed to consist of 60 % $N_2(X^1\Sigma_g^+, v = 0)$, 15 % $N_2(X^1\Sigma_g^+, v > 0)$ and 25 % $N_2(A^3\Sigma_u^+)$. He detected no systematic difference in results between the two beams, indicating that the cross sections for the dissociation of vibrationally and electronically excited molecules are not very different from the cross section for dissociation of the ground state molecule $N_2(X^1\Sigma_g^+, v = 0)$. A comparison with the result of Winters reveals a significant discrepancy between the two cross sections. Therefore, Cosby recommended a cross section that was a weighted average of both cross sections. Mi and Bonham (1998) measured the cross section at two energies. The results were in good agreement with

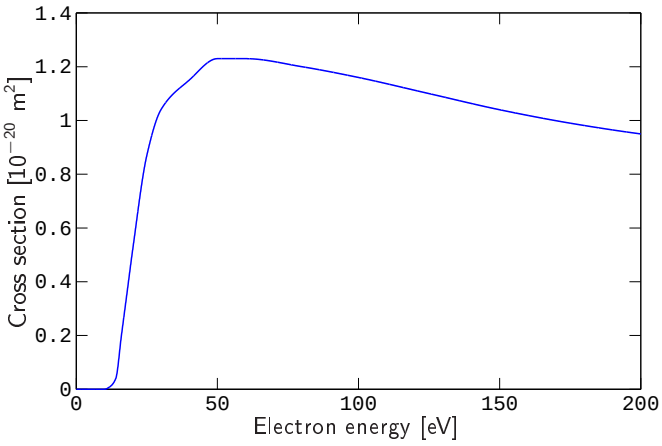

Figure 3.1: The cross section for the electron impact dissociation of the ground state nitrogen molecule $N_2(X^1\Sigma_g^+, v = 0)$ versus electron energy as recommended by Cosby (1993). The cross section is a weighted average of the cross sections measured by Winters (1966) and Cosby (1993).

the cross section recommended by Cosby (1993). Furthermore, recent compilations of electron-N_2 collision data (Tabata et al., 2006; Itikawa, 2006) support the use of Cosby's recommended cross section. This cross section is shown in figure 3.1

Like Itikawa (2006) pointed out, further research is needed concerning the state of the dissociation products. Although theory predicts that the least energy is needed for producing two atoms in the ground state, no sophisticated measurements or simulations have been made to explicitly obtain the overall product branching ratio in the electron impact dissociation of N_2. Nevertheless, the product branching ratio has been measured repeatedly for the dissociative recombination of N_2^+, as mentioned in section 3.4.1. With an analysis of translational energy release distribution, Cosby (1993) saw an indication of $N(^4S)$ + $N(^2D)$ being the dominant channel, with $N(^4S)$ + $N(^4S)$ and $N(^4S)$ + $N(^2P)$ being minor channels, and $N(^2D)$ + $N(^2D)$ being a negligible channel. Subsequent measurements of product yields in the predissociation of highly excited levels of N_2 by Walter et al. (1993) show

that while the ground state atom $N(^4S)$ is always produced, two $N(^4S)$ atoms are almost never produced in a single dissociation event. The other product was found to be either the metastable $N(^2D)$ or the metastable $N(^2P)$, with the former being more likely. This is in agreement with the suggestion of Kaplan (1932), that argued that at least one of the products had to be in a metastable state, most probably the $N(^2D)$, contrary to yet earlier belief (Mulliken, 1932) of both the atoms being in the ground state. We therefore assume that there is only a single dissociation channel, $N(^4S) + N(^2D)$, with the creation of the higher metastable atom $N(^2P)$ being negligible in comparison.

Other than what is mentioned above about Cosby's measurement, there is no information regarding the state of the reactant molecule. Thus, approximations must be made to obtain cross sections for electron impact dissociation of excited nitrogen molecules. In the case of the electron impact ionization of the nitrogen molecule (see section 3.2.1), threshold reduction is much more important than scaling the cross section for ionization of the ground state molecule in order to approximate the cross section for ionization of the metastable molecule. One could even argue that the scaling is not appropriate, as the difference in magnitude is within the error limits of the corresponding cross sections. This is even more true for the dissociation of N_2, now under discussion, because of the lack of any specific measurements or predictions. Even though it is only an approximation, using a threshold reduced cross section is at least more appropriate than just disregarding dissociation from excited molecules altogether. We will therefore take this approach for the electron impact dissociation of vibrationally and electronically excited nitrogen molecules.

3.2 Electron impact ionization

Ionization is a crucial part of any discharge, since the amount of free electrons is largely defined by the efficiency of the ionization reactions. In low pressure discharges, electron impact ionization is the dominating ionization mechanism, whereas in discharges operating at higher pressure associative or Penning ionization may dominate (Guerra et al., 2004). Here we will discuss the electron impact ionization of nitrogen molecules and atoms. The ionization potential for the ground state nitrogen molecule $N_2(X^1\Sigma_g^+, v = 0)$ is 15.6 eV and for the ground state nitrogen atom $N(^4S)$ 14.5 eV (Lias, 2005).

3.2.1 Electron impact ionization of the nitrogen molecule

Ionization of nitrogen molecules can occur in a number of ways, but since we only take into account singly ionized particles, our scope tightens to the direct and dissociative ionization of the nitrogen molecule, that is

$$e + N_2 \longrightarrow N_2^+ + 2e \tag{3.2}$$

and

$$e + N_2 \longrightarrow N^+ + N + 2e \tag{3.3}$$

$$\longrightarrow N^+ + N^+ + 3e \tag{3.4}$$

respectively. The direct ionization, reaction (3.2), should be much more likely than the dissociative ionization, reactions (3.3) and (3.4).

Several groups have measured or calculated a cross section for the direct ionization, reaction (3.2), but do not specify the state of the molecule being ionized,

although their nitrogen molecules are likely dominated by ground state nitrogen molecules. Itikawa (2006) recommended the cross section given by Lindsay and Mangan (2003), which in turn based their cross section on a slightly modified data of Straub et al. (1996) and the widely known measurements of Rapp and Englander-Golden (1965). Other authors have measured or theoretically predicted the cross section and most (Halas and Adamczyk, 1972; Crowe and McConkey, 1973; Krishnakumar and Srivastava, 1990; Tian and Vidal, 1998; Hudson et al., 2003; Freund et al., 1990; Daly and Powell, 1966) are in an excellent agreement with Straub et al. (1996). Because of the high level of agreement with other measurements and the claimed measurement error of only 5.5%, we will consider the the cross section measured by Straub et al. as the point of reference for the ionization of ground state nitrogen molecules, reaction 3.2. A few more studies (Cook and Peterson, 1962; Märk, 1975; Bacri and Medani, 1982; Abramzon et al., 1999) measure or calculate the cross section as well, but are less consistent with the data above. Armentrout et al. (1981) measured the cross sections for the direct ionization of both ground state and metastable nitrogen molecules. Freund et al. (1990) repeated the measurements in order to improve the reliability of the measurement of the metastable ionization cross section. The measurement for the ground state ionization was content with the previous result and consistent with the cross section measured by Straub et al. (1996) and Tian and Vidal (1998).

As for the dissociative ionization, we notice a lack of product branching ratios, with most authors only measuring the production of N^+ from electron impact on N_2 (Straub et al., 1996; Krishnakumar and Srivastava, 1990; Crowe and McConkey, 1973; Rapp et al., 1965; Cook and Peterson, 1962; Daly and Powell, 1966). Tian and Vidal (1998) measured the cross section for reactions (3.2), (3.3) and (3.4) independently with the use of covariance mapping mass spectroscopy. As with

the previously mentioned N^+ production cross sections, their cross sections also include contribution from N_2^{2+} production, being indistinguishable in a mass spectrometer because of equal mass to charge ratio. They estimate the contribution of N_2^{2+} production to be negligible, while Halas and Adamczyk (1972) measured the contribution to be as much as 10%, decreasing with increasing energy to being negligible near threshold. Lindsay and Mangan (2003) estimated the contribution to be less than 0.5%, agreeing with Tian and Vidal (1998). We will follow the latter and more common conclusion and ignore the contribution of N_2^{2+} to the N^+ production cross sections.

Since the data of Tian and Vidal (1998) is nearly identical to the corresponding cross sections of Straub et al. (1996), it is regarded to be reliable as well, both for direct and dissociative ionization. We will therefore use both the direct and dissociative ionization cross sections for ground state ionization from Tian and Vidal in the model. The electron impact cross sections for direct and dissociative ionization of the nitrogen molecule is shown in figure 3.2. Very few measurements or calculations of the cross section for electron impact ionization of excited states of the nitrogen molecule exist. Armentrout et al. (1981) and Freund et al. (1990) measured the cross section for the direct ionization of the metastable molecule $N_2(A^3\Sigma_u^+)$, whereas Bacri and Medani (1982) used a weighted cross section calculation to predict it theoretically. The metastable ionization cross sections of those two are in a reasonable agreement, although their ground state ionization cross sections are not. However, the cross section for the electron impact ionization of the ground state nitrogen molecule measured by Freund et al. (1990) is consistent with the cross section measured by Straub et al. (1996), whereas the cross section by Bacri and Medani (1982) is not. We will therefore use the cross section from Freund et al. (1990) for the direct ionization of the metastable nitrogen molecule.

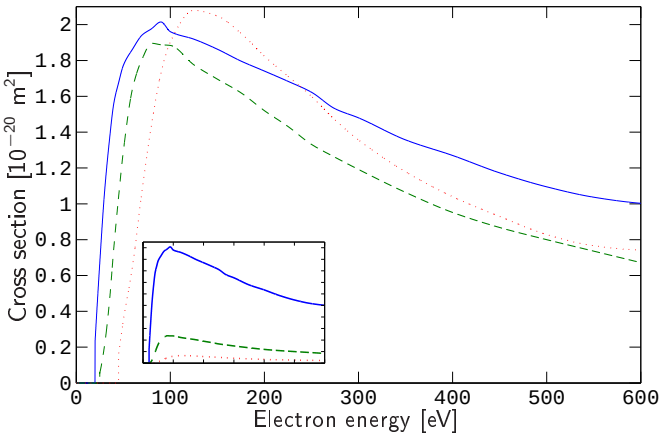

Figure 3.2: The cross section for the electron impact ionization of the ground state nitrogen molecule versus electron energy (Tian and Vidal, 1998). The solid, dashed and dotted lines refer to the production of N_2^+, $N(^2D)$ + N^+ and N^+ + N^+, respectively. The dashed line has been multiplied by 4, and the dotted by 16, for a more detailed representation, but are shown in their original scale on the inset graph. The corresponding cross sections for the ionization of excited nitrogen molecules are threshold reduced and scaled versions of the above cross sections (see text), and are therefore not shown.

As no cross section data exists for the dissociative ionization of excited nitrogen molecules, we will approximate them by scaling the magnitude and reducing the threshold of other cross sections. A comparison of the cross sections for the ionization of the ground state and the metastable molecules, as measured by Freund et al. (1990), can be used to determine the scaling and threshold reduction. Applying the result to the cross section of Tian and Vidal (1998) should yield a reliable cross section for the direct ionization of the metastable nitrogen molecule, $N_2(A^3\Sigma_u^+)$. As illustrated in figure 3.3, making the ground state cross section of Freund et al. 20% larger and reducing the threshold by 6.17 eV, the energy of which the metastable $N_2(A^3\Sigma_u^+)$ lies above the ground state nitrogen molecule $N_2(X^1\Sigma_g^+, v = 0)$, gave a good match to the metastable ionization cross section also measured by Freund et al. (1990). A better match at high energies could have

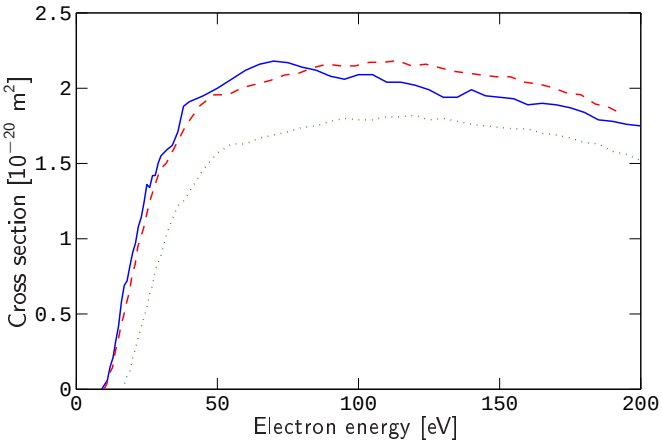

Figure 3.3: The electron impact ionization cross section for the nitrogen molecule. Comparison of the cross sections from Freund et al. (1990) for ionization of $N_2(A^3\Sigma_u^+)$ (solid line) and $N_2(X^1\Sigma_g^+, v = 0)$ before (dotted line) and after (dashed line) scaling and reducing the threshold of the ground state ionization cross section.

been achieved by different scaling of the cross section magnitude, but we regard the low energy accuracy to be more desireable.

A similar method can be used to find cross sections for ionization of vibrationally excited molecules. We assume that only the $N_2(X^1\Sigma_g^+, v = 0)$ is present in the impact molecule beam in the above data, but no experiments are to be found that attempt to measure the cross section for ionization of molecules in a specific vibrationally excited state. An approximation would be to only shift the threshold the energy of which each state lies above the ground state $N_2(X^1\Sigma_g^+, v = 0)$, without scaling the magnitude of the cross section. The calculations of Cacciatore et al. (1982) show that this is approximately correct, as the ionization cross sections have reduced thresholds but a similar magnitude with increasing vibrational level of $N_2(X^1\Sigma_g^+, v)$. The result is most likely satisfactory and in any case better than disregarding ionization from vibrational states altogether.

Since no information was found regarding the state of the neutral atom produced

in reaction (3.3), and taking into account the branching ratios from dissociative recombination (sec 3.4.1), we will simply assume that $N(^2D)$ is the only product. This may not be very accurate, perhaps even inaccurate, but this channel is likely to be of no importance for neutral nitrogen atom production anyway, although it might be important in the production of the atomic ion N^+.

Electron energy loss

For the calculation of the collisional energy loss due to collisions with ground state nitrogen molecules, $\mathcal{E}_c$, given by equation (2.31), the individual cross sections for reactions (3.2), (3.3) and (3.4), shown in figure 3.2, are not necessary. Instead, it will be adequate to use the total cross section for the ionization of the nitrogen molecule, the sum of the three individual cross sections measured by Tian and Vidal (1998) and shown in figure 3.2. Furthermore, to obtain the threshold of the ionization of the nitrogen molecule, we will use the value given by Lias (2005) for the energy loss associated with the production of N_2^+, 15.6 eV.

3.2.2 Electron impact ionization of the nitrogen atom

The overall cross section for the electron impact ionization of the nitrogen atom,

$$e + N \longrightarrow N^+ + 2e \tag{3.5}$$

has been both predicted theoretically (Seaton, 1959; Peach, 1970, 1971; Omidvar et al., 1972; McGuire, 1971; Yu et al., 2006) and measured (Smith et al., 1962; Brook et al., 1978). These cross sections include contribution from multiple ionization of nitrogen atoms and do not discriminate the state of the nitrogen atom before impact. However, all the measurements and theoretical predictions are in quite good agreement with each other, indicating that the overall cross section is reliable.

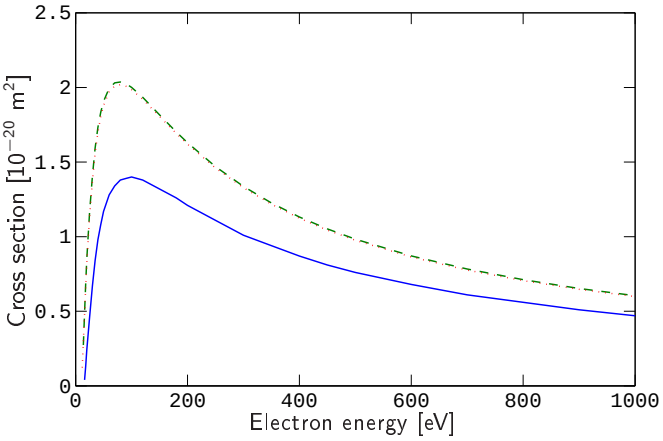

Figure 3.4: The cross section for electron impact ionization of the nitrogen atom calculated by Kim and Desclaux (2002). The solid line corresponds to the ionization from the ground state nitrogen atom, N(^{4}S). The dashed and dotted lines, nearly indistinguishable, correspond to the ionization from the metastable atoms N(^{2}D) and N(^{2}P).

Kim and Desclaux (2002) calculated the cross sections for the electron impact ionization of N(^{4}S), N(^{2}D) and N(^{2}P), individually. Their results are in agreement with the overall cross section measurements of Brook et al. (1978), indicating that the calculation is reliable as well. We will therefore use the cross sections calculated by Kim and Desclaux (2002) for ionization of each of the neutral atoms we include in the model. The cross sections are in part shown in figure 3.4, excluding the data in the range 1000 – 5000 eV.

Electron energy loss

For the electron energy loss due to collision with the ground state nitrogen atom, N(^{4}S), we will use the cross section calculated by Kim and Desclaux (2002), consistent with our choice above. Furthermore, for the threshold of the ionization of the ground state nitrogen atom, we will use the value given by Lias (2005), 14.5 eV.

3.3 Electron impact excitation

If gas species in excited levels are considered, the reactions responsible for their excitation are very important. The dominating excitation mechanism is generally the electron impact excitation, which we will discuss here. The excited species considered in this study are the two metastable nitrogen atoms $N(^2D)$ and $N(^2P)$, with excitation energies of 2.38 eV and 3.58 eV, respectively (Ralchenko et al., 2008), the metastable nitrogen molecule $N_2(A^3\Sigma_u^+)$, having an excitation energy of roughly 6.17 eV (Lofthus and Krupenie, 1977), as well as the first six vibrational levels of the ground state nitrogen molecule, $N_2(X^1\Sigma_g^+, v = 1-6)$, having vibrational energies of 0.29, 0.57, 0.86, 1.13, 1.41 and 1.68 eV, respectively (Ren et al., 2005; Lofthus and Krupenie, 1977).

3.3.1 Electron impact electronic excitation of the nitrogen molecule

In the current study we are only interested in the lowest lying metastable state of the nitrogen molecule, so electron impact electronic excitation simply refers to the reaction

$$e + N_2(X^1\Sigma_g^+, v) \quad \longrightarrow \quad N_2(A^3\Sigma_u^+) + e \tag{3.6}$$

Bacri and Medani (1982) calculated the cross section for the excitation of the ground state nitrogen molecule and compared the result to the various measurements and calculations that had been performed up to that time. The cross section, being in a surprisingly good agreement with the measurement of Borst (1972), is inconsistent with the cross section measurement of Cartwright et al. (1977), the most reliable cross section in the comparison. A renormalization of the measurement of

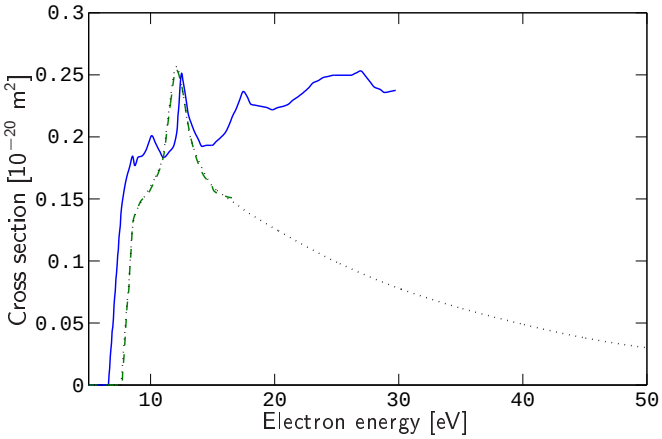

Figure 3.5: Electron impact electronic excitation of the ground state nitrogen molecule $N_2(X^1\Sigma_g^+, v = 0)$ to $N_2(A^3\Sigma_u^+)$. Comparison of the cross sections calculated by da Costa and Lima (2007) (solid line) and by Gillan et al. (1996) (dashed line). The dotted line shows the cross section recommended by Itikawa (2006), assembled from the cross section calculated by Gillan et al. (1996) at low energy and several measured cross sections at high energy.

Cartwright et al. (1977) by members of the same group, only further emphasized the inconsistency. Several measurements (Ohmori et al., 1988; Campbell et al., 2001; Johnson et al., 2005) and calculations (da Costa and Lima, 2007; Tashiro and Morokuma, 2007; Gillan et al., 1996; Huo et al., 1987; Phelps and Pitchford, 1985) show considerable variation in results. Most of the calculated cross sections have a similar behavior at low electron energy, the only exception being the cross section calculated by da Costa and Lima (2007), where the apparent threshold is considerably lower than in the other calculations (see figure 3.5). The measurements, on the other hand, are in quite good agreement at high electron energy. Itikawa (2006) assembled a cross section using the theoretical calculation of Gillan et al. (1996) for low electron energy, and a weighted average of several measurements at higher electron energy.

Although the apparent threshold observed in the calculation of da Costa and

Lima (2007) is closer than other calculations to what we would expect of 6.17 eV, the high energy part of the cross section is inconsistent with all other cross section calculations or measurements. Thus, we discard their cross section calculation altogether. Furthermore, recent cross section calculations (Tashiro and Morokuma, 2007) are also in good agreement with the cross section of Gillan et al. (1996), and therefore with the low energy part of the cross section recommended by Itikawa (2006). Therefore, we will use the cross section suggested by Itikawa (2006) for reaction (3.6), shown in figure 3.5 as a dotted line.

Electronic excitation of a vibrationally excited nitrogen molecule is also likely an important factor in the creation of $N_2(A^3\Sigma_u^+)$. However, little information is available in the literature on this reaction, in particular on specific vibrational states. All of the experiments mentioned above for the excitation of a ground state molecule probably include contributions of excitation from vibrationally excited molecules. Cacciatore et al. (1982) calculated the cross section for the excitation to $N_2(A^3\Sigma_u^+)$, $N_2(C^3\Pi_u)$, $N_2(b^1\Pi_u)$, $N_2(B^3\Pi_g)$ and $N_2(a^1\Pi_g)$ by electron impact excitation of $N_2(X^1\Sigma_g^+, v)$. Unfortunately, the excitation of the first metastable level was only calculated for electron impact on $N_2(X^1\Sigma_g^+, v = 0)$, whereas the cross sections for the latter four levels were calculated for impact with $N_2(X^1\Sigma_g^+, v = 0\,, 5\,, 10)$. The cross section for the excitation of the first level was shown to be in a reasonable agreement with the cross section measured by Cartwright et al. (1977), which in turn is in good agreement with the cross section recommended by Itikawa (2006). The cross sections for excitations of the vibrationally excited molecules not only shifted to lower electron energy, but also increased in magnitude with increasing vibrational level of the reactant molecule. Although the reduction in threshold energy was roughly the same, the magnitude increase was irregular and different for each of the four electronic levels. This makes it impossible for

us to apply any kind of scaling rule to obtain cross sections for the excitation of $N_2(A^3\Sigma_u^+)$ from vibrational levels of $N_2(X^1\Sigma_g^+, v)$. To obtain these cross sections we will simply reduce the threshold of the cross section, assuming there is no change in magnitude for this particular excitation.

Electron energy loss

For the calculation of the collisional energy loss, $\mathcal{E}_c$, we will use the same cross section for the excitation of the first excited level, the metastable $N_2(A^3\Sigma_u^+)$, as found above and shown in figure 3.5. For the electronic excitation of higher levels we will solely rely on the cross sections given by Itikawa (2006), in total considering the first 10 electronically excited levels. The cross sections are shown in figures 3.6 (a) and (b). Furthermore, we will use the values given in the review by Lofthus and Krupenie (1977) for the energy of which each electronically excited species lies above the absolute ground state molecule, $N_2(X^1\Sigma_g^+, v = 0)$.

The determination of the cross section for the rotational excitation of the nitrogen molecule,

$$e + N_2(X^1\Sigma_g^+, v = 0, j = 0) \longrightarrow N_2(X^1\Sigma_g^+, v = 0, j = 2) + e \tag{3.7}$$

is difficult both theoretically and experimentally, especially at energies above 1 eV. The available data was reviewed by Itikawa (2006) and Brunger et al. (2003), both recommending the use of the swarm-derived data of Robertson et al. (1997) and Morrison et al. (1997) for energy under 1.25 eV. For higher energy, Itikawa (2006) recommended the theoretical cross section of Kutz and Meyer (1995), given for energy in the range 1 – 1000 eV, but on an arbitrary scale and thus needing a suitable normalization. According to Itikawa (2006), the cross section is too large in the resonance region but otherwise consistent with experiments. Using vibrational

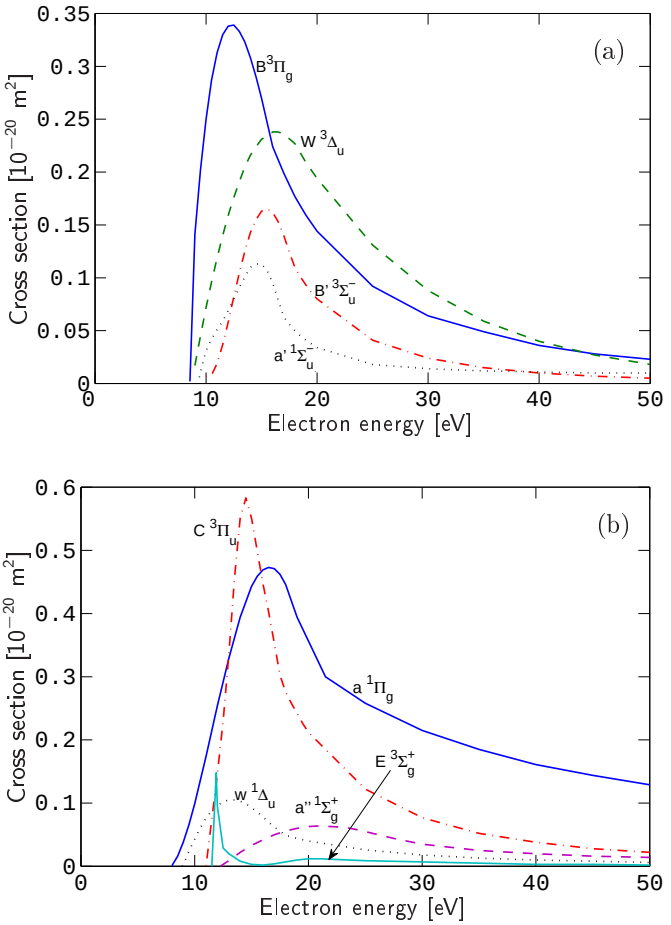

Figure 3.6: The cross sections for the electron impact excitation of (a) the $B^3\Pi_g$, $W^3\Delta_u$,$B'^3\Sigma_u^-$ and $a''^1\Sigma_u^-$ electronic states and (b) the $a^1\Pi_g$, $w^1\Delta_u$, $C^3\Pi_u$, $E^3\Sigma_g^+$ and $a"^1\Sigma_g^+$ electronic states of nitrogen molecule. The cross section for the excitation to the $N_2(A^3\Sigma_u^+)$ metastable molecule is shown in figure 3.5.

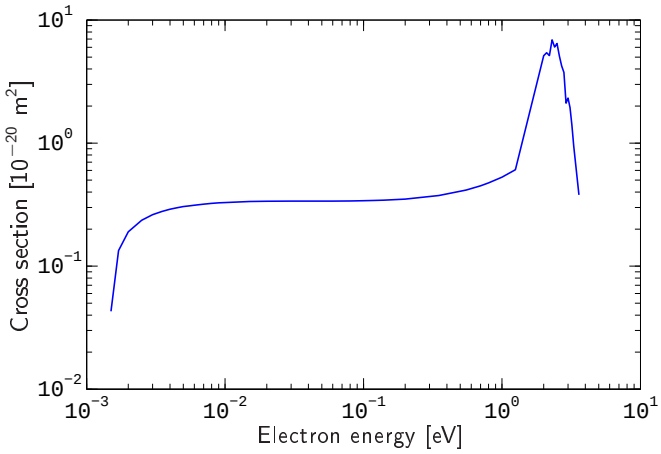

Figure 3.7: The cross section for the rotational excitation of the nitrogen molecule. It is assembled from the cross section recommended by Brunger et al. (2003) in the energy range 1.5 meV – 1.25 eV and the cross section approximated by Phelps (2008) in the energy range 2 – 3.6 eV.

cross section data, Phelps (2008) approximated the cross section for rotational vibration, resulting in non-zero values in the range 1.2 – 3.6 eV, essentially in the resonance region. The resonance peak is significantly smaller than the peak in the cross section calculation of Kutz and Meyer (1995), indicating that for this energy this cross section is more appropriate. We will therefore assemble and use a cross section consisting of the cross section recommended by Brunger et al. (2003) for the energy range 1.5 meV – 1.25 eV and the cross section approximation given by Phelps (2008) in the energy range 2 – 3.6 eV. The result is shown in figure 3.7. Furthermore, we will use the value given by Itikawa (2006) for the excitation energy of the first rotational excitation, $j = 0 \rightarrow 2$, or 1.48×10^{-3}. The threshold for the rotational excitation is therefore 3 – 4 orders of magnitude smaller than of the other electron energy loss processes. This makes it very unlikely for the rotational excitation cross section to be important at all for the collisional energy loss, especially since the cross section is not unusually large.

3.3.2 Electron impact vibrational excitation of the ground state nitrogen molecule

Vibrational levels of the ground state $N_2(X^1\Sigma_g^+, v)$ are thought to be very important in nitrogen discharges. The vibrational excitation of the nitrogen molecule,

$$e + N_2(X^1\Sigma_g^+, v = i) \longrightarrow N_2(X^1\Sigma_g^+, v = j) + e \qquad j > i \qquad (3.8)$$

is important in order to realize the correct population distribution among the vibrationally excited nitrogen molecules. That in turn is important for various processes within the discharge, such as ionization, dissociation and electronic excitation of the nitrogen molecule because of the lowered threshold for those reactions. To get an accurate image of the vibrational level population distribution, we need to have reliable cross sections for all of the vibrational excitations.

While a great number of vibrational states of the ground state nitrogen molecule exist, the first 10 levels are the most well documented, with the $v = 0 \rightarrow v = 1$ excitation being the single most studied (Sun et al., 1995; Feng et al., 2003; Robertson et al., 1997; Allan, 2005). If the first 10 vibrational levels are included there are 55 excitations possible ($\frac{1}{2}v(v+1)$), as well as the same number of de-excitations. Here we will restrict the calculations to the first 6 levels, $v = 0 - 6$, since more data is available for these in the literature.

Schulz (1964) measured the cross section for vibrational excitation from the ground state, $v = 0$, of the nitrogen molecule. Although the cross sections are on an arbitrary scale, they are commonly used (Phelps, 2008; Mihajlov et al., 1999) after having been normalized with other absolute measurements, since their high resolution captures the resonant structure observed in some of the subsequent measurements and calculations. Of those, probably the most significant are the

measurements of Allan (1985) and Vicic et al. (1996), and the calculations of Morgan (1986) and Huo et al. (1987). It is evident after analyzing these cross sections that simply using a threshold reduction would be highly inaccurate, even incorrect, when vibrational excitation is concerned. As the cross section is dominated by its resonant part, the apparent threshold is not directly related to the energy difference of vibrational levels. Furthermore, the maximum value of the largest peak decreases with vibrational level, with the resonant structure changing as well.

Even though most of both the experimental and theoretical data are in good agreement with each other, this is still an active subject, for example with the measurements of Ristić et al. (2007) and the calculation of Sarma et al. (2007) being quite recent. The review by Campbell et al. (2004) includes a compilation of cross sections for the first 10 levels using the swarm experiment data of Ohmori et al. (1988). Additionally, they took into account the previous compilation of Brunger and Buckman (2002) and the swarm data calculation of Robertson et al. (1997). With all the cross sections mentioned being in a reasonably good agreement, the choice of cross sections for the $v = 0 \rightarrow v = 1 - 6$ transitions is probably not very important. The cross sections measured by Ristić et al. are an appropriate choice, being both recent and in good agreement with other measurements.

There is much less data available for transitions within vibrational levels than is for vibrational excitation from the ground state, $v = 0$. Threshold reduction alone can not be utilized because of the inaccuracy of its use in vibrational excitation, as previously mentioned. Therefore experimentally or theoretically predicted cross sections must be used. To calculate the cross sections for the excitation from one vibrationally excited level v to a higher vibrationally excited level k, Mihajlov et al.

(1999) used a semi-empirical equation,

$$\sigma_{vk}(\mathcal{E}) = \frac{\mathcal{E}+\mathcal{E}_v}{\mathcal{E}} \frac{\sigma_{0v}(\mathcal{E}+\mathcal{E}_v)\sigma_{0k}(\mathcal{E}+\mathcal{E}_v)}{\sigma_{00}(\mathcal{E}+\mathcal{E}_v)} \tag{3.9}$$

where $\mathcal{E}_v$ is the energy of vibrational level v with respect to the ground state. The cross section calculation for any given transition $v = j \rightarrow k$ needs three cross sections; the elastic scattering cross section, the cross sections for the transition $v = 0 \rightarrow j$ and the cross section for the transition $v = 0 \rightarrow k$. Their calculated cross sections therefore strongly depend on the quality of those three cross sections obtained from other literature data. For ground state vibrational excitations they used the cross sections given by Phelps (2008) that are based on the previously mentioned measurement of Schulz (1964). In their survey, Campbell et al. (2004) recommended using the cross sections calculated by Dubé and Herzenberg (1979) for the $v = 1 - 5 \rightarrow v = 2 - 6$ transitions, as the corresponding data of Chen (1964) was not in as good agreement with the data for the ground state excitation. Campbell et al. indicated that no other data were available for these excitations within higher states, not mentioning the work of Mihajlov et al. (1999).

By comparing the various transitions given by Mihajlov et al. (1999) and Dubé and Herzenberg (1979) we see how the cross sections of Dubé and Herzenberg are more consistent with each other. We feel that the inconsistency observed in the cross sections by Mihajlov et al. is an error, rather than a physical property of vibrational excitations. The error might simply be because of the relatively poor vibrational excitation cross sections used in the calculation by Mihajlov et al. (1999), and thus it would be interesting to see the calculation repeated using, for example, the vibrational excitation cross sections of Ristić et al. (2007). Unsure of which of the sets for vibrational level transition cross sections would be correct we tried running the model with both. When using the cross sections of Mihajlov

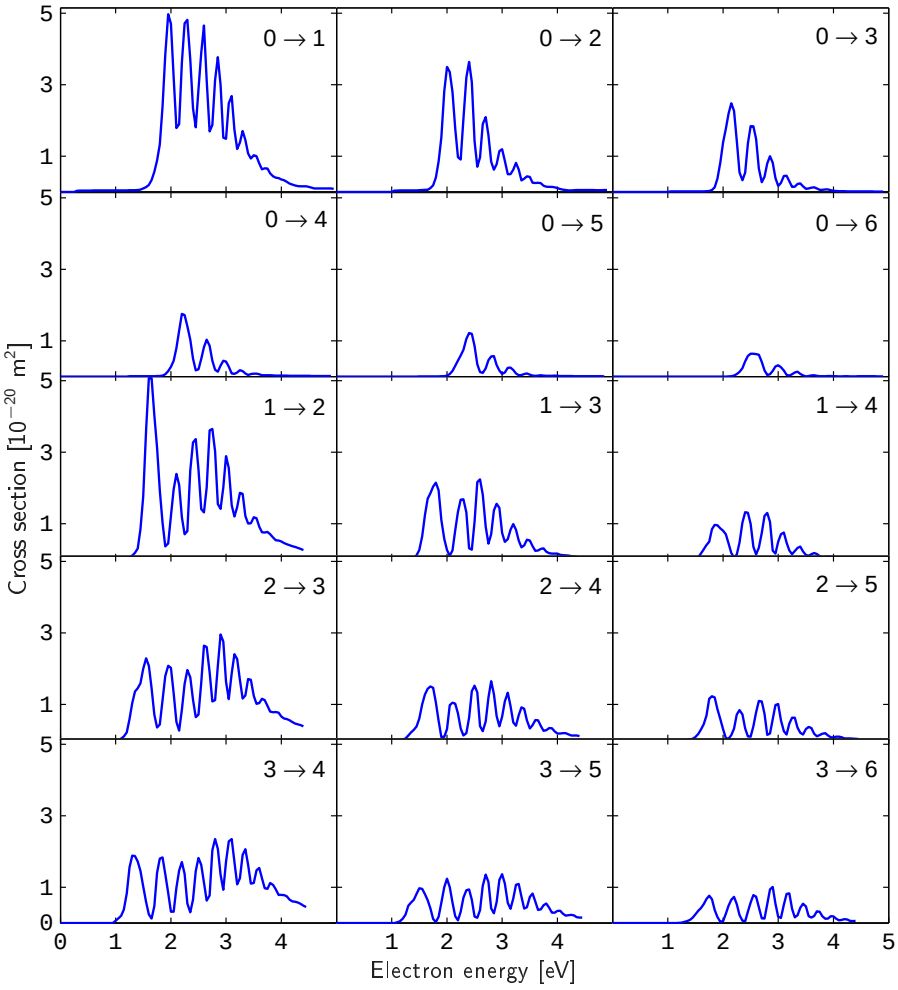

Figure 3.8: Cross sections for electron impact vibrational excitation of $N_2(X^1\Sigma_g^+, v)$ versus electron energy. The vibrational transition is indicated by the label on each graph. The cross sections for excitations from the ground state were calculated by Ristić et al. (2007) while the cross sections for the excitations from the vibrationally excited states were calculated by Dubé and Herzenberg (1979).

et al. (1999), the population within vibrational levels was inconsistent, with a non-uniform density decrease or increase with vibrational level. This is not likely to be physically accurate, as indicated by the various vibrational population distributions that have been calculated or measured (Capitelli et al., 2007; Ono and Teii, 1983;

Nagpal and Ghosh, 1990; Biloiu et al., 2007a; White and Ross, 1976; Darracht et al., 1993). When using the cross sections of Dubé and Herzenberg (1979) the density profile of vibrational levels was much more believable, uniformly decreasing with vibrational level. Furthermore, this test showed that the overall result depends very strongly on this choice, as densities of vibrational levels were much higher with the former set, which in turn generally increases the density of atoms. Although it may be necessary to use the semi-empirical formula, equation (3.9), on our choice of cross sections for vibrational excitation of $v = 0$, those measured by Ristić et al. (2007), we will simply use the cross sections for transitions within vibrational levels calculated by Dubé and Herzenberg (1979). The cross sections for both vibrational excitation from ground state and other vibrational states can be seen on figure 3.8.

The remaining vibrational excitation cross sections, the ones Dubé and Herzenberg (1979) did not calculate, need to be approximated somehow or else the population in the affected vibrational levels may be underestimated. By analyzing the pattern in the change of maximum value of the cross sections between vibrational level transitions, we fitted an exponential function, $A\exp(-B\zeta)+C$, in an attempt to extrapolate a value for the missing transitions. Our approximation of these cross sections will therefore be found by using both threshold reduction and decreasing the absolute value of the cross section in accordance to this extrapolation. The process for the scaling extrapolation is demonstrated in figure 3.9.

The electron impact vibrational relaxation of nitrogen molecules is just as important as the corresponding excitation processes. If it is not fully included in the reaction set, the population in the vibrational levels will be overestimated. Dubé and Herzenberg (1979) calculated some of these cross sections, either with the same method as for the vibrational excitation cross sections or by simply applying the

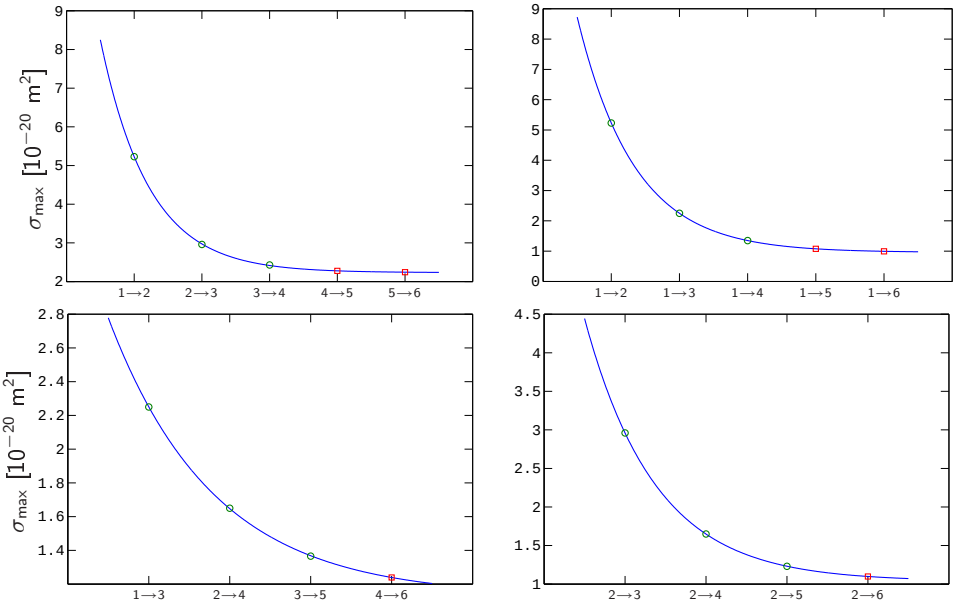

Figure 3.9: The procedure used to approximate the cross section scaling of missing vibrational transitions. The circles ○ are the maximum values of the cross sections for the transitions given by Dubé and Herzenberg (1979). The solid line is the exponential function fitted to a particular pattern of those points, giving the scaling of the missing values, displayed as squares □.

principle of detailed balancing on the direct cross sections, shown in figure 3.8. In any case, the given cross sections were said to conform to the principle of detailed balancing. Since Dubé and Herzenberg (1979) did not calculate all the vibrational relaxation cross sections, not giving a complete inverse set of the given excitation cross sections, we opt to simply apply the principle of detailed balancing, equation (2.40), on all the vibrational excitation cross sections to obtain the corresponding vibrational relaxation cross sections. The agreement of the result with the relaxation cross section given by Dubé and Herzenberg (1979) was excellent, with the cross sections being practically identical.

Electron energy loss

Consistent with the discussion above, we will use the cross sections given by Ristić et al. (2007) for the excitation of the ground state nitrogen molecule $N_2(X^1\Sigma_g^+, v = 0)$ to the first 6 vibrational levels, $v = 0 \rightarrow 1, 2, 3, 4, 5, 6$. Cross sections for excitations of the ground state molecules to vibrational levels as high as $v = 17$ are available (Allan, 1985; Huo et al., 1987). As can be seen in figure 3.8 for $v = 0 \rightarrow 1, 2, 3, 4, 5, 6$, the magnitude of the vibrational cross sections decreases quite rapidly with vibrational level, as well as the threshold shifts to higher energy. The evolution is the same with higher transitions, and therefore it will be sufficient to include only the transitions from the ground state to the first six levels in the calculation of the collisional energy loss, $\mathcal{E}_c$. Furthermore, we will use the widely accepted values given in the review by Lofthus and Krupenie (1977) for the energy of which each vibrational level is above the absolute ground state, $N_2(X^1\Sigma_g^+, v = 0)$.

3.3.3 Electron impact excitation of the nitrogen atom

Since we only take into account the first two metastable levels of nitrogen atoms, the electron impact excitation of the nitrogen atom consists of three reactions, on one hand the excitation of the ground state nitrogen atom,

$$\mathrm{e} + \mathrm{N}(^4\mathrm{S}) \longrightarrow \mathrm{N}(^2\mathrm{D}) + \mathrm{e} \tag{3.10}$$

$$\longrightarrow \mathrm{N}(^2\mathrm{P}) + \mathrm{e} \tag{3.11}$$

and on the other hand the excitation of the first metastable atom,

$$\mathrm{e} + \mathrm{N}(^2\mathrm{D}) \longrightarrow \mathrm{N}(^2\mathrm{P}) + \mathrm{e} \tag{3.12}$$

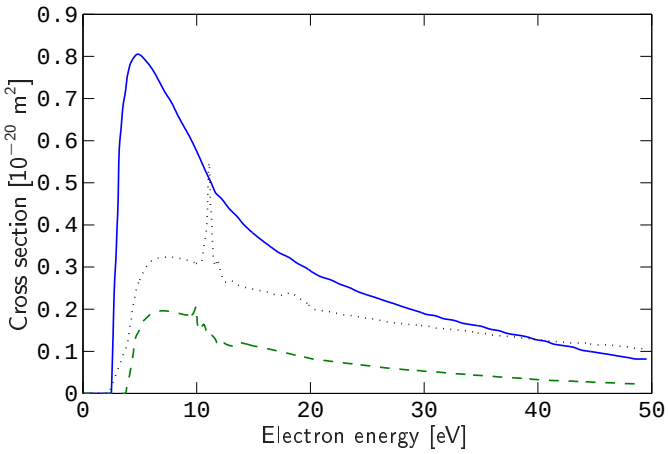

Figure 3.10: The cross sections for the electron impact excitation of the nitrogen atom calculated by Tayal and Zatsarinny (2005). Solid line: ^{4}S→^{2}D, reaction (3.10). Dashed line: ^{4}S→^{2}P, reaction (3.11). Dotted line: ^{2}D→^{2}P, reaction (3.12).

Kato (1994) reviewed the available electron impact excitation data for nitrogen (Smith et al., 1967; Henry et al., 1969; Ormonde et al., 1973; Thomas and Nesbet, 1975; Berrington et al., 1975) and recommended the best cross sections for the various excitations. No experimental data was available at the time and all the cross sections for reactions (3.10), (3.11) and (3.12) were all theoretical predictions. Although all the available data was in a rather good agreement, Kato regarded the calculations of Berrington et al. (1975) to be the most reliable cross sections available.

Ramsbottom and Bell (1994) calculated the cross sections for reactions (3.10), (3.11) and (3.12), with results very similar to the calculation of Berrington et al. (1975). Yang and Doering (1996) measured the cross section for reaction (3.10) with the result being in a good agreement with the results of Berrington et al..

Tayal and Zatsarinny have done a more sophisticated calculation of this electron impact excitation by including more states than the previous calculations (Tayal and Beatty, 1999; Tayal, 2000; Tayal and Zatsarinny, 2005). The most ad-

vanced calculation (Tayal and Zatsarinny, 2005) includes 39 states, compared to the 8 states included in the calculations of Berrington et al. (1975), for example. The differences of the two are however quite minor, but for reaction (3.10) the cross section of Tayal and Zatsarinny (2005) is closer to the measurements of Yang and Doering (1996). Because of the good agreement with all the aforementioned data, we will use the cross sections calculated by Tayal and Zatsarinny (2005) for reactions (3.10), (3.11) and (3.12). The cross sections are shown in figure 3.10.

Electron energy loss

As well as calculating the cross section for the two lowest lying metastable atoms, $N(^2D)$ and $N(^2P)$, Tayal and Zatsarinny (2005) calculated the cross sections for the higher lying levels $3s^4P$, $2s2p^{4\,4}P$, $4s^4P$ and $3d^4P$. As revealed in the review by Kato (1994), other cross section determinations for the higher lying levels exist, but are mostly for the same levels as Tayal and Zatsarinny (2005) calculated for. Frost et al. (1998) studied the various transitions in atomic nitrogen both theoretically and experimentally. Although the metastable levels were not considered, rate coefficients for five transitions from the ground state to the higher lying levels were given, including for two transitions not given by Tayal and Zatsarinny (2005). For the three transitions given in both studies, the rate coefficients given by Frost et al. (1998) are similar to the corresponding Maxwellian rate coefficients derived from the cross sections given by Tayal and Zatsarinny (2005). However, since only the Maxwellian averaged rate coefficients are given, and no cross sections, the data is of limited use to us. For the electron energy loss, we will therefore solely rely on the cross sections calculated by Tayal and Zatsarinny (2005). The cross sections for the higher level excitations are shown in figure 3.11. Furthermore, we will use data from the NIST database (Ralchenko et al., 2008) for the energy levels of the

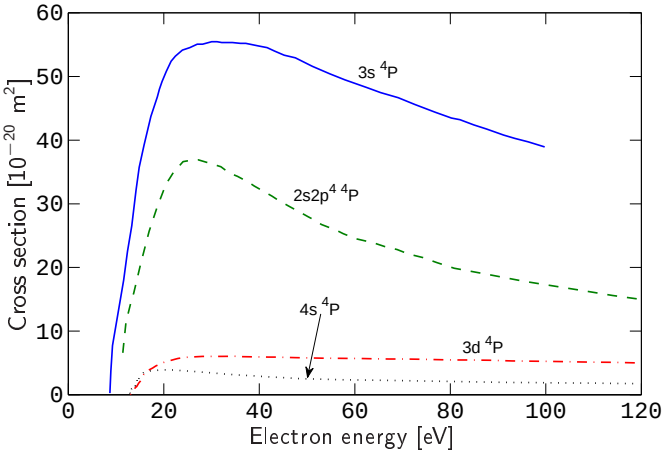

Figure 3.11: The cross sections for the excitation to the $3s^4P$, $2s2p^4\,^4P$, $4s^4P$ and $3d^4P$ levels of the nitrogen atom versus electron energy as calculated by Tayal and Zatsarinny (2005).

excited atomic species, both for the metastable atoms and the higher lying excited levels.

3.4 Collisions of electrons with ions

Collision of an electron and an ion can lead to the recombination of the electron with the ion. However, since momentum transfer prevents two bodies from merging directly, the product is likely to dissociate. The recombination of an electron and an atomic ion is only possible by optical emission, believed to be a much slower reaction than the electron simply detaching again, and therefore not important in low-pressure discharges (Lieberman and Lichtenberg, 2005, p. 295). We will therefore only consider electron collisions with the nitrogen molecular ions N_2^+, N_3^+ and N_4^+.

3.4.1 Dissociative recombination of the N_2^+ ion

Dissociative recombination of N_2^+ occurs when an electron collides with a molecular positive ion, combines with it, resulting with the neutral molecule subsequently dissociating,

$$e + N_2^+ \longrightarrow N(^2D) + N(^2D) \tag{3.13}$$

$$\longrightarrow N(^4S) + N(^2D) \tag{3.14}$$

$$\longrightarrow N(^4S) + N(^2P) \tag{3.15}$$

$$\longrightarrow N(^4S) + N(^4S) \tag{3.16}$$

The dissociative recombination has been of considerable interest among researchers. Many studies have taken place that either measure or theoretically predict the absolute rate coefficient or cross section. However, with the process having no threshold almost all rate coefficients (or cross sections) are only given for the electron temperature below 1 V. This is a problem for our application as the model is only valid in the regime $1 < T_e < 10$ V. Although an electron impact cross section does not necessarily need to be given over this entire electron energy range, it is important that it is at least valid somewhere on the interval, or the tail and even the main part of the electron energy distribution function will be disregarded, resulting in an invalid rate coefficient for electron temperature larger than 1 V. This is the case for each and every theoretical (Guberman, 1991) and experimental (Peterson et al., 1998; Zipf, 1980; Mehr and Biondi, 1969; Cunningham and Hobson, 1972; Noren et al., 1989; Sheehan and St.-Maurice, 2004; Mul and McGowan, 1979; Canosa et al., 1991; Kasner, 1967; Geoghegan et al., 1991) data for dissociative recombination of N_2^+ that we have explored.

Peterson et al. (1998) used a storage ring to measure the absolute rate coefficient

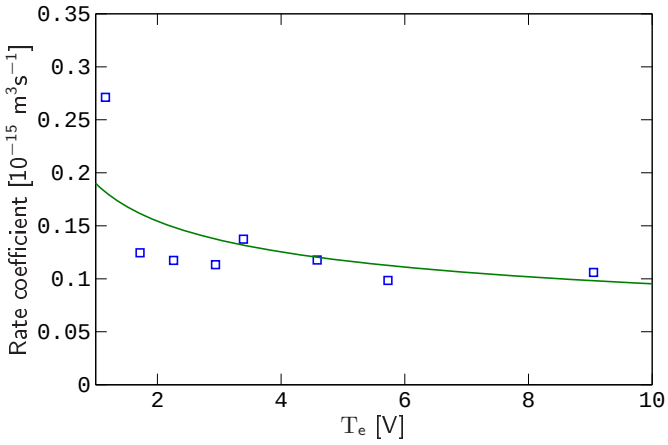

Figure 3.12: The overall rate coefficient for dissociative recombination of N_2^+ as a function of the electron temperature. The squares □ are the portion of the rate coefficients measured by Peterson et al. (1998) that are in the electron temperature range $1 - 10$ V. The solid line is a fit to the measured data points to give $1.9 \times 10^{-14} T_e{}^{-0.3}$.

as a function of electron energy in the range 1 meV to 10 eV for the dissociative recombination of ground state N_2^+. A deconvolution procedure, described by Mowat et al. (1995), was then used to acquire a cross section in the electron energy range 1 meV to 1 eV. This procedure, likely being the inverse process of obtaining a rate coefficient from a cross section with equation (2.17), required the assumption of a specific electron energy distribution function, in this case the Maxwellian distribution. Thus, we conclude that the absolute rate coefficient measured by Peterson et al. (1998) can be used directly in the model, without any assumption of the EEDF. The rate coefficient is shown in figure 3.12 along with the fit used in the model to give $1.9 \times 10^{-14} T_e{}^{-0.3}$ m^3/s.

The branching ratio for the dissociative recombination of a wide range of ions was reviewed by Florescu-Mitchell and Mitchell (2006). Branching of the total rate coefficient for the dissociative recombination of N_2^+ has been measured by Kella et al. (1996), resulting in the ratios 0.46:0.46:0.08:0 for reactions (3.13):(3.14):(3.15):

(3.16), respectively. Oddone et al. (1997) had similar results, although with the peculiar ratios 0.53:0.53:0.12:0 for the same reactions. Peterson et al. (1998) measured the branching ratios along with the aforementioned rate coefficient; 0.47:0.34:0.19:0. All authors agree that reaction (3.16) is negligible. For the sake of consistency, and with all authors being in a relatively good agreement, we will use both the branching ratio and rate coefficient measured by Peterson et al. (1998) for reactions (3.13) to (3.16).

3.4.2 Dissociative excitation and ionization of the N_2^+ ion

If the electron does not succeed in combining with the ion in an electron-ion collision, there are still several possibilities for a reaction to proceed. The ion could simply be excited from the ground state, later releasing the energy by spontaneous emission. It could also be ionized further (single ionization; the formation of N_2^{2+}) or it could dissociate. Since no excited ions or multiple-ionized ions are included in the current study, we will consider the electron impact dissociation of the N_2^+ ion. The dissociation is normally followed by either an excitation or ionization of the resulting nitrogen atom,

$$\begin{aligned} e + N_2^+ &\longrightarrow N^+ + N(^2D) + e \qquad (3.17) \\ &\longrightarrow N^+ + N^+ + 2e \qquad (3.18) \end{aligned}$$

which are referred to as dissociative excitation and dissociative ionization, respectively.

Van Zyl and Dunn (1967) measured the total cross section for production of N^+ and N_2^{2+}, the sum of single ionization and reactions (3.17) and (3.18). Noren et al. (1989) measured the cross section near threshold (7 – 12 eV), but their

data was very scattered, not exhibiting any clear trend. Peterson et al. (1998) measured the dissociative excitation cross section, reaction (3.17), but only with a purpose of probing the internal states of the ions, before ultimately doing the primary measurement of the dissociative recombination (see section 3.4.1). With an estimated error of $\pm 20\%$, this measurement is not very accurate, although it has a magnitude similar to some of the data points of Noren et al. (1989). By subtracting the dissociative excitation cross section from the total cross section of Van Zyl and Dunn, Peterson et al. also extracted an approximation to the dissociative ionization cross section. But since the dissociative excitation cross section was only measured for energies up to 50 eV, only $3 - 4$ eV above the dissociative ionization threshold, the result is probably mostly invalid.

Kim et al. (2000) calculated the cross section for the total ionization of N_2^+, that is the sum of single ionization and dissociative ionization, reaction (3.18). The cross section calculation performed by Deutsch et al. (2002) is furthermore consistent with the calculation of Kim et al..

Bahati et al. (2001) measured the individual cross sections for the dissociative excitation and the dissociative ionization, as well as for single ionization. The dissociative ionization cross section is the only credible cross section we could find, aside from the one approximated by Peterson et al. (1998), making it hard to compare to anything. A comparison of the dissociative excitation cross section with that of Peterson et al. (1998) shows a significant discrepancy, or of about a factor of 3. Bahati et al. were aware of this discrepancy and tried to explain it with various tests, but with no success. The total dissociation cross section, the sum of the single ionization and dissociative ionization cross sections, is also in a poor agreement with the results of Kim et al. (2000) and Deutsch et al. (2002), although only of a factor of about 1.5. It is thus obvious that an appropriate choice

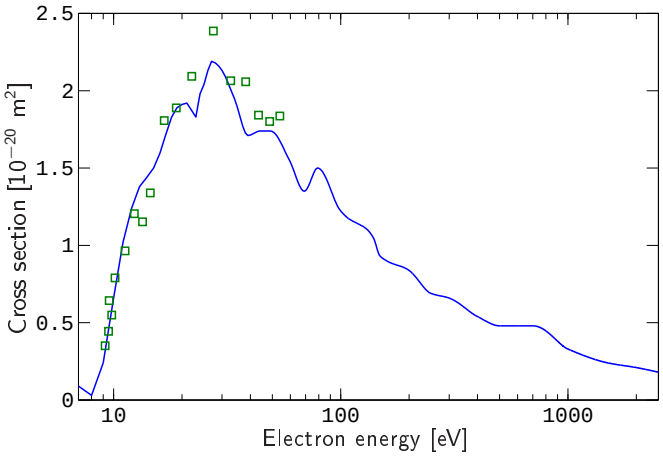

Figure 3.13: The cross section for the dissociative excitation of N_2^+, reaction (3.17), versus electron energy. The solid line is the cross section of Bahati et al. (2001) scaled up by a factor of 3. The squares □ are the cross section measurement points of Peterson et al. (1998).

of cross section for reactions (3.17) and (3.18) is not straightforward. In view of the product separation technique used by Bahati et al. (2001), of the three measured cross sections the single ionization cross section is the most likely to be correct. This is further supported with the single ionization cross section being assigned the least estimated error. With that in mind, a comparison with the total ionization calculations of Kim et al. (2000) and Deutsch et al. (2002) can give us an indication of how far off the dissociative ionization cross section is. In that way, we found that the discrepancy is near identical to the dissociative excitation discrepancy with Peterson et al. (1998), or about a factor of 3 too small. Rather than using the cross sections measured by Bahati for reactions (3.17) and (3.18) unmodified, it is probably a better choice to first scale them up by a factor of 3. This way, we get a very good agreement with the measurement of Peterson et al. for reaction (3.17) but with the cross section extending to much higher electron energy, as seen in figure 3.13. Additionally, we get a good agreement with the total ionization

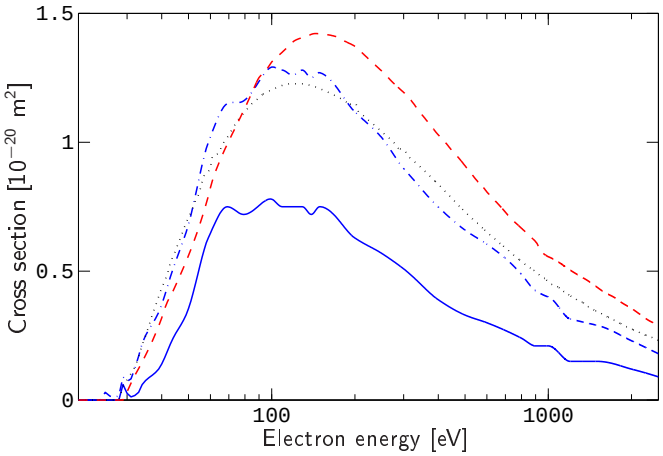

Figure 3.14: The cross section for the dissociative ionization of N_2^+, reaction (3.18), versus electron energy. The solid line is the cross section of Bahati et al. (2001), scaled upwards by a factor of 3. For comparison to calculations, the dash-dot line is the sum of the single ionization cross section of Bahati et al. and the solid line. The dotted line is the corresponding cross section of Kim et al. (2000) and the dashed line is the calculation of Deutsch et al. (2002).

calculations of Kim et al. (2000) and Deutsch et al. (2002), as seen on figure 3.14, assuming the single ionization cross section of Bahati et al. is accurate. There is still a possibility that all the cross section measurements of Bahati et al. are accurate with the other measurements and calculations being in error, although this is statistically the less likely scenario. Therefore, we will use the solid line cross sections in figures 3.13 and 3.14 in the model for the dissociative excitation and dissociative ionization of N_2^+, respectively. Those reactions are not expected to contribute a lot to our overall calculation result anyway, but this choice of cross sections should provide an upper limit of their contribution. If the reactions prove to be important, using the original values from Bahati et al. instead could give an indication of the quality of their unmodified cross sections, as well as demonstrating how sensitive the overall result is to those reactions.

The product atom in reaction (3.17) is assumed to be $N(^2D)$. None of the

experiments mentioned above specify the state of the atom, but since the atom is probably the N(^{2}D) metastable atom we will simply assume that other atoms are not formed in this reaction. How inaccurate this may be should not be important since this reaction should be negligible in the production of nitrogen atoms. However, the reaction might be an important channel for the production of atomic nitrogen ions, and can thus not be excluded either.

3.4.3 Dissociative recombination of N_3^+

The dissociative recombination of N_3^+ can follow two paths, one creating a molecule, the other only atoms,

$$e + N_3^+ \longrightarrow N + N_2 \tag{3.19}$$

$$\longrightarrow N + N + N \tag{3.20}$$

As with dissociative recombination of N_2^+ a measured cross section in the energy range of interest could not be found. We are therefore forced to use energy dependent rate coefficients that we assume to be valid in our range. Recently, Zhaunerchyk et al. (2007) measured the cross section and branching ratios of the reaction above, using the same or similar equipment as Peterson et al. (1998) used for his measurements of dissociative recombination of N_2^+. A rate coefficient of 6.47×10^{-13} m^3/s was only obtained for electron temperature of 25 meV, which is of limited use to us. Instead we will use the temperature dependent value recommended by Kossyi et al. (1992), $3.22 \times 10^{-14} T_e{}^{-1/2}$ m^3/s, having a room temperature value of 2×10^{-13} m^3/s for comparison.

As for the branching ratio, Zhaunerchyk et al. found that the reaction has a strong tendency towards the creation of N + N_2, or over 90%. Therefore the

latter reaction above, (3.20), will not be considered at all. As with the dissociative recombination of N_2^+, we will assume that at least one of the products is in an excited state. Therefore, reaction (3.19) follows two channels, $N_2(A^3\Sigma_u^+)$ + $N(^4S)$ and $N_2(X^1\Sigma_g^+, v = 0)$ + $N(^2P)$. Rather arbitrarily, we will also assume that these channels have a 0.5:0.5 branching ratio.

3.4.4 Dissociative recombination of N_4^+

For the dissociation of N_4^+ we will only consider the reaction

$$e + N_4^+ \longrightarrow N_2 + N_2 \tag{3.21}$$

The rate coefficient for the dissociative recombination of N_4^+ has been measured or recommended by several authors (Kossyi et al., 1992; Fitaire et al., 1984; Whitaker et al., 1981; Cao and Johnsen, 1991). The results were in excellent agreement with each other, with the exception of Cao and Johnsen (1991) who found about one order of magnitude larger rate coefficient. However, the electron energy associated with these rate coefficients is far below our range of interest. As we did with the dissociative recombination of N_3^+, we will use the rate coefficient recommended by Kossyi et al. (1992), $3.2\times10^{-13}{T_e}^{-1/2}$ m^3/s, assuming the temperature dependence holds in the interval $1 < T_e < 10$ V. Furthermore, we will assume that one of the molecules formed is in an excited state, as is generally the case for dissociative recombination and has been suggested for reaction (3.21) (Cao and Johnsen, 1991), such that the metastable nitrogen molecule $N_2(A^3\Sigma_u^+)$ is always produced along with the ground state nitrogen molecule $N_2(X^1\Sigma_g^+, v = 0)$ in reaction (3.21).

3.5 Reactions of gaseous species

Reactions involving no electrons are independent of the electron temperature, but depend on the gas temperature; the temperature of the colliding gaseous species. The rate coefficients are therefore independent of the electron energy distribution function, and a rate coefficient describing the behavior with gas temperature is sufficient instead of a cross section. The most extensive collection of rate coefficients between gaseous species are those by Kossyi et al. (1992), Herron (1999) and Schofield (1973, 1979).

3.5.1 Charge transfer

Since the ionization energy of the nitrogen atom is about 1.1 eV less than that of the molecule, the reaction

$$N_2^+ + N \longrightarrow N_2 + N^+ \tag{3.22}$$

has no threshold and may have a large rate coefficient. We will use the rate coefficient given in the review by Kossyi et al. (1992), $7.2 \times 10^{-19}(300/T_g)^{-1}$ m^3/s. This is about a factor of 10 smaller than the maximum value given by Albritton (1978). Furthermore, we will assume the rate coefficient is independent of the state of the neutral reactant atom, applying to collisions with both ground state and metastable nitrogen atoms. We will also assume that the produced nitrogen molecule is in a state roughly 1.1 eV above the energy of the reactant atom, the charge transfer being near resonant.

The inverse reaction,

$$N^+ + N_2 \longrightarrow N + N_2^+ \tag{3.23}$$

has an energy threshold of approximately 1.1 eV, thus having a small rate coefficient. However, when the reactant nitrogen molecule is in an excited state more than 1.1 eV above the ground state, the reaction has no threshold and the rate coefficient may be large. For collisions with nitrogen molecules in vibrational levels above $v = 3$ and in the metastable state, $A^3\Sigma_u^+$, we will use the rate coefficient used by Tao et al. (2002), 2×10^{-17} m^3/s. The rate coefficient decreases exponentially with energy threshold, being very small for a $v = 3$ reactant and negligible for reactants in lower vibrationally excited states. Therefore, for a charge transfer with a $v = 3$ reactant we will multiply the rate coefficient with the exponential factor $\exp(-2829/T_g)$, but disregard any charge transfers with reactants in the lower vibrational levels $v = 0 - 2$. Furthermore, we will assume that the produced nitrogen atom is in a state having 1.1 eV less energy than the reactant molecule, the charge transfer being near resonant.

3.5.2 Quenching by the nitrogen molecule

Vibrational excitation

The vibration – translation energy exchange, i.e. the quenching of vibrationally excited ground state molecules $N_2(X^1\Sigma_g^+, v > 0)$ by a collision with other ground state nitrogen molecules,

$$N_2(X^1\Sigma_g^+, v = j) + N_2(X^1\Sigma_g^+, v) \longrightarrow N_2(X^1\Sigma_g^+, v = j - 1) + N_2(X^1\Sigma_g^+, v) \tag{3.24}$$

has a small rate coefficient for relatively small values of j, whereas it has a large coefficient for quenching of vibrational levels much exceeding $v = 6$. Billing and Fisher (1979) calculated the rate coefficient at various temperatures, yielding values

in the range $0.4 - 22 \times 10^{-25}$ m^3/s for a 500 K temperature, increasing with vibrational level j. These rate coefficients are commonly used in kinetic modeling of nitrogen discharges (Guerra and Loureiro, 1997, 1995; Guerra et al., 2004) and have been shown to be in excellent agreement with more recent and presumably more accurate calculations (Cacciatore et al., 2005; Adamovich et al., 1998; Adamovich, 2001). We will therefore use the values calculated by Billing and Fisher (1979) for temperatures in the range 400 – 700 K, after fitting them to the usual power law dependence with the gas temperature.

The calculations by Adamovich (2001) indicate that quenching of vibrational energy by two or more levels has a rate coefficient at least $6-7$ orders of magnitude smaller than for the single level quenching of reaction (3.24). We will therefore assume that quenching by multiple vibrational levels is negligible, and will only include the single vibrational level quenching of reaction (3.24).

The quenching of vibrational excitation of the ground state nitrogen molecule by a collision with the metastable molecule $N_2(A^3\Sigma_u^+)$ can occur by the intermediate reaction

$$N_2(A^3\Sigma_u^+) + N_2(X^1\Sigma_g^+, v \geq 5) \longrightarrow N_2(B^3\Pi_g) + N_2(X^1\Sigma_g^+, v = 0) \qquad (3.25)$$

Since the energy of the fifth vibrational level is larger than the energy level difference of $N_2(A^3\Sigma_u^+)$ and $N_2(B^3\Pi_g)$, the above reaction is exothermic and can have a large rate coefficient. The reaction was studied by Piper (1989a) who found a rate coefficient of 3×10^{-17} m^3/s. Since the $B^3\Pi_g$ level is not metastable and has a lifetime of only several microseconds (Piper et al., 1989), it radiates quickly back to the metastable state $A^3\Sigma_u^+$. We will therefore assume that effectively, quenching of vibrational excitation of the ground state nitrogen molecule by a collision with

the metastable $N_2(A^3\Sigma_u^+)$ proceeds by the reaction

$$N_2(A^3\Sigma_u^+) + N_2(X^1\Sigma_g^+, v \geq 5) \longrightarrow N_2(A^3\Sigma_u^+) + N_2(X^1\Sigma_g^+, v = 0) \tag{3.26}$$

that we will assume to have the same rate coefficient as reaction (3.25), 3×10^{-17} m^3/s. When the ground state reactant molecule is in a vibrational level below $v = 5$ the reaction is endothermic, and the rate coefficient decreases exponentially with the threshold energy, i.e. $\exp(-T_a/T_g)$ where $T_a = eE_a/k$. We will therefore assume an exponential temperature factor of $T_a = 533$ K and $T_a = 3757$ K when the ground state nitrogen molecule is in vibrational levels $v = 4$ and $v = 3$, respectively, whereas the rate coefficients for reactants in lower vibrational levels are assumed to be negligible.

Electronic excitation

The quenching of the metastable nitrogen molecule $N_2(A^3\Sigma_u^+)$ by the nitrogen molecule,

$$N_2(A^3\Sigma_u^+) + N_2 \longrightarrow N_2(X^1\Sigma_g^+, v = 0) + N_2 \tag{3.27}$$

is relatively well documented, but the discrepancy between some of the available data (Clark and Setser, 1980; Kossyi et al., 1992; Herron, 1999), as much as by a factor of 200, makes the choice for the rate coefficient difficult. Piper (1989a) even found a rate coefficient $4 - 6$ orders of magnitude larger, 3.7×10^{-18} m^3/s, only further emphasizing the uncertainty of even the order of magnitude of this rate coefficient. Given the wast disagreement with the other measurements, we will assume that the large value given by Piper (1989a) is not accurate. Instead, we will use the value recommended by both Kossyi et al. (1992) and Herron (1999),

3×10^{-24} m^3/s, given as an upper limit at a gas temperature of 300 K. Furthermore, we will assume that the rate coefficient applies to collisions with ground state nitrogen molecules in any vibrational state. However, given that the pooling of the metastable nitrogen molecule $N_2(A^3\Sigma_u^+)$,

$$N_2(A^3\Sigma_u^+) + N_2(A^3\Sigma_u^+) \longrightarrow N_2 + N_2(B, C, C')\,, \tag{3.28}$$

has a rate coefficient roughly 8 orders of magnitude larger (Kossyi et al., 1992; Hays and Oskam, 1973; Clark and Setser, 1980), we believe the small quenching rate coefficient mentioned above does not apply to the self quenching of $N_2(A^3\Sigma_u^+)$. The excited levels resulting from the pooling, $N_2(B^3\Pi_g)$, $N_2(C^3\Pi_u)$ and $N_2(C'^3\Pi_u)$, are not metastable and radiate back to $N_2(A^3\Sigma_u^+)$ with a lifetime ranging from a few hundredths of a microsecond to a few microseconds (Piper et al., 1989; Dilecce et al., 2007). The metastable nitrogen molecule $N_2(A^3\Sigma_u^+)$ has on the other hand a radiative lifetime on the order of a few seconds (Piper, 1993). We therefore assume that the reaction

$$N_2(A^3\Sigma_u^+) + N_2(A^3\Sigma_u^+) \longrightarrow N_2(A^3\Sigma_u^+) + N_2(X^1\Sigma_g^+, v = 0) \tag{3.29}$$

effectively has the same rate coefficient as the pooling of $N_2(A^3\Sigma_u^+)$. We will use the mean value of the overall rate coefficient suggested by Herron (1999), taken from the measurement of Piper (1988), 3.5×10^{-16} m^3/s.

The rate coefficient for the quenching of the metastable atom $N(^2D)$ by the nitrogen molecule,

$$N(^2D) + N_2 \longrightarrow N(^4S) + N_2 \tag{3.30}$$

was measured by Sugawara et al. (1980) to be 1.3×10^{-20} m^3/s. This value is quite close to the rate coefficient suggested by other studies (Herron, 1999; Kossyi et al., 1992; Schofield, 1979) and we will therefore use this value. Furthermore, we will assume the rate coefficient applies to impacts with both ground state and excited nitrogen molecules.

The quenching of the metastable atom N(^{2}P) by the nitrogen molecule,

$$\mathrm{N}(^2\mathrm{P}) + \mathrm{N}_2 \longrightarrow \mathrm{N}(^4\mathrm{S}) + \mathrm{N}_2 \tag{3.31}$$

$$\longrightarrow \mathrm{N}(^2\mathrm{D}) + \mathrm{N}_2 \tag{3.32}$$

was also studied by Sugawara et al. (1980). They obtained a rate coefficient of 3.3×10^{-23} m^3/s for the production of N(^{4}S), but found no indication of any N(^{2}D) production. This rate coefficient is roughly 10 times larger than values suggested in other studies (Schofield, 1979; Gordiets et al., 1995; Kossyi and Silakov, 2005), but is the basis in the recommendation of Herron (1999). We will therefore use the rate coefficient of Sugawara et al. (1980). Furthermore, we will assume that the metastable nitrogen atom N(^{2}P) is only quenched to the ground state, N(^{4}S), by impact with nitrogen molecules, and that the rate coefficient is independent of the state of the quencher molecule.

3.5.3 Quenching by the nitrogen atom

The quenching of vibrational energy of the ground state nitrogen molecule by a collision with the neutral nitrogen atom is generally negligible for low vibrational levels. Guerra et al. (2004) disregarded the effect altogether for vibrational levels below $v = 7$, assuming the rate coefficient vanishes for such low vibrational levels. This approximation is justifiable since the rate coefficient is very small, on the

order of 10^{-27} m^3/s, for nitrogen molecules in low vibrational levels (Esposito and Capitelli, 2006; Esposito et al., 2006). We will therefore follow suit and assume that the rate coefficients are negligible, not including any quenching of vibrational energy by collisions with atoms for the relatively low vibrational levels considered in the current study.

The rate coefficient for the quenching of the metastable nitrogen atom $N(^2P)$ by other nitrogen atoms,

$$N(^2P) + N \longrightarrow N(^4S) + N \tag{3.33}$$

$$\longrightarrow N(^2D) + N \tag{3.34}$$

has been measured only by Young and Dunn (1975), reporting a value of 6.2×10^{-19} m^3/s. Because of the complexity of the measurement, the rate coefficient was not expected to be accurate to more than 20 %. Although other authors recommend larger values (Schofield, 1979; Gordiets et al., 1995; Kossyi et al., 1992), Herron (1999) suggested using the value measured by Young and Dunn (1975). Thus, we will use the above rate coefficient as well as assuming that the product atom is always the ground state nitrogen atom, as was suggested by Herron (1999). Furthermore, we will assume that this rate coefficient is independent of the state of the quencher atom.

The rate coefficient for the quenching of the metastable nitrogen atom $N(^2D)$ by other neutral nitrogen atoms was included in none of the collections of nitrogen reaction rate coefficients (Schofield, 1979; Guerra et al., 2004; Gordiets et al., 1995; Tatarova et al., 2005; Herron, 1999; Kossyi et al., 1992), although Schofield (1979) mentioned that no measurements had been reported for the reaction. Therefore, we will simply assume that the reaction is negligible. However, given that the effective

quenching of the $N(^2D)$ by atomic oxygen can have a considerable effect on the density of $N(^2D)$ in the upper atmosphere (Piper, 1989c), this assumption is not necessarily accurate and should be taken with a grain of salt. If the quenching of the metastable atom $N(^2P)$ turns out to be important in the overall destruction mechanism of $N(^2P)$, the quenching of the $N(^2D)$ is probably important as well.

3.5.4 Transfer of excitation

Vibrational excitation

The vibration - vibration energy exchange, i.e. the near resonant transfer of vibrational excitation between two colliding ground state molecules,

$$N_2(v = j) + N_2(v = k) \longrightarrow N_2(v = j + 1) + N_2(v = k - 1) \tag{3.35}$$

is believed to be responsible for the high density of highly vibrationally excited ground state molecules, often observed in the afterglow of nitrogen discharges at higher pressure (Guerra et al., 2004). The rate coefficient is known to depend strongly on the vibrational level, as well as the gas temperature, such that it is not possible to use a single value for the general reaction given above. There exist a number of studies that have attempted to calculate or formulate the rate coefficients for various vibrational levels as a function of gas temperature (da Silva et al., 2008; Adamovich et al., 1998; Adamovich, 2001; Cacciatore et al., 2005). However, the rate coefficients calculated by Billing and Fisher (1979) are generally used as a point of reference in those studies and are commonly used in discharge modelling studies (Guerra and Loureiro, 1995; Fisher, 1997; Guerra et al., 2004). Furthermore, they have been shown to be in a quite good agreement with experimental data (Ahn et al., 2004). However, although the rate coefficients are generally given for a wide

range of j values, numeric values are never given for other values of k than 1. We will use the Schwartz, Slawsky and Herzfeld theory (Schwartz et al., 1952; Schwartz and Herzfeld, 1954; Keck and Carrier, 1965; Bray, 1968) to derive the missing rate coefficients for $k = 2 - 6$ from the rate coefficients given by Billing and Fisher (1979) for $k = 1$. Assuming that the anharmonicity of the nitrogen molecule has a negligible contribution for the relatively low values of j and k considered in this study, the transition probability is given (Bray, 1968)

$$P_{k,k-1}^{j,j+1} = Q(T)k(j+1)F(y_{k,k-1}^{j,j+1}) \tag{3.36}$$

where $y_{k,k-1}^{j,j+1} \propto |k-j-1|$. We can therefore derive the rate coefficient from another given rate coefficient with $k = 1$ and $j = j'$, that is

$$K_{k,k-1}^{j,j+1} = \frac{k(j+1)}{j'+1} K_{1,0}^{j',j'+1} \exp\left(\frac{\Delta E - \Delta E'}{2kT}\right) \qquad j' = |k-j-1| \tag{3.37}$$

where $\Delta E = E_k + E_j - E_{k-1} - E_{j+1}$ and $\Delta E' = E_1 + E_{j'} - E_0 - E_{j'+1}$ are the vibrational energy defects of the two transitions. Now, since

$$\Delta E \simeq \begin{cases} \Delta E' & j' = k-j-1 \\ -\Delta E' & j' = j+1-k \end{cases} \tag{3.38}$$

the rate coefficient is given by

$$K_{k,k-1}^{j,j+1} \simeq \begin{cases} \frac{k(j+1)}{j'+1} K_{1,0}^{j',j'+1} & j' = k-j-1 \\ \frac{k(j+1)}{j'+1} K_{1,0}^{j',j'+1} \exp\left(-\frac{\Delta E}{kT}\right) & j' = j+1-k \end{cases} \tag{3.39}$$

This is a familiar relation, since it is apparent that transitions for $j + 1 < k$ are slightly endothermic by the negative vibrational energy defect, resulting in

a smaller expected rate coefficient. The activation barrier, $T_a = e\Delta E/k$, varies from about 40 to 200 K for the vibrational levels considered in the current study. Furthermore, the relation is consistent with the expression for the rate coefficient in more accurate theories (Adamovich et al., 1998; Adamovich, 2001), as given by Ahn et al. (2004). The rate coefficients $K_{1,0}^{j',j'+1}$, used to calculate the missing transitions, are taken from Billing and Fisher (1979), after fitting them to the usual power law dependence with gas temperature in the range $300 - 1000$ K. The resulting values for the various transitions are tabulated in table A.2.

The calculations of Adamovich (2001) indicate that vibrational energy jumps of more than one level, i.e. when the reactants and products differ by two or more vibrational levels, have a rate coefficient roughly $3 - 4$ orders of magnitude smaller than for the single level jumps. Therefore, we will assume that jumps by multiple vibrational levels are negligible and will only include the vibrational energy transfer of reaction (3.35).

Electronic excitation

The transfer of electronic excitation from the neutral nitrogen molecule to the neutral nitrogen atom,

$$\mathrm{N_2}(A^3\Sigma_u^+) + \mathrm{N}(^4\mathrm{S}) \longrightarrow \mathrm{N_2}(X^1\Sigma_g^+, v = 0) + \mathrm{N}(^2\mathrm{P}) \tag{3.40}$$

$$\longrightarrow \mathrm{N_2}(X^1\Sigma_g^+, v = 0) + \mathrm{N}(^2\mathrm{D}) \tag{3.41}$$

has been discussed in several studies, all resulting in similar rate coefficients (Gordiets et al., 1995; Herron, 1999; Kossyi et al., 1992). We will use the value measured by Piper (1989b), 4×10^{-17} m^3/s. Furthermore, we will assume that the product atom is always the higher lying metastable atom $\mathrm{N}(^2\mathrm{P})$ (Meyer et al., 1970; Piper, 1989b), i.e. the latter channel in the reaction above is assumed to be negligible.

3.5.5 Dissociation of ions

The dissociation of the N_4^+ ion by the nitrogen atom,

$$N_4^+ + N \longrightarrow N^+ + N_2 + N_2 \tag{3.42}$$

has a rate coefficient of 1×10^{-17} m^3/s as recommended by Kossyi et al. (1992). We will use this rate coefficient and assume that it is independent of the state of the reactant atom and that the produced molecules will have a combined energy roughly corresponding to the energy level of the reactant atom.

An upper limit of the rate coefficient for the dissociation of the N_4^+ ion by a collision with the neutral nitrogen molecule,

$$N_4^+ + N_2 \longrightarrow N_2^+ + N_2 + N_2 \tag{3.43}$$

was given by Kossyi et al. (1992) as a function of gas temperature, yielding roughly 1×10^{-12} m^3/s at 500 K, whereas Tatarova et al. (2005) and Gordiets et al. (1995) used a rate coefficient that was roughly ten order of magnitudes smaller, or $2.1 \times 10^{-22} \exp(T_g/121)$ m^3/s. This brute discrepancy is strange, especially since both authors cite the same source for the rate coefficient. However, the recommendation by Kossyi et al. (1992) is abnormally large while the value used by Gordiets et al. is closer to what to normally expect from a gaseous reaction rate coefficient. Since the rate coefficient used by Gordiets et al. and Tatarova et al. is not of the Arrhenius form, unlike all other rate coefficients used in the model, we refitted their rate coefficient on the interval $300 < T_g < 900$ K, resulting in $8.67 \times 10^{-23}(300/T_g)^{-6.45} \exp(900/T_g)$ m^3/s. Furthermore, we will assume that the rate coefficient is independent of the state of the reactant molecule and that the additional neutral molecule product will be in the ground state.

3.5.6 Rearrangement of chemical bonds

One channel for the formation of the N_3^+ ion is the rearrangement of atoms due to the collision of an ion and a neutral nitrogen molecule,

$$N_2^+ + N_2 \longrightarrow N_3^+ + N \tag{3.44}$$

In a study of the formation of N_3^+ from excited states of the N_2^+ ion, Bowers et al. (1974) suggested a rate coefficient of 5.5×10^{-17} m^3/s, although without specifying the state of the nitrogen molecule. This is consistent with the upper limit of the rate coefficient given by Kossyi et al. (1992), 3×10^{-16} m^3/s. Jaffe et al. (1973) found a rate coefficient of about factor of 20 smaller than the rate coefficient by Bowers et al. (1974). Although this is consistent with the upper limit value given by Kossyi et al. (1992), we believe the rate coefficient is too small. Thus, we will use the rate coefficient measured by Bowers et al. (1974) for reaction (3.44). The reaction is only possible if either the ion or the molecule reactants are in an excited level since the appearance energy of N_3^+ is about $21 - 23$ eV (Bowers et al., 1974), i.e. roughly $5.4 - 7.4$ eV above the ionization energy of the N_2^+ ion. Since we do not discriminate between the states of the N_2^+ ion in our global model calculations, we will assume that the rate coefficient is only applicable when the neutral nitrogen molecule is the metastable $N_2(A^3\Sigma_u^+)$, as indicated by Kossyi et al. (1992). Furthermore, we will assume that the produced neutral atom is in the ground state.

The inverse reaction of reaction (3.44), the destruction of N_3^+ by the rearrangement of chemical bonds,

$$N_3^+ + N \longrightarrow N_2^+ + N_2 \tag{3.45}$$

should have no energy threshold in contrast to the threshold predicted for reaction

(3.44). However, this is not necessarily the case since the reaction might proceed through an intermediate step having a some energy threshold. We will use the rate coefficient suggested by Kossyi et al. (1992), 6.6×10^{-17} m^3/s, which is of similar magnitude as the rate coefficient used for reaction (3.44). Furthermore, we will assume that the reaction has no threshold, such that the rate coefficient is the same for reactant atoms in any state and that the neutral molecule produced is always the metastable nitrogen molecule $N_2(A^3\Sigma_u^+)$.

3.5.7 Three body association

Association generally can only occur through three body collisions, as momentum conservation does not allow two bodies to directly form a single body. Thus, association of two bodies is generally explained by the assistance of a third body.

Association of two neutral species

The rate coefficient for the association of two atoms by a collision with the nitrogen molecule,

$$N + N + N_2 \longrightarrow N_2 + N_2 \tag{3.46}$$

will be assigned the value $8.27 \times 10^{-46} \exp(500/T_g)$ m^6/s (Gordiets et al., 1995; Kossyi et al., 1992) which was given for the interaction of ground state particles. It is in relatively good agreement with the rate coefficient measured by Yamashita (1979), 7.2×10^{-45} m^6/s. We will assume that the rate coefficient applies to interactions of atoms and molecules in both ground and excited states. Furthermore, we will assume that the produced molecule is in an excited state according to the combined energy level of the atoms it is composed of (Kossyi et al., 1992).

The association of nitrogen atoms by a collision with other nitrogen atoms,

$$N + N + N \longrightarrow N_2 + N \tag{3.47}$$

was suggested to have a rate coefficient of 1×10^{-44} m^6/s or 1.9×10^{-45} m^6/s, depending on the state of the produced molecule (Gordiets et al., 1995). We will use the larger value, assuming it represents an upper limit of this rate coefficient. Furthermore, we will assume that the rate coefficient applies to collisions of atoms in both the ground state and in excited states, and that the product molecule is in a state according to the combined energy level of the atoms it is composed of.

Association of an ion and a neutral species

The ion-atom association

$$N^+ + N + N_2 \longrightarrow N_2^+ + N_2 \tag{3.48}$$

has the rate coefficient 1×10^{-41} m^6/s as (Kossyi et al., 1992). We will assume that the rate coefficient is the same for collisions of neutral atoms and molecules in any state.

The conversion of the N_2^+ ion to the N_4^+ ion by a collision with the nitrogen molecule,

$$N_2^+ + N_2 + N_2 \longrightarrow N_4^+ + N_2 \tag{3.49}$$

has been well studied. As well as measuring the rate coefficient, Guthrie et al. (1991) reviewed the available data, showing that the results were mostly in a good agreement. Other rate coefficients found for the same reaction are also of the same

order of magnitude (Gordiets et al., 1995; Kossyi et al., 1992; Phillips, 1990; Bates, 1989) and therefore we will use the rate coefficient measured by Guthrie et al. (1991), $5.2 \times 10^{-41}(300/T_g)^{2.2}$ m^6/s. Furthermore, we will assume that the rate coefficient applies to collisions of both ground state and excited nitrogen molecules.

Guthrie et al. (1991) also measured the rate coefficient for the conversion of the N^+ ion to the N_3^+ ion by a collision with the nitrogen molecule,

$$N^+ + N_2 + N_2 \longrightarrow N_3^+ + N_2 \tag{3.50}$$

finding a value of $1.7 \times 10^{-41}(300/T_g)^{2.1}$ m^6/s, which is in a reasonable agreement with other experimental values (Kossyi et al., 1992). We will therefore use this rate coefficient and assume it is valid for collisions of both excited and ground state molecules with the N^+ ion.

The rate coefficient for the association of the N_2^+ ion and a neutral nitrogen atom to form the N_3^+ ion, by a collision with a neutral nitrogen molecule,

$$N_2^+ + N + N_2 \longrightarrow N_3^+ + N_2 \tag{3.51}$$

is given the value $9 \times 10^{-42} \exp(400/T_g)$ m^6/s (Kossyi et al., 1992), and is assumed to apply to collisions of both ground state and excited molecules and atoms.

3.5.8 Ionization

The formation of the N_2^+ ion by the association of two atoms,

$$N + N \longrightarrow N_2^+ + e \tag{3.52}$$

can have a large rate coefficient when the sum of the excitation energy of the reactants and the dissociation energy of N_2^+ is larger than the ionization energy of the N_2 molecule. We will use the rate coefficient recommended by Kossyi et al. (1992), 1×10^{-18} m^3/s, when at least one of the reactants is the N(^{2}P) metastable atom.

The formation of the N_4^+ ion by the association of two molecules,

$$N_2 + N_2 \longrightarrow N_4^+ + e \tag{3.53}$$

can have a large rate coefficient when the nitrogen molecules have a sufficiently high combined excitation energy such that the ionization energy of N_4^+ is surpassed. Unfortunately, this energy threshold is likely higher than the combined energy of two $N_2(A^3\Sigma_u^+)$ metastable molecules. In the pressure regime $1 - 100$ mTorr, electron impact ionization is generally the dominating pathway for creation of ions. However, since the N_4^+ ion has no neutral counterpart in the current reaction set, associative ionization is probably the dominating pathway in its creation. Therefore, we can not exclude the reaction, as we would normally do, but we will instead try to use a rate coefficient that is representative of an effective rate coefficient for the creation of the ion N_4^+. Gordiets et al. (1995) gave a rate coefficient for a similar reaction, deviating from the above reaction only in one of the reactants being vibrationally excited with $v \gtrsim 30$, instead of also being an $N_2(A^3\Sigma_u^+)$. We will assume that the rate coefficient, 1×10^{-19} m^3/s, applies to the reaction above as well. Kossyi et al. (1992) suggested a value nearly two orders of magnitude larger for a similar reaction when one of the reactants is the higher lying metastable molecule $N_2(a'\,^1\Sigma_u^-)$, not considered in the current study. Thus, the assumption of reaction (3.53) is likely appropriate, with the rate coefficient probably not being much larger than would be observed effectively in an experiment.

Penning ionization, such as the reaction

$$N_2 + N_2 \longrightarrow N_2^{2+} + N_2 + e \tag{3.54}$$

is believed to be a negligible part of the overall ionization mechanism in the low pressure regime of $1 - 100$ mTorr, even though it has been found to be important in higher pressure discharges (Guerra et al., 2004). The reaction can have a large rate coefficient when the combined excitation energy of the reactants surpasses the ionization energy of the N_2 molecule. The combined excitation energy of two metastable molecules $N_2(A^3\Sigma_u^+)$ is about 3 eV below the ionization energy of the N_2 molecule. The reaction can therefore only proceed if a higher lying metastable species, such as the $N_2(a'^1\Sigma_u^-)$, were included in the model, as was the case with the associative ionization. Thus, instead of approximating the rate coefficient, as we did for reaction (3.53), we will simply exclude reaction (3.54) from the reaction set, since it is almost certainly negligible for the creation of N_2^+.

3.6 Optical emission of excited species

Each excited species eventually returns to some lower energy level by, for example, spontaneously emitting a light of a specific wavelength corresponding to the decrease in energy. The strongest optical emission is by electric dipole radiation, which is only permitted for a given excited level if a set of selection rules is fulfilled. If the electric dipole radiation is not permitted, optical emission can only occur by magnetic dipole radiation or other mechanisms that are much weaker than electric dipole radiation. Particles in a specific excited level thus have a specific lifetime, varying from level to level, before spontaneously emitting light and returning to some lower energy level. From some energy levels no electric dipole radiation is

permitted. These levels are called metastable and have much longer lifetime, τ_{rad}, than other excited levels, much exceeding 10^{-6} sec. Metastable species can therefore be present in a considerable quantity in a gas discharge. Because of the high lifetime of metastable particles, the spontaneous emission is not believed to play an important role in the loss of metastable particles. We will however include the process, just to confirm that it is of no importance. An extensive collection of lifetimes of excited nitrogen atoms is given in the compilation by Wiese et al. (1996). Furthermore, a collection of lifetimes of excited nitrogen molecules is given in the compilation by Lofthus and Krupenie (1977).

Since the nitrogen molecule has no permanent dipole moment (Patel, 1964; Weber and Deutsch, 1966), electric dipole radiation from the vibrational levels of the ground state nitrogen molecule is not permitted. The lifetime of vibrationally excited molecules can therefore be expected to be very long, and since no data could be found regarding their lifetime we will simply assume that spontaneous emission from vibrational levels is negligible.

3.6.1 Emission from $\mathrm{N}_2(A^3\Sigma_{\mathrm{u}}^+)$

Piper (1993) measured the lifetime for the transition

$$\mathrm{N}_2(A^3\Sigma_{\mathrm{u}}^+, v) \longrightarrow \mathrm{N}_2(X^1\Sigma_{\mathrm{g}}^+, v = 0) + \hbar\omega \tag{3.55}$$

for several vibrational levels of the metastable molecule. We will use the $v = 0$ value of 2.37 sec, which is in a reasonably good agreement with other reported values for the lifetime (Shemansky and Carleton, 1969; Lofthus and Krupenie, 1977; Meyer et al., 1971).

3.6.2 Emission from N(^{2}P)

The Einstein coefficient, $1/\tau_{\rm rad}$, for the transition

$$\mathrm{N}(^2\mathrm{P}) \longrightarrow \mathrm{N}(^4\mathrm{S}) + \hbar\omega \tag{3.56}$$

was measured by Piper (1998). We will use his value of 185 sec, which was found to be in a reasonable agreement with earlier theoretical calculations (Godefroid and Fischer, 1984). Furthermore, it is in a reasonable agreement with the largest value given in the compilation by Wiese et al. (1996).

The lifetime for the transition

$$\mathrm{N}(^2\mathrm{P}) \longrightarrow \mathrm{N}(^2\mathrm{D}) + \hbar\omega \tag{3.57}$$

is assigned the value 18.9 sec, originating from the largest theoretical Einstein coefficient given in the compilation by Wiese et al. (1996).

3.6.3 Emission from N(^{2}D)

The lifetime for the transition

$$\mathrm{N}(^2\mathrm{D}) \longrightarrow \mathrm{N}(^4\mathrm{S}) + \hbar\omega \tag{3.58}$$

is much higher than for the other two atomic transitions, or $\tau_{\rm rad} = 5.3 \times 10^4$ sec, originating from the largest theoretical Einstein coefficient given in the compilation by Wiese et al. (1996). Thus, it is apparent that the metastable atom N(^{2}D) is the most stable of the metastable atoms and molecules included in the model.

3.7 Elastic electron scattering

As there is no loss or generation of a species involved in elastic collisions, the elastic scattering cross section does not play a role in the particle balance equations (2.56). However, it plays a vital role in the determination of the collisional energy loss, $\mathcal{E}_c$, given by equation (2.31), which is an important parameter in the energy balance equation (2.57). The total electron impact scattering cross section is the sum of all possible electron collision cross sections, and can be important in determining the maximum value of a particular inelastic collision cross section. Elastic collisions are those where the kinetic energy is conserved, with the internal energy of the particles being unchanged. While inelastic collisions have a particular energy threshold, elastic processes do not, and thus the low energy part of the total scattering cross section consists only of the elastic scattering cross section. The elastic cross section therefore has to cover a wide range of electron energy in order for the rate coefficient to be accurate, preferably from a few meV to a few keV. This can often only be accomplished by assembling the cross section from more than one measurement or calculation, as most authors only cover a subset of the energy range needed.

3.7.1 Elastic scattering by the $N_2(X^1\Sigma_g^+, v = 0)$ molecule

The elastic scattering of electrons by impact with the nitrogen molecule has been quite well studied, both theoretically (Shyn and Carignan, 1980; Morrison et al., 1987; Gillan et al., 1988; Sun et al., 1995; Szmytkowski et al., 1996; Feng et al., 2003) and experimentally (DuBois and Rudd, 1976; Nickel et al., 1988; Randell et al., 1994; Gote and Ehrhardt, 1995; Sun et al., 1995; Allan, 2005). Furthermore, several authors have reviewed the available data and recommended the best cross sections (Itikawa et al., 1986; Brunger and Buckman, 2002; Buckman et al., 2003; Itikawa, 2006). Allan (2005) measured the differential elastic cross section in the

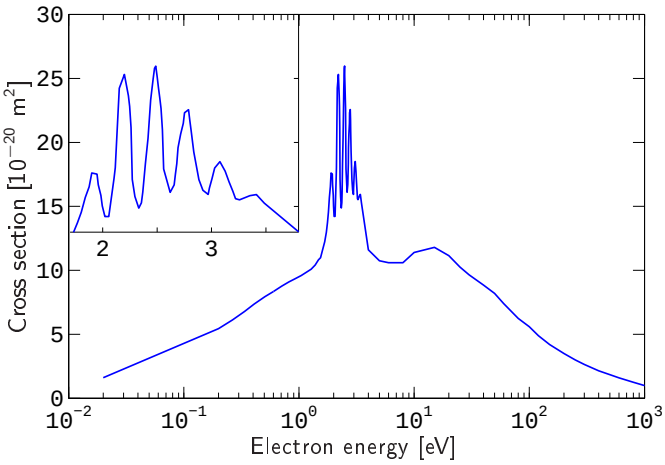

Figure 3.15: The elastic scattering cross section of electron-N_2 collisions. The data in the range 20 meV – 3.5 eV is a part of the theoretical elastic scattering cross section of Feng et al. (2003), and the data in the range 4 – 1000 eV is a part of the elastic scattering cross section recommended by Itikawa (2006). The inset reveals the resonant structure in more detail with the energy on a linear scale.

resonance region, 0.5 – 5 eV. The result is in agreement with previous measurements and recommendations, but since this integral elastic cross section consists of only 3 measurement points, there is not enough detail in the resonance region for the cross section to be usable. Although a detailed integral cross section could be derived from the detailed differential cross sections given by Allan (2005), we will use other similarly accurate integral cross sections that are more detailed. Feng et al. (2003) calculated the differential and integral elastic scattering cross section in the energy range 20 meV – 10 eV. Their differential cross sections were in an excellent agreement with those of Allan (2005) at low energy, at approximately 0.5 – 3 eV, but were slightly larger at higher energy. A comparison to the measurements of Sun et al. (1995) reveals a similar high energy overestimation of the cross section. The cross section is furthermore in good agreement with the cross section recommended by Itikawa (2006) below 0.5 eV. We therefore will use the theoretical cross section

of Feng et al. (2003) in the energy range 20 meV – 3.5 eV. In the energy range 4 – 1000 eV we will use the cross section recommended by Itikawa (2006), which is in part unchanged since his previous elastic cross section recommendation (Itikawa et al., 1986), and thus should be quite accurate. The resulting cross section is shown in figure 3.15.

3.7.2 Elastic scattering by the N(^{4}S) atom

Although there exist many calculations of the cross section for the elastic electron scattering by the nitrogen atom (Robinson, 1957; Smith et al., 1967; Thompson, 1971; Ormonde et al., 1973; Burke et al., 1974; Thomas and Nesbet, 1975; Berrington et al., 1975; John and Williams, 1977; Ramsbottom and Bell, 1994), the cross section has only been measured twice (Neynaber et al., 1963; Miller et al., 1970). Most of the data is very dated, especially the measurements, with the theoretical calculation of Ramsbottom and Bell (1994) being the most recent. At high energy, larger than 2 eV, most of the calculated cross section are similar, all being larger than the measurement of Neynaber et al. (1963) by at least a factor of two. However, for energy lower than 2 eV some of the cross sections begin to deviate from the rest, eventually exhibiting a very strong resonant peak at several meV. The other cross sections simply decrease uniformly with decreasing energy. The low energy measurement of Miller et al. (1970), even though suggested to be taken with a grain of salt, supports the former result, increasing with decreasing energy and thus indicating the existence of the low energy resonance. Ramsbottom and Bell (1994) could reproduce excellent agreement with both instances in their calculations, showing that the difference only lies in the assumption of the existence of a bound state of N^-. Taking into account the measurement of Miller et al. (1970) and the fact that there is no experimental evidence of a bound N^- state,

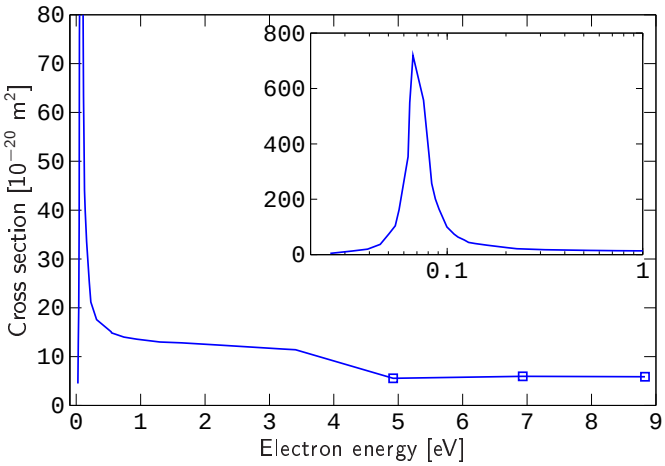

Figure 3.16: The elastic scattering cross section for the collision of electrons and nitrogen atoms versus electron energy. The data in the range 25 meV – 3.5 eV is a part of the theoretical elastic scattering cross section of Ramsbottom and Bell (1994). The data in the range 5 – 9 eV is the most reliable portion of the elastic scattering cross section measured by Neynaber et al. (1963), the data points being represented by squares □. The inset reveals the resonant peak in more detail with the energy on a logarithmic scale.

Ramsbottom and Bell regard the cross section with the resonant peak to be the more accurate.

As the experimental data is relatively poor, we prefer to use of the theoretical cross sections. Given the relatively good agreement with experimental data, we will use the most recent calculation of Ramsbottom and Bell (1994) in the energy range 0.025 – 3.5 eV. To extend the cross section to higher energy we will use the three measurement points of Neynaber et al. (1963), in the energy range 5 – 9 eV, that were assigned the least error. For this elastic scattering, no data could be found that gave the cross section at any higher energy. The resulting cross section is shown in figure 3.16.

3.8 Wall interactions

Wall interactions are very important in low pressure discharges. Wall recombination of neutral atoms is sometimes the only significant sink of atoms, even though its probability is often very low. Positive ions are also lost rapidly to the walls, whereas negative ions are not present at the wall and therefore not lost in that manner. The wall can also act as a sink for excitation energy, commonly quenching excited molecules and atoms quite effectively.

3.8.1 Wall recombination coefficient

The wall recombination coefficient, $\gamma_{\rm rec}$, is a very important discharge parameter. At low pressure, when heavy particle collisions are less likely, wall recombination of atoms is believed to be the dominating pathway of atom loss. It has been shown (Lee and Lieberman, 1995) that the value of the wall recombination coefficient $\gamma_{\rm rec}$ may decide the fractional dissociation, $n_{\rm at}/n_{\rm g}$, in the discharge. Depending on the application, the fractional dissociation is regarded as one of the most important parameters in a processing plasma, and thus the importance of the wall recombination coefficient can not be taken lightly. The recombination coefficient does however change not only with the wall material, but also with the quality of the surface, such as its roughness and purity. For a given chamber, the wall material or its coating might thus have been chosen to fulfill a specific requirement of fractional dissociation. Furthermore, the wall recombination coefficient $\gamma_{\rm rec}$ may depend on pressure, as is the case with the oxygen discharge (Gudmundsson and Thorsteinsson, 2007b), and with gas temperature as well.

Singh et al. (2000) measured the recombination coefficient for neutral oxygen and nitrogen atoms on a stainless steel surface in a low pressure inductive discharge chamber. The wall recombination coefficient obtained, an average of values

measured while varying the discharge pressure and power, was $\gamma_{\rm rec} = 0.07$.

A variety of other experimental and theoretical determinations exist for the wall recombination coefficient, $\gamma_{\rm rec}$, in a nitrogen discharge. In a study of the effect of wall material in an N_2–O_2 post-discharge, Kutasi and Loureiro (2007) reviewed some of the available data for various surface materials. The majority of the studies are for the recombination of atoms on a glass, pyrex, quartz or other silica surface materials (Capitelli et al., 2007; Herron et al., 1959; Young, 1961; Sancier et al., 1962; Lefèvre et al., 2000; Belmonte et al., 1999; Gordiets et al., 1996; Yamashita, 1979; Tunis Wentink et al., 1958), yielding wall recombination coefficients of approximately $10^{-6} - 10^{-4}$ in the pressure regime $0.1 - 11$ Torr. The wall recombination coefficient has also been determined for iron (Belmonte et al., 1999; Lefèvre et al., 1999), iron-nitride (Belmonte et al., 1998), molybdenum (Hays et al., 1974; Marković et al., 1994), aluminum (Sarrette et al., 2006; Adams and Miller, 2000), stainless steel (Adams and Miller, 2000) and copper wall surfaces in the same pressure regime, yielding values of approximately 10^{-3}, 10^{-2}, $10^{-4} - 10^{-2}$, 10^{-3}, 5×10^{-3} and 10^{-2}, respectively. Because of the pressure dependence, these measurements are of limited use to us, all being above the operating pressure regime of interest here. However, they do indicate that the recombination coefficient is considerably smaller for glass, quartz and pyrex than it is for a chamber made of stainless-steel, iron or aluminum, for example. Since the power is generally coupled to the plasma through a dielectric window in an inductively coupled plasma chamber or a electron cyclotron discharge, at least some part of the chamber must exhibit this low wall recombination coefficient, effectively lowering the overall wall recombination coefficient of the chamber.

In a study of the dissociation degree in a low pressure inductively coupled discharge, Nakano et al. (2002) estimated the wall recombination coefficient of the

discharge chamber, made mostly of aluminum oxide, to be in the range 0.17 – 0.093 for a pressure of 5 mTorr, assuming the gas temperature to be between 300 and 1000 K. This is in agreement with the aforementioned measurement of Singh et al. (2000), indicating the wall recombination coefficient is significantly larger in the pressure regime 1 – 100 mTorr, compared to the pressure regime of the other studies, 0.1 – 11 Torr.

Since we assume the chamber in our global model study is made of stainless steel, we prefer to use the wall recombination coefficients measured by Singh et al. (2000). Although the measurement demonstrates that the wall recombination coefficient has an inverse dependence on pressure, we are not able to derive a pressure dependent wall recombination coefficient as was done in the O_2/Ar discharge model (Gudmundsson and Thorsteinsson, 2007b). The wall recombination coefficient was only measured in the pressure regime 15 – 30 mTorr, which is too narrow to extrapolate a pressure dependent wall recombination coefficient that is valid for pressure below 10 mTorr. We will therefore simply use the aforementioned average wall recombination coefficient reported by Singh et al. (2000), $\gamma_{\mathrm{rec}} = 0.07$, for the recombination of both ground state and metastable atoms on the wall, and assume that it is constant with pressure. We will also assume the resulting molecule is in the ground state, $N_2(X^1\Sigma_g^+, v = 0)$, as predicted by Capitelli et al. (2007) for a silica surface. Furthermore, we will assume that the measured wall recombination coefficient represents an overall value for the chamber, including the effect of the lower wall recombination coefficient at dielectric windows.

3.8.2 Wall quenching coefficients

Quenching of excited species by impact with the wall can be an important factor in their loss. However, excited species are also lost rapidly through other channels,

such as electron impact de-excitation, which reduces the impact of wall quenching on excited particle densities.

Wall quenching of vibrationally excited molecules

Black et al. (1974) measured the vibrational relaxation of $N_2(X^1\Sigma_g^+, v = 1)$ by a collision with various surface materials at pressure above 7.5 Torr. The wall quenching coefficients were found to be in the range 2×10^{-4} for pyrex to 5×10^{-3} for aluminum. Morgan and Schiff (1963) estimated the wall quenching coefficients for vibrationally excited ground state nitrogen molecules on a pyrex surface to be roughly 4.5×10^{-4}. Egorov et al. (1973) measured the vibrational deactivation probability in a collision with a glass surface for a wall temperature in the range $282 - 603$ K and pressure in the range $1.85 - 6.3$ Torr. Egorov et al. then found an equation describing the behavior of the quenching coefficient with pressure p and wall temperature T,

$$\gamma_{N_2(X,v)} = 0.39 \times 10^{-3} \exp(1000/RT) + \frac{0.415}{p} \exp(-6000/RT) \tag{3.59}$$

which, for a 600 K gas temperature, would result in a wall quenching coefficient of about 2 at 1 mTorr, i.e. two molecules quenching for each collision of a single vibrationally excited molecule on the wall. This discrepancy, along with the fact that the limited pressure range is about $2 - 3$ orders of magnitudes above ours, prevents us from using this equation directly. However, the implied pressure dependence indicates that the vibrationally excited molecules are quenched quite effectively in the pressure regime $1 - 100$ mTorr. Thus, in spite of the relatively low values found at much higher pressure, we will assume the wall quenching coefficient for vibrationally excited molecules has reached unity in the operating pressure regime of an inductively coupled discharge, that is $\gamma_{N_2(X,v)} = 1$.

Wall quenching of the metastable molecule $N_2(A^3\Sigma_u^+)$

Meyer et al. (1971) found that the $N_2(A^3\Sigma_u^+)$ metastable nitrogen molecule is quenched with approximately 30% efficiency on a quartz surface at a 3 Torr pressure. Given the general inverse dependence of the quenching coefficient with pressure (Egorov et al., 1973; Kozlov et al., 1987a), it is not unreasonable to assume that at the much lower pressure of $1 - 100$ mTorr essentially all $N_2(A^3\Sigma_u^+)$ molecules colliding with the wall are quenched to the ground state, $N_2(X^1\Sigma_g^+, v = 0)$. Furthermore, Clark and Setser (1980) found that essentially all metastable $N_2(A^3\Sigma_u^+)$ are quenched on a pyrex/quartz wall under similar conditions as those in the measurement of Meyer et al. (1971). We will therefore simply use a unity value for the wall quenching coefficient, $\gamma_{N_2(A)} = 1$, and assume that it applies to a stainless steel chamber at $1 - 100$ mTorr.

Wall quenching of the metastable atoms $N(^2D)$ and $N(^2P)$

As well as recombining to form a molecule, as mentioned above, excited atoms are quenched to the ground state when they collide with the wall. A common assumption (Gordiets et al., 1995; Guerra et al., 2002; Guerra and Loureiro, 1997) is that all excited atoms that do not combine with other atoms on the wall are instead quenched. Furthermore, Lin and Kaufman (1971) found that $N(^2D)$ and $N(^2P)$ are quenched very efficiently on a pyrex wall with a $3 - 16$ Torr pressure, or with approximately a unity wall quenching coefficient. On a gold surface, Kozlov et al. (1987b) found a quenching probability coefficient of $0.1 - 0.72$ for a temperature in the range $300 - 670$ K and pressure in the range 50 mTorr to 1.25 Torr. This value, although low compared to the mentioned quartz value, is still relatively large, and supports the use of a near unity quenching coefficient. Therefore, we will simply assume that $\gamma_{N(^2D)} = \gamma_{N(^2P)} = 1 - \gamma_{rec} = 0.93$.

3.8.3 Wall recombination of ions

We assume all positive ions recombine on the wall, and therefore all the ions we consider in the nitrogen discharge. Thus, the nitrogen ions N_2^+ and N^+ recombine to form their neutral counterparts N_2 and N, respectively, with a rate given by equation (2.49). However, the heavier ions we consider as well, N_3^+ and N_4^+, can not recombine in the same way since we do not consider the heavy neutrals N_3 and N_4. As an approximation, we will assume the heavy molecular ion N_3^+ recombines on the wall and subsequently dissociates to produce both a neutral nitrogen molecule and an atom. Similarly, we will assume the heavier ion N_4^+ recombines on the wall to form two neutral nitrogen molecules. Since these heavy molecular ions are expected to have a rather weak bond, the approximation is likely satisfactory. Furthermore, assuming the neutral counterparts N_3 and N_4 are formed in the wall recombination, we expect their bond to be weak and the molecules to dissociate quickly, such that their formation can in effect be ignored altogether. This assessment is further supported by the scarcity of data found regarding those two heavy neutrals.

3.9 Scattering cross sections

In order to calculate the mean free path of a given particle, given by equation (2.5), the scattering cross section of impacts of that particle with all species in the discharge must be known. In an argon discharge the ion-neutral scattering cross section is approximately $1 \times 10^{-18}\,\mathrm{m}^2$ (Lieberman and Lichtenberg, 2005, p. 80). In order to acquire a simple estimate of the mean free path, this value is commonly used as a rough approximation of the cross sections in other similar gases as well. Another common approximation is the so called hard sphere model. It assumes that all discharge particles are hard spheres and the scattering cross section is

simply given by

$$\sigma_{\mathrm{sc}} = \pi(a_1 + a_2)^2 \tag{3.60}$$

where a_1 and a_2 are the radii of the incident and target particles. Since atoms do not behave as hard spheres nor have a precisely defined radius, this model is probably not very accurate. Furthermore, molecules are generally not sphere shaped, the nitrogen molecule being closer to a cylindrical shape, for example. However, the scattering cross section, and therefore the mean free path of the incident particle, are likely to depend on the size of both the incident and target particles, such as predicted by the hard sphere model. We will assume that the scattering cross sections scale proportionally with the combined number of atoms of the incident and target particles, that is

$$\sigma_{\mathrm{sc}} \propto A_1 + A_2 \tag{3.61}$$

where A_1 and A_2 are the number of atoms in the incident and target particles. By defining an effective radius of a molecule as the radius of a sphere with the same volume as confined by the molecule, we found this to approximately correspond to the square dependency of the combined radius as predicted by the hard sphere model.

Phelps (1991) determined the cross sections for collisions of the nitrogen molecule with itself and the ions N^+ and N_2^+ in the energy range $0.1 - 10$ keV. Since the gas temperature is assumed to be 600 K, we extrapolate the cross sections to lower energy, 50 meV, in order to find a suitable cross section value (Lieberman and Lichtenberg, 2005, p. 80). Furthermore, for the collision of the neutral nitrogen molecule with the neutral nitrogen atom, Phelps (1991) recommended using 60%

Table 3.1: The scattering cross sections, σ_{sc} [10^{-20} m^2], for the various collisions in the discharge. The cross sections are assumed to be independent of the excitation level of the particles. The values marked with a star are derived from the cross sections given by Phelps (1991). The unmarked values are derived from the marked values according to equation (3.61). The ion-ion scattering cross sections are all assumed to be negligible.

σ_{sc} [10^{-20} m^2]	N_2	N	N_2^+	N^+	N_3^+	N_4^+
N_2	50*	35	250*	150*	310	380
N	35	25	180	100	250	310
N_2^+	250*	180	0	0	0	0
N^+	150*	100	0	0	0	0
N_3^+	310	250	0	0	0	0
N_4^+	380	310	0	0	0	0

of the $N_2 - N_2$ cross section, scaling with approximately the square of the combined number of atoms.

Stallcop et al. (1991) calculated the cross section for the charge transfer in $N - N^+$ collisions, giving a value of $4 \times 10^{-19}\,m^2$ for a 600 K gas temperature. Although the charge transfer collision contributes to the scattering cross section, the momentum transfer collision is generally just as important and thus the value does not necessarily correspond to the entire scattering cross section. We will therefore scale the cross section values of Phelps (1991) instead, according to equation (3.61), to obtain values for the scattering cross sections of collisions of the neutral nitrogen atom with itself and the ions N^+, N_2^+, N_3^+ and N_4^+. Furthermore, we will assume that all ion-ion scattering cross sections are negligible and that the scattering cross section is not dependent on the excitation level of particles. The resulting scattering cross section values are summarized in table 3.1

3.10 Gas temperature

The gas temperature defines the mean thermal velocity of gas particles and can affect the rate coefficients of reactions involving the collision of two heavy species.

Furthermore, the temperature of the gas species is necessary in order to determine their density from the discharge pressure. Even though the gas temperature can therefore be regarded as an important parameter in plasma discharge modelling, it is commonly simply assumed to be equal to the room temperature. This may be a satisfactory approximation for simple modelling of some plasma discharges, but in the current study of the inductively coupled nitrogen discharge we will use a more suitable value, obtained from specific measurements of the gas temperature.

In a capacitively coupled discharge the gas temperature is close to the room temperature, roughly $300 - 400$ K. However, the gas temperature is generally much higher in an inductively coupled discharge, often assumed to be 600 K, which is the temperature we have used in previous models of the oxygen discharge (Gudmundsson et al., 1999; Gudmundsson and Thorsteinsson, 2007b; Patel, 1998; Gudmundsson et al., 2000, 2001). The gas temperature is known to vary with gas species and discharge conditions. The gas temperature in an inductively coupled chlorine discharge is for example known to be as high as 1250 K, depending on the discharge power and pressure (Donnelly and Malyshev, 2000). The high temperature is associated with the unusually high dissociation degree observed in chlorine discharges. We expect the gas temperature in the nitrogen discharge to be significantly lower, given its relatively low degree of dissociation.

The gas temperature is generally determined by a spectroscopic method, rather than by direct temperature measurement, such as by a thermocouple. Since the temperature of the chamber walls does not represent the temperature of the gas species in the plasma bulk, ranging from 320 K to 340 K on the walls of a stainless steel chamber (Singh et al., 2000), a direct gas temperature measurement would need to be done within the discharge chamber. Because of its sensitivity and simplicity, the spectroscopic method is therefore the most common method used to

determine the gas temperature (Biloiu et al., 2007b). Several studies have determined the gas temperatures specifically for inductively coupled discharges in the pressure range 1 – 100 mTorr and with a 50 – 1000 W input power. Bakowski et al. (2004) measured the gas temperature in a magnetically confined inductively coupled discharge chamber as a function of power in the range 100 – 400 W. The gas temperature exhibited an apparent linear increase with increasing power, varying from 300 K to 460 K, while its dependence with pressure was found to be negligible. Tuszewski (2006) measured the gas temperature as a function of both power and pressure in a low-frequency inductively coupled nitrogen discharge, finding a weak increase with pressure but a stronger dependence with power, increasing linearly from 400 K to 600 K for an applied power in the range 200 to 900 W. Shimada et al. (2006), Britun et al. (2007) and Bol'shakov et al. (2004) measured the gas temperature as a function of nitrogen content in rare gas inductively coupled discharges diluted with nitrogen, finding a 450 – 550 K gas temperature for high nitrogen content at various input powers. Biloiu et al. (2007b) found a gas temperature of 400 – 500 K in a low-pressure helicon nitrogen discharge operating at a 600 W input power. Although no dependence of power or pressure was reported, a higher gas temperature was obtained for a measurement taken in the axial direction compared to a measurement taken in the radial direction of the discharge chamber. Linss et al. (2005) measured the gas temperature as a function of both pressure and power in an rf magnetron discharge. A two temperature fit to the spectroscopic data gave a gas temperature of about 410 – 470 K as the power was increased from 50 to 500 W while showing little dependence with pressure, whereas a "conventional fit" gave a much steeper and unexpected increase with pressure.

The determinations of the gas temperature mentioned above were all for nitrogen discharges in the pressure range 1 – 100 mTorr. Since the studies indicated

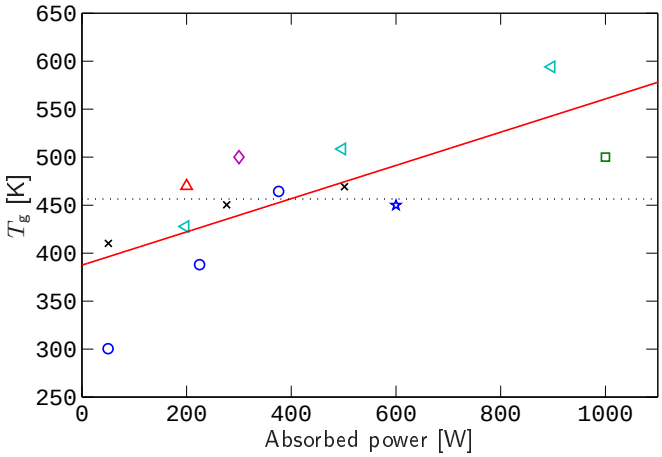

Figure 3.17: The gas temperature T_g in low-pressure (1 – 100 mTorr) nitrogen discharges as a function of input power P_{abs}. The measured data is taken from, ○ Bakowski et al. (2004), ◁ Tuszewski (2006), □ Shimada et al. (2006), △ Britun et al. (2007), ♢ Bol'shakov et al. (2004), ☆ Biloiu et al. (2007b) and × Linss et al. (2005). The solid line is a linear fit to the measured data, $T_g = 0.17 \times P_{abs} + 387$ K, and the dotted line is the average gas temperature, 456 K.

only a weak dependence with pressure, we will assume that the gas temperature is constant within that range. A gas temperature of 600 K found at a 1 Torr pressure and 1000 W power in an rf nitrogen discharge (Porter and Harshbarger, 1979), further supports this assessment. However, it is apparent that the gas temperature depends strongly enough on the discharge power such that it can not be ignored. The various findings of the gas temperature are summarized in figure 3.17 as a function of the discharge power along with a linear fit to the data, describing the dependence with power, and the average temperature value (a constant temperature fit). In the low power region, i.e. as the discharge enters the capacitively coupled mode (E-mode) and exits the inductively coupled mode (H-mode), the gas temperature is likely to exhibit a more complex behavior with discharge power than is predicted by the linear fit in figure 3.17. Taking into account the measurement of Bakowski et al. (2004), the decrease in temperature is more rapid at lower power,

ultimately reaching a gas temperature of close to 300 K. Saturation of temperature can also be expected at very high powers. However, since the global model is only valid within the inductively coupled regime and fails at lower power, we will assume the linear fit is satisfactory within the operating parameters of the discharge.

Tuszewski (2006) found that the temperature of ions is approximately $2 - 2.5$ larger than of the neutral species in a 0.46 MHz inductively coupled discharge, or about 1000 K. This behavior was assumed to be a result of the lower frequency used in the discharge compared to in other measurements that use a 13.56 MHz driving frequency and find equal temperatures of ions and neutrals. We will assume the power in the global model is driven with a frequency of 13.56 MHz, and therefore that all nitrogen gas species, ions and neutrals, have an equal temperature as a function of power P_{abs}, $T_{\mathrm{i}} = T_{\mathrm{g}} = 0.17 \times P_{\mathrm{abs}} + 387$ K, in the steady state global model calculations. However, in the time dependent part of this study the power is pulsed with a frequency much smaller than the driving frequency, or $1 - 1000$ kHz, such that the electrons and ions can respond to the slower fields and be considerably hotter than the neutral gas particles in the discharge. We could therefore assume that the temperature of positive nitrogen ions is roughly 2.25 times higher than the temperature of neutral species in the pulsed power global model calculations. However, in order to see more clearly the difference between the pulsed and steady state model, we will assume that the gas temperature is the same in the pulsed model as in the the steady state model and has the same dependence on average absorbed power as in the steady state model. In any case, we expect the ion heating to have an insignificantly effect on the outcome. A steady state calculation, where the temperature of ions was increased gradually from the neutral gas temperature to 1000 K, demonstrated that the ion densities, neutral densities and the electron temperature remained virtually constant with varying temperature of ions.

Chapter 4

The steady state discharge

We assume a cylindrical stainless steel chamber of radius R and length L. A steady flow Q of neutral species is introduced through the inlet.The content of the chamber is assumed to be nearly spatially uniform and the power deposited uniformly into the plasma bulk. The discharge is assumed to consist of 15 species of nitrogen; the seven lowest lying vibrational levels of the ground state nitrogen molecule $N_2(X^1\Sigma_g^+, v = 0 - 6)$, the metastable nitrogen molecule $N_2(A^3\Sigma_u^+)$, the ground state nitrogen atom $N(^4S)$, the metastable nitrogen atoms $N(^2D)$ and $N(^2P)$, and the ions N_2^+, N^+, N_3^+ and N_4^+. The neutral molecules N_3 and N_4 are assumed to be unstable in the discharge and will not be included, supported by the absence of rate coefficients for reactions with these particles. All negative ions are also assumed to be unstable and will therefore be excluded, supported by the extremely low lifetime of for example the N_2^- ion, roughly 10^{-14} sec (Mihajlov et al., 1999). The reaction set used is summarized in appendix A, tables A.1 to A.8. The electrons are generally assumed to have a Maxwellian-like energy distribution in the range 1 – 10 eV, but the electron energy distribution function will also be allowed to vary

corresponding to the general distribution function given by equation (2.13).

4.1 Comparison with measurements

Singh and Graves (2000a,b) measured the electron temperature, T_e, electron density, fractional dissociation and the fractional density of ions at various pressures and discharge powers in an inductively coupled discharge in a stainless steel chamber with the dimensions $R = 10$ cm and $L = 10$ cm. The gas flow rate into the chamber was not specified and we will therefore assume a 50 sccm gas flow rate in the calculation. Since only the total rf-power was specified for the measurement, we will assume a 75 % power coupling efficiency, i.e. $P_{abs}/P_{rf} = 0.75$ (Hopwood, 1994). The measured electron density and electron temperature are compared to our calculations in figure 4.1. The measured dissociation fraction and the fraction of ion densities are compared to our calculations in figure 4.2. The agreement of the model and measurements is quite good for the electron density, the electron temperature, the $[N^+]/[N_2^+]$ ratio and the $[N_3^+]/[N_2^+]$ ratio. However, the measured dissociation fraction is much lower than what the model predicts, the model seemingly overestimating the atomic density by a factor of roughly $3-5$, depending on absorbed power. Furthermore, we predict a linear increase of dissociation fraction with absorbed power, whereas the measurements show relatively little variation with absorbed power. This could be the result of incorrectly assuming that the gas flow in the measurement was 50 sccm, but since assuming a gas flow of 500 sccm would only decrease the dissociation fraction by less than 2 %, it can not be the only explanation. The ion fraction measurement seems to contradict the dissociation fraction measurement, with one indicating a rather atomic nature of the discharge, while the other indicates the molecules are the dominating species. To reproduce the low dissociation fraction in our model for this chamber we could either signifi-

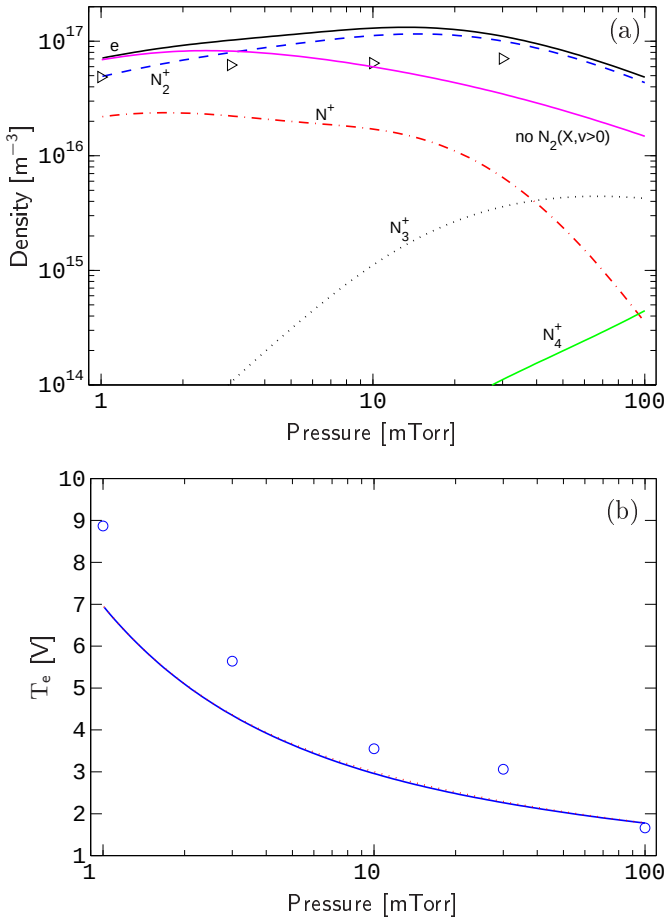

Figure 4.1: Calculations and measurements of (a) the densities of ions and electrons and (b) the electron temperature as a function of reactor pressure. In (a), the triangles are the electron density measured by Singh and Graves (2000a) and the lower solid line is the electron density calculated while excluding all vibrationally excited ground state molecules $N_2(X^1\Sigma_g^+, v = 1-6)$. In (b), the circles ○ are the effective electron temperatures measured by Singh and Graves (2000a) and the solid and dotted lines, nearly indistinguishable, are the electron temperature calculated while including and excluding $N_2(X^1\Sigma_g^+, v = 1-6)$, respectively. The gas flow rate was 50 sccm and the absorbed power 240 W in the calculation, whereas the total rf-power was 320 W in the measurement. The chamber was made of stainless steel, with the dimensions $R = 10$ cm and $L = 10$ cm.

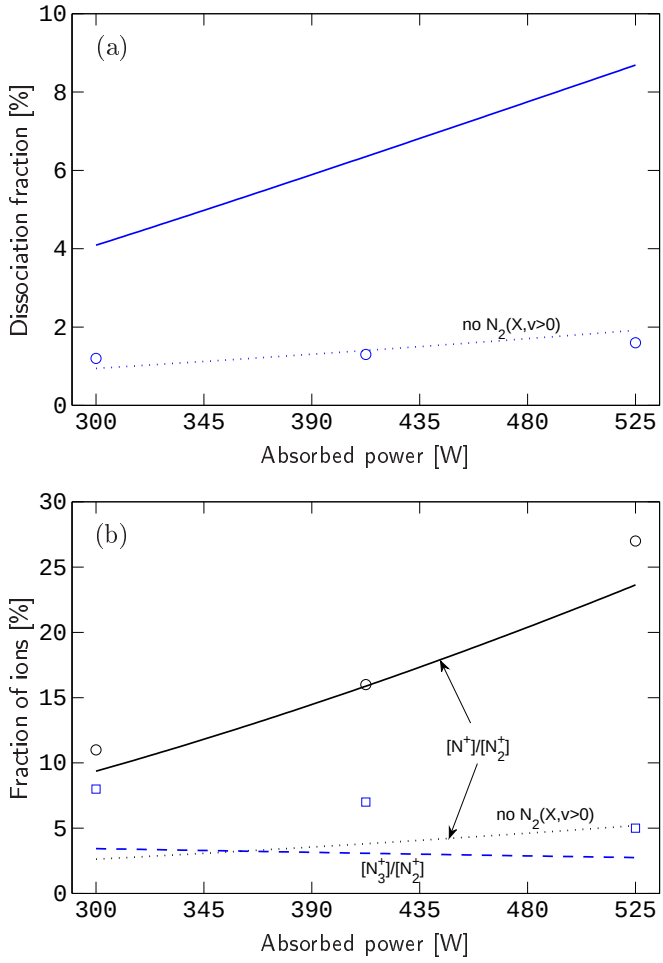

Figure 4.2: Calculations and measurements of (a) the fraction of atomic neutral species and (b) the fraction of ions as a function of absorbed power. In (a), the circles are the $[N]/[N_2]$ density ratio measured by Singh and Graves (2000b). In (b), the circles and squares are ○ the $[N^+]/[N_2^+]$ density ratio and □ the $[N_3^+]/[N_2^+]$ density ratio measured by Singh and Graves (2000b), respectively. The dotted lines represent the calculation when excluding vibrationally excited ground state nitrogen molecules, $N_2(X^1\Sigma_g^+, v = 1-6)$. The gas flow was 50 sccm and the reactor pressure was 30 mTorr. The total rf-power reported for the measurement was scaled down 25% to roughly correspond to the absorbed power used in the calculation. The chamber was made of stainless steel, with the dimensions $R = 10$ cm and $L = 10$ cm.

cantly increase the wall recombination coefficient, γ_{rec}, or decrease the dissociation cross section. As the wall recombination coefficient we use was measured by the same author for the same chamber and is already at the upper limit of commonly used values, we will consider the latter route. By trial and error, we found that the dissociation cross section would need to be scaled down by a factor of $4-5$. As expected, this also decreased the $[N^+]/[N_2^+]$ fraction significantly, then being in a poor agreement with the measurement. Although the dissociation cross section might be too large, a discrepancy of a factor of $4-5$ from the true value has to be considered an unlikely event. However, since it has been suggested elsewhere in the literature that the cross section may be too large by a factor of 10 (Cenian and Chernukho, 2003), a discrepancy of a factor of 5 is not necessarily that far fetched. The fact that this has merely been suggested only underlines the doubt that surrounds this particular cross section. When dissociation of vibrationally excited ground state nitrogen molecules was excluded in our calculations, such that only the $N_2(X^1\Sigma_g^+, v=0)$ and $N_2(A^3\Sigma_u^+)$ dissociate, we got a much better agreement of the dissociation fraction with the measurement. Furthermore, when the model was run without including any of the vibrationally excited ground state nitrogen molecules, an excellent agreement with the dissociation fraction measurement was achieved. This is shown by the dotted line in figure 4.2(a). The electron density, the lower solid line in figure 4.1(a), decreased more rapidly with pressure than with the vibrationally excited molecules included, but was still in good agreement with the measurement. Excluding vibrationally excited molecules had a negligible effect on the electron temperature, demonstrated by the dotted line being almost indistinguishable from the solid line in figure 4.1(b). However, excluding the vibrational excited molecules had roughly the same effect on the $[N^+]/[N_2^+]$ fraction, shown by the dotted line in figure 4.2, as on the dissociation fraction, being significantly

smaller and therefore in poor agreement with the measurement.

It is possible that the dissociation cross section, believed to apply solely to the dissociation of $N_2(X^1\Sigma_g^+, v = 0)$, includes a significant contribution from the dissociation of vibrationally excited ground state molecules. Additionally, the cross sections for the dissociation of vibrationally excited molecules may be significantly smaller than for the $N_2(X^1\Sigma_g^+, v = 0)$, and not only with a reduced threshold as we assume in the current study. The atomic density discrepancy is likely to be caused by a combination of these factors. Instead of arbitrarily configuring them to reach an agreement with the dissociation fraction measurement, meanwhile losing the good agreement with the atomic ion fraction, we will use the cross section unmodified in the current study and try to discuss and explain the discrepancy we observe between calculation and measurement.

Agarwal et al. (2003) measured the absolute atomic and metastable molecule densities in an inductively coupled discharge. The chamber was made of stainless steel, 30 cm in diameter and 18 cm in length (Aydil, 2003). The flowrate was fixed at 50 sccm. The power reported for the measurement was the total rf-power (Aydil, 2003) and was fixed at 750 W. In order to approximate the power absorbed by the plasma we will assume the same power coupling efficiency as before, or 75 %, yielding an absorbed power of approximately 563 W. Most of the metastable molecule signal was attributed to the $N_2(A^3\Sigma_u^+)$ molecule, whereas the state of the observed atoms was not discussed. We will assume the measured atomic density consists of both ground state and metastable atoms, and therefore we will compare the measurement to the sum of all the neutral atom densities predicted by our model. As is evident in figure 4.3(a) there is quite high discrepancy between our calculation of the atomic density and the measurement. The difference is even greater than the discrepancy between the dissociation fraction measure-

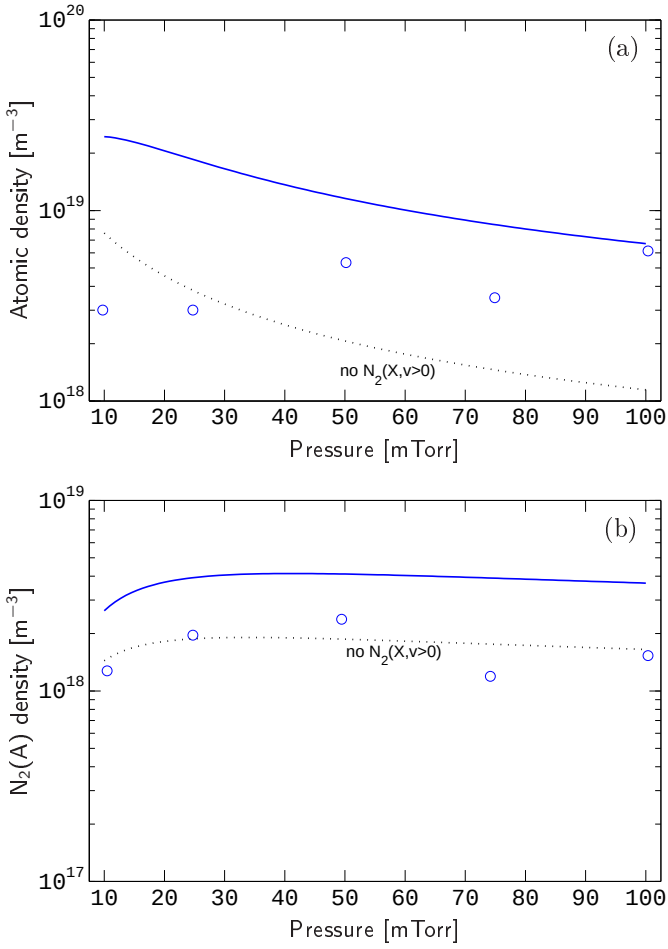

Figure 4.3: Calculations and measurements of (a) the density of nitrogen atoms and (b) the density of $N_2(A^3\Sigma_u^+)$ as a function of pressure. The circles ○ are the atomic nitrogen density and metastable nitrogen molecule density measured by Agarwal et al. (2003). The dotted lines represent the calculation when excluding vibrationally excited ground state nitrogen molecules, $N_2(X^1\Sigma_g^+, v = 1-6)$. The absorbed power was 563 W in the calculation, whereas the total rf-power reported in the measurement was 750 W (Aydil, 2003). The gas flowrate was 50 sccm in both the measurement and calculation. The chamber was made of stainless steel, with the dimensions $R = 15$ cm and $L = 18$ cm (Aydil, 2003).

ment of Singh and Graves (2000b). The calculated atomic density is roughly an order of magnitude larger than the measured density at 10 mTorr, but less than factor of two larger at 100 mTorr. Furthermore, we predict that the atomic density decreases significantly with pressure, whereas the measurement shows little variation of atomic density with pressure. Thus, this measurement mostly confirms our suspicion that the model overestimates the neutral atomic density considerably. When vibrationally excited molecules were excluded in the calculations, the atomic density decreased significantly, as shown by the dotted line in figure 4.3(a), and was in acceptable agreement with the measurement by Agarwal et al. (2003). It is possible that the measurement only captured the signal from either the ground state or metastable atoms, instead of the total atomic density, which would in part explain the difference from our calculation. However, we have no firm reason to believe this is the case and it is more likely that some or all of the dissociation cross sections are too large. The measured and calculated metastable molecule $N_2(A^3\Sigma_u^+)$ density are compared in figure 4.3(b). Although the model seems to overestimate the $N_2(A^3\Sigma_u^+)$ density, the agreement with the measurement is acceptable. The agreement is excellent when the calculation is performed without including the vibrationally excited levels $N_2(X^1\Sigma_g^+, v = 1-6)$. Similarly to dissociation, this indicates that the cross sections for electron impact excitation of vibrationally excited ground state molecules to $N_2(A^3\Sigma_u^+)$ are somewhat too large, likely not simply being threshold reduced counterparts of the cross section for the excitation from $N_2(X^1\Sigma_g^+, v = 0)$, as we assume in the current study.

Hancock et al. (2006) measured the density of $N_2(A^3\Sigma_u^+)$ as a function of pressure and power in an inductively coupled plasma chamber with a 35 cm diameter and a 17 cm length. The gas flowrate was not specified in the measurement, but we will assume a 50 sccm flowrate for the calculation. Since only the to-

tal rf-power, and not the absorbed power, was specified in the measurement, we will assume a 75 % power coupling efficiency, as before, to obtain an estimate of the absorbed power. As shown in figures 4.4(a) and (b), the agreement of our calculation with the measurement of the $N_2(A^3\Sigma_u^+)$ density is not quite as good as in figure 4.3(b). The agreement is good at low pressure in figure 4.4(a). A rapid decrease of $N_2(A^3\Sigma_u^+)$ density with increasing pressure is observed in the measurement, whereas the model predicts the density to be nearly constant, only decreasing slightly with pressure above 40 mTorr. This indicates that the $N_2(A^3\Sigma_u^+)$ is quenched much more effectively by ground state nitrogen molecules $N_2(X^1\Sigma_g^+, v = 0-6)$, whose density increases rapidly with pressure, than the current rate coefficient implies. At 100 mTorr the model predicts a density a factor of 20 larger than in the measurement. The total $N_2(A^3\Sigma_u^+)$ density in the measurement was determined from a measured $N_2(A^3\Sigma_u^+, v = 0)$ density by assuming a certain pressure independent vibrational temperature of the $N_2(A^3\Sigma_u^+, v = 0)$. We show later that the density of $N_2(X^1\Sigma_g^+, v > 0)$ decreases rapidly with decreasing pressure, i.e. the vibrational temperature depends strongly on discharge pressure. Thus, assuming a similar behavior of $N_2(A^3\Sigma_u^+, v)$, the decrease of the total $N_2(A^3\Sigma_u^+)$ density that is observed with pressure is possibly because of an underestimation of the $N_2(A^3\Sigma_u^+, v > 0)$ density with increasing pressure. As can be seen in figure 4.4(b), the $N_2(A^3\Sigma_u^+)$ density behaves similarly with power in the measurement and simulation, the model predicting a density roughly a factor of $3-5$ larger than in the measurement, depending on power. The agreement with the measurement is better when the calculation is performed without including $N_2(X^1\Sigma_g^+, v = 1-6)$, the metastable molecule density decreasing by roughly a factor of 2. The rapid decrease in $N_2(A^3\Sigma_u^+)$ density with pressure, as observed in the measurement in figure 4.4(a), is still not reproduced in the calculation. Thus,

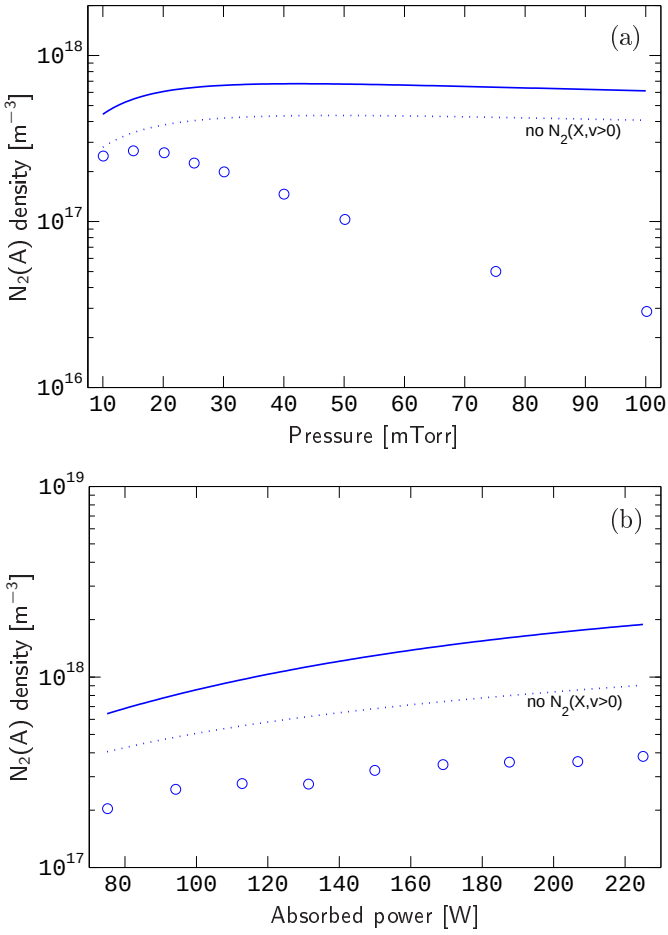

Figure 4.4: Calculations and measurements of the total $N_2(A^3\Sigma_u^+)$ density as (a) a function of pressure with the absorbed power fixed at 75 W and (b) as a function of absorbed power with the pressure fixed at 25 mTorr. The circles ○ are the metastable nitrogen molecule densities measured by Hancock et al. (2006). The dotted lines represent the calculation when excluding vibrationally excited ground state nitrogen molecules, $N_2(X^1\Sigma_g^+, v = 1-6)$. The total rf-power reported for the measurement was scaled down 25% to roughly correspond to the absorbed power used in the calculation. The gas flow rate was assumed to be 50 sccm. The discharge chamber had the dimensions $R = 17.5$ cm and $L = 17$ cm.

in this case, the disagreement between the measurement and the calculation can not be explained only by the cross sections for the excitation of $N_2(A^3\Sigma_u^+)$ from $N_2(X^1\Sigma_g^+, v = 1-6)$ being too large.

Cho et al. (2001) measured the electron density and the ratio of the ions N_2^+ and N^+ as a function of power and pressure in a cylindrical inductively coupled plasma chamber with a 50 cm diameter and a 56 cm length. The gas flowrate was not specified, but we will assume a 50 sccm flowrate for the calculation. Only the total rf-power was reported for the measurement, and therefore we will assume a 75 % power coupling efficiency to obtain the absorbed power to use in the calculation. The calculation is in an excellent agreement with the measurement of the electron density, as seen in figure 4.5(a). However, the calculation predicts a significantly lower density of the atomic ion N^+ than found in the measurement. The high ratio of N^+ is inconsistent with the low dissociation fraction measurement in figure 4.2(a) and the low atomic density measurement in figure 4.3, but is consistent with the measured large ion ratio shown in figure 4.2(b). All of the measurements therefore indicate a high ratio of atomic ions but a low ratio of neutral atoms, which is very hard to believe to be physically accurate. As seen in figure 4.5(b), the N^+ ratio is even higher at higher pressure, being roughly equal to the N_2^+ density at 2 mTorr. The agreement of the electron density calculation with the measurement gets worse at higher pressure, being roughly a factor of 2 smaller at 2 mTorr. Excluding $N_2(X^1\Sigma_g^+, v = 1-6)$ in the calculations has a negligible effect on the electron density, shown by the dotted lines in figures 4.5(a) and (b).

Zhu and Pu (2008) measured the electron density as a function of power and the electron temperature as a function of reactor pressure in an inductively coupled plasma chamber with a 60 cm diameter and a 40 cm length. The gas flowrate was not specified, but we will assume a 50 sccm flowrate in the calculation. Only the

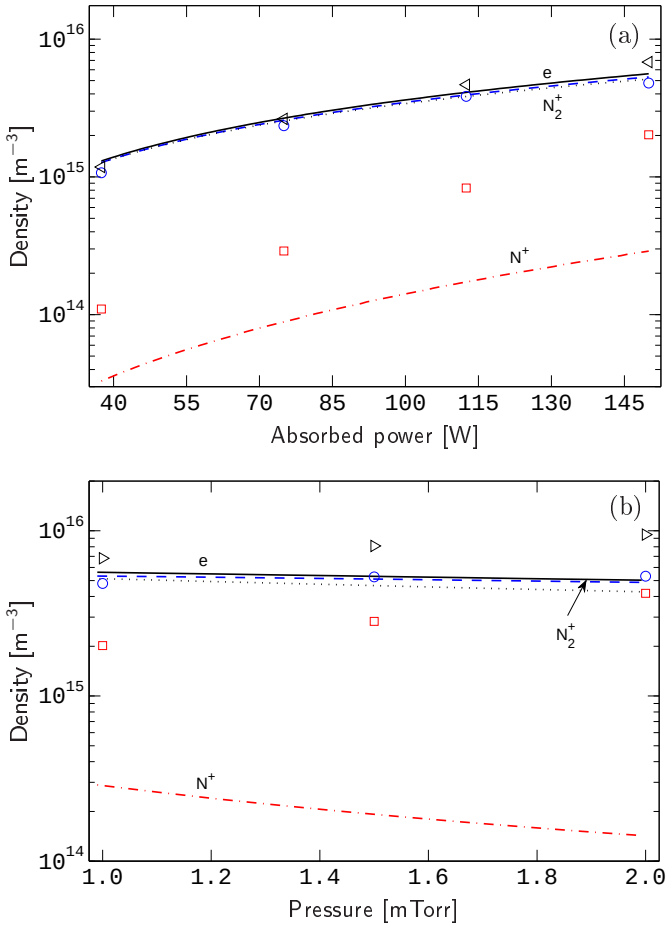

Figure 4.5: Calculations and measurements of the density of ions and electrons as (a) a function of absorbed power with the pressure fixed at 1 mTorr and (b) as a function of pressure with the absorbed power fixed at 150 W. The circles, squares and triangles are ○ the N_2^+ density, □ the N^+ density and ▷ the electron density measured by Cho et al. (2001). The dotted lines represent the calculation when vibrationally excited ground state nitrogen molecules, $N_2(X^1\Sigma_g^+, v = 1-6)$, are excluded. The rf-power reported for the measurement was scaled down 25% to roughly correspond to the absorbed power used in the calculation. The gas flow rate was assumed to be 50 sccm. The discharge chamber had the dimensions $R = 25$ cm and $L = 56$ cm.

total rf-power was specified, and therefore we will assume a 75 % power coupling efficiency to obtain the absorbed power to use in the calculation. The calculated electron density is in good agreement with the measurement, as can be seen in figure 4.6(a). The agreement is best at the highest absorbed power, but slightly worse at lower power. Excluding $N_2(X^1\Sigma_g^+, v = 1-6)$ has a considerable effect on the electron density, the lower solid line in figure 4.6(a), particularly as the absorbed power is increased, although it is still in relatively good agreement with the measurement. The measured and calculated electron temperature, compared in figure 4.6(b), are in good agreement as well. As in figure 4.1(b), excluding $N_2(X^1\Sigma_g^+, v = 1-6)$ in the calculations has no effect on the electron temperature.

Biloiu et al. (2007a) measured the dissociation fraction in a helicon discharge chamber with a 15 cm diameter and 30 cm length. A single value of 13 % was reported when the discharge was operating in H-mode with a 10 mTorr discharge pressure 500 W total rf-power. Using an absorbed power of 375 W and a gas flowrate of 50 sccm in the calculation, we found exactly the same value for the dissociation fraction, 13 %. This indicates that there is a disagreement between different measurements of the atomic density or dissociation fraction. In an inductively coupled discharge with a low aspect ratio, Czerwiec et al. (2005) found a dissociation fraction of up to 70 %, showing that the high dissociation fraction predicted by our model is not unheard of experimentally. Biloiu et al. (2007b) reported on a similar value when applying the same method, as was used to find the aforementioned 13 % value, to the data given by Czerwiec et al. (2005), showing the similarity of the methods.

Nakano et al. (2002) measured the electron density, electron temperature and the dissociation fraction in an inductively coupled plasma as a function of pressure and power. The electron density was almost one order of magnitude larger

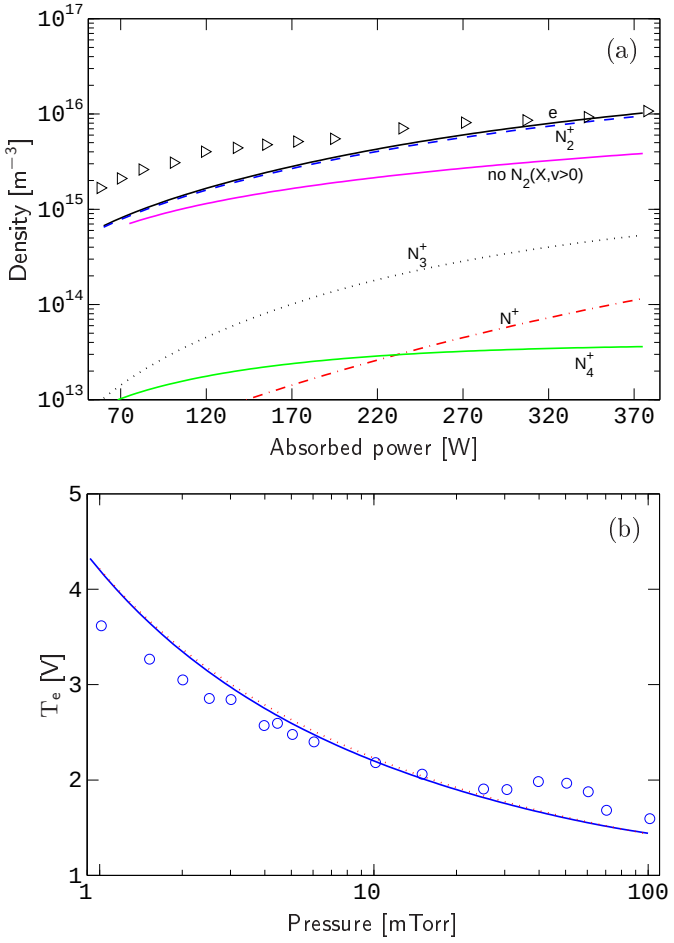

Figure 4.6: Calculations and measurements of (a) the electron density as a function of absorbed power with the pressure fixed at 15 mTorr and (b) the electron temperature as a function of pressure with the absorbed power fixed at 450 W. In (a), the triangles ▷ are the electron density measured by Zhu and Pu (2008) and the lower solid line is the electron density calculated with all vibrationally excited ground state nitrogen molecules, $N_2(X^1\Sigma_g^+, v = 1-6)$, excluded. In (b), the circles ○ are the electron temperature measured by Zhu and Pu (2008) and the dotted line, nearly indistinguishable from the solid line, is the electron temperature calculated while excluding $N_2(X^1\Sigma_g^+, v = 1-6)$. The total rf-power reported for the measurement was scaled down 25% to roughly correspond to the absorbed power used in the calculation. The gas flow rate was assumed to be 50 sccm. The discharge chamber had the dimensions $R = 30$ cm and $L = 40$ cm.

than our corresponding calculations, although the calculation and measurement exhibited similar behavior with absorbed power and discharge pressure. The electron temperature in the measurement was of similar value and had a similar trend with pressure as the electron temperature given by our calculation, although the measured electron temperature showed significant variation with absorbed power instead of being constant with power as we anticipated. The measured dissociation fraction increases with increasing power as in the calculations, but is almost constant with pressure instead of increasing rapidly with decreasing pressure as predicted by our model. The dissociation fraction is significantly lower than our calculations as well, being anywhere between 2 and 13 times lower. It is apparent that our model is not in particularly good agreement with the measurements by Nakano et al. (2002), but given the the peculiar power dependence of the electron temperature we feel these measurements are not as reliable as the other measurements. Nevertheless, the measurement of the dissociation fraction is one more indication of the atomic density being overestimated by our model.

Kitajima et al. (2008) measured the dissociation fraction in an inductively coupled discharge. Since the dimensions of the chamber were not specified for the measurement we were not able to compare the result to our calculations. The measured dissociation fraction was smaller than what is normally observed, always being less than 1 %. However, the trend of the measured dissociation fraction data is in agreement with the behavior normally observed in the calculations, increasing with increasing power and decreasing with increasing pressure.

Shin et al. (2008) measured the dissociation fraction, electron temperature and the electron density in a inductively coupled discharge. The dissociation fraction was measured by two different methods, yielding vastly different results. The dissociation fraction found by mass spectroscopy was very large, even exceeding the

value predicted by our model for the same chamber and conditions, and increased significantly with pressure rather than decreasing as predicted by our model. The dissociation fraction measured by actinometry was about an order of magnitude lower than the other measurement and decreased with increasing power. This is in contrast to other measurements and our calculations that predict that the dissociation fraction increases with absorbed power. Furthermore, the two measurements are not consistent with each other with regards to their behavior with pressure and power. The dissociation fraction we calculated for the same chamber and conditions lies somewhere between the two measurements, being somewhat closer to the optical measurement. The measured electron density was significantly smaller than predicted by our calculations, although exhibiting the expected behavior with power. The measured electron temperature decreased slightly with increasing power, but otherwise had a value close to what predicted by our model.

Given the relatively good agreement of the calculations with all the measurements in figures 4.1(a), 4.5(a), 4.5(b) and 4.6(a), the model seems to describe the electron density quite well. There is also a relatively good agreement with the electron temperature measurements in figures 4.1(b) and 4.6(b). The disagreement of calculations and measurements for the neutral atom density shown in figures 4.2(a) and 4.3(a) indicates that the model overestimates the density of neutral atoms considerably. However, we believe that the low dissociation fraction and relatively large $[N^+]/[N_2^+]$ ratio reported by measurements are contradictory, preventing us from concluding that the model is actually overestimates the atomic density. The calculated density of the metastable $N_2(A^3\Sigma_u^+)$ seems to be a bit too large in comparison to the measurements shown in figures 4.3(b) and 4.4, although the two measurements do not agree on the dependence of pressure.

4.2 Densities and electron temperature

The reactor chamber was assumed to be cylindrical with a 20 cm diameter and a 10 cm length. The absorbed power was fixed at 500 W, the discharge pressure at 10 mTorr and the gas flow rate at 50 sccm. The steady state calculation results are summarized in figures 4.7 to 4.15 as a function of absorbed power, discharge pressure, gas flowrate, electron energy distribution function, gas temperature, wall quenching coefficient, wall recombination coefficient, chamber radius and chamber length. Each of the figures consists of four parts. In figure (a) the density of the neutrals are displayed as a function of the varying parameter. The densities of $N_2(X^1\Sigma_g^+, v = 2-5)$ always lie between the densities of $N_2(X^1\Sigma_g^+, v = 1)$ and $N_2(X^1\Sigma_g^+, v = 6)$, generally equally spaced. Thus, it serves no purpose to display them specifically in the already somewhat crowded figure (a). In figure (b) the electron density and the densities of each ion are shown. The density of the ion N_4^+ is sometimes so low that only show parts of it are shown. In figure (c) the dissociation fraction and the fraction of N^+ of the total ion density are shown with the scale on the left axis. On the right axis we show the ratio of the neutral N atom flux versus the positive ion flux in the axial direction, i.e.

$$\frac{\Gamma_N}{\Gamma_i} = \frac{\frac{1}{4} v_N n_N}{u_{B,i} n_i h_L} \tag{4.1}$$

where v_N, $u_{B,i}$ and h_L are given by equations (2.4), (2.2) and (2.11), respectively. Note that only the dissociation and ion fraction are in %, whereas the flux ratio is generally much larger than 1 and is therefore shown on a different scale, although sometimes incidentally equal to the left axis scale. In figure (c) the electron temperature and the corresponding collisional energy loss, $\mathcal{E}_c$, are shown.

4.2.1 Absorbed power

The atomic density increases significantly with absorbed power as can be seen in figure 4.7(a). When the absorbed power is less than 100 W the atomic density is negligible, whereas at 2000 W the discharge is essentially atomic with atomic radicals representing roughly 65 % of the total neutral density. The fraction of excited species increases significantly as well, although not as rapidly. The vibrational level of the ground state molecule has an order of magnitude lower density than the $N_2(X^1\Sigma_g^+, v = 0)$ at low power, whereas at high power the difference

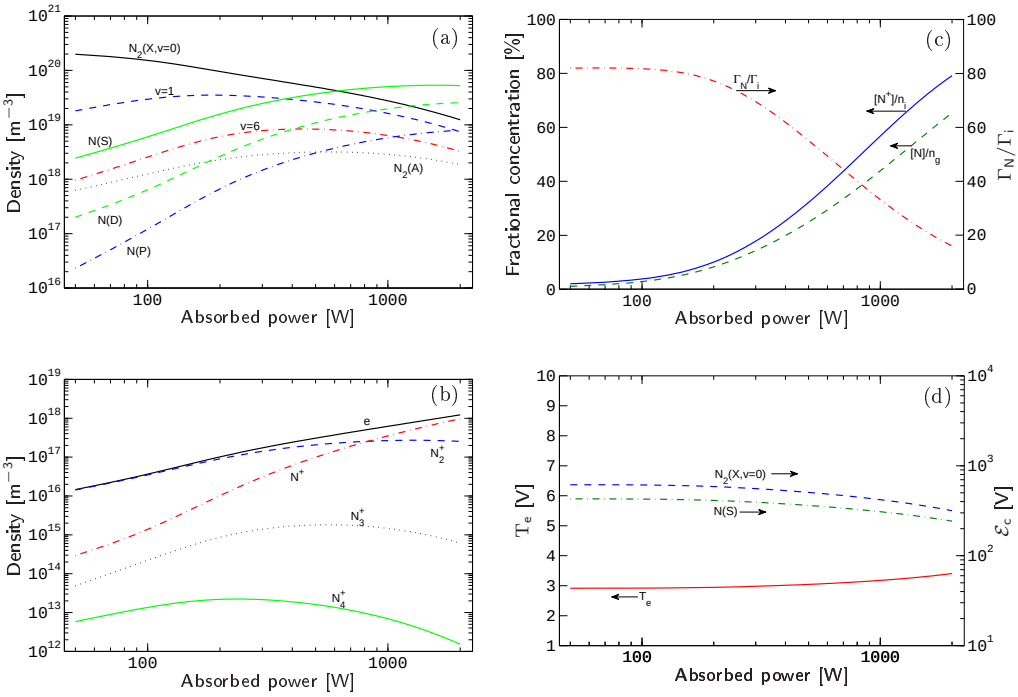

Figure 4.7: The plasma parameters as a function of absorbed power for the steady state discharge. (a) the densities of neutral species, (b) the densities of charged species, (c) the dissociation fraction $[N]/n_g$, the fraction of the N^+ ion of the total ion density $[N^+]/n_i$, the ratio of the neutral N atom flux versus the positive ion flux in the axial direction Γ_N/Γ_i and (d) the electron temperature and the collisional energy loss of $N_2(X^1\Sigma_g^+, v = 0)$ and $N(^4S)$.

is less than a factor of 2. The density of the metastable $N_2(A^3\Sigma_u^+)$ is relatively constant with absorbed power, but peaks at roughly 600 W. It is a significant part of the total molecular density at high absorbed power, being roughly 10 % of the $N_2(X^1\Sigma_g^+, v = 0)$ density at 2000 W, but is less important at low power. The density of the metastable atom $N(^2D)$ is similarly insignificant at low power, but increases to be roughly half the $N(^4S)$ density at 2000 W. At this high power even the metastable atom $N(^2P)$ is comparable to that of the ground state nitrogen molecule $N_2(X^1\Sigma_g^+, v = 0)$, which really puts into perspective how atomic the discharge is at these conditions.

The electron density increases near linearly with power, as can be seen in figure 4.7(b). The N_2^+ ion is the dominating ion below roughly 800 W absorbed power, with the atomic ion N^+ having a higher density at higher absorbed power. The densities of the N_3^+ and N_4^+ ions peak at roughly 600 W and 250 W, respectively, and represent a negligible part of the total ion density, irrespective of power.

The fraction of N^+ ions in the total ion density is similar to the dissociation fraction and has the same basic behavior with power, as can be seen in figure 4.7(c), although it increases more rapidly. The ratio of the neutral atomic flux versus the total ion flux in the axial direction increases rapidly with decreasing power, but saturates at roughly 80 for absorbed power below 150 – 200 W. At 2000 W the ratio is roughly 16.

The electron temperature in figure 4.7(d) shows only a very small variation with power, varying from 2.9 to 3.4 V when the power is varied from 50 – 2000 W. This is a well known characteristic that we can now confirm is no different in the nitrogen discharge model. The collisional energy loss decreases somewhat with increasing absorbed power, varying from 620 – 320 V for the molecule and 430 – 240 V for the atom for absorbed power in the range 50 – 2000 W.

4.2.2 Discharge pressure

As can be seen from figure 4.8(a), the density of the $N_2(X^1\Sigma_g^+, v = 0)$ increases almost linearly with pressure as the atomic density peaks at intermediate pressure. The vibrationally excited ground state molecules are a negligible part of the overall molecular density at low pressures, but increase such that at 100 mTorr the $N_2(X^1\Sigma_g^+, v = 1)$ density is comparable to the $N_2(X^1\Sigma_g^+, v = 0)$ density and the $N_2(X^1\Sigma_g^+, v = 6)$ is only a factor of 3 lower. The density of the metastable atoms is similarly closer to the ground state atom density at higher pressure, but

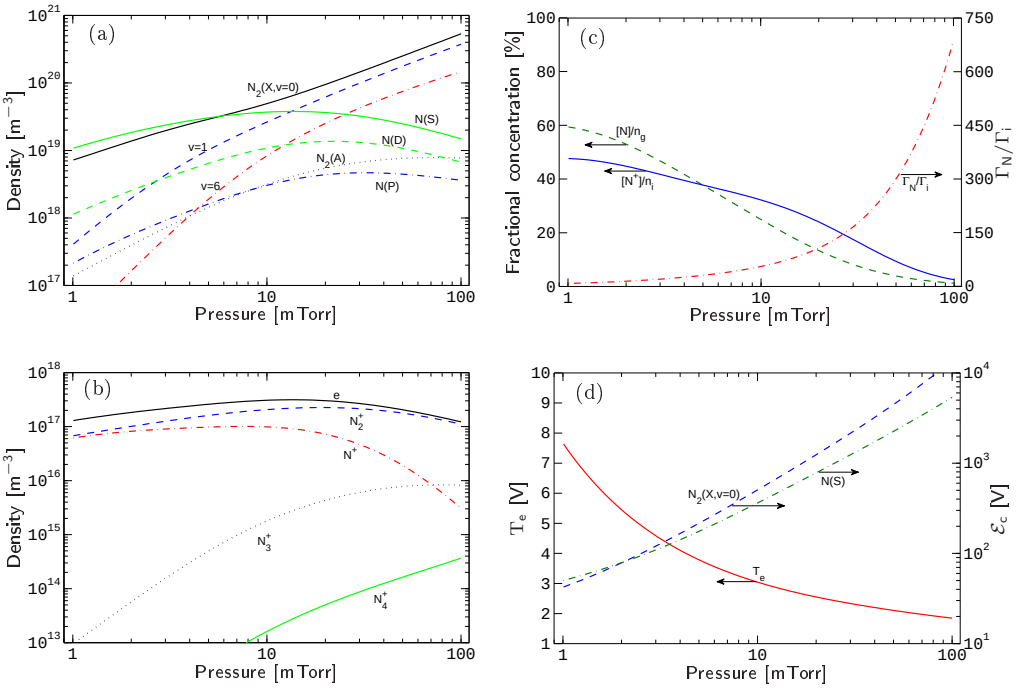

Figure 4.8: The plasma parameters as a function of discharge pressure for the steady state discharge. (a) the densities of neutral species, (b) the densities of charged species, (c) the dissociation fraction $[N]/n_g$, the fraction of the N^+ ion of the total ion density $[N^+]/n_i$, the ratio of the neutral N atom flux versus the positive ion flux in the axial direction Γ_N/Γ_i and (d) the electron temperature and the collisional energy loss of $N_2(X^1\Sigma_g^+, v = 0)$ and $N(^4S)$.

are negligible at low pressure.

The electron density, shown in figure 4.8(b), is relatively constant with pressure, but peaks at roughly 10 – 15 mTorr. The N_2^+ is the dominating ion at intermediate and high pressures, but is comparable to the N^+ density at lower pressure, although slightly larger. The density of the N^+ ion decreases so rapidly with pressure that the N_3^+ ion has a larger density above 70 mTorr. At 100 mTorr the N_3^+ ion represents roughly 10 % of the total ion density. The density of the N_4^+ ion increases rapidly with pressure as well, but is still an insignificant part of the total ion density at 100 mTorr.

The dissociation fraction, shown in figure 4.8(c), is large at low pressure, roughly 60 % at 1 mTorr, but decreases so rapidly with pressure that it is just above 1 % at 100 mTorr. The fraction of the N^+ ion has a similar behavior to the dissociation fraction, the two curves never being considerably different in magnitude, although the N^+ fraction decreases slower than the dissociation fraction when the pressure is below 10 mTorr and decreases faster at higher pressure. The fraction of neutral atomic flux versus total ionflux in the axial direction depends very strongly on pressure, from being about 8 at 1 mTorr to almost 700 at 100 mTorr.

The electron temperature and the corresponding collisional energy loss are shown in figure 4.8(d). The electron temperature is strongly affected by pressure, as already demonstrated in figures 4.1(b) and 4.6(b), being larger than 7 V at 1 mTorr and only 2 V at 100 mTorr. The collisional energy loss, inversely dependent on the electron energy, meanwhile increases significantly with pressure, from about 40 V at 1 mTorr to roughly 13.5 kV at 100 mTorr for the molecule.

4.2.3 Gas flow into the chamber

The gas flowrate has a relatively small effect on the neutral densities, shown in figure 4.9(a), particularly in comparison with the effect of absorbed power and pressure. In fact, when the flowrate is below 100 sccm all the densities are practically constant. As the gas flowrate is increased to 1000 sccm, the density of $N_2(X^1\Sigma_g^+, v = 0)$ increases considerably on account of the atomic density which decreases by approximately a factor of 2. Even at 1000 sccm, the densities of the vibrationally excited ground state molecules $N_2(X^1\Sigma_g^+, v = 1-6)$ and the metastable molecule $N_2(A^3\Sigma_u^+)$ have changed very insignificantly.

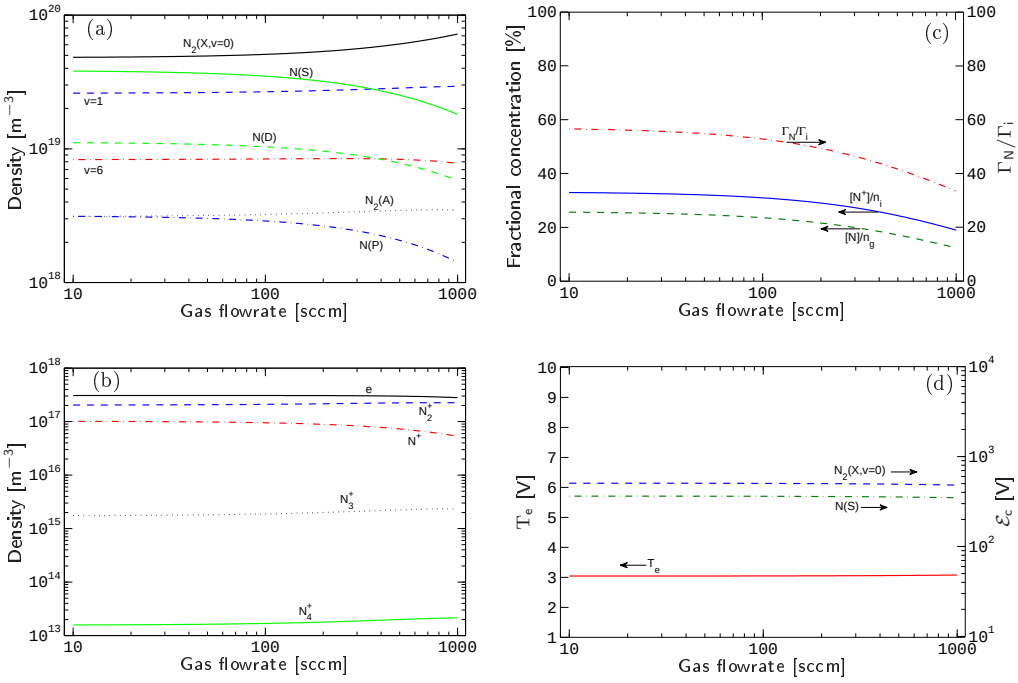

Figure 4.9: The steady state results as a function of gas flowrate. (a) the densities of neutral species, (b) the densities of charged species, (c) the dissociation fraction $[N]/n_g$, the fraction of the N^+ ion of the total ion density $[N^+]/n_i$, the ratio of the neutral N atom flux versus the positive ion flux in the axial direction Γ_N/Γ_i and (d) the electron temperature and the collisional energy loss of $N_2(X^1\Sigma_g^+, v = 0)$ and $N(^4S)$.

The density of charged species is shown in figure 4.9(b). The electron density is essentially independent of the gas flowrate, only decreasing slightly when the density of the atomic ion decreases above 100 sccm. The density of N_2^+ changes very little with gas flow, growing only slightly when the gas flowrate is increased to 1000 sccm. The densities of the ions N_3^+ and N_4^+ are not affected as well, being negligible.

The dissociation fraction is practically constant when the gas flow is less than 100 sccm, as can be seen in figure 4.9(c), but decreases significantly when it is increased to 1000 sccm, or roughly by a factor of 2. The behavior of the N^+ ion fraction is almost identical, simply being several percent above the dissociation fraction. The flux ratio also decreases by less than a factor of two, being roughly 57 at 10 sccm and 33 at 1000 sccm, the majority of this variation occurring above 100 sccm.

The electron temperature, shown in figure 4.9(d), is simply independent of the gas flow rate, being constant at roughly 3 V. The collisional energy loss is therefore almost constant as well, being roughly 500 V for the molecule and 350 V for the atom.

It is apparent that the gas flowrate is not a very effective control parameter in the current study. Its effect is particularly weak in comparison to the effect of pressure or absorbed power. Since the majority of the measurements we compared to our calculations in section 4.1 did not specify the gas flowrate, the assumption of 50 sccm is likely sufficiently accurate, with the gas flowrate having such a little effect on the results as demonstrated in figure 4.9.

4.2.4 Electron energy distribution function

The neutral densities are not significantly affected by the electron energy distribution function, as seen in figure 4.10(a). In fact, the $N_2(A^3\Sigma_u^+)$ density is almost constant with x. The densities of $N_2(X^1\Sigma_g^+, v = 1)$ and $N(^4S)$ decrease only slightly when the distribution function is varied from Maxwellian to Druyvesteyn by varying the parameter x in equation (2.13). The densities of $N(^2D)$ and $N(^2P)$ decrease by roughly a factor of 2. The most significant decrease is the density

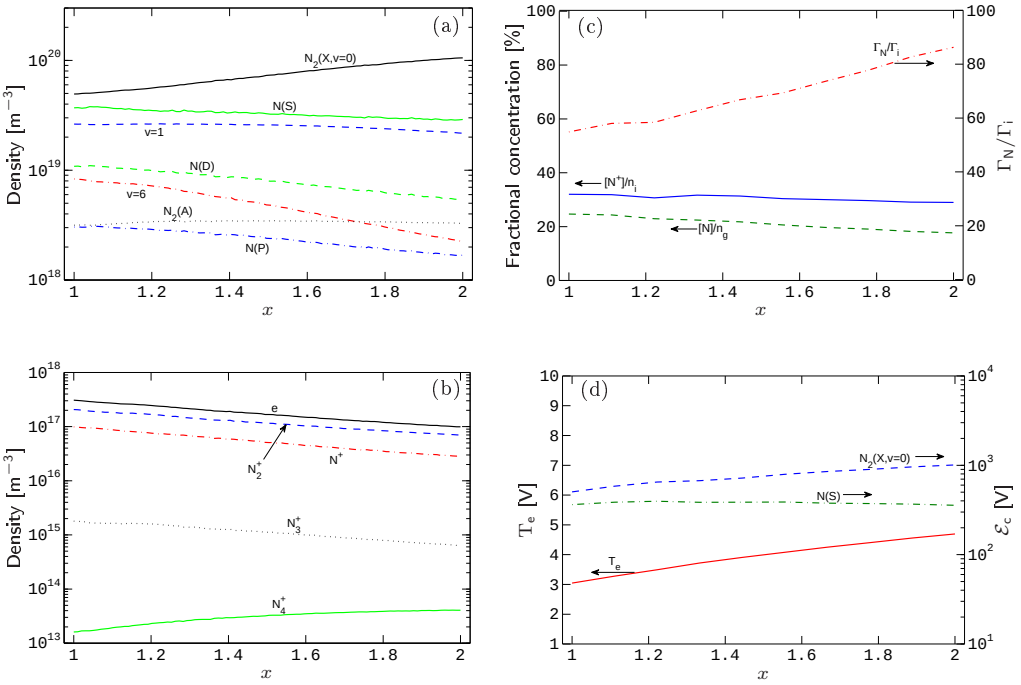

Figure 4.10: The plasma parameters for the steady state discharge versus the electron energy distribution function, varying from Maxwellian-like ($x = 1$) to Druyvesteyn ($x = 2$) distribution function according to equation (2.13). (a) the densities of neutral species, (b) the densities of charged species, (c) the dissociation fraction $[N]/n_g$, the fraction of the N^+ ion of the total ion density $[N^+]/n_i$, the ratio of the neutral N atom flux versus the positive ion flux in the axial direction Γ_N/Γ_i and (d) the electron temperature and the collisional energy loss of $N_2(X^1\Sigma_g^+, v = 0)$ and $N(^4S)$.

of $N_2(X^1\Sigma_g^+, v = 6)$ which decreases by roughly a factor of 4. All of the density decreases seem to accumulate in the $N_2(X^1\Sigma_g^+, v = 0)$, its density increasing considerably with increasing x, or roughly by a factor of 2.

The electron density, shown in figure 4.10(b), decreases significantly with varying electron energy distribution function, being roughly a factor of 3 lower with a Druyvesteyn distribution than with a Maxwellian distribution. The densities of the N_2^+, N^+ and N_3^+ ions behave similarly with increasing x, their ratio not changing significantly with x. However, the density of the N_4^+ ion increases somewhat with x, although its density is negligible.

The fractional concentration of atomic neutrals and ions does not change significantly with electron energy distribution function, as seen in figure 4.10(c). The dissociation fraction decreases from roughly 25 % to 18 %, while the N^+ ion fraction is almost independent of the electron energy distribution function, roughly 30 %. The flux ratio changes relatively subtly as well, increasing from 55 to 86 with increasing x.

The effect of the electron energy distribution function on the electron temperature is more pronounced, as seen in figure 4.10(d), increasing from roughly 3 V with a Maxwellian distribution to 4.7 V with a Druyvesteyn distribution. The collisional energy loss does not exhibit the usual inverse behavior with the electron temperature, but rather increases with increasing x as the electron temperature. The collisional energy loss increases from roughly 500 V to 1000 V for the molecule, whereas is is almost independent of x for the atom, being fixed at roughly 360 V.

4.2.5 Gas temperature

Although the gas temperature is not considered a control parameter, it is important to see the effect of incorrectly assuming its value. The neutral densities, shown in figure 4.11(a), all decrease with increasing gas temperature. This is a normal behavior since, according to the ideal gas law, the densities are inversely proportional to the gas temperature when the pressure is kept constant. The densities of excited atoms and molecules decrease significantly faster than of ground state atoms and molecules, the decrease of the $N_2(X^1\Sigma_g^+, v = 6)$ density being the most

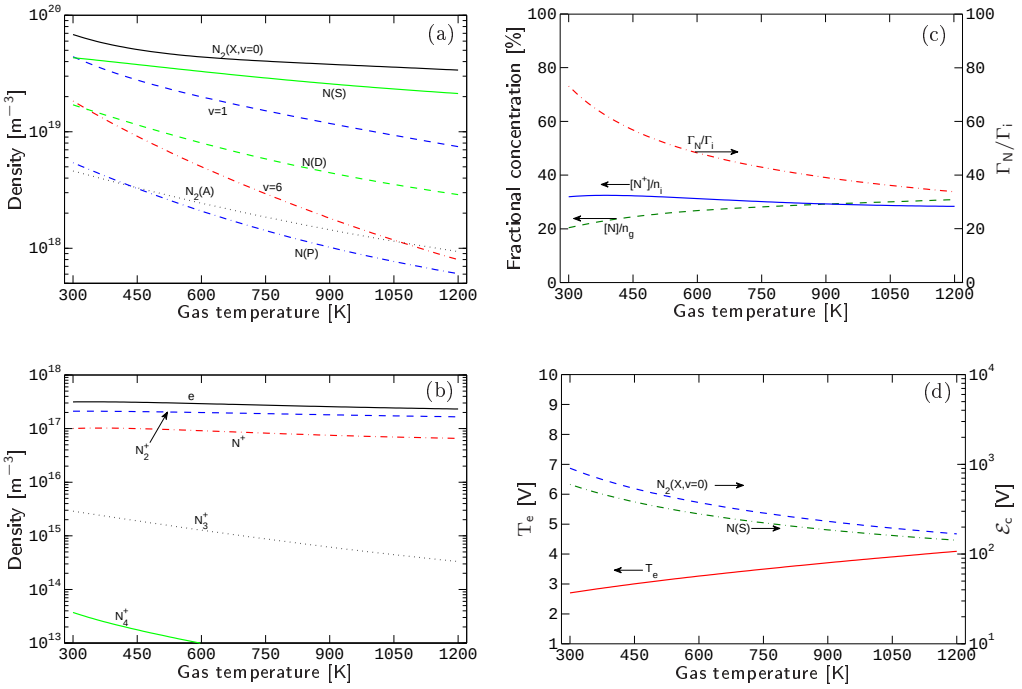

Figure 4.11: The steady state results as a function of the gas temperature. (a) the densities of neutral species, (b) the densities of charged species, (c) the dissociation fraction $[N]/n_g$, the fraction of the N^+ ion of the total ion density $[N^+]/n_i$, the ratio of the neutral N atom flux versus the positive ion flux in the axial direction Γ_N/Γ_i and (d) the electron temperature and the collisional energy loss of $N_2(X^1\Sigma_g^+, v = 0)$ and $N(^4S)$.

significant, being roughly 25 times smaller at 1200 K than at 300 K.

In light of the significant drop in neutral density with gas temperatures it is quite surprising to see that the densities of the corresponding ions are nearly independent of the gas temperature, as seen in figure 4.11(b). The electron density is therefore almost constant with gas temperature as well. Since the N_3^+ and N_4^+ ions are not created by electron impact as the other ions, their density drops with the neutral density and therefore the gas temperature, although both of these ions, in particular the N_4^+, are negligible in the discharge for any gas temperature.

As seen in figure 4.11(c), the dissociation fraction changes somewhat with gas temperature, from roughly 20 % at 300 K to about 31 % at 1200 K. The fraction of the N^+ ion is however roughly constant, only decreasing slightly with gas temperature from 32 % at 300 K to 28 % at 1200 K. The atom/ion flux ratio decreases by over a factor of 2 with increasing gas temperature, being roughly 73 at 300 K and 34 at 1200 K. This is a much more significant change than implied by the dissociation and N^+ ion fraction.

The electron temperature, shown in figure 4.11(d), increases as the gas temperature is increased, although not proportionally. At 300 K it is roughly 2.7 V, whereas at 1200 K it has increased to about 4.1 V. The collisional energy loss decreases accordingly when the gas temperature is increased from 300 K to 1200 K, from roughly 900 V to 170 V for the molecule and from roughly 600 V to 140 V for the atom.

Neither the electron density nor the dissociation fraction were heavily affected by the gas temperature. The gas temperature may therefore be in a significant error without significantly affecting the results of our model.

4.2.6 Wall quenching coefficient

Although it is possible to only investigate the effect of the quenching coefficient for a specific excited species, such as for the quenching of $N_2(A^3\Sigma_u^+)$ on the wall for example, here we varied the wall quenching coefficient from 0.01 to 1 for all the excited species simultaneously.

As seen in figure 4.12(a), the wall quenching coefficient mainly affects the density of excited species, being quenched more efficiently on the wall when the value increases. The densities of the ground state atoms and molecules increases accord-

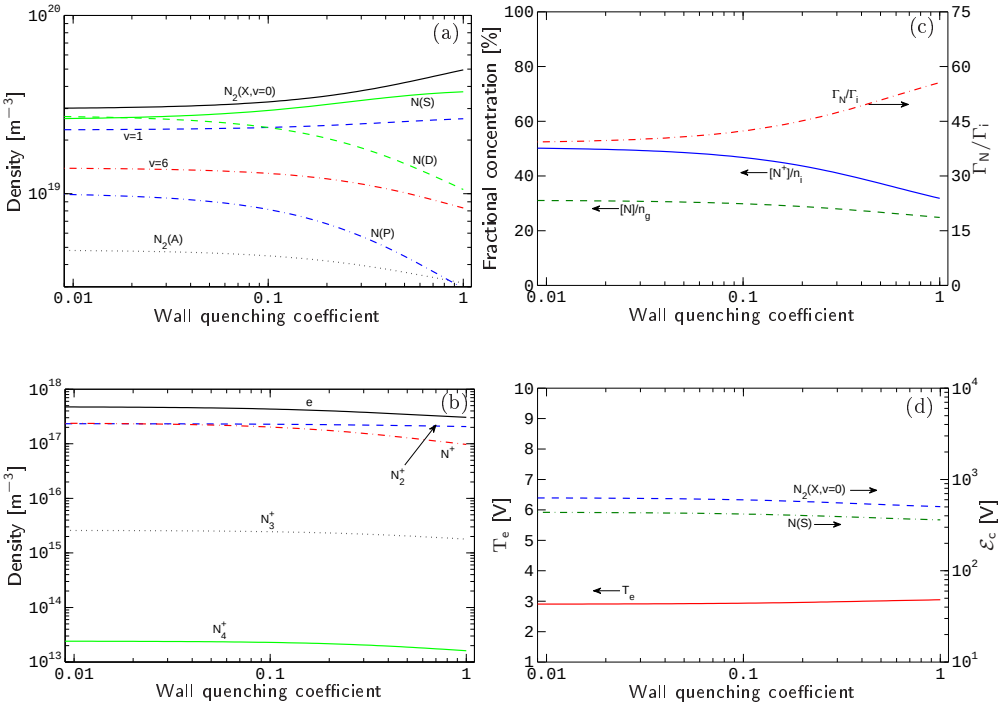

Figure 4.12: The steady state results as a function of the wall quenching coefficient of all excited species. (a) the densities of neutral species, (b) the densities of charged species, (c) the dissociation fraction $[N]/n_g$, the fraction of the N^+ ion of the total ion density $[N^+]/n_i$, the ratio of the neutral N atom flux versus the positive ion flux in the axial direction Γ_N/Γ_i and (d) the electron temperature and the collisional energy loss of $N_2(X^1\Sigma_g^+, v = 0)$ and $N(^4S)$.

ing to the drop in excited species density, the exception being the density of the $N_2(X^1\Sigma_g^+, v = 1)$ which increases slightly with increasing quenching coefficient. Although the wall quenching coefficient has a significant effect on the excited species density when it is varied in the range $0.1 - 1$, wall quenching becomes a negligible loss pathway of excited species when the value is less than 0.1. In fact, although not shown in figure 4.12(a), when the quenching coefficient was in the range 0.001 – 0.01 the densities of the excited species were not affected at all.

Although constant when the wall quenching coefficient is less than 0.1, the electron density decreases slightly with wall quenching coefficient above 0.1, as seen in figure 4.12(b). This decrease is a result of the drop in N^+ density above 0.1, being equal to the N_2^+ density when wall quenching is negligible but a factor of 2 lower when wall quenching is perfectly efficient. Meanwhile, the density of N_2^+ is almost fully independent on the wall quenching coefficient.

The dissociation fraction is almost constant with the wall quenching coefficient, as seen in figure 4.12(d), although decreasing slightly with increased wall quenching, or from roughly 31 % to 25 %. The fraction of the N^+ ion is more significantly affected, decreasing from roughly 50 % to 32 % with increasing wall quenching coefficient. The flux ratio meanwhile increases somewhat with the wall quenching coefficient, the neutral atomic flux being about 39 times larger than the ion flux in the axial direction when wall quenching is negligible, but 56 times larger when wall quenching is efficient.

The electron temperature, shown in figure 4.12(d), increases very subtly with the wall quenching coefficient, being in the range 2.9 V to 3.1 V. The corresponding collisional energy loss decreases insignificantly as well, being roughly $630 - 500$ V for the molecule and $440 - 360$ V for the atom.

4.2.7 Wall recombination coefficient

Although it is possible to investigate the effects of the wall recombination coefficient for a specific neutral atom, here we have varied the wall recombination coefficient from 10^{-3} to 1 for all the neutral atoms simultaneously.

When the recombination coefficient is small the discharge is atomic in nature, with the ground state atom N(^{4}S) density being approximately a factor of 5 larger than the density of the ground state nitrogen molecule $N_2(X^1\Sigma_g^+, v = 0)$, as seen in figure 4.13(a). The molecular density increases with increasing wall recombination

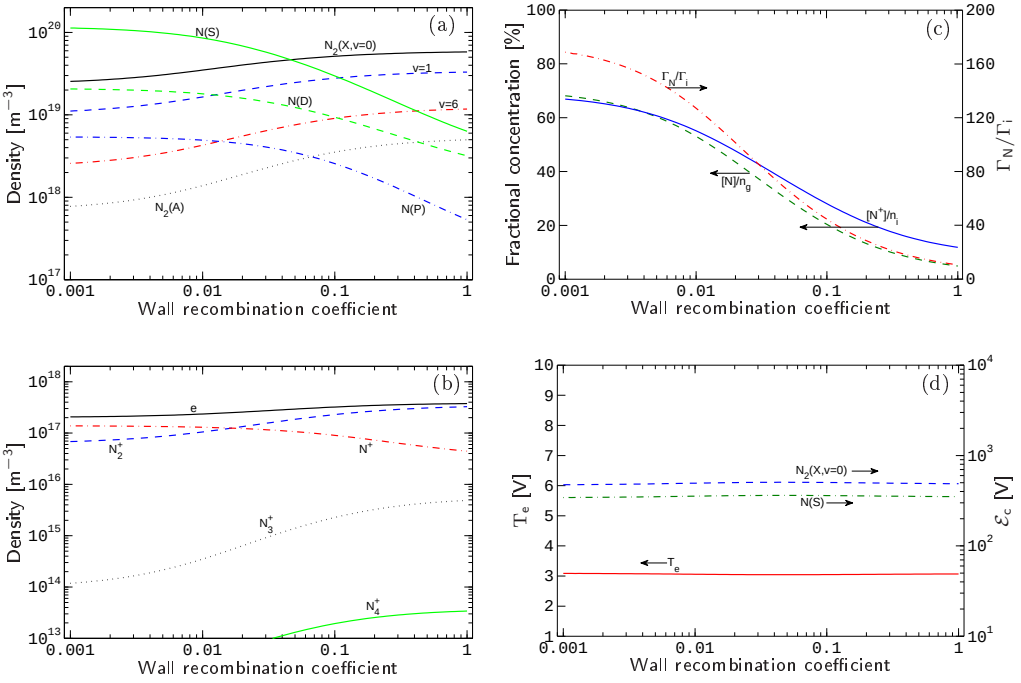

Figure 4.13: The steady state results as a function of the wall recombination coefficient of atoms. (a) the densities of neutral species, (b) the densities of charged species, (c) the dissociation fraction $[N]/n_g$, the fraction of the N^+ ion of the total ion density $[N^+]/n_i$, the ratio of the neutral N atom flux versus the positive ion flux in the axial direction Γ_N/Γ_i and (d) the electron temperature and the collisional energy loss of $N_2(X^1\Sigma_g^+, v = 0)$ and N(^{4}S).

coefficient as the atomic density drops. When the recombination coefficient is larger than roughly 0.05 the density of the $N_2(X^1\Sigma_g^+, v = 0)$ molecule becomes larger than the $N(^4S)$ density. When all atoms bombarding the wall are recombined into molecules the density of the ground state atom is about an order of magnitude lower than of the $N_2(X^1\Sigma_g^+, v = 0)$, being comparable to the $N_2(A^3\Sigma_u^+)$ density. The distribution of most excited species is roughly the same for all values of the wall recombination coefficient, the exception being the $N(^2D)$ metastable atom, whose density is significantly closer to the $N(^4S)$ density when the efficiency of wall recombination is high.

The electron density, shown in figure 4.13(b), increases considerably as the wall recombination coefficient is increased from 0.01 to 1. This is a result of the increased N_2^+ density, which increases as the neutral molecular density increases. The N_2^+ ion is the dominant ion when the wall recombination coefficient is 1, whereas the N^+ ion is the dominant ion in the discharge when wall recombination is inefficient. With the molecular density increasing, the densities of the N_3^+ and N_4^+ ions increase as well, although their density is never above the N^+ density.

The dissociation fraction, shown in figure 4.13(c), is quite sensitive to the wall recombination coefficient, being almost 70 % when the coefficient is 10^{-3} but only roughly 5 % when it is unity. The fractional density of the N^+ ion behaves similarly, decreasing from nearly 70 % to about 12 % with increasing wall recombination coefficient. The flux ratio is also heavily affected, being 170 times the axial ion flux when the wall recombination coefficient is small and only 10 when it is 1.

Although the densities are heavily affected, the electron temperature is independent on the wall recombination coefficient, being fixed at 3.1 V as shown in figure 4.13(d). The collisional energy loss is similarly constant, being about 500 V for the molecule and 350 V for the atom.

4.2.8 Chamber radius

Since the chamber volume and the axial part of the surface area are proportional to the square of the chamber radius, we can expect quite large variation of results when changing this dimension. This is indeed the case with neutral densities, shown in figure 4.14(a). The density of $N_2(X^1\Sigma_g^+, v = 0)$ increases as almost all other densities decrease uniformly with the chamber radius. This is caused by the increased area for wall quenching and wall recombination. The density of $N_2(X^1\Sigma_g^+, v = 1)$ peaks at roughly $15 - 20$ cm, and the $N_2(X^1\Sigma_g^+, v = 6)$ at roughly

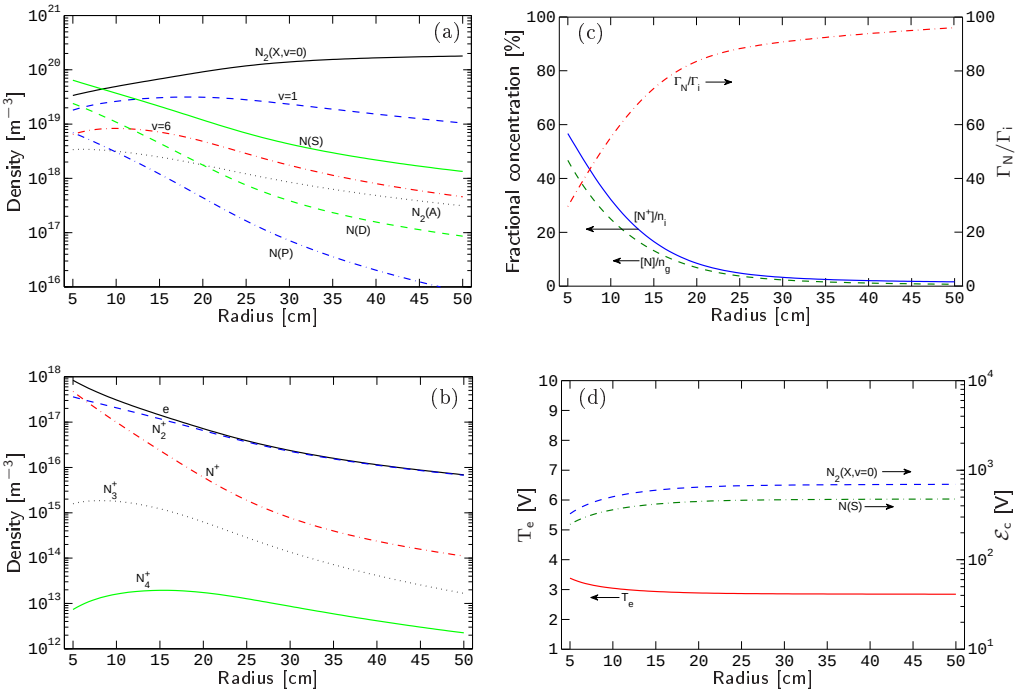

Figure 4.14: The steady state results as a function of the reactor chamber radius. (a) the densities of neutral species, (b) the densities of charged species, (c) the dissociation fraction $[N]/n_g$, the fraction of the N^+ ion of the total ion density $[N^+]/n_i$, the ratio of the neutral N atom flux versus the positive ion flux in the axial direction Γ_N/Γ_i and (d) the electron temperature and the collisional energy loss of $N_2(X^1\Sigma_g^+, v = 0)$ and $N(^4S)$.

10 cm, but are then uniformly decreasing as well. The densities of the metastable atoms $N(^2D)$ and $N(^2P)$ decrease somewhat faster than the $N(^4S)$ density.

The electron density, shown in figure 4.14(b), is heavily affected by an increased radius, falling about 2 orders of magnitude when the radius is increased from 5 cm to 50 cm. This is caused by the increased area for recombination of ions on the wall as the radius increases, effectively losing free electrons from the discharge. Although the N^+ density is comparable to the N_2^+ density when the chamber has a low radius, it falls very sharply when the radius is increased. The density of the N_3^+ ion decreases rapidly with increased radius as well, whereas the N_4^+ density peaks at roughly 15 cm and then decreases less rapidly, although both of these ions are negligible.

The dissociation fraction, shown in figure 4.14(c), decreases rapidly with radius, being nearly 50 % when the radius is 5 cm but less than 1 % when it is 50 cm. Similarly applies to the N^+/n_i fraction, approximately following the dissociation fraction decrease, although being somewhat larger overall. The flux fraction has an inverse behavior to the density fractions, increasing from about 30 to nearly 100 with increasing radius.

Given the strong dependence of the densities of the chamber radius it is peculiar to see in figure 4.14(d) the electron temperature being almost independent of this parameter. The electron temperature is practically constant when the radius is larger than 15 cm, roughly 2.8 V, but increases slightly when the radius is decreased further, being roughly 3.4 V at 5 cm. The same applies to the collisional energy loss, increases from about 330 V to 700 V for the molecule and from roughly 250 V to 480 V for the atom with increasing radius.

4.2.9 Chamber length

Interestingly, several of the neutral densities have a non-uniform behavior with chamber length. The N(^{4}S) density decreases uniformly with increasing chamber length, as seen in figure 4.15(a) The metastable atoms, however, peak at roughly 10 cm, being a negligible part of the total atomic density when the length is 1 cm. The density of the ground state molecule $N_2(X^1\Sigma_g^+, v = 0)$ has a minimum at roughly 15 cm length, whereas the $N_2(X^1\Sigma_g^+, v = 1)$ increases uniformly with length. The $N_2(X^1\Sigma_g^+, v = 6)$ density peaks at roughly 20 – 30 cm, indicating the

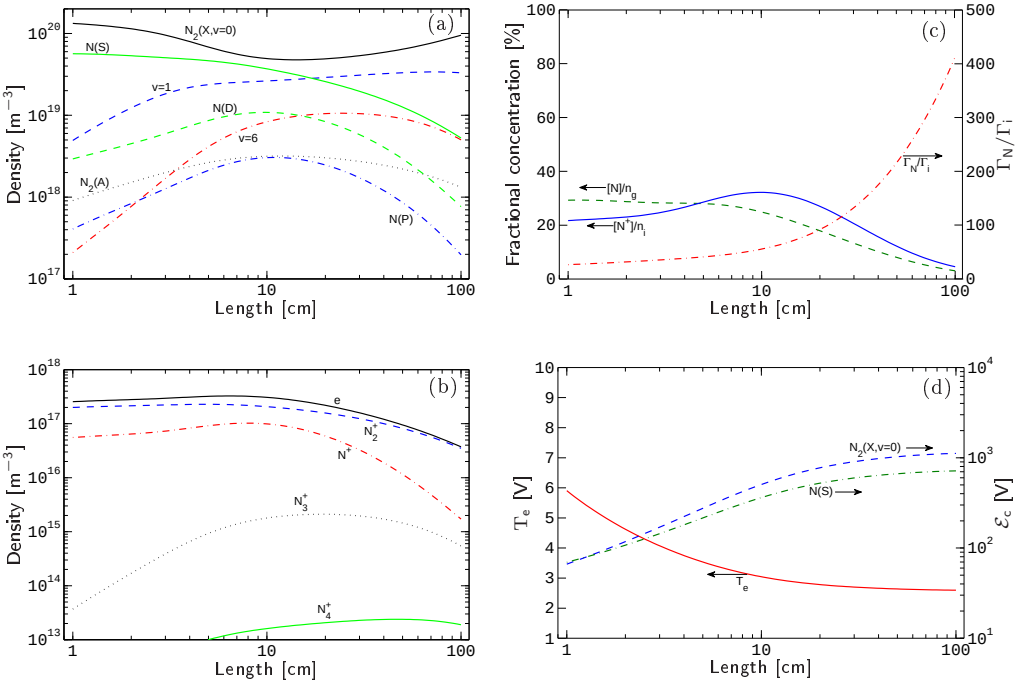

Figure 4.15: The steady state results as a function of the chamber axial length. (a) the densities of neutral species, (b) the densities of charged species, (c) the dissociation fraction $[N]/n_g$, the fraction of the N^+ ion of the total ion density $[N^+]/n_i$, the ratio of the neutral N atom flux versus the positive ion flux in the axial direction Γ_N/Γ_i and (d) the electron temperature and the collisional energy loss of $N_2(X^1\Sigma_g^+, v = 0)$ and N(^{4}S).

peak is at longer length for $N_2(X^1\Sigma_g^+, v < 6)$. When the chamber is 1 cm long the densities of all excited species are very small, most of the discharge being composed of ground state molecules and atoms. When the chamber is 100 cm long the only significant species other than $N_2(X^1\Sigma_g^+, v = 0)$ is the $N_2(X^1\Sigma_g^+, v = 1)$, the atomic density only being comparable to the $N_2(X^1\Sigma_g^+, v = 6)$ density.

The electron density, shown in figure 4.15(b), is quite constant when the chamber length is less than 10 cm, but decreases significantly when the length increases beyond that. The N_2^+ ion is always the dominating ion, with the N^+ density being somewhat lower when the chamber length is less than 10 cm and decreasing rapidly when the length is increased to 100 cm. Although a negligible part of the total ion density, the N_3^+ and N_4^+ densities peak at roughly 20 and 50 cm chamber length.

As seen in figure 4.15(c), the dissociation fraction decreases from roughly 30 % when the chamber is 1 – 10 cm long to 3 % when it is 100 cm long. The fraction of the N^+ ion is roughly 22 % when the chamber is 1 cm long and increases with length until it peaks at 32 % when the length is 10 cm. The N^+ ion fraction then decreases rapidly when the length is increased any further to be roughly 5 % at 100 cm length. The flux ratio is also heavily affected by the chamber length, the neutral atomic flux being 26 times the axial ion flux when the chamber is 1 cm long and increasing rapidly, particularly when the chamber is longer than 10 cm, to be roughly 410 times the axial ion flux when the chamber is 100 cm long.

The electron temperature increases rapidly when the chamber length is decreased from 10 cm to 1 cm, as seen in figure 4.15(d), being about 5.9 V when the chamber is 1 cm long but roughly 2.6 V when it is 100 cm long. The collisional energy increases accordingly with length, being little less than 70 V for both the atom and the molecule when the chamber is 1 cm long, but about 1100 V for the molecule and 700 V for the atom at 100 cm chamber length.

4.3 Reaction Rates

The overall creation and destruction mechanisms of molecules, atoms and electrons are evaluated in figures 4.16, 4.17 and 4.18. The reaction rates for the creation and destruction of every particle, except for $N_2(X^1\Sigma_g^+, v = 2-5)$, are analyzed in figures 4.19 to 4.29 as a function of pressure. In all the calculations, the absorbed power is fixed at 500 W and the gas flow rate is fixed at 50 sccm. The chamber is assumed to be made of stainless steel, cylindrical with radius $R = 10$ cm and length $L = 10$ cm. Furthermore, the electron energy distribution is assumed to be Maxwellian-like ($x = 1$).

The reaction rates for the overall creation and destruction of neutral nitrogen molecules are shown in figures 4.16(a) and (b), respectively. Neutral molecules are mostly created by wall recombination of neutral atoms, the recombination of $N(^4S)$ being responsible for $40-50$ % of the overall molecule creation mechanism. Pumping of $N_2(X^1\Sigma_g^+, v = 0)$ into the chamber has a roughly 40 % contribution at high and low pressure, but is lower at intermediate pressure, roughly 20 %. Wall recombination of N_2^+ is significant at low pressure, but has no more than 25 % contribution at 1 mTorr.

As seen in figure 4.16(b), the pumping of species out of the chamber is responsible for roughly 25 % of the total loss of molecules at low and intermediate pressure, but increases to over 60 % at 100 mTorr. At low pressure the dissociation of $N_2(X^1\Sigma_g^+, v = 0)$ has over 30 % contribution, but at higher pressure the dissociation of $N_2(X^1\Sigma_g^+, v > 0)$ is more important, its contribution reaching a maximum of over 40 % at 20 mTorr. Furthermore, ionization is a significant factor in the overall loss of neutral molecules at low and intermediate pressure, at most roughly 35 % at 1 mTorr.

The reaction rates for the overall creation and destruction of neutral nitrogen

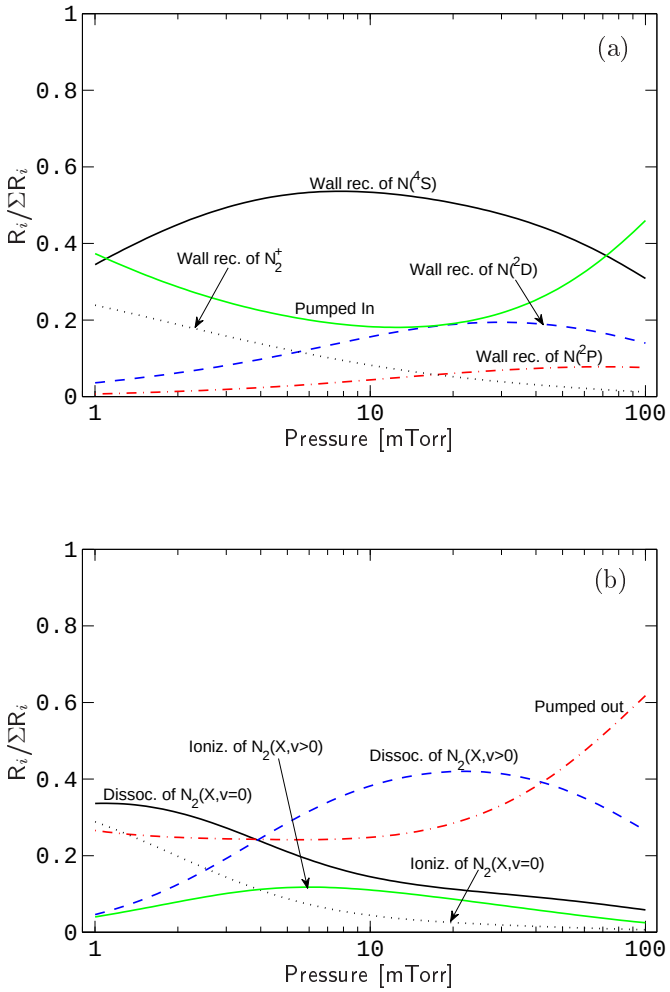

Figure 4.16: The reaction rates for (a) the overall creation and (b) the overall loss of neutral nitrogen molecules versus discharge pressure.

atoms are shown in figures 4.17(a) and (b), respectively. Neutral nitrogen atoms are mostly created by dissociation over the entire pressure range, dissociation of $N_2(X^1\Sigma_g^+, v > 0)$ dominating at intermediate and high pressures. The contribution of dissociation of $N_2(X^1\Sigma_g^+, v = 0)$ is roughly 40 % at 1 mTorr, but decreases and is less than 20 % at 100 mTorr. Wall recombination of N^+ is very important at

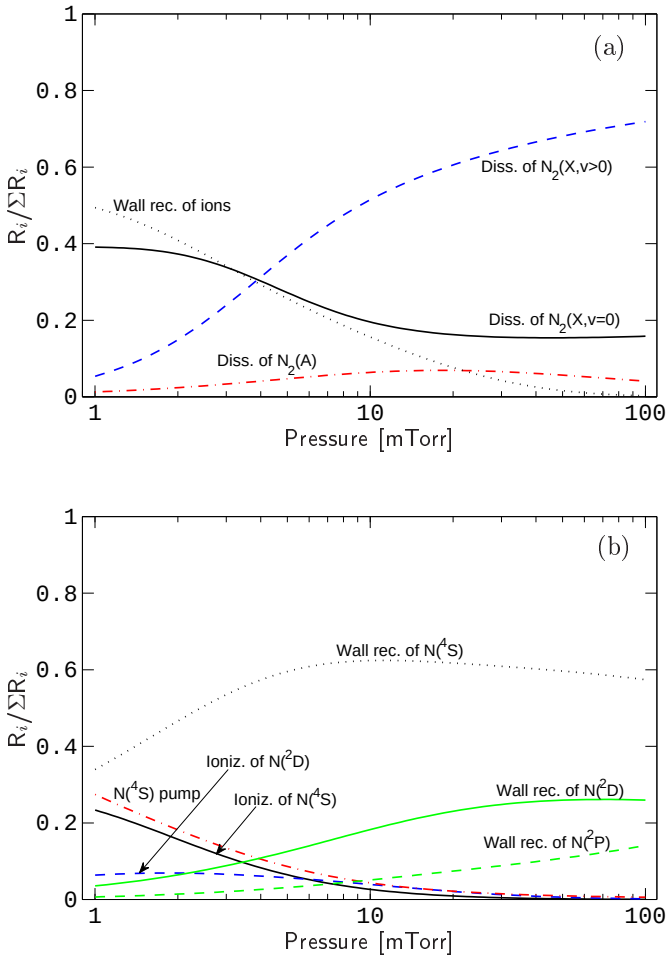

Figure 4.17: The reaction rates for (a) the overall creation and (b) the overall loss of neutral nitrogen atoms versus discharge pressure.

low pressure, having a contribution of roughly 50 % at 1 mTorr, but is negligible at high pressure.

Neutral nitrogen atoms are lost mainly to wall recombination, as shown in figure 4.17(b). Pumping of $N(^4S)$ out of the chamber and ionization of $N(^4S)$ are significant loss processes at low pressure, having a near identical contribution of roughly $20 - 25$ % at 1 mTorr.

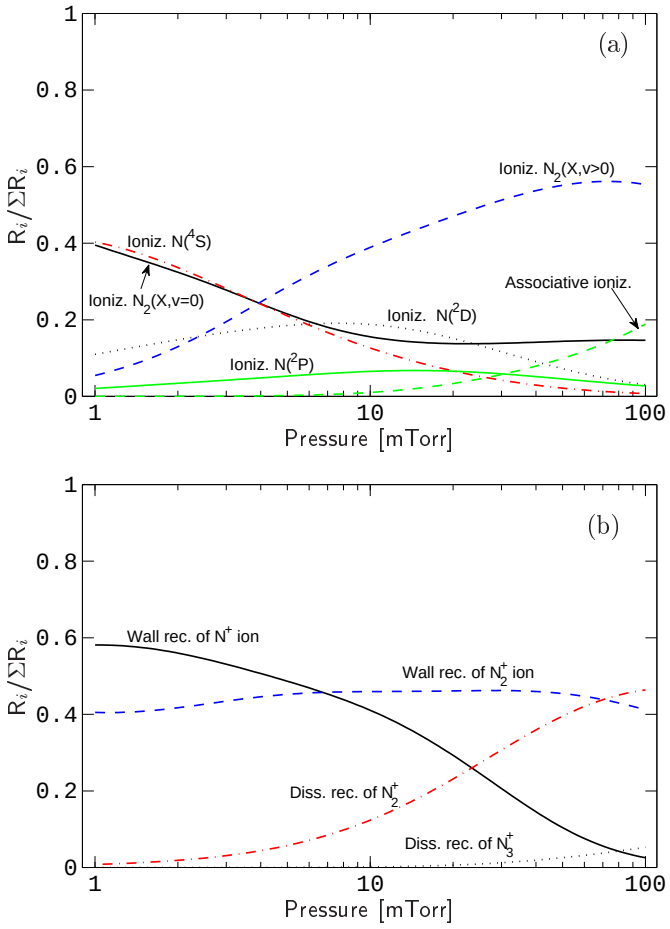

Figure 4.18: The reaction rates for (a) the creation and (b) the loss of free electrons versus discharge pressure.

The reaction rates for the overall creation and destruction of electrons are shown in figures 4.18(a) and (b), respectively. Electron impact ionization is responsible for nearly all creation of free electrons. Ionization of $N_2(X^1\Sigma_g^+, v > 0)$ is the dominating process at intermediate and high pressure. Ionization of $N(^4S)$ and ionization of $N_2(X^1\Sigma_g^+, v = 0)$ have a similar contribution, each contributing roughly 40 % at low pressure, but are much less important at higher pressure. Ionization of $N(^2D)$ is

significant, having $10-20$ % contribution at low and intermediate pressure. Associative ionization of atoms and molecules, reactions (3.52) and (3.53), is significant at high pressure, however the contribution is no more than 20 % at 100 mTorr.

As seen in figure 4.18(b), electrons are mainly lost at the wall, the wall recombination of N^+ being the most important process at low pressure and the wall recombination of N_2^+ having a $40-45$ % contribution over the entire pressure range. Dissociative recombination of N_2^+ has a significant contribution at high pressure, reaching roughly 50 % at 100 mTorr. Dissociative recombination of N_3^+ has a slight contribution at 100 mTorr, less than 5 %, but is negligible otherwise.

The reaction rates for the creation and destruction of $N_2(X^1\Sigma_g^+, v=0)$ are shown in figures 4.19(a) and (b), respectively. The wall quenching of vibrational and metastable states of N_2 is responsible for most of the creation of $N_2(X^1\Sigma_g^+, v=0)$ at intermediate pressure, with its contribution peaking at $3-4$ mTorr. At higher pressure electron impact de-excitation is more important, being roughly 70% at 100 mTorr. At low pressure the recombination of ions and atoms and pumping of gas into the chamber are the most important processes for the creation of $N_2(X^1\Sigma_g^+, v=0)$, each having a contribution of about $20-30$% at 1 mTorr.

As seen in figure 4.19(b), the $N_2(X^1\Sigma_g^+, v=0)$ is mainly lost to electron impact excitation at intermediate and high pressures, whereas dissociation, ionization and pumping are the most important destruction processes at low pressure.

The reaction rates for the creation and destruction of $N_2(X^1\Sigma_g^+, v=1)$ are shown in figures 4.20(a) and (b), respectively. The $N_2(X^1\Sigma_g^+, v=1)$ is mainly created by electron impact excitation of the $N_2(X^1\Sigma_g^+, v=0)$, contributing around 50 % over the entire pressure range. Electron impact de-excitation of $N_2(X^1\Sigma_g^+, v>1)$ and wall quenching of $N_2(X^1\Sigma_g^+, v=2)$ are responsible for the rest at high and low pressure, respectively.

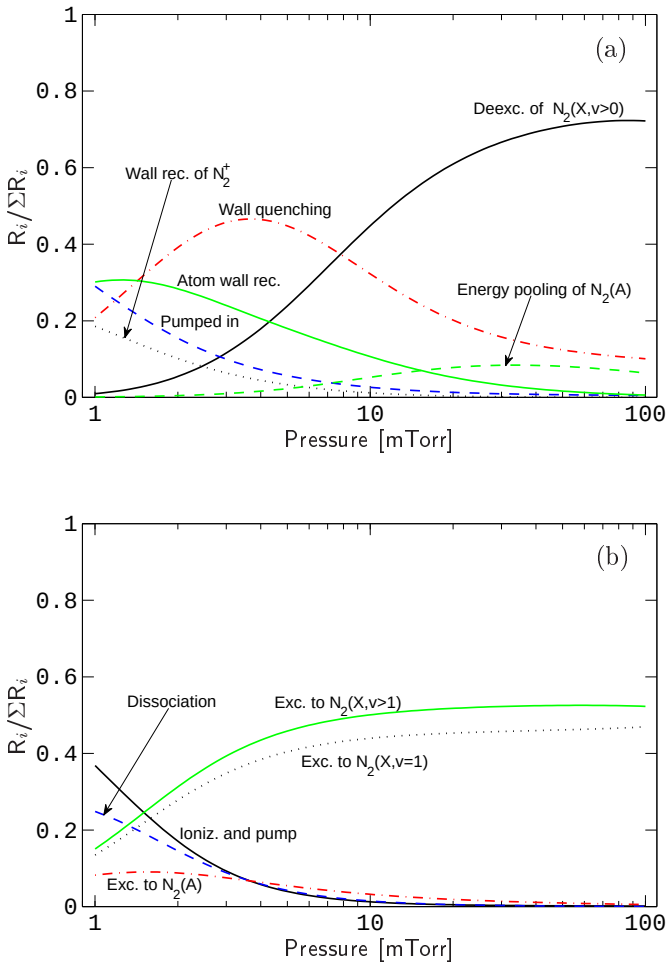

Figure 4.19: The reaction rates for (a) the creation and (b) the destruction of the $N_2(X^1\Sigma_g^+, v = 0)$ molecule versus discharge pressure.

As seen in figure 4.20(b), $N_2(X^1\Sigma_g^+, v = 1)$ is mainly lost by wall quenching at low pressure and by electron impact excitation and de-excitation at higher pressure. Ionization, pumping and dissociation have a small contribution, at most roughly 15% combined at 1 mTorr.

The reaction rates for the creation and destruction of $N_2(X^1\Sigma_g^+, v = 6)$ are

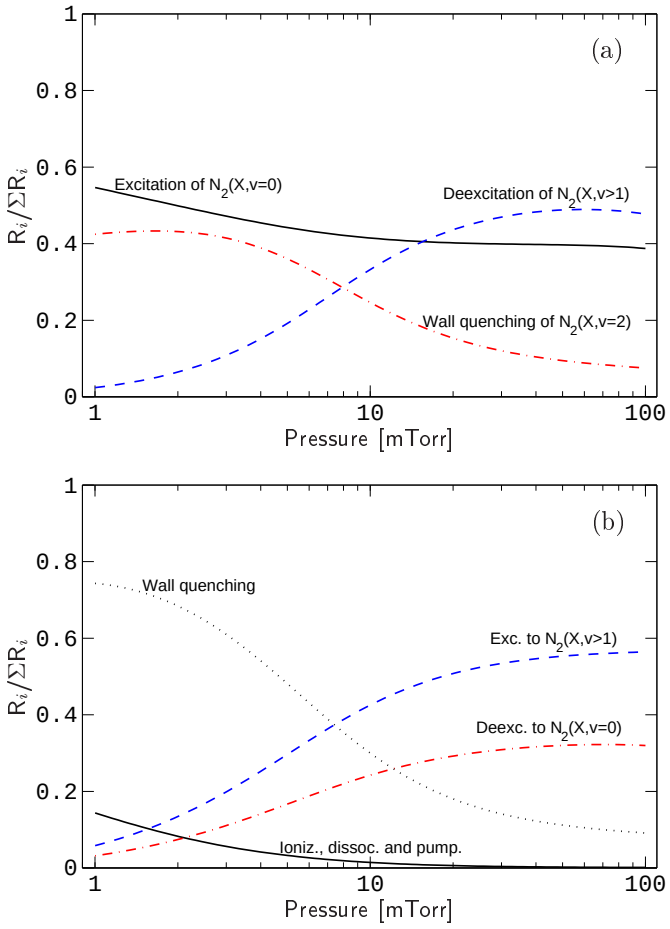

Figure 4.20: The reaction rates for (a) the creation and (b) the destruction of the $N_2(X^1\Sigma_g^+, v = 1)$ molecule versus discharge pressure.

shown in figures 4.21(a) and (b), respectively. $N_2(X^1\Sigma_g^+, v = 6)$ is mostly created by electron impact excitation of other ground state nitrogen molecules at intermediate and high pressures. The electron impact excitation of $N_2(X^1\Sigma_g^+, v = 0)$ is the most important process at low pressure. The energy pooling of two colliding $N_2(X^1\Sigma_g^+, v = 5)$ into $N_2(X^1\Sigma_g^+, v = 4)$ and $N_2(X^1\Sigma_g^+, v = 6)$ has a significant contribution at high pressure, although not more than 10 % at 100 mTorr.

As seen in figure 4.21(b), the $N_2(X^1\Sigma_g^+, v = 6)$ is mostly lost by wall quenching

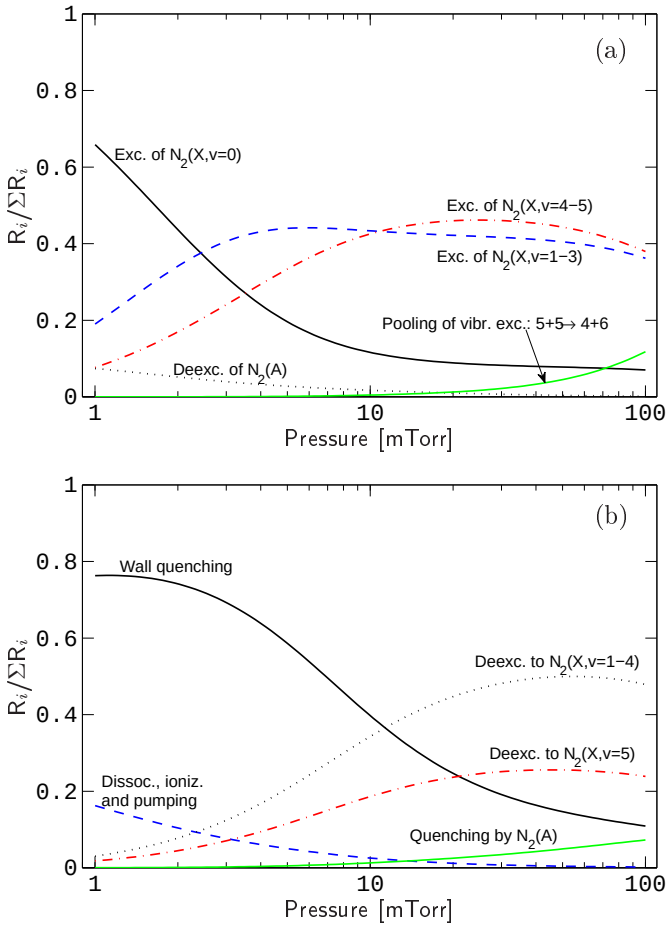

Figure 4.21: The reaction rates for (a) the creation and (b) the destruction of the $N_2(X^1\Sigma_g^+, v = 6)$ molecule versus discharge pressure.

at low pressure, contributing nearly 80 % at 1 mTorr but only about 10 % at 100 mTorr. Electron impact de-excitation is responsible for most of the $N_2(X^1\Sigma_g^+, v = 6)$ destruction at high pressure, but is negligible at 1 mTorr. Ionization, pumping and dissociation contribute at most less than 20% at 1 mTorr, combined.

The reaction rates for the creation and destruction of $N_2(A^3\Sigma_u^+)$ are shown in figures 4.22(a) and (b), respectively. The metastable $N_2(A^3\Sigma_u^+)$ is near entirely created by electron impact excitation of ground state nitrogen molecules, with the

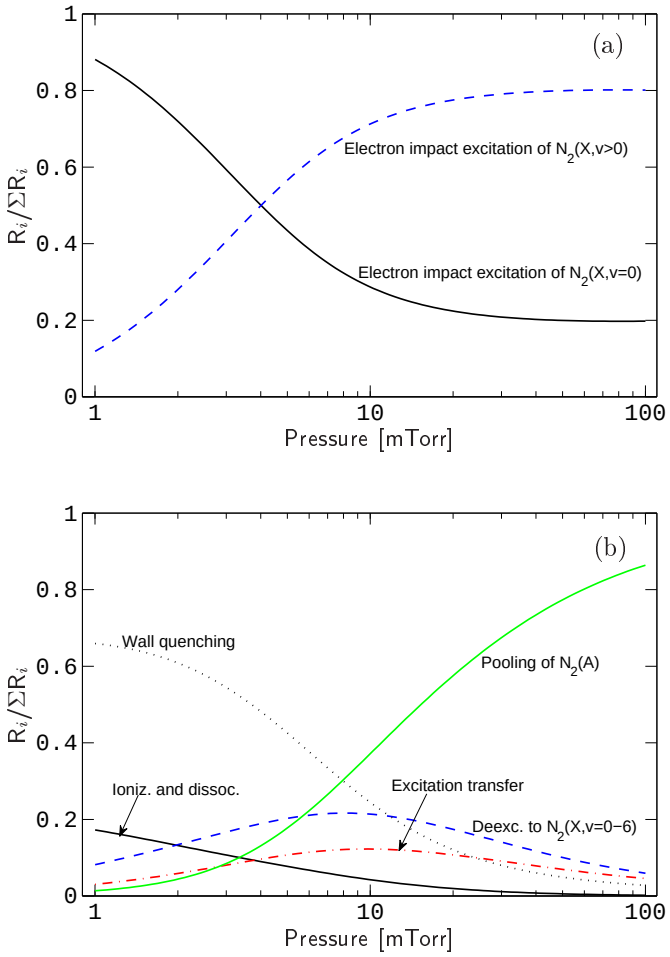

Figure 4.22: The reaction rates for (a) the creation and (b) the destruction of the $N_2(A^3\Sigma_u^+)$ metastable molecule versus discharge pressure.

contribution of any other process being negligible in comparison. At low pressure the excitation of $N_2(X^1\Sigma_g^+, v = 0)$ dominates, but at higher pressure the excitation of $N_2(X^1\Sigma_g^+, v > 0)$ is more important.

As seen in figure 4.22(b), the metastable $N_2(A^3\Sigma_u^+)$ is mainly lost to wall quenching at low pressure, but at high pressure pooling of excitation energy in a collision of two $N_2(A^3\Sigma_u^+)$ molecules, reaction (3.29), is the dominating loss

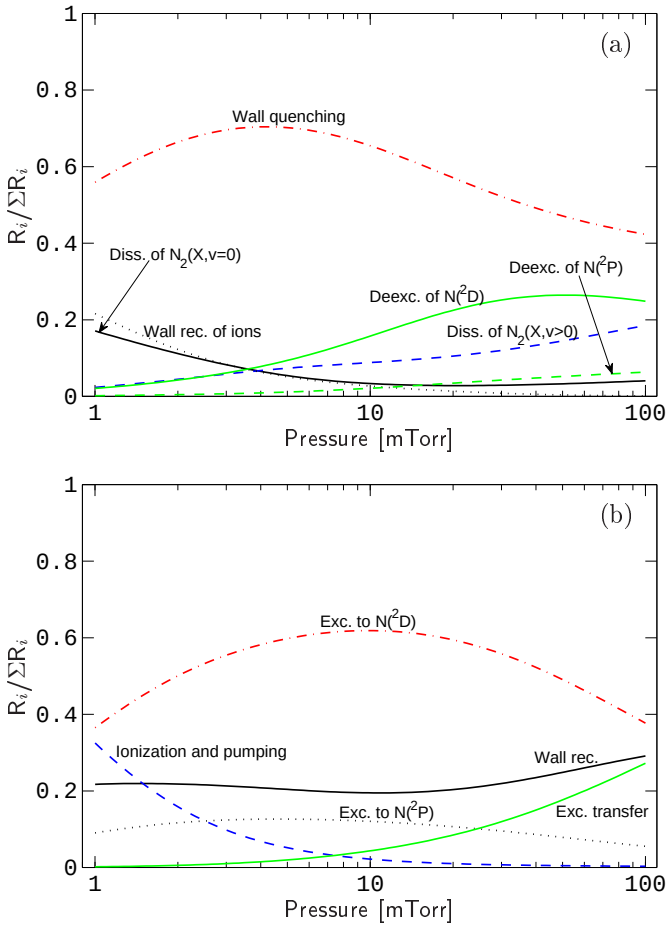

Figure 4.23: The reaction rates for (a) the creation and (b) the destruction of the N(^{4}S) atom versus discharge pressure.

process. The contribution of electron impact de-excitation and the transfer of excitation from $N_2(A^3\Sigma_u^+)$ to N(^{2}P), reaction (3.40), peak at roughly 10 and 20 % at intermediate pressure, respectively. Furthermore, the various ionization and dissociation processes have a combined contribution of less than 20 % at 1 mTorr, being negligible at 100 mTorr.

The reaction rates for the creation and destruction of N(^{4}S) are shown in figures

4.23(a) and (b), respectively. The ground state nitrogen atom, $N(^4S)$, is created mostly by wall quenching of metastable atoms, having a contribution no less than 40 % even at high pressure. Electron impact de-excitation of $N(^2D)$ has around 30 % contribution at high pressure. Wall recombination of N^+ ions is at most 20 % of the total $N(^4S)$ creation at 1 mTorr, but is negligible at intermediate and high pressures. Electron impact dissociation of $N_2(X^1\Sigma_g^+, v = 0)$ has a similar contribution, but the dissociation of $N_2(X^1\Sigma_g^+, v > 0)$ becomes more important with pressure and is roughly 20 % at 100 mTorr.

As seen in figure 4.23(b), the $N(^4S)$ atom is mostly lost to electron impact excitation of $N(^2D)$, peaking at 10 mTorr with a roughly 60 % contribution. The transfer of excitation from metastable nitrogen molecules to atoms, reaction (3.40), has roughly 30 % contribution at 100 mTorr, but is negligible at low pressure. The formation of molecules by wall recombination of atoms is also a strong factor in the loss of $N(^4S)$, or about 20-30%. Pumping of $N(^4S)$ out of the chamber and electron impact ionization contribute about the same, at most about 30% combined at 1 mTorr.

The reaction rates for the creation and destruction of $N(^2D)$ are shown in figures 4.24(a) and (b), respectively. The $N(^2D)$ metastable atom is created mostly by excitation from the ground state atom, $N(^4S)$. Dissociation has a similar contribution as in the creation of $N(^4S)$, dissociation of $N_2(X^1\Sigma_g^+, v = 0)$ being important at low pressure, whereas the dissociation of $N_2(X^1\Sigma_g^+, v > 0)$ is more important at high pressure.

As seen in figure 4.24(b), the $N(^2D)$ is mostly lost to wall quenching, counting for roughly 80 % at 1 mTorr, but decreasing to roughly 40 % at 100 mTorr. Electron impact de-excitation is also important at intermediate and high pressures, contributing to around 35 % at 100 mTorr. As in the loss mechanism of $N(^4S)$,

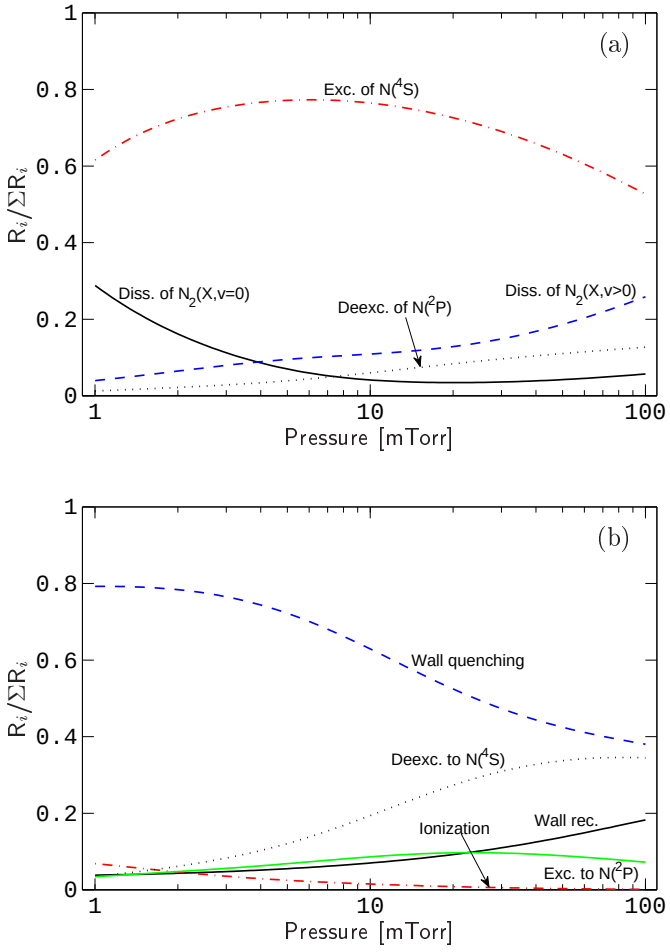

Figure 4.24: The reaction rates for (a) the creation and (b) the destruction of the $N(^2D)$ metastable atom versus discharge pressure.

formation of molecules by association of $N(^2D)$ at the wall is insignificant at low pressure, but increases to near 20% at 100 mTorr.

The reaction rates for the creation and destruction of $N(^2P)$ are shown in figures 4.25(a) and (b), respectively. The $N(^2P)$ is created mostly by electron impact excitation at low and intermediate pressures. The transfer of excitation from the metastable molecule $N_2(A^3\Sigma_u^+)$, reaction (3.40), is very important at high and

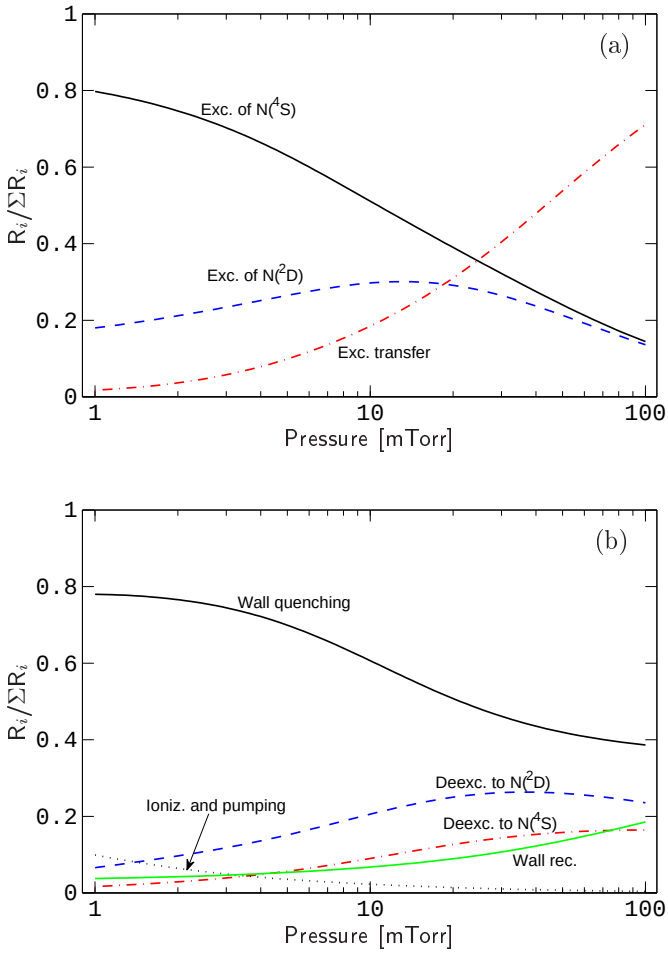

Figure 4.25: The reaction rates for (a) the creation and (b) the destruction of the N(^{2}P) metastable atom versus discharge pressure.

intermediate pressures, dominating at 100 mTorr.

As seen in figure 4.25(b), the loss scheme for the metastable atom N(^{2}P) is near identical with that of the metastable atom N(^{2}D), wall quenching being the most important loss mechanism over the entire pressure range. Electron impact de-excitation and wall recombination of atoms are important at higher pressure, whereas the combined effect of ionization and pumping is small, being at most

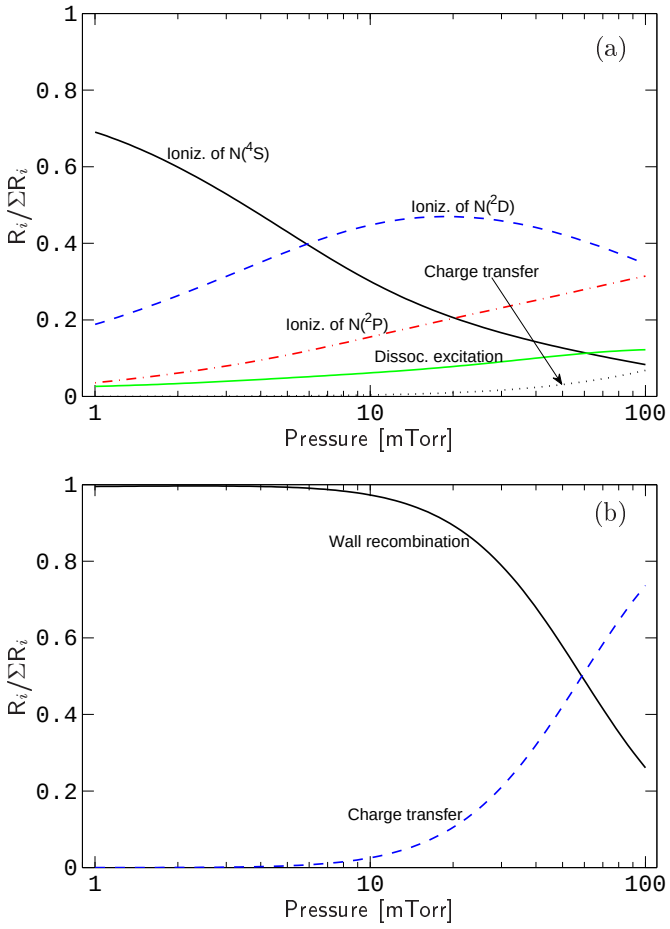

Figure 4.26: The reaction rates for (a) the creation and (b) the destruction of the N^+ ion versus discharge pressure.

roughly 10 % at 1 mTorr.

The reaction rates for the creation and destruction of N^+ are shown in figures 4.26(a) and (b), respectively. The atomic ion N^+ is, as the ion N_2^+, is mostly formed by electron impact ionization of its neutral counterpart. The ionization of the ground state atom dominates at low pressure while ionization of metastable atoms is more important at high and intermediate pressures. Electron impact dissociative

excitation of N_2^+, reaction (3.17), has a significant contribution, increasing from roughly 3 % at 1 mTorr to 12 % at 100 mTorr. Charge transfer, reaction (3.22), is only noticeable at high pressure with a 7 % contribution at its maximum.

As seen in figure 4.26(b), wall recombination is the dominating loss mechanism of the atomic ion N^+ at low and intermediate pressure, having a contribution of roughly $95 - 100$ % at $10 - 100$ mTorr. However, charge transfer, reaction (3.23), is very important at high pressure, being responsible for roughly 75 % of the total N^+ loss at 100 mTorr.

The reaction rates for the creation and destruction of N_2^+ are shown in figures 4.27(a) and (b), respectively. The N_2^+ ion is mostly created by electron impact ionization of $N_2(X)$. At low pressure the ionization of $N_2(X^1\Sigma_g^+, v = 0)$ is the dominating process, whereas at high and intermediate pressures the ionization of $N_2(X^1\Sigma_g^+, v > 0)$ is more important. Associative ionization of ground state and excited atoms, reaction (3.52), and charge transfer, reaction (3.23), each have a significant contribution at high pressure, roughly $7 - 15$ % at 100 mTorr.

As seen in figure 4.27(b), the N_2^+ ion is lost mainly by wall recombination over the entire pressure range, having a contribution no less than 40 % at 100 mTorr. Dissociative recombination is very important at intermediate and high pressure, having a roughly 45 % contribution at 100 mTorr. The molecular decomposition of N_2^+ to form the N_3^+ ion, reaction (3.44), only has a noticeable contribution at high pressure, being roughly 10 % at 100 mTorr.

The reaction rates for the creation and destruction of N_3^+ are shown in figures 4.28(a) and (b), respectively. Since the N_3^+ ion has no neutral counterpart in the model, there are a limited number of pathways to consider for the creation of ion. As a consequence, the N_3^+ ion is entirely created by molecular decomposition of N_2^+, reaction (3.44). Third order reactions, the other possible pathway considered

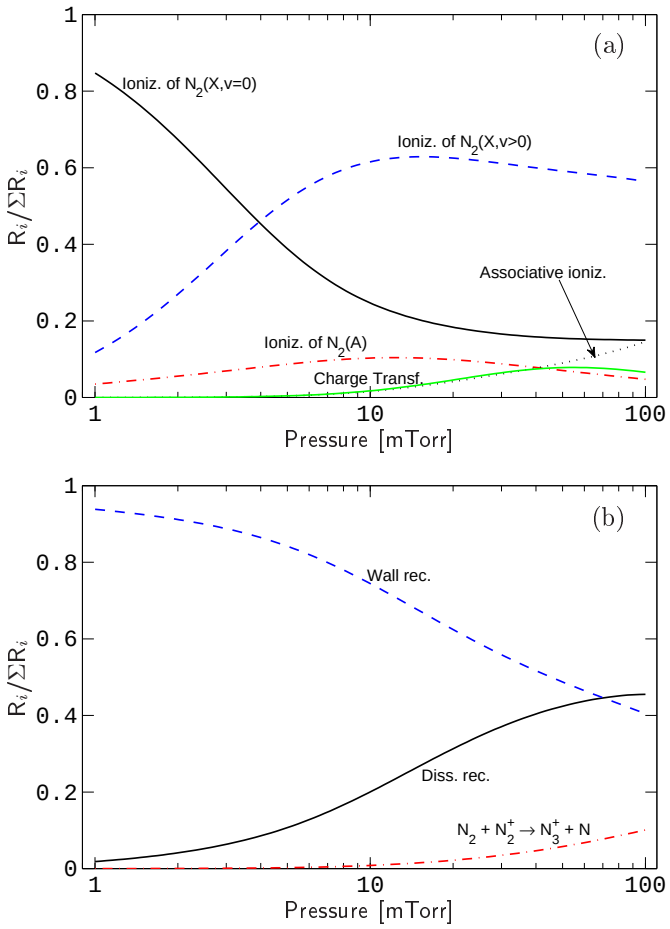

Figure 4.27: The reaction rates for (a) the creation and (b) the destruction of the N_2^+ ion versus discharge pressure.

for the formation of the ion, have a negligible contribution.

As seen in figure 4.28(b), the N_3^+ ion is lost mainly to wall recombination at low and intermediate pressures. At high pressure the dissociative recombination of N_3^+, reactions (3.19) and (3.20), becomes the most important loss mechanism, with a roughly 50 % contribution at 100 mTorr. Molecular decomposition of N_3, reaction

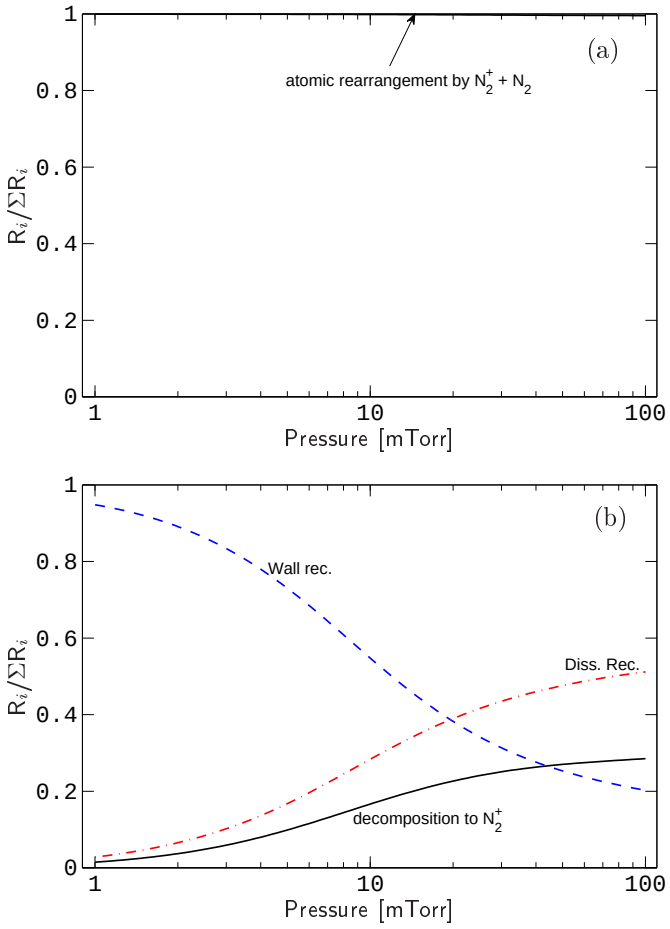

Figure 4.28: The reaction rates for (a) the creation and (b) the destruction of the N_3^+ ion versus discharge pressure.

(3.45), is also important at intermediate and high pressures, being responsible for roughly 30 % of the total N_3^+ loss at 100 mTorr.

The reaction rates for the creation and destruction of N_4^+ are shown in figures 4.29(a) and (b), respectively. The N_4^+ ion is almost entirely created by associative ionization, reaction (3.53). The formation of the N_4^+ ion is the only instance where third order reactions are not negligible. Combined, they have a noticeable effect at high pressure, roughly 30 % at 100 mTorr.

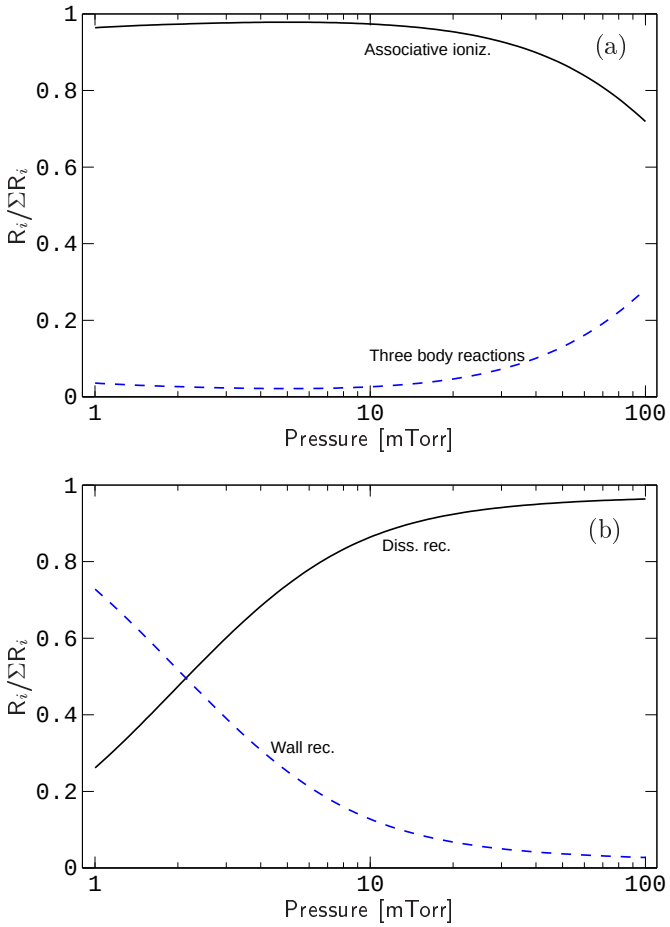

Figure 4.29: The reaction rates for (a) the creation and (b) the destruction of the N_4^+ ion versus discharge pressure.

As seen in figure 4.29(b), the N_4^+ ion is lost very effectively by dissociative recombination, being the dominant channel at high and intermediate pressure. Wall recombination is however the dominant process at low pressure, having a roughly 70 % contribution at 100 mTorr.

Chapter 5

The pulsed-power discharge

We assume a cylindrical stainless steel chamber. The content of the chamber is assumed to be nearly spatially uniform and the power uniformly deposited into the plasma bulk. The discharge is assumed to consist of 15 species of nitrogen; the seven lowest lying vibrational levels of the ground state nitrogen molecule $N_2(X^1\Sigma_g^+, v = 0 - 6)$, the metastable nitrogen molecule $N_2(A^3\Sigma_u^+)$, the ground state nitrogen atom $N(^4S)$, the metastable nitrogen atoms $N(^2D)$ and $N(^2P)$, and the ions N_2^+, N^+, N_3^+ and N_4^+. The electrons are assumed to have a Maxwellian-like energy distribution. The reaction set is summarized in tables A.1 to A.8 in Appendix A. The pulsed model is essentially identical to the steady state model, discussed in chapter 4, the only difference being that the absorbed power is no longer constant over time. Although the power can be modulated with any given waveform, we choose to modulate it with a rectangular wave in the current study.

The time dependent power can be described by (Ashida et al., 1995)

$$P_{\mathrm{abs}}(t) = \begin{cases} P_{\max} & 0 \le t < \alpha/f \\ P_{\min} & \alpha/f \le t < 1/f \end{cases} \tag{5.1}$$

where f is the pulse frequency, α is the duty ratio, and $P_{\max}$ and $P_{\min}$ are the absorbed power during the on- and off-periods, respectively. The average power, given by

$$\overline{P}_{\mathrm{abs}} = \alpha P_{\max} - (\alpha - 1) P_{\min} \tag{5.2}$$

is kept constant when the duty ratio or minimum power are varied. To be able to get a fair comparison of a pulsed power simulation and a steady state calculation, the average power must be the same in both cases.

When using initial values corresponding to zero radical and electron density, the simulation must be carried out for a very large number of periods before the time averaged densities, the dissociation fraction in particular, settle to constant values. When using initial values obtained from a steady state calculation, the simulation only needs to be carried out for a relatively few number of pulses before the time averaged results stabilize. Thus, the initial values are chosen to be the results of a steady state calculation for the same conditions. The simulation is then carried out until the results are stable with time. Since the outlet-flow pressure is kept constant during the simulation, and not the reactor pressure as in the steady state calculations, the reactor pressure may be slightly different at the end of the simulation than the chosen initial reactor pressure.

5.1 Densities and electron temperature

The stainless steel reactor chamber was assumed to be cylindrical with a 20 cm diameter and a 10 cm length. The average absorbed power was fixed at 500 W, the initial reactor pressure was 10 mTorr (the outlet-flow pressure being fixed at roughly 5 mTorr) and the gas flow rate was fixed at 50 sccm. The pulsed power calculation results are summarized in figures 5.1 to 5.3 as a function of time, frequency and duty ratio.

5.1.1 Time

The results in figure 5.1 represent two 10 kHz pulses with a 25 % duty ratio, acquired after simulating for 5 msec from a steady state, constant power, initial value. The actual discharge pressure varied from 10.2 – 10.3 mTorr during each pulse, increasing slightly from the 10 mTorr initial discharge pressure.

The densities of excited species, shown in figure 5.1(a), increase during the on-periods of the pulses, but drop again during the off-period. We consider the discharge to have reached stability when the density drop of each species equals the increase over one period. The density of $N_2(X^1\Sigma_g^+, v = 1)$ is almost constant with time, but the densities of all other excited species change considerably over a pulse period. The drop in excited species density accumulates mostly in the $N_2(X^1\Sigma_g^+, v = 0)$ density, although the $N(^4S)$ density increases slightly as well during the off-period of the pulse.

Densities of all charged species, shown in figure 5.1(b), increase during the on-period and decrease during the off-period. The time averaged electron density seems to have increased considerably from the steady state results, or almost by a factor of 2. Having increased by roughly a factor of 2 – 3 from its steady state value, the N^+ density seems to be mostly responsible for this increase in electron

density. The N_2^+ density responds more dynamically to the power than the N^+ density, having a larger density at its peak than the N^+, but then drops rapidly during the off-period and is roughly a factor of $3-4$ below its peak value at the end of the period. Neither of the N_3^+ or N_4^+ ion densities increase by pulsing the power and are so insignificant that we have omitted the N_4^+ density altogether from figure 5.1(b).

Although the dissociation fraction does not increase or decrease significantly within each pulse period, as seen in figure 5.1(c), this is the parameter that takes

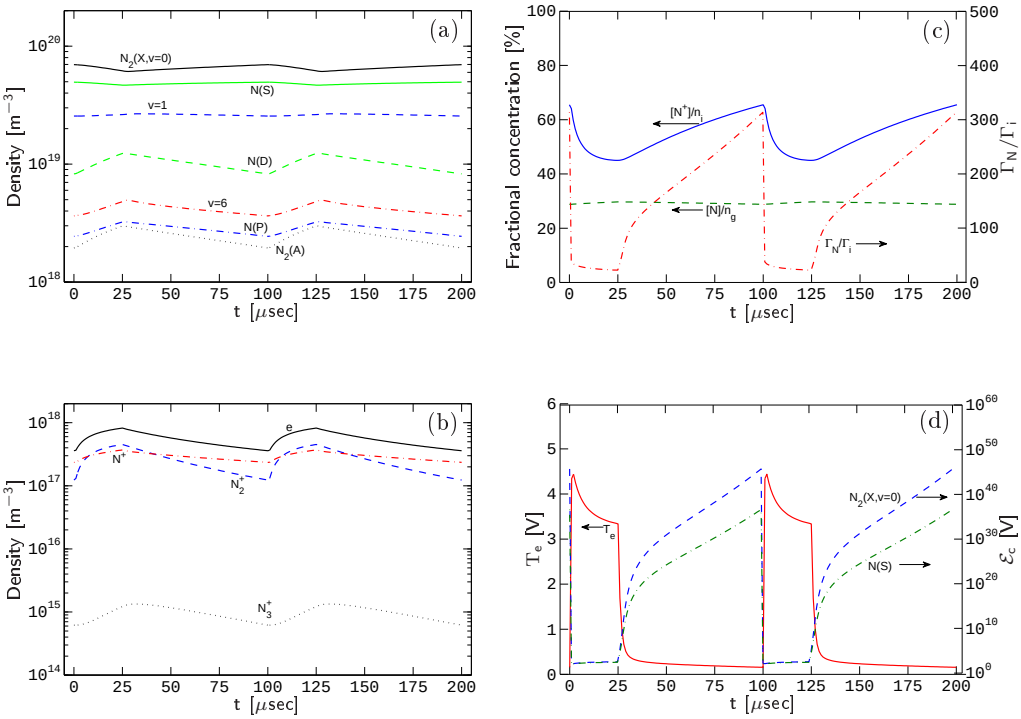

Figure 5.1: The plasma parameters as a function of time for the pulsed nitrogen discharge. (a) the densities of neutral species, (b) the densities of charged species, (c) the dissociation fraction $[\mathrm{N}]/n_\mathrm{g}$, the fraction of the N^+ ion of the total ion density $[\mathrm{N}^+]/n_\mathrm{i}$, the ratio of the neutral N atom flux versus the positive ion flux in the axial direction $\Gamma_\mathrm{N}/\Gamma_\mathrm{i}$ and (d) the electron temperature and the collisional energy loss of $N_2(X^1\Sigma_\mathrm{g}^+, v=0)$ and $N(^4S)$. The frequency was 10 kHz and the duty ratio was 25 %.

the longest to stabilize with time. The dissociation fraction has increased somewhat from the steady state initial value, increasing from 25 % to about 29 % by pulsing the power. The N^+ ion fraction is much more dynamic with power than the dissociation fraction, peaking at the end of the off-period at 65 %, but decreasing rapidly when the power is applied to a minimum of 45 %. This is a very significant increase from the steady state value, having been only about 32 % when the power was constant, significantly lower than the minimum value when the power is pulsed. The flux ratio responds even more dynamically to the power than the ion ratio, the neutral atom flux being roughly 25 times larger than the axial ion flux during the on-period, but then increases rapidly to roughly 300 at the end of the off-period.

The electron temperature is extremely dynamic with respect to the power, as seen in figure 5.1(d), falling near instantly to a very low value, several tenths of a V, when the power is turned off, but then decreasing slowly until the power is turned on again. This is somewhat peculiar, given that the electron temperature is known to be nearly independent of the absorbed power in the steady state calculations, demonstrated in figure 4.7(d). Furthermore, unlike the behavior of the densities, the peak value of the electron temperature is not at the end of the on-period, but rather at the start of it. The electron temperature therefore jumps instantly from several tenths of a V to 4.4 V when the power is turned off, but then relatively slowly decreases until the power is turned off again, then being roughly 3.3 V, 0.3 V above the steady state value of 3 V. Also shown in figure 5.1(d) is the collisional energy loss, increasing exponentially when the power is turned off, from roughly 300 V when the power is on to about $10^{35} - 10^{45}$ at the end of the off-period.

5.1.2 Frequency

The results shown in figure 5.2 represent a time average over 5 pulses, sampled after having carried out the simulation for 5 msec. The frequency was varied from 1 kHz to 1 MHz while the duty ratio was fixed at 25 %. The actual discharge pressure varied slightly with frequency, being roughly 10.25 mTorr when the frequency was below 100 kHz but decreasing to about 10 mTorr at 1 MHz.

The neutral densities, shown in figure 5.2(a), do not depend strongly on the pulse frequency, although there are some variations with frequency. The densities of

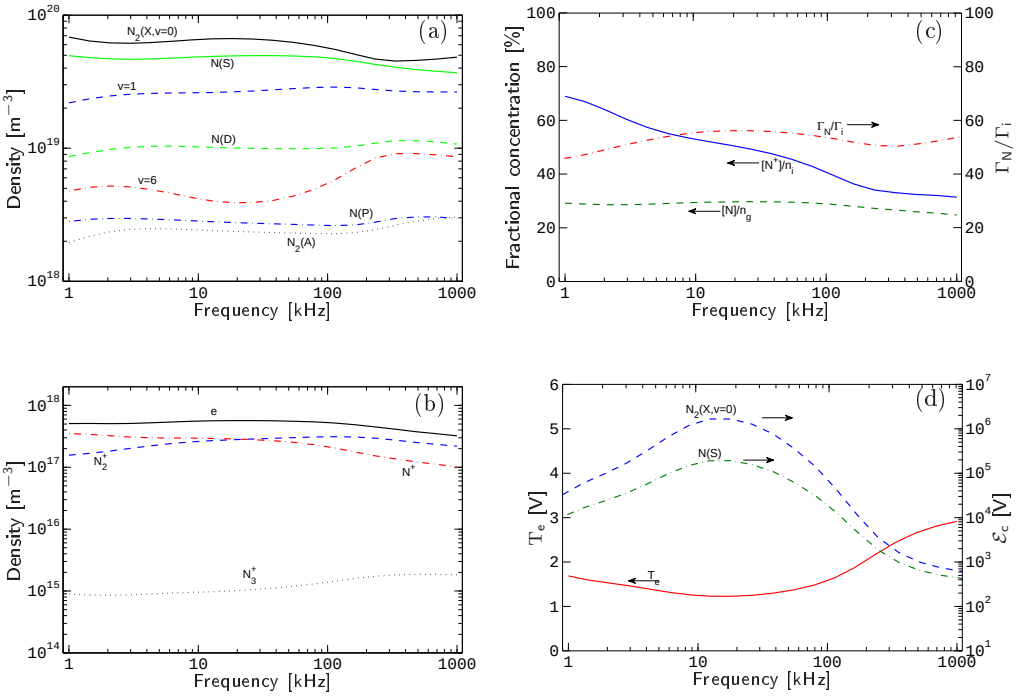

Figure 5.2: The plasma parameters as a function of modulation frequency for the pulsed nitrogen discharge. (a) the densities of neutral species, (b) the densities of charged species, (c) the dissociation fraction $[\mathrm{N}]/n_\mathrm{g}$, the fraction of the N^+ ion of the total ion density $[\mathrm{N}^+]/n_\mathrm{i}$, the ratio of the neutral N atom flux versus the positive ion flux in the axial direction $\Gamma_\mathrm{N}/\Gamma_\mathrm{i}$ and (d) the electron temperature and the collisional energy loss of $\mathrm{N}_2(X^1\Sigma_\mathrm{g}^+, v = 0)$ and $\mathrm{N}(^4\mathrm{S})$. The duty ratio was fixed at 25 %.

excited species remain relatively constant when the frequency is below $50-100$ kHz, but then increase somewhat with higher frequency, in particular the $N_2(X^1\Sigma_g^+, v = 6)$ density. The densities of ground state species decrease accordingly, although it is considerably less pronounced for $N(^4S)$ than for $N_2(X^1\Sigma_g^+, v = 0)$.

The electron density, shown in figure 5.2(b), is almost constant for frequencies lower than 100 kHz, but drops considerably when the frequency is increased, although having dropped by less than a factor of two at 1 MHz. The densities of the ions N^+ and N_2^+ are significantly affected by frequency, the N^+ being the dominating ion at low frequencies and the N_2^+ ion at high frequencies. Although both are negligible in the discharge, the densities of the N_3^+ and N_4^+ ions increase somewhat with frequency.

The dissociation fraction, shown in figure 5.2(c), is relatively independent of frequencies lower than 100 kHz, or about 29 %, but then decreases to roughly 25 % at 1 MHz. The fraction of the N^+ ion decreases significantly with frequency, from about 69 % at 1 kHz to roughly 31 % at 1 MHz. Thus, it seems to be possible to reach very high ratio of atomic ions in spite of a relatively low dissociation fraction if the pulse frequency is sufficiently low. The flux ratio is unusually constant with frequency, the N atom flux being between 45 and 55 times the axial ion flux for this range of frequencies.

As seen in figure 5.2(d), the time averaged electron temperature reaches a minimum of 1.2 V when the frequency is roughly 15 kHz. At 1 kHz it is roughly 1.7 V, but is almost equal to the steady state value of 3 V when the frequency is 1 MHz. The collisional energy loss is inversely dependent on the electron temperature, as usual, peaking at roughly 2×10^6 V for the molecule and 2×10^5 V for the atom when the frequency is 15 kHz.

5.1.3 Duty ratio

The results shown in figure 5.3 represent a time average over 10 pulses, sampled after having carried out the simulation for a minimum of 12 msec. The duty ratio was varied from 0.1 % to 100 % while the frequency was fixed at 10 kHz. The actual discharge pressure varied somewhat with decreasing duty ratio, being roughly 11.5 mTorr at 0.4 % duty ratio, an increase of about 15 % from the 10 mTorr initial pressure. Although this may be a relatively large deviation from

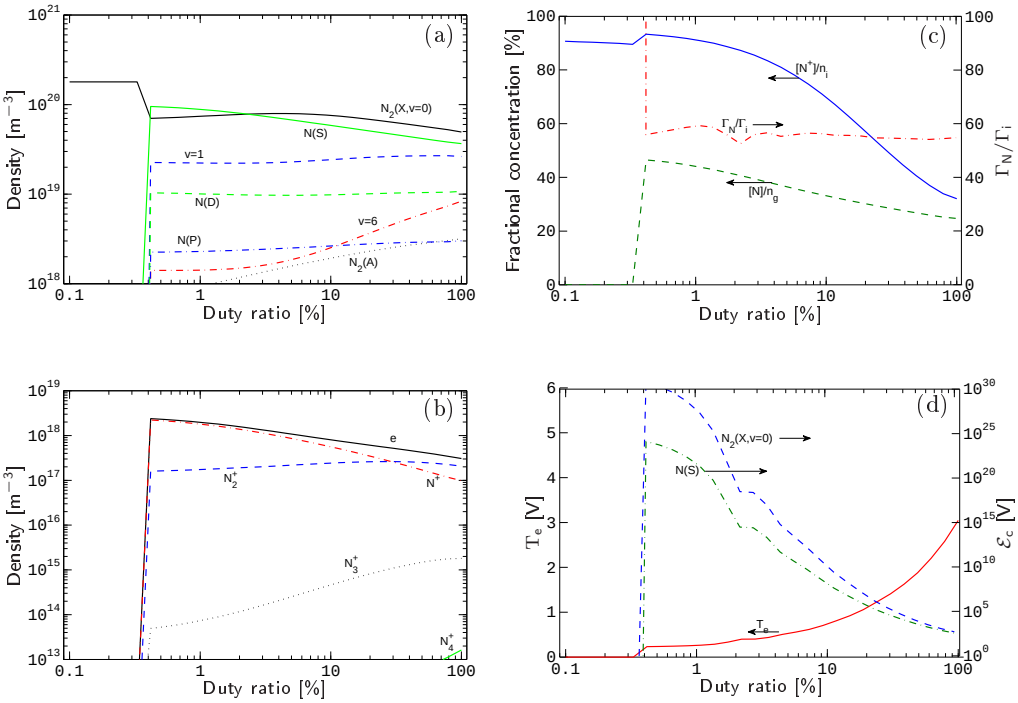

Figure 5.3: The plasma parameters as a function of modulation frequency for the pulsed nitrogen discharge. (a) the densities of neutral species, (b) the densities of charged species, (c) the dissociation fraction $[\mathrm{N}]/n_\mathrm{g}$, the fraction of the N^+ ion of the total ion density $[\mathrm{N}^+]/n_\mathrm{i}$, the ratio of the neutral N atom flux versus the positive ion flux in the axial direction $\Gamma_\mathrm{N}/\Gamma_\mathrm{i}$ and (d) the electron temperature and the collisional energy loss of $\mathrm{N}_2(X^1\Sigma_\mathrm{g}^+, v=0)$ and $\mathrm{N}(^4\mathrm{S})$. The frequency was fixed at 10 kHz. The peak power was adjusted with varying duty ratio to maintain an average absorbed power of 500 W.

the initial discharge pressure, the effect is not very significant, as seen in figure 4.8. The electron temperature and all the radical and charged species densities are negligible when the duty ratio is below 0.4 %. Although this describes a discharge that is turned off, this behavior might simply be the result of a calculation error, preventing us from concluding there is actually a specific minimum duty ratio that is needed to sustain the discharge from steady state. Thus, our discussion of the plasma parameters in figure 5.3 will only refer to when the duty ratio is above 0.4 %. When the duty ratio is 100 % the discharge is in fact not pulsed and the results are simply steady state values.

Most of the neutral densities, shown in figure 5.3(a), are relatively constant with duty ratio. The $N_2(X^1\Sigma_g^+, v = 0)$ density is almost constant for duty ratios below 10 %, but decreases considerably when the duty ratio is increased to 100 %. The density of $N(^4S)$ decreases uniformly with increasing duty ratio, being larger than the $N_2(X^1\Sigma_g^+, v = 0)$ density at duty ratios below 2 % but somewhat smaller at 100 % duty ratio. The density of the metastable nitrogen atoms $N(^2D)$ and $N(^2P)$ is however almost independent of duty ratio, increasing slightly with increasing duty ratio. The density of all excited nitrogen molecules increases with duty ratio, most significantly the $N_2(X^1\Sigma_g^+, v = 6)$ density which increases by almost a factor of 5 when the duty ratio is increased from roughly 5 % to 100 %.

The density of charged species, shown in figure 5.3(b), is strongly affected by the duty ratio. The electron density decreases uniformly with increasing duty ratio, being almost an order of magnitude larger when the duty ratio is 0.4 % than in the steady state, i.e. when the duty ratio is 100 %. Although the N_2^+ density increases only slightly with increasing duty ratio, the N^+ density decreases rapidly with increasing duty ratio, having over a 20 times larger density when the duty ratio is 0.4 % than in the steady state. The N_3^+ and N_4^+ densities decrease substantially

when the duty ratio is decreased from 100 % to 0.4 % and are always negligible in comparison to the other ions.

As seen in figure 5.3(c), the dissociation fraction increases significantly when the duty ratio is decreased from 100 % to 0.4 %, or from roughly 25 % to about 47 %. The corresponding increase in the N^+ ion fraction is considerably more pronounced, being roughly 32 % in the steady state but almost double the dissociation fraction when the duty ratio is 0.4 %, or about 93 %. Similarly to the frequency dependence in figure 5.2(c), the flux ratio is relatively independent of the duty ratio, the N atom flux being between 50 and 60 times the axial ion flux. By increasing the number of points in the $1 - 10$ % duty ratio region, we found that the irregularity in the flux ratio actually has a more detailed structure, somewhat resembling a sinc-function, and is therefore probably not some sort of averaging error as we expected at first.

The electron temperature, shown in figure 5.3(d), increases with increasing duty ratio, as expected, being roughly 0.2 V at 0.4 % duty ratio and about 3 V in the steady state. The time averaged electron temperature is heavily affected by the length of the off-period, and therefore the duty ratio, because of its dynamic behavior with time, although the electron temperature during the on-time is much higher. The time averaged collisional loss is extremely large at low duty ratios, or roughly $10^{20} - 10^{30}$ V, but decreases to about 400 V for the atom and the molecule when the duty ratio is 100 %.

5.2 Reaction rates

The chamber was assumed to be made of stainless steel, cylindrical with radius $R = 10$ cm and length $L = 10$ cm. The initial reactor pressure was 10 mTorr, but since the outlet-flow pressure was fixed at roughly 5 mTorr during the simulation the actual reactor pressure increased slightly, varying from $10.2 - 10.3$ mTorr during each period. The gas flow rate was 50 sccm. The power was pulsed with a 10 kHz frequency and a 25 % duty ratio rectangular waveform, described by equation (5.1). The average absorbed power was fixed at 500 W and the minimum power was fixed at 0 W, such that the maximum power was 2000 W. Furthermore, the electron energy distribution was assumed to be Maxwellian, $x = 1$. The overall reaction rates for the creation and destruction of neutral molecules, neutral atoms and electrons are evaluated as a function of time over a single pulsed power period in figures 5.5, 5.4 and 5.6, respectively. Additionally, the reaction rates for the creation and destruction of every gas species, except $N_2(X^1\Sigma_g^+, v = 2 - 5)$, are shown in figures 5.7 to 5.17.

The reaction rates for the overall creation and destruction of neutral nitrogen molecules are shown in figures 5.4(a) and (b), respectively. Neutral nitrogen molecules are mostly created from wall recombination of $N(^4S)$ during both the on- and off-period. Wall recombination of the metastable atoms $N(^2D)$ and $N(^2P)$ and pumping of $N_2(X^1\Sigma_g^+, v = 0)$ into the chamber have a similar contribution, or about $15 - 20$ %, during both the on- and off-period. Recombination of N_2^+ on the wall is significant during the on-period, being roughly $10 - 15$ %, but becomes negligible soon after the power is turned off.

As seen in figure 5.4(b), neutral nitrogen molecules are almost entirely lost by pumping out of the chamber during the off-period, other processes having a negligible effect. The situation is vastly different during the on-period, with pumping

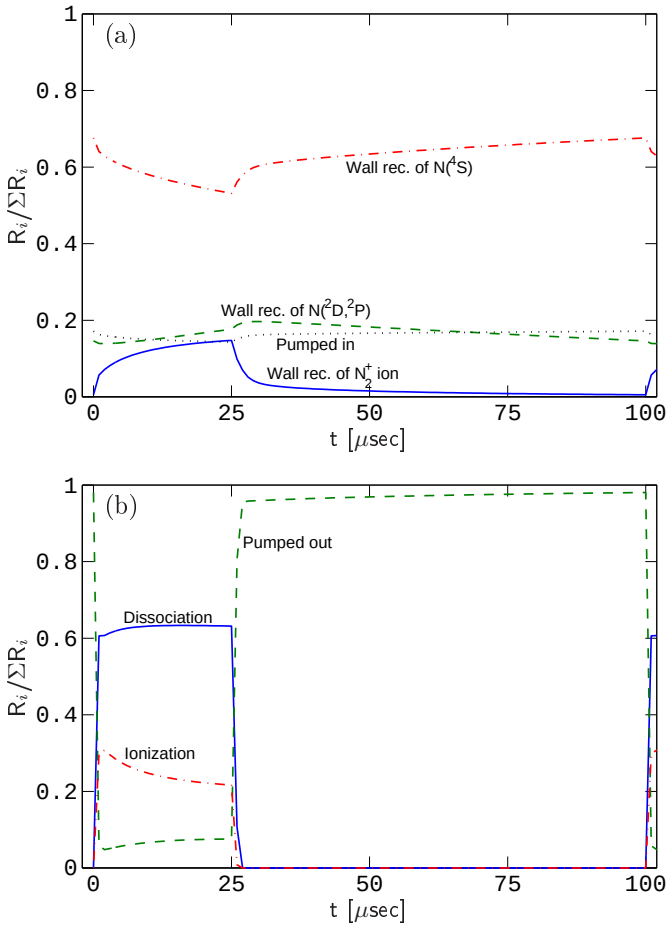

Figure 5.4: The reaction rates for (a) the overall creation and (b) the overall destruction of neutral nitrogen molecules versus time over a single pulsed power period.

being responsible for less than 10 % of the total loss but electron impact dissociation and electron impact ionization of $N_2(X^1\Sigma_g^+, v = 1-6)$ being responsible for roughly 60 % and 25 % of the total loss, respectively.

The reaction rates for the overall creation and destruction of neutral nitrogen atoms are shown in figures 5.5(a) and (b), respectively. Roughly half of the neutral nitrogen atoms are created by electron impact dissociation of $N_2(X^1\Sigma_g^+, v = 0-6)$

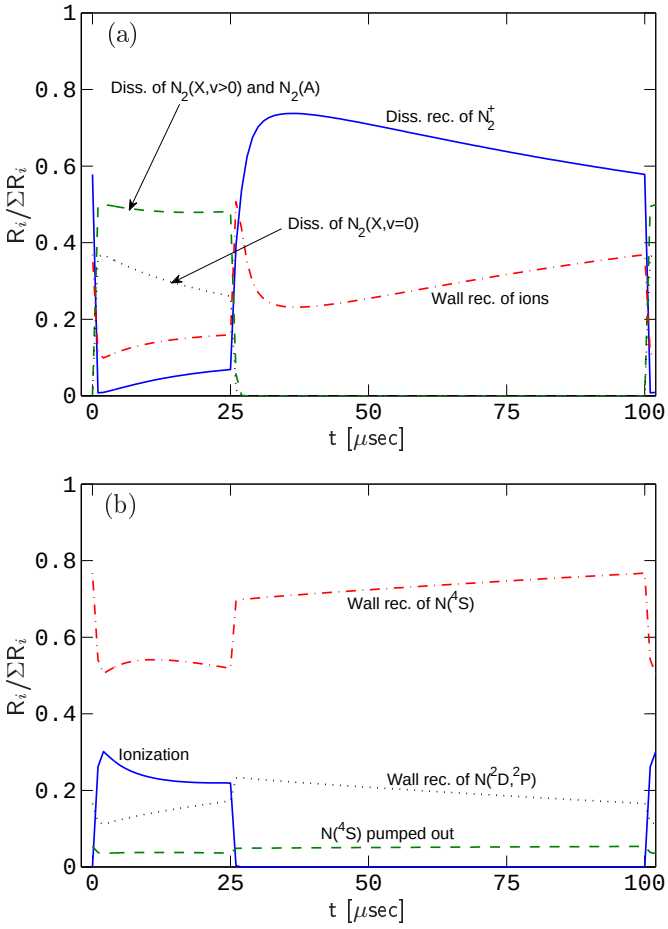

Figure 5.5: The reaction rates for (a) the overall creation and (b) the overall destruction of neutral nitrogen atoms versus time over a single pulsed power period.

(and a small contribution of $N_2(A^3\Sigma_u^+)$) during the on-period, the dissociation of $N_2(X^1\Sigma_g^+, v = 0)$ meanwhile being responsible for about 26 – 36 %. However, as soon as the power is turned off the electron impact dissociation processes become negligible. Dissociative recombination of N_2^+, reactions (3.13) – (3.15), quickly becomes the dominant creation process after the power is turned off, its contribution being between 58 % and 74 %. The importance of recombination of N^+ on the wall

increases during both the on- and off-period, having a contribution of about 23 – 37 % during the off-period and 10 – 16 % during the on-period.

As seen in figure 5.5(b), neutral nitrogen atoms are mostly lost by wall recombination of $N(^4S)$ during both periods, being roughly 70 – 77 % during the off-period but slightly above 50 % during the on-period. Wall recombination of the metastable atoms is significant as well, being 17 – 23 % and 11 – 17 % during the off- and on-period, respectively. Electron impact ionization of nitrogen atoms has a significant contribution during the on-period, roughly 22 – 30 %, but is negligible when the power is off. Pumping of $N(^4S)$ out of the chamber is small, being roughly 4 – 5 % of the total atom loss whether the power is on or off.

The reaction rates for the overall creation and destruction of electrons are shown in figures 5.6(a) and (b), respectively. Electrons are entirely created by electron impact ionization during the on-period, the ionization of atoms and molecules having a contribution of about 32 – 41 % and 53 – 65 %, respectively. When the power is turned off the electron impact processes become negligible almost instantly and electrons are instead entirely created by associative ionization. The associative ionization of two nitrogen atoms, reaction (3.52), is much more important than the ionization of two molecules, reaction (3.53), being responsible for roughly 95 % of electron creation during the off-period.

As seen in figure 5.6(b), electrons are lost by the same three processes during both the on- and off-period. Wall recombination of the N^+ ion is the most important process when the power is on, being roughly 48 – 73 % of the total electron loss, and still has a significant contribution when the power is off, or roughly 21 – 35 %. Dissociative recombination of N_2, reactions (3.13) – (3.15), is the dominating process when the power is off, having a contribution of roughly 55 – 68 %, but about 5 – 21 % when it is on. Wall recombination of N_2^+ is much less important

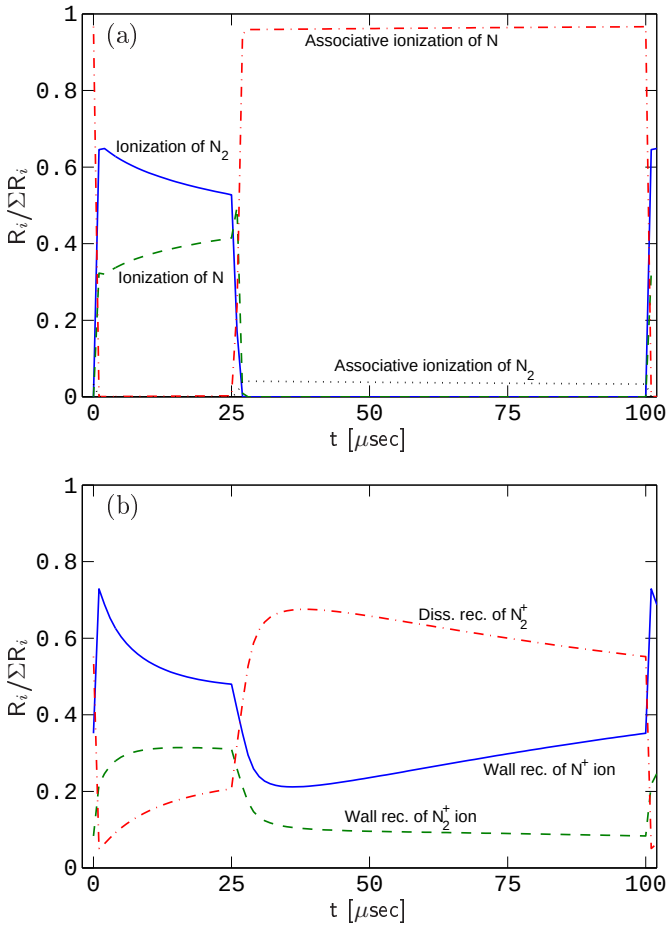

Figure 5.6: The reaction rates for (a) the overall creation and (b) the overall destruction of free electrons versus time over a single pulsed power period.

during both periods, being roughly 8 – 10 % and about 31 % during the off- and on-periods, respectively.

The reaction rates for the creation and destruction of the ground state nitrogen molecule $N_2(X^1\Sigma_g^+, v = 0)$ are shown in figures 5.7(a) and (b), respectively. The $N_2(X^1\Sigma_g^+, v = 0)$ is created mainly by electron impact de-excitation of $N_2(X^1\Sigma_g^+, v = 1 - 6)$ when the power is off, contributing at most 73 % soon after the power is turned off, but then decreases and is negligible at the end of the

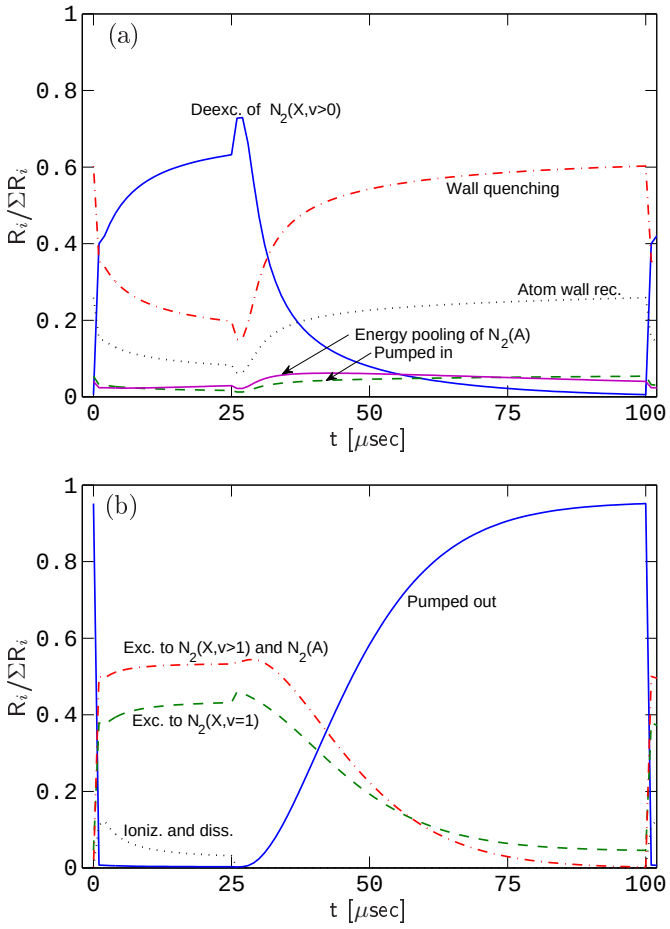

Figure 5.7: The reaction rates for (a) the creation and (b) the destruction of the $N_2(X^1\Sigma_g^+, v = 0)$ molecule versus time over a single pulsed power period.

off-period. Wall quenching of $N_2(X^1\Sigma_g^+, v = 1)$ and $N_2(A^3\Sigma_u^+)$ is the dominating process when the power is turned off, contributing at most roughly 60 % at the end of the pulse, but is also significant during the on-period. Wall recombination of neutral atoms is also a significant creation process after the power has been turned off, being about 26 % at the end of the pulse. Furthermore, energy pooling of $N_2(A^3\Sigma_u^+)$, reaction (3.29), and pumping of gas into the chamber each contribute around 5 % when the power is turned off.

As seen in figure 5.7(b), the pumping of species out of the chamber is the dominating loss mechanism of $N_2(X^1\Sigma_g^+, v = 0)$ after the power is turned off. Electron impact excitation is the dominating process when the power is on, electron impact ionization and dissociation being responsible for the rest, or roughly 3 – 12 %, and pumping out of the chamber having practically no contribution. The excitation processes do not become negligible very fast, as would be expected from any electron impact process, given how fast the electron temperature decreases when the power is turned off.

The reaction rates for the creation and destruction of the vibrationally excited ground state nitrogen molecule $N_2(X^1\Sigma_g^+, v = 1)$ are shown in figures 5.8(a) and (b), respectively. Once the power has been turned off, the wall quenching of $N_2(X^1\Sigma_g^+, v = 2)$ becomes the dominating process in the creation of $N_2(X^1\Sigma_g^+, v = 1)$, meanwhile being responsible for $10 - 20$ % of the creation when the power is on. Electron impact excitation of $N_2(X^1\Sigma_g^+, v = 0)$ is the dominating process during the on-period, being roughly 60 %, but rather quickly becomes negligible after the power is turned off. Electron impact de-excitation of $N_2(X^1\Sigma_g^+, v = 2 - 6)$ has a contribution of about $23 - 31$ % when the power is on, increasing to almost 50 % soon after the power is turned off, but then decreasing rather slowly for an electron impact process, being negligible at the end of the pulse.

As seen in figure 5.8(b), the $N_2(X^1\Sigma_g^+, v = 1)$ molecules are predominantly lost by wall quenching when the power has been turned off. During the on-period electron impact processes dominate, the contribution of electron impact excitation to $N_2(X^1\Sigma_g^+, v > 1)$ being largest, or roughly $39 - 51$ %. Electron impact de-excitation to $N_2(X^1\Sigma_g^+, v = 0)$ has about $21 - 29$ % contribution, while ionization, dissociation and pumping out of the chamber only account for roughly $2 - 7$ %. Wall quenching is responsible for the rest of the $N_2(X^1\Sigma_g^+, v = 1)$ loss during the

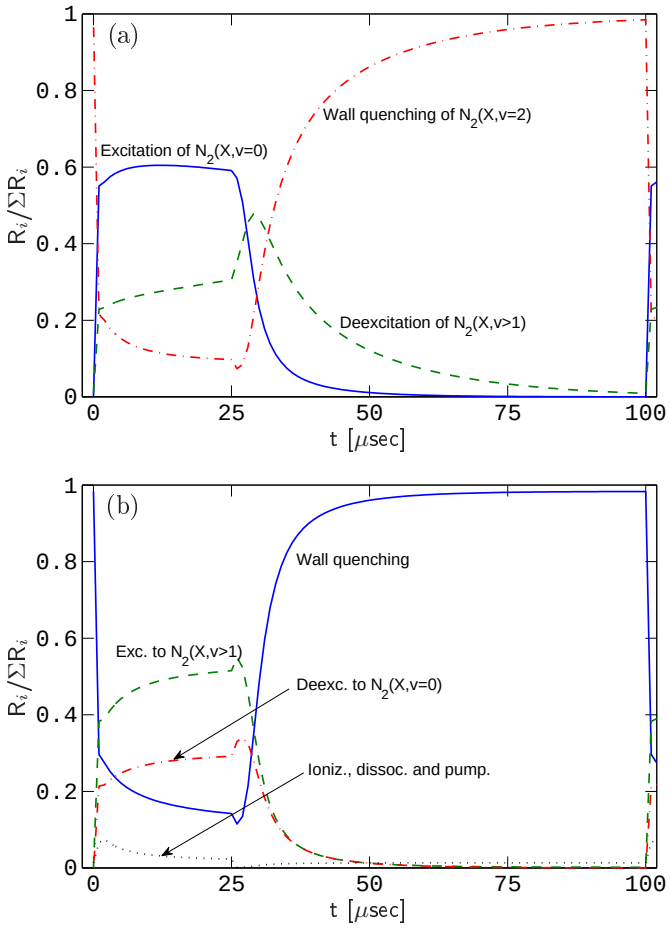

Figure 5.8: The reaction rates for (a) the creation and (b) the destruction of the $N_2(X^1\Sigma_g^+, v = 1)$ molecule versus time over a single pulsed power period.

on-period, or roughly $14 - 30$ %.

The reaction rates for the creation and destruction of the vibrationally excited ground state nitrogen molecule $N_2(X^1\Sigma_g^+, v = 6)$ are shown in figures 5.9(a) and (b), respectively. The creation scheme of $N_2(X^1\Sigma_g^+, v = 6)$ is somewhat complicated, although it is entirely created from excitation or de-excitation of other $N_2(X^1\Sigma_g^+, v)$ molecules. Electron impact excitation of $N_2(X^1\Sigma_g^+, v = 0)$ and $N_2(X^1\Sigma_g^+, v = 1 - 3)$ each contribute around 19 % and 47 % when the power

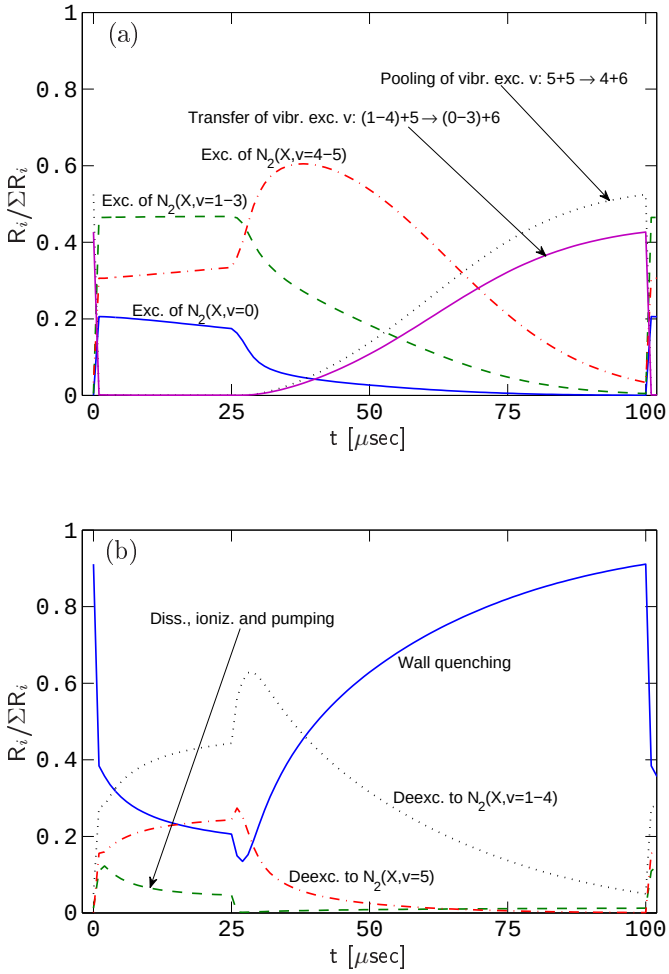

Figure 5.9: The reaction rates for (a) the creation and (b) the destruction of the $N_2(X^1\Sigma_g^+, v = 6)$ molecule versus time over a single pulsed power period.

is on, respectively, but decrease rapidly when the power is turned off and are negligible at the end of the pulse. The electron impact excitation of $N_2(X^1\Sigma_g^+, v = 4-5)$ has a peculiar behavior when the power is turned off. Instead of decreasing as the other electron impact excitations, its contribution increases from about 32 % when the power is on to roughly 60 % when 13 μsec have passed since turning off the

power, only then decreasing to less than 4 % at the end of the off-period. Transfer of vibrational excitation, reaction (3.35), is negligible when the power is on, but increases once the power has been turned off. The contribution of the pooling of $N_2(X^1\Sigma_g^+, v = 5)$ is larger than the combined contribution of transfer of vibrational excitation from $N_2(X^1\Sigma_g^+, v = 1 - 4)$ to $N_2(X^1\Sigma_g^+, v = 5)$, being 52 % and 43 % at the end of the pulse, respectively.

As seen in figure 5.9(b), wall quenching to $N_2(X^1\Sigma_g^+, v = 5)$ is the dominating mechanism for $N_2(X^1\Sigma_g^+, v = 6)$ loss when the power is turned off, but has a $21 - 38$ % contribution during the on-period. Electron impact de-excitation to $N_2(X^1\Sigma_g^+, v = 1 - 4)$, being the dominant loss process during the on-period with a $28 - 44$ % contribution, is also significant during the off-period, its contribution peaking at roughly 63 % soon after the power is turned off but decreasing after that. Electron impact de-excitation of $N_2(X^1\Sigma_g^+, v = 5)$ is significant during the on-period with a $16 - 24$ % contribution, decreasing rapidly after the power is turned off. Together with pumping of out the chamber, electron impact dissociation and ionization of $N_2(X^1\Sigma_g^+, v = 6)$ contribute about $5 - 12$ % during the on-period, but are negligible during the off period.

The reaction rates for the creation and destruction of the metastable nitrogen molecule $N_2(A^3\Sigma_u^+)$ are shown in figures 5.10(a) and (b), respectively. $N_2(A^3\Sigma_u^+)$ is predominantly lost by dissociative recombination of N_3^+, reaction (3.19), when the power is off but is negligible when it is on. Although negligible during the on-period as well, the rearrangement of the chemical bonds of N_3^+, reaction (3.45), has a significant contribution to the creation of $N_2(A^3\Sigma_u^+)$ during the off-period, or roughly $16 - 20$ %. Additionally, dissociative recombination of N_4^+, reaction (3.21), has around 3 % contribution during the off-period. Electron impact excitation of $N_2(X^1\Sigma_g^+, v)$ is entirely responsible for the creation of $N_2(A^3\Sigma_u^+)$ during the on-

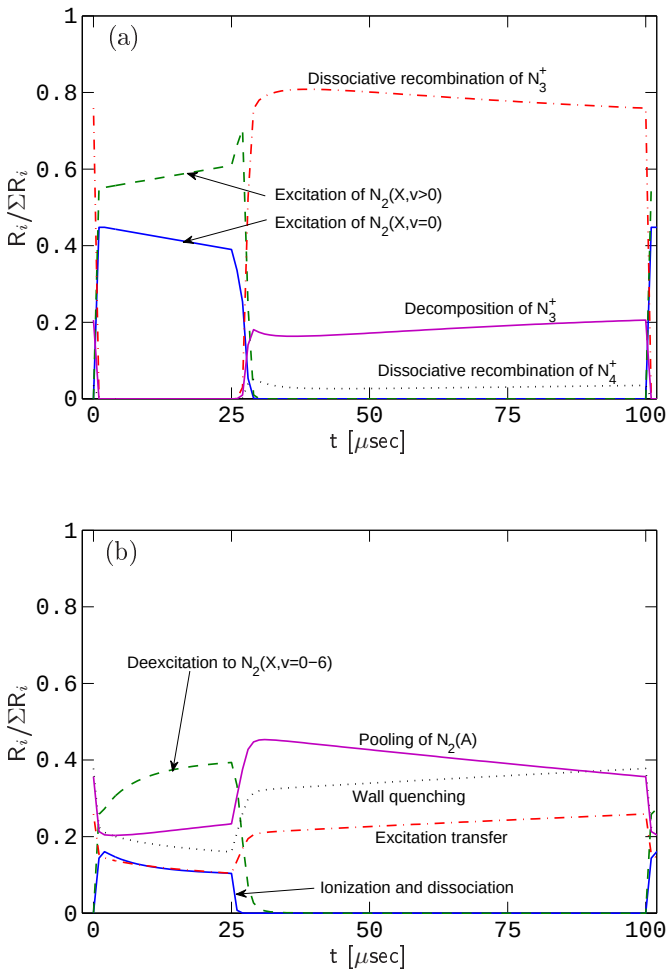

Figure 5.10: The reaction rates for (a) the creation and (b) the destruction of the $N_2(A^3\Sigma_u^+)$ molecule versus time over a single pulsed power period.

period, the combined contribution of excitation from $N_2(X^1\Sigma_g^+, v = 1-6)$ being roughly $55-61$ %, the excitation of $N_2(X^1\Sigma_g^+, v = 0)$ representing the rest.

As seen in figure 5.10(b), there are no dominating processes in the loss of $N_2(A^3\Sigma_u^+)$. During the on-period, electron impact de-excitation of $N_2(A^3\Sigma_u^+)$ to $N_2(X^1\Sigma_g^+, v)$ has a roughly $26-39$ % contribution and the combined contribution of electron impact ionization and dissociation is roughly $10-16$ %, both processes

being negligible when the power is off. Pooling of $N_2(A^3\Sigma_u^+)$, reaction (3.29), has the largest contribution during the off-period, or about 36 – 45 %, but about 20 – 23 % when the power is on. Quenching of $N_2(A^3\Sigma_u^+)$ on the wall has a roughly 31 – 37 % contribution during the off period but 16 – 21 % during the on-period. Excitation transfer, reaction (3.40), has a roughly 20 – 26 % contribution during the off-period but 10 – 16 % during the on-period.

The reaction rates for the creation and destruction of the ground state nitrogen atom $N(^4S)$ are shown in figures 5.11(a) and (b), respectively. The ground state nitrogen atom $N(^4S)$ is predominantly created by wall quenching of $N(^2D)$ and $N(^2P)$ during the off-period, having a 34 – 38 % contribution when the power is on. Electron impact de-excitation of $N(^2D)$ has a 10 – 25 % contribution during the on-period, but decreasing rapidly when the power is turned off. Wall recombination of N^+ only has a slight effect, being around 6 % when the power is on and around 2 % when it is off. Electron impact dissociation of $N_2(X^1\Sigma_g^+, v)$ are significant processes during the on-period, combined contributing roughly 25 – 46 %.

As seen in figure 5.11(b), $N(^4S)$ atoms are lost predominantly by wall recombination during the off-period and by electron impact excitation to $N(^2D)$ during the on-period. Excitation transfer, reaction (3.40), has a roughly 11 – 16 % contribution during the off-period, but is negligible during the on-period. The combined contribution of electron impact ionization and pumping of $N(^4S)$ out of the chamber is roughly 6 % when the power is off, but is negligible when the power is on. Electron impact excitation to $N(^2P)$ has around 15 % contribution during the on-period, but is negligible when the power is off.

The reaction rates for the creation and destruction of the metastable nitrogen atom $N(^2D)$ are shown in figures 5.12(a) and (b), respectively. The $N(^2D)$ is entirely created by dissociative recombination, reactions (3.13) – (3.15), during the

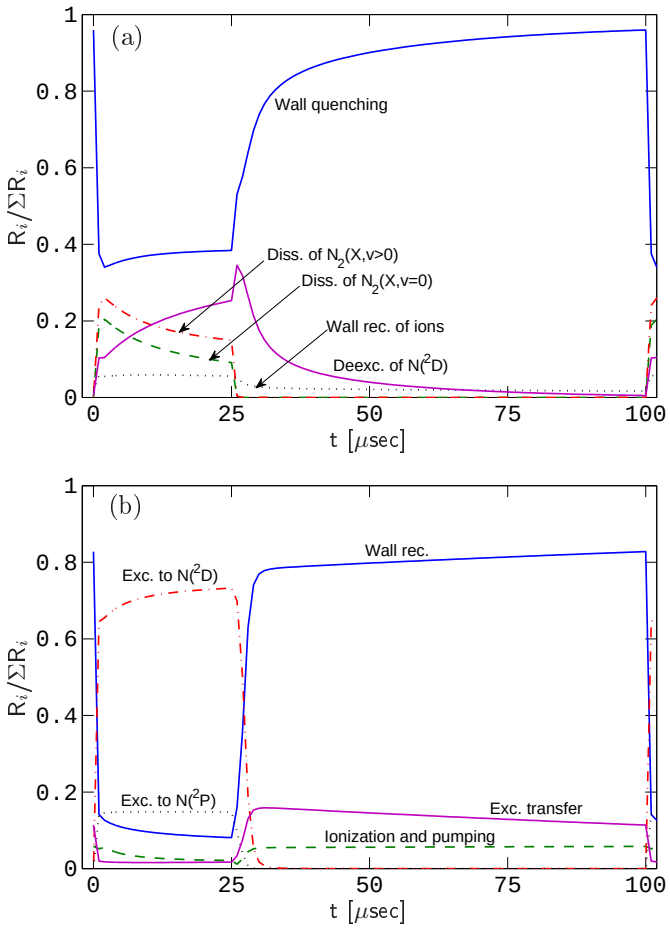

Figure 5.11: The reaction rates for (a) the creation and (b) the destruction of the N(^{4}S) atom versus time over a single pulsed power period.

off-period, whereas electron impact excitation of N(^{4}S) is the dominating process when the power is off, with a roughly 65 – 76 % contribution. Electron impact dissociation of $N_2(X^1\Sigma_g^+, v = 0-6)$ has a combined contribution of about 15 – 32 % during the on-period, but is negligible when the power is off.

As seen in figure 5.12(b), N(^{2}D) atoms are mostly lost by quenching at the wall,

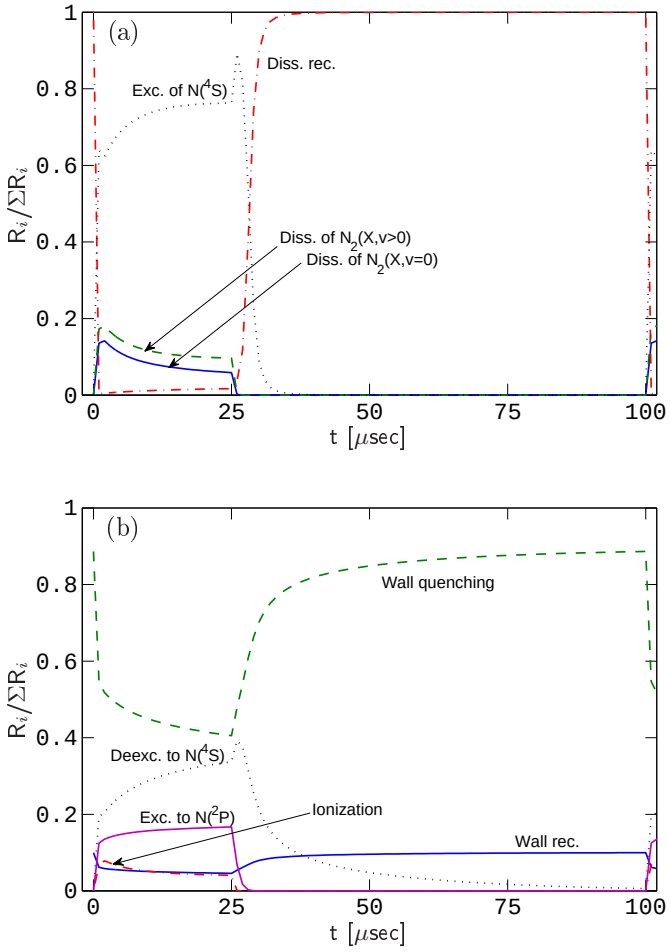

Figure 5.12: The reaction rates for (a) the creation and (b) the destruction of the N(^{2}D) atom versus time over a single pulsed power period.

contributing 41 – 55 % during the on-period but increasing to about 89 % at the end of the off-period. Electron impact de-excitation to N(^{4}S) has about 20 – 34 % contribution when the power is on, but decreasing rapidly once the power has been turned off. Electron impact excitation to N(^{2}P) is responsible for about 13 – 17 % of the N(^{2}D) loss during the on-period, but is negligible when the power is off. Recombination of N(^{2}D) on the wall has around 10 % contribution during

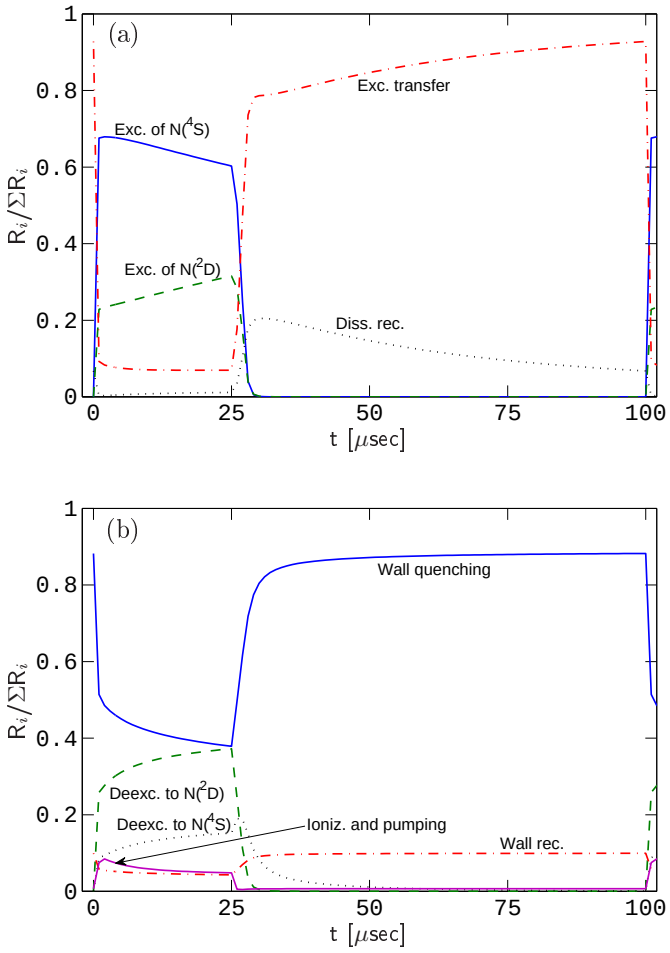

Figure 5.13: The reaction rates for (a) the creation and (b) the destruction of the $N(^2P)$ atom versus time over a single pulsed power period.

the off-period, but around 5 % when the power is on, which is very similar to the electron impact ionization contribution.

The reaction rates for the creation and destruction of the metastable nitrogen atom $N(^2P)$ are shown in figures 5.13(a) and (b), respectively. Although only having a 7 % contribution during the on-time, the metastable nitrogen atom $N(^2P)$ is mostly created by transfer of excitation from $N_2(A^3\Sigma_u^+)$, reaction (3.40), when

the power is off. Dissociative recombination, reaction (3.15), is responsible for the rest of the $N(^2P)$ creation during the off-period, having a contribution of roughly 7 – 21 %. Electron impact excitation of $N(^4S)$ and $N(^2D)$ is the dominating creation mechanism when the power is on, each contributing roughly 60 – 68 % and 23 – 32 %, respectively.

As seen in figure 5.13(b), $N(^2P)$ atoms are primarily lost by wall quenching, the contribution being around 87 % during the off-period and about 38 – 51 % during the on-period. Wall recombination is small during both periods, its contribution being around 10 % when the power is off and around 5 % when it is on. Electron impact ionization and pumping of $N(^2P)$ out of the chamber have a combined contribution of about 5 – 9 % when the power is on, but are negligible when it is off. Electron impact de-excitation to $N(^4S)$ and $N(^2D)$ is responsible for the rest of the $N(^2P)$ creation during the on-time, each having a contribution of roughly 8 – 15 % and 26 – 37 %, respectively.

The reaction rates for the creation and destruction of the N^+ ion are shown in figures 5.14(a) and (b), respectively. The atomic ion N^+ is entirely created by charge transfer, reaction (3.22), when the power is off, although that process is negligible when the power is on. The electron impact ionization of $N(^4S)$, $N(^2D)$ and $N(^2P)$ are responsible for most of the N^+ creation during the on-period, each having a contribution of roughly 34 – 49 %, 31 – 41 % and 10 – 13 %, respectively. Dissociative excitation, reaction (3.17), has no contribution during the off-period or at the start of the pulse, but increases to roughly 11 % at the end of the on-period.

As seen in figure 5.14(b), the N^+ ion is almost entirely lost to wall recombination during the on-period. The contribution of charge transfer, reaction (3.23), increases when the power is turned off, but is at most roughly 10 % at the end of the pulse, wall recombination being responsible for the rest.

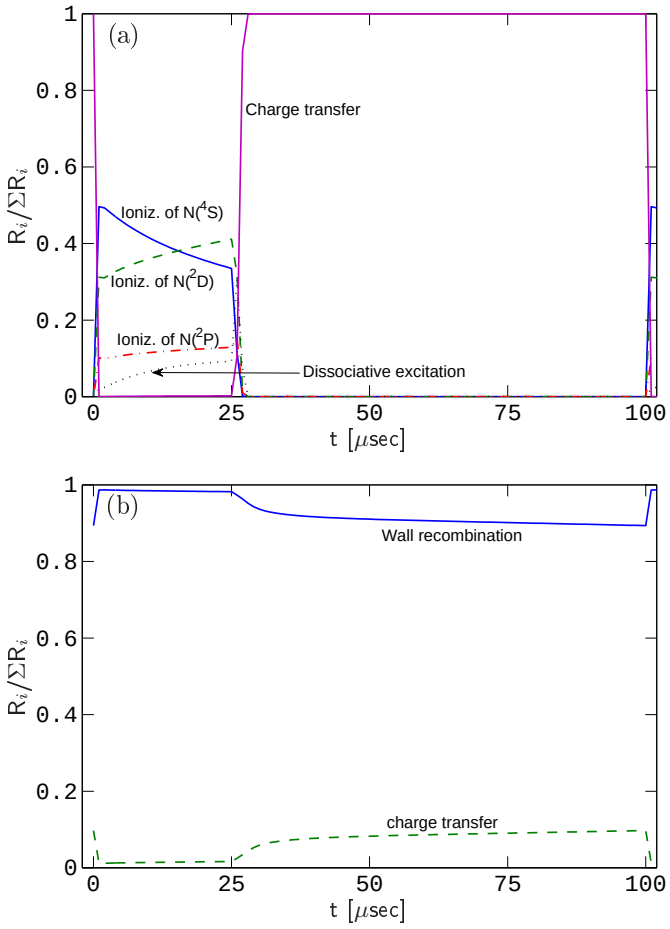

Figure 5.14: The reaction rates for (a) the creation and (b) the destruction of the N^+ ion versus time over a single pulsed power period.

The reaction rates for the creation and destruction of the N_2^+ ion are shown in figures 5.15(a) and (b), respectively. The N_2^+ ion is entirely created by charge transfer, reaction (3.23), and associative ionization, reaction (3.52) when the power is off, each having a contribution of around 31 and 69 %, respectively. Electron impact ionization of $N_2(X^1\Sigma_g^+, v = 0)$, $N_2(X^1\Sigma_g^+, v = 1-6)$ and $N_2(A^3\Sigma_u^+)$ are responsible for the N_2^+ creation during the on-period, each having a contribution

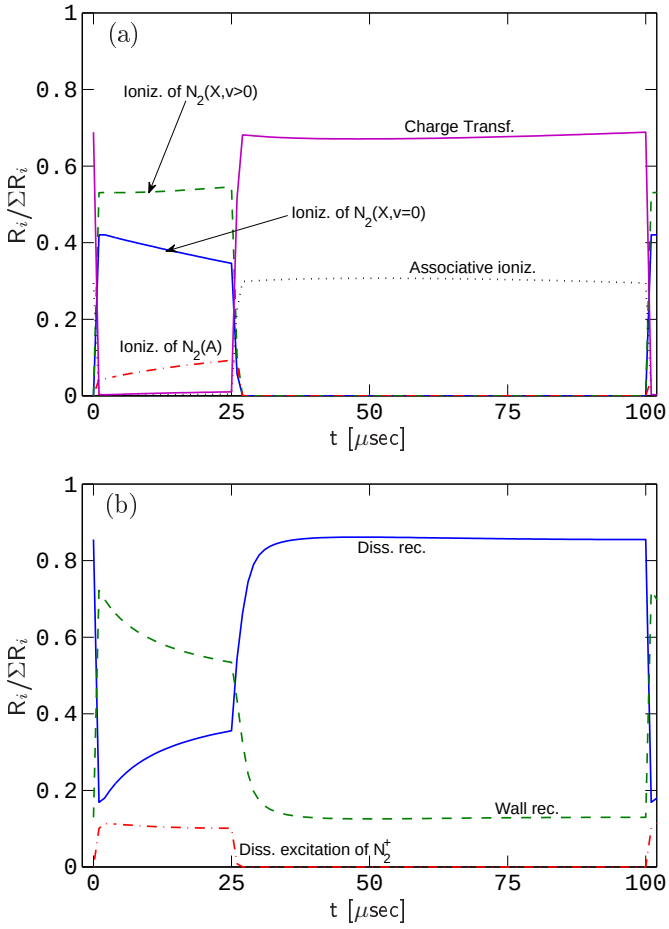

Figure 5.15: The reaction rates for (a) the creation and (b) the destruction of the N_2^+ ion versus time over a single pulsed power period.

of roughly $35-42$ %, $53-55$ % and $4-9$ %, respectively.

As seen in figure 5.15(b), dissociative recombination of N_2^+, reactions (3.13) to (3.15), is the primary loss channel of N_2^+ when the power is off, having around 86 % contribution, but is also very important during the on-period, having a contribution of roughly $17-36$ %. Recombination of N_2^+ on the wall is responsible for the rest of the loss during the off-period and is the primary loss channel when the power is

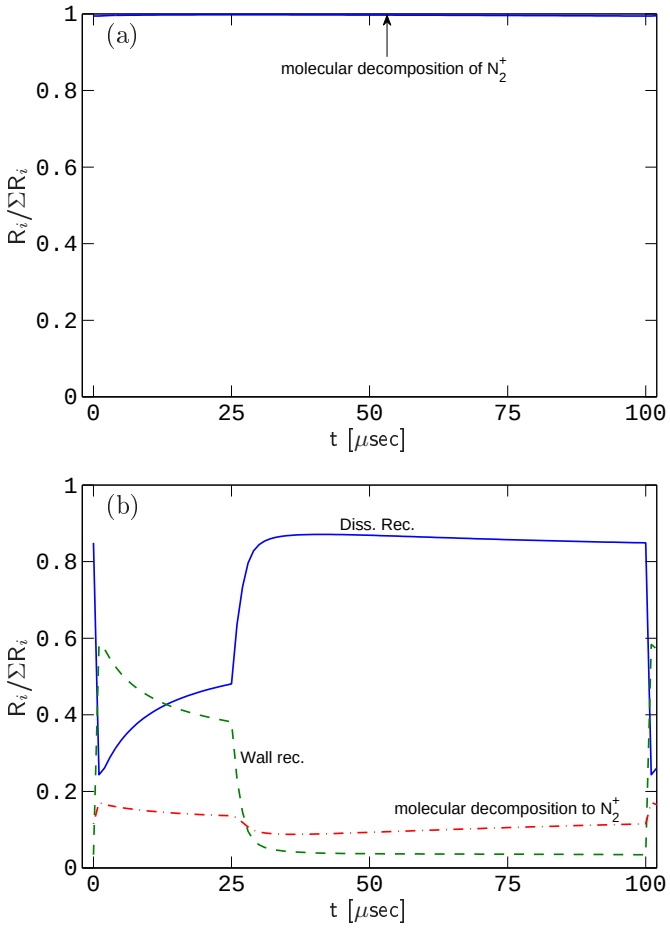

Figure 5.16: The reaction rates for (a) the creation and (b) the destruction of the N_3^+ ion versus time over a single pulsed power period.

on, having a contribution of roughly 53 – 72 %. Dissociative excitation, reaction (3.17), is negligible during the off-period, but has around 10 % contribution when the power is on.

The reaction rates for the creation and destruction of the N_3^+ ion are shown in figures 5.16(a) and (b), respectively. The creation mechanism for N_3^+ does not change when the power is pulsed, the rearrangement of N_2^+ chemical bonds, reaction (3.44), being entirely responsible for all N_3^+ creation during both on- and

off-periods.

As seen in figure 4.28(b), with a contribution of around 86 %, N_3^+ is predominantly lost by dissociative recombination, reaction (3.19), during the off-period. Dissociative recombination is also very important when the power is on, having about 24 – 48 % contribution. Recombination of N_3^+ on the wall has less than 4 % contribution during the off-period, but is very important during the on-period, having roughly 38 – 58 % contribution. The decomposition of N_3^+, reaction (3.45), has around 15 % contribution when the power is on, decreasing to around 10 % after the power has been turned off

The reaction rates for the creation and destruction of the N_4^+ ion are shown in figures 5.17(a) and (b), respectively. N_4^+ ions are predominantly created by associative ionization, reaction (3.53), the contribution being over 90 % whether the power is on or off. The combined contribution of three body association, reaction (3.49), is at most roughly 8 % soon after the power is turned on, but decreases to around 5 % towards the end of the pulse.

As seen in figure 5.17(b), N_4^+ are entirely lost by dissociative recombination of N_4^+, reaction (3.21), when the power is off and is also the dominant loss mechanism during the on-period. Recombination of N_4^+ on the wall is responsible for the rest of the N_4^+ loss during the on-period, having a contribution of roughly 6 – 15 %.

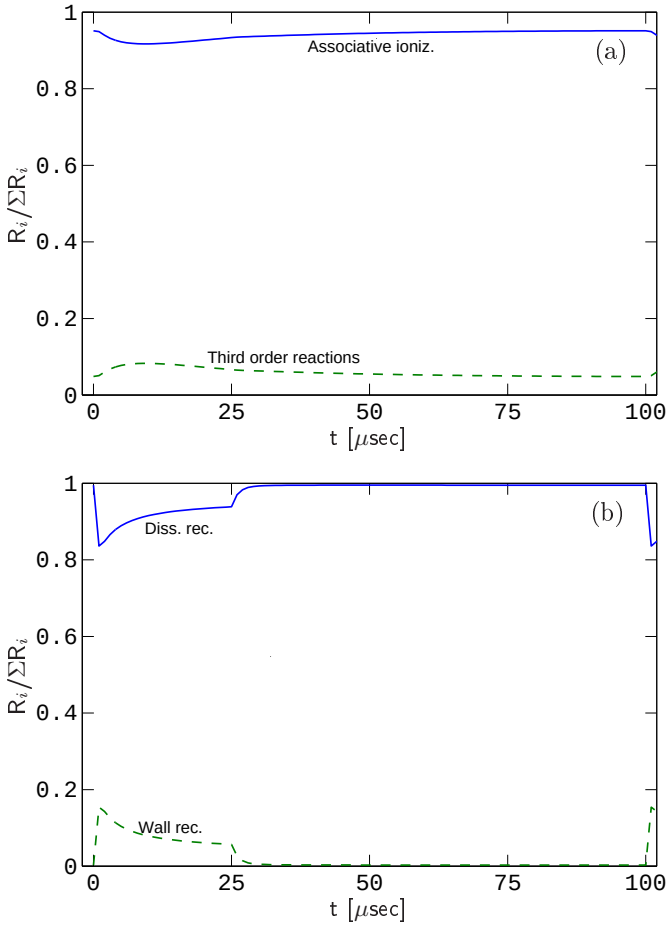

Figure 5.17: The reaction rates for (a) the creation and (b) the destruction of the N_4^+ ion versus time over a single pulsed power period.

Chapter 6

Conclusion

We find that the nitrogen discharge is essentially atomic when the pressure is around 1 mTorr but is highly molecular when the pressure is 100 mTorr. The model calculations of the electron temperature, electron density and ion fractions are in good agreement with measurements. However, our prediction of the density of neutrals, in particular the atomic density, are significantly larger than measured values. This indicates that the dissociation cross section is still questionable, likely being significantly too large, particularly for the dissociation of $N_2(X^1\Sigma_g^+, v > 0)$. The density of vibrationally excited ground state molecules $N_2(X^1\Sigma_g^+, v > 1)$ is negligible when the pressure is about 1 mTorr but increases rapidly as the pressure is increased, being a substantial part of the total molecular density when the pressure is above 10 mTorr. The atomic density also depends strongly on the absorbed power, the discharge being essentially atomic when the absorbed power is very high but highly molecular when the absorbed power is very low. The gas flowrate has very little effect on the plasma parameters when below 100 sccm, the discharge becoming somewhat more molecular when the flowrate is increased to 1000 sccm. Changing

the electron energy distribution function from Maxwellian to Druyvesteyn affects mostly the density of excited species, ground state species being more important when the distribution is Druyvesteyn-like. The gas temperature has a similar effect, the density of excited species decreasing with increasing gas temperature. The wall quenching coefficient of the excited species in the discharge must be relatively large, above roughly 0.1, to have any effect on the plasma parameters, then only decreasing the excited species density. The wall recombination coefficient controls the dissociation fraction in the discharge, being highly molecular when the value is unity and highly atomic when the value approaches zero. Yet, the electron temperature is independent of the wall recombination coefficient. The atomic density and electron density decrease rapidly when the chamber dimensions are increased, although a unity aspect ratio seems to be preferred. Neutral atoms are mostly created by electron impact dissociation of neutral nitrogen molecules, although the contribution of wall recombination of N^+ increases with decreasing pressure and accounts for about half the overall creation of neutral atoms at 1 mTorr. Neutral atoms are similarly lost mostly by recombination at the wall, except at 1 mTorr where pumping of atoms out of the chamber and electron impact ionization account for more than half the loss. Dissociative recombination of N_2^+ is very important for the loss of free electrons at high pressure. When the power is pulsed the density of the atomic ion N^+ is most significantly affected, with the $[N^+]/n_e$ fraction increasing far beyond the dissociation fraction when the modulation frequency or duty ratio is low. As a consequence the electron density increases compared to the corresponding steady state calculation. Electron collision processes generally dominate the creation and loss of the various species in the discharge when the power is turned on. When the power is off the electron temperature drops rapidly and, as a consequence, the contribution of conventional electron-neutral collision

processes quickly becomes negligible. As such, neutral atoms are created mostly by dissociative recombination of N_2^+ during the off-period, but by electron impact dissociation during the on-period. Dissociative recombination of N_2^+ is also the dominant loss process of N_2^+ during the off-period. The loss mechanism of N^+ does however not change significantly when the power is turned off, the ion being primarily lost by wall recombination with the power either on or off.

Overall, the model seems to describe the nitrogen discharge quite well in comparison to measurements. The exception to this is the density of neutral atoms which seems to be significantly too large. However, the measurements themselves are not all in good agreement with each other. In some cases, the atomic density has been measured simultaneously by two or more different methods, yielding vastly different results. Assuming that the model actually overestimates the density of neutral atoms, the fault must be that the electron impact dissociation cross section is substantially too large. This may well be the case, since it has been suggested elsewhere that the dissociation cross section may be too large by a factor of 10. The dissociation cross section must therefore be considered to be in doubt. However, if the fraction of neutral atoms decreases in our model, the fraction of the N^+ ion would inevitably be much lower as well, which is in disagreement with measurements. In this respect, we feel that the measurements are also inconsistent. Given the apparent difficulty with the measurement of the only parameter that our model is not in good agreement with, we are quite satisfied with the accuracy of the model calculations. Since nitrogen discharges are commonly diluted, the most straightforward addition to this model is to dilute the nitrogen with argon. The addition of hydrogen to the gas is much more complicated, but may nevertheless be of even more interest. This will hopefully be the subject of future studies.

Acknowledgments

I would like to thank my advisor, Dr. Jón Tómas Guðmundsson, for the invaluable guidance and input on this project throughout. I would also like to thank my parents for all the support during my studies, without which would not have been possible. Past and present members of *Team Tumi* are thanked as well for keeping the good team spirit.

This work was partially supported by the Icelandic Research Fund, the University of Iceland Research Fund and the Icelandic Research Fund for Graduate Students.

Appendix A

The nitrogen reaction set

The reactions that are used in the model and their rate coefficients are given in the tables below. The usage of the reactions and rate coefficient is identical to the representation here, since the tables are automatically generated each time the model is loaded. In table A.1 is a summary of electron collision reactions and their rate coefficients, calculated for a Maxwellian distribution of electron energy. A summary of reactions involving collisions of two and three heavy species and their rate coefficients as a function of gas temperature is given in tables A.2 and A.3, respectively. In table A.4 interactions with the wall and the equations used to calculate the corresponding rate coefficients are summarized. The transition frequency for optical emission from excited species is summarized in table A.5. Reactions representing pumping of gaseous species in and out of the gas chamber and the equations describing their rate coefficient are summarized in table A.6. Furthermore, a summary of the rate coefficients and the energy losses of processes leading to the loss of electron energy is given in tables A.7 and A.8 for collisions with the ground state nitrogen molecule and the ground state nitrogen atom, respectively.

Table A.1: Electron impact rate coefficients.

Reaction	Rate coefficient [m^3/s]	Reference
$e + N_2^+ \longrightarrow N(D) + N(D)$	$8.93 \times 10^{-15}\ T_e^{-0.30}$	175‡
$e + N_2^+ \longrightarrow N(S) + N(D)$	$6.46 \times 10^{-15}\ T_e^{-0.30}$	175‡
$e + N_2^+ \longrightarrow N(S) + N(P)$	$3.61 \times 10^{-15}\ T_e^{-0.30}$	175‡
$e + N_2^+ \longrightarrow N(D) + N^+ + e$	$3.72 \times 10^{-14}\ T_e^{0.24}\ e^{-8.63/T_e}$	16‡
$e + N_2^+ \longrightarrow N^+ + N^+ + e + e$	$3.74 \times 10^{-16}\ T_e^{1.48}\ e^{-25.00/T_e}$	16‡
$e + N_3^+ \longrightarrow N_2(A) + N(S)$	$1.61 \times 10^{-14}\ T_e^{-0.50}$	124‡
$e + N_3^+ \longrightarrow N_2(X, v{=}0) + N(P)$	$1.61 \times 10^{-14}\ T_e^{-0.50}$	124‡
$e + N_4^+ \longrightarrow N_2(X, v{=}0) + N_2(A)$	$3.20 \times 10^{-13}\ T_e^{-0.50}$	124
$e + N_2(X, v{=}0) \longrightarrow N_2^+ + e + e$	$1.17 \times 10^{-14}\ T_e^{0.67}\ e^{-17.84/T_e}$	231
$e + N_2(X, v{=}0) \longrightarrow N(D) + N^+ + e + e$	$5.88 \times 10^{-16}\ T_e^{1.17}\ e^{-22.36/T_e}$	231
$e + N_2(X, v{=}0) \longrightarrow N^+ + N^+ + e + e + e$	$9.95 \times 10^{-16}\ T_e^{0.56}\ e^{-43.62/T_e}$	231
$e + N_2(X, v{=}1) \longrightarrow N_2^+ + e + e$	$1.41 \times 10^{-14}\ T_e^{0.60}\ e^{-18.06/T_e}$	231*
$e + N_2(X, v{=}1) \longrightarrow N(D) + N^+ + e + e$	$4.95 \times 10^{-16}\ T_e^{1.22}\ e^{-21.66/T_e}$	231*
$e + N_2(X, v{=}1) \longrightarrow N^+ + N^+ + e + e + e$	$9.86 \times 10^{-16}\ T_e^{0.56}\ e^{-43.32/T_e}$	231*
$e + N_2(X, v{=}2) \longrightarrow N_2^+ + e + e$	$1.32 \times 10^{-14}\ T_e^{0.62}\ e^{-17.65/T_e}$	231*
$e + N_2(X, v{=}2) \longrightarrow N(D) + N^+ + e + e$	$4.14 \times 10^{-16}\ T_e^{1.28}\ e^{-20.95/T_e}$	231*
$e + N_2(X, v{=}2) \longrightarrow N^+ + N^+ + e + e + e$	$9.77 \times 10^{-16}\ T_e^{0.56}\ e^{-43.03/T_e}$	231*
$e + N_2(X, v{=}3) \longrightarrow N_2^+ + e + e$	$1.13 \times 10^{-14}\ T_e^{0.67}\ e^{-17.03/T_e}$	231*
$e + N_2(X, v{=}3) \longrightarrow N(D) + N^+ + e + e$	$4.06 \times 10^{-16}\ T_e^{1.28}\ e^{-20.65/T_e}$	231*
$e + N_2(X, v{=}3) \longrightarrow N^+ + N^+ + e + e + e$	$9.68 \times 10^{-16}\ T_e^{0.57}\ e^{-42.74/T_e}$	231*
$e + N_2(X, v{=}4) \longrightarrow N_2^+ + e + e$	$1.57 \times 10^{-14}\ T_e^{0.56}\ e^{-17.62/T_e}$	231*
$e + N_2(X, v{=}4) \longrightarrow N(D) + N^+ + e + e$	$4.11 \times 10^{-16}\ T_e^{1.28}\ e^{-20.45/T_e}$	231*
$e + N_2(X, v{=}4) \longrightarrow N^+ + N^+ + e + e + e$	$9.59 \times 10^{-16}\ T_e^{0.57}\ e^{-42.46/T_e}$	231*
$e + N_2(X, v{=}5) \longrightarrow N_2^+ + e + e$	$1.53 \times 10^{-14}\ T_e^{0.57}\ e^{-17.31/T_e}$	231*
$e + N_2(X, v{=}5) \longrightarrow N(D) + N^+ + e + e$	$4.29 \times 10^{-16}\ T_e^{1.26}\ e^{-20.31/T_e}$	231*
$e + N_2(X, v{=}5) \longrightarrow N^+ + N^+ + e + e + e$	$9.50 \times 10^{-16}\ T_e^{0.57}\ e^{-42.18/T_e}$	231*
$e + N_2(X, v{=}6) \longrightarrow N_2^+ + e + e$	$1.57 \times 10^{-14}\ T_e^{0.56}\ e^{-17.13/T_e}$	231*
$e + N_2(X, v{=}6) \longrightarrow N(D) + N^+ + e + e$	$4.25 \times 10^{-16}\ T_e^{1.26}\ e^{-20.05/T_e}$	231*
$e + N_2(X, v{=}6) \longrightarrow N^+ + N^+ + e + e + e$	$9.42 \times 10^{-16}\ T_e^{0.57}\ e^{-41.90/T_e}$	231*
$e + N_2(A) \longrightarrow N_2^+ + e + e$	$1.08 \times 10^{-14}\ T_e^{0.71}\ e^{-12.04/T_e}$	231*‡
$e + N_2(A) \longrightarrow N(D) + N^+ + e + e$	$6.47 \times 10^{-16}\ T_e^{1.17}\ e^{-16.80/T_e}$	231*‡
$e + N_2(A) \longrightarrow N^+ + N^+ + e + e + e$	$9.51 \times 10^{-16}\ T_e^{0.61}\ e^{-37.29/T_e}$	231*‡
$e + N(S) \longrightarrow N^+ + e + e$	$4.99 \times 10^{-15}\ T_e^{0.77}\ e^{-15.24/T_e}$	119
$e + N(D) \longrightarrow N^+ + e + e$	$1.67 \times 10^{-14}\ T_e^{0.50}\ e^{-13.07/T_e}$	119
$e + N(P) \longrightarrow N^+ + e + e$	$9.42 \times 10^{-15}\ T_e^{0.67}\ e^{-11.25/T_e}$	119
$e + N_2(X, v{=}0) \longrightarrow N(S) + N(D) + e$	$1.13 \times 10^{-14}\ T_e^{0.52}\ e^{-13.56/T_e}$	53
$e + N_2(X, v{=}1) \longrightarrow N(S) + N(D) + e$	$1.08 \times 10^{-14}\ T_e^{0.53}\ e^{-13.20/T_e}$	53*
$e + N_2(X, v{=}2) \longrightarrow N(S) + N(D) + e$	$1.07 \times 10^{-14}\ T_e^{0.53}\ e^{-12.94/T_e}$	53*
$e + N_2(X, v{=}3) \longrightarrow N(S) + N(D) + e$	$7.62 \times 10^{-15}\ T_e^{0.64}\ e^{-11.90/T_e}$	53*
$e + N_2(X, v{=}4) \longrightarrow N(S) + N(D) + e$	$7.56 \times 10^{-15}\ T_e^{0.65}\ e^{-11.67/T_e}$	53*
$e + N_2(X, v{=}5) \longrightarrow N(S) + N(D) + e$	$1.04 \times 10^{-14}\ T_e^{0.54}\ e^{-12.20/T_e}$	53*
$e + N_2(X, v{=}6) \longrightarrow N(S) + N(D) + e$	$8.82 \times 10^{-15}\ T_e^{0.59}\ e^{-11.58/T_e}$	53*
$e + N_2(A) \longrightarrow N(S) + N(D) + e$	$6.33 \times 10^{-15}\ T_e^{0.67}\ e^{-7.32/T_e}$	53*
$e + N_2(X, v{=}0) \longrightarrow N_2(A) + e$	$1.53 \times 10^{-14}\ T_e^{-0.49}\ e^{-8.68/T_e}$	108
$e + N_2(X, v{=}1) \longrightarrow N_2(A) + e$	$1.52 \times 10^{-14}\ T_e^{-0.49}\ e^{-8.44/T_e}$	108*
$e + N_2(X, v{=}2) \longrightarrow N_2(A) + e$	$1.42 \times 10^{-14}\ T_e^{-0.47}\ e^{-8.09/T_e}$	108*
$e + N_2(X, v{=}3) \longrightarrow N_2(A) + e$	$1.37 \times 10^{-14}\ T_e^{-0.46}\ e^{-7.81/T_e}$	108*
$e + N_2(X, v{=}4) \longrightarrow N_2(A) + e$	$1.34 \times 10^{-14}\ T_e^{-0.46}\ e^{-7.55/T_e}$	108*
$e + N_2(X, v{=}5) \longrightarrow N_2(A) + e$	$1.30 \times 10^{-14}\ T_e^{-0.46}\ e^{-7.30/T_e}$	108*
$e + N_2(X, v{=}6) \longrightarrow N_2(A) + e$	$1.27 \times 10^{-14}\ T_e^{-0.45}\ e^{-7.05/T_e}$	108*
$e + N_2(X, v{=}0) \longrightarrow N_2(X, v{=}1) + e$	$7.85 \times 10^{-14}\ T_e^{-1.45}\ e^{-2.44/T_e}$	194

*Obtained by reducing the threshold of the cross section.
†Obtained by applying the principle of detailed balancing on the cross section.
‡Magnitude of cross section changed (see text).

Table A.1: (continued)

Reaction	Rate coefficient [m^3/s]	Reference
$e + N_2(X, v{=}0) \longrightarrow N_2(X, v{=}2) + e$	$4.00 \times 10^{-14}\ T_e^{-1.46}\ e^{-2.38/T_e}$	194
$e + N_2(X, v{=}0) \longrightarrow N_2(X, v{=}3) + e$	$2.22 \times 10^{-14}\ T_e^{-1.47}\ e^{-2.38/T_e}$	194
$e + N_2(X, v{=}0) \longrightarrow N_2(X, v{=}4) + e$	$1.33 \times 10^{-14}\ T_e^{-1.47}\ e^{-2.42/T_e}$	194
$e + N_2(X, v{=}0) \longrightarrow N_2(X, v{=}5) + e$	$9.23 \times 10^{-15}\ T_e^{-1.48}\ e^{-2.53/T_e}$	194
$e + N_2(X, v{=}0) \longrightarrow N_2(X, v{=}6) + e$	$5.87 \times 10^{-15}\ T_e^{-1.48}\ e^{-2.68/T_e}$	194
$e + N_2(X, v{=}1) \longrightarrow N_2(X, v{=}2) + e$	$6.79 \times 10^{-14}\ T_e^{-1.43}\ e^{-2.30/T_e}$	64
$e + N_2(X, v{=}1) \longrightarrow N_2(X, v{=}3) + e$	$3.17 \times 10^{-14}\ T_e^{-1.44}\ e^{-2.31/T_e}$	64
$e + N_2(X, v{=}1) \longrightarrow N_2(X, v{=}4) + e$	$1.75 \times 10^{-14}\ T_e^{-1.46}\ e^{-2.40/T_e}$	64
$e + N_2(X, v{=}2) \longrightarrow N_2(X, v{=}3) + e$	$5.88 \times 10^{-14}\ T_e^{-1.41}\ e^{-2.40/T_e}$	64
$e + N_2(X, v{=}2) \longrightarrow N_2(X, v{=}4) + e$	$2.82 \times 10^{-14}\ T_e^{-1.42}\ e^{-2.37/T_e}$	64
$e + N_2(X, v{=}2) \longrightarrow N_2(X, v{=}5) + e$	$1.71 \times 10^{-14}\ T_e^{-1.44}\ e^{-2.39/T_e}$	64
$e + N_2(X, v{=}3) \longrightarrow N_2(X, v{=}4) + e$	$5.37 \times 10^{-14}\ T_e^{-1.40}\ e^{-2.42/T_e}$	64
$e + N_2(X, v{=}3) \longrightarrow N_2(X, v{=}5) + e$	$2.62 \times 10^{-14}\ T_e^{-1.41}\ e^{-2.41/T_e}$	64
$e + N_2(X, v{=}3) \longrightarrow N_2(X, v{=}6) + e$	$1.57 \times 10^{-14}\ T_e^{-1.43}\ e^{-2.46/T_e}$	64
$e + N_2(X, v{=}1) \longrightarrow N_2(X, v{=}0) + e$	$7.83 \times 10^{-14}\ T_e^{-1.45}\ e^{-2.16/T_e}$	64†
$e + N_2(X, v{=}2) \longrightarrow N_2(X, v{=}1) + e$	$6.74 \times 10^{-14}\ T_e^{-1.42}\ e^{-2.01/T_e}$	64†
$e + N_2(X, v{=}2) \longrightarrow N_2(X, v{=}0) + e$	$4.01 \times 10^{-14}\ T_e^{-1.46}\ e^{-1.81/T_e}$	64†
$e + N_2(X, v{=}3) \longrightarrow N_2(X, v{=}2) + e$	$5.83 \times 10^{-14}\ T_e^{-1.41}\ e^{-2.10/T_e}$	64†
$e + N_2(X, v{=}3) \longrightarrow N_2(X, v{=}1) + e$	$3.19 \times 10^{-14}\ T_e^{-1.45}\ e^{-1.76/T_e}$	64†
$e + N_2(X, v{=}3) \longrightarrow N_2(X, v{=}0) + e$	$2.20 \times 10^{-14}\ T_e^{-1.47}\ e^{-1.51/T_e}$	64†
$e + N(S) \longrightarrow N(D) + e$	$2.74 \times 10^{-14}\ T_e^{-0.40}\ e^{-3.35/T_e}$	228
$e + N(S) \longrightarrow N(P) + e$	$9.11 \times 10^{-15}\ T_e^{-0.45}\ e^{-4.80/T_e}$	228
$e + N(D) \longrightarrow N(P) + e$	$1.01 \times 10^{-14}\ T_e^{-0.18}\ e^{-3.94/T_e}$	228
$e + N_2(A) \longrightarrow N_2(X, v{=}0) + e$	$4.95 \times 10^{-15}\ T_e^{-0.47}\ e^{-2.50/T_e}$	108†
$e + N(P) \longrightarrow N(D) + e$	$1.64 \times 10^{-14}\ T_e^{-0.17}\ e^{-2.69/T_e}$	228†
$e + N(D) \longrightarrow N(S) + e$	$1.00 \times 10^{-14}\ T_e^{-0.36}\ e^{-0.83/T_e}$	228†
$e + N(P) \longrightarrow N(S) + e$	$5.45 \times 10^{-15}\ T_e^{-0.41}\ e^{-1.05/T_e}$	228†
$e + N_2(X, v{=}1) \longrightarrow N_2(X, v{=}5) + e$	$1.40 \times 10^{-14}\ T_e^{-1.46}\ e^{-2.40/T_e}$	64*‡
$e + N_2(X, v{=}1) \longrightarrow N_2(X, v{=}6) + e$	$1.29 \times 10^{-14}\ T_e^{-1.46}\ e^{-2.40/T_e}$	64*‡
$e + N_2(X, v{=}2) \longrightarrow N_2(X, v{=}6) + e$	$1.53 \times 10^{-14}\ T_e^{-1.44}\ e^{-2.39/T_e}$	64*‡
$e + N_2(X, v{=}4) \longrightarrow N_2(X, v{=}5) + e$	$4.49 \times 10^{-14}\ T_e^{-1.39}\ e^{-2.17/T_e}$	64*‡
$e + N_2(X, v{=}4) \longrightarrow N_2(X, v{=}6) + e$	$2.12 \times 10^{-14}\ T_e^{-1.41}\ e^{-2.16/T_e}$	64*‡
$e + N_2(X, v{=}5) \longrightarrow N_2(X, v{=}6) + e$	$3.93 \times 10^{-14}\ T_e^{-1.39}\ e^{-1.95/T_e}$	64*‡
$e + N_2(X, v{=}5) \longrightarrow N_2(X, v{=}1) + e$	$1.11 \times 10^{-14}\ T_e^{-1.45}\ e^{-1.27/T_e}$	64†‡
$e + N_2(X, v{=}6) \longrightarrow N_2(X, v{=}1) + e$	$9.52 \times 10^{-15}\ T_e^{-1.46}\ e^{-1.01/T_e}$	64†‡
$e + N_2(X, v{=}6) \longrightarrow N_2(X, v{=}2) + e$	$1.35 \times 10^{-14}\ T_e^{-1.43}\ e^{-1.27/T_e}$	64†‡
$e + N_2(X, v{=}5) \longrightarrow N_2(X, v{=}4) + e$	$4.17 \times 10^{-14}\ T_e^{-1.39}\ e^{-1.88/T_e}$	64†‡
$e + N_2(X, v{=}6) \longrightarrow N_2(X, v{=}4) + e$	$1.96 \times 10^{-14}\ T_e^{-1.42}\ e^{-1.64/T_e}$	64†‡
$e + N_2(X, v{=}6) \longrightarrow N_2(X, v{=}5) + e$	$3.73 \times 10^{-14}\ T_e^{-1.41}\ e^{-1.71/T_e}$	64†‡
$e + N_2(X, v{=}4) \longrightarrow N_2(X, v{=}1) + e$	$1.74 \times 10^{-14}\ T_e^{-1.45}\ e^{-1.55/T_e}$	64†
$e + N_2(X, v{=}4) \longrightarrow N_2(X, v{=}2) + e$	$2.83 \times 10^{-14}\ T_e^{-1.43}\ e^{-1.81/T_e}$	64†
$e + N_2(X, v{=}5) \longrightarrow N_2(X, v{=}2) + e$	$1.69 \times 10^{-14}\ T_e^{-1.43}\ e^{-1.53/T_e}$	64†
$e + N_2(X, v{=}4) \longrightarrow N_2(X, v{=}3) + e$	$5.29 \times 10^{-14}\ T_e^{-1.39}\ e^{-2.12/T_e}$	64†
$e + N_2(X, v{=}5) \longrightarrow N_2(X, v{=}3) + e$	$2.57 \times 10^{-14}\ T_e^{-1.40}\ e^{-1.84/T_e}$	64†
$e + N_2(X, v{=}6) \longrightarrow N_2(X, v{=}3) + e$	$1.59 \times 10^{-14}\ T_e^{-1.43}\ e^{-1.65/T_e}$	64†
$e + N_2(X, v{=}4) \longrightarrow N_2(X, v{=}0) + e$	$1.32 \times 10^{-14}\ T_e^{-1.47}\ e^{-1.28/T_e}$	194†
$e + N_2(X, v{=}5) \longrightarrow N_2(X, v{=}0) + e$	$9.19 \times 10^{-15}\ T_e^{-1.47}\ e^{-1.12/T_e}$	194†
$e + N_2(X, v{=}6) \longrightarrow N_2(X, v{=}0) + e$	$5.87 \times 10^{-15}\ T_e^{-1.48}\ e^{-1.00/T_e}$	194†
$e + N_2(A) \longrightarrow N_2(X, v{=}1) + e$	$4.79 \times 10^{-15}\ T_e^{-0.47}\ e^{-2.50/T_e}$	108†
$e + N_2(A) \longrightarrow N_2(X, v{=}2) + e$	$4.65 \times 10^{-15}\ T_e^{-0.46}\ e^{-2.51/T_e}$	108†
$e + N_2(A) \longrightarrow N_2(X, v{=}3) + e$	$4.48 \times 10^{-15}\ T_e^{-0.45}\ e^{-2.50/T_e}$	108†
$e + N_2(A) \longrightarrow N_2(X, v{=}4) + e$	$4.35 \times 10^{-15}\ T_e^{-0.45}\ e^{-2.51/T_e}$	108†

*Obtained by reducing the threshold of the cross section.
†Obtained by applying the principle of detailed balancing on the cross section.
‡Magnitude of cross section changed (see text).

Table A.1: (continued)

Reaction	Rate coefficient [m^3/s]	Reference
$e + N_2(A) \longrightarrow N_2(X, v{=}5) + e$	$4.17 \times 10^{-15}\ T_e^{-0.44}\ e^{-2.50/T_e}$	108†
$e + N_2(A) \longrightarrow N_2(X, v{=}6) + e$	$4.02 \times 10^{-15}\ T_e^{-0.43}\ e^{-2.50/T_e}$	108†

†Obtained by applying the principle of detailed balancing on the cross section.

Table A.2: Rate coefficients for collisions of two gaseous species

Reaction	Rate coefficient [m^3/s]	Reference
$N(S) + N_2^+ \longrightarrow N_2(X, v{=}3) + N^+$	$7.20 \times 10^{-19}\ (300/T_g)^{-1.00}$	124
$N(D) + N_2^+ \longrightarrow N_2(X, v{=}6) + N^+$	$7.20 \times 10^{-19}\ (300/T_g)^{-1.00}$	124
$N(P) + N_2^+ \longrightarrow N_2(X, v{=}6) + N^+$	$7.20 \times 10^{-19}\ (300/T_g)^{-1.00}$	124
$N_2(X, v{=}3) + N^+ \longrightarrow N(S) + N_2^+$	$2.00 \times 10^{-17}\ e^{-2829/T_g}$	223
$N_2(X, v{=}4) + N^+ \longrightarrow N(S) + N_2^+$	2.00×10^{-17}	223
$N_2(X, v{=}5) + N^+ \longrightarrow N(S) + N_2^+$	2.00×10^{-17}	223
$N_2(X, v{=}6) + N^+ \longrightarrow N(S) + N_2^+$	2.00×10^{-17}	223
$N_2(A) + N^+ \longrightarrow N(P) + N_2^+$	2.00×10^{-17}	223
$N_2(X, v{=}0) + N_2(A) \longrightarrow N_2(X, v{=}0) + N_2(X, v{=}0)$	3.00×10^{-24}	124, 102
$N_2(X, v{=}1) + N_2(A) \longrightarrow N_2(X, v{=}0) + N_2(X, v{=}1)$	3.00×10^{-24}	124, 102
$N_2(X, v{=}2) + N_2(A) \longrightarrow N_2(X, v{=}0) + N_2(X, v{=}2)$	3.00×10^{-24}	124, 102
$N_2(X, v{=}3) + N_2(A) \longrightarrow N_2(X, v{=}0) + N_2(X, v{=}3)$	3.00×10^{-24}	124, 102
$N_2(X, v{=}4) + N_2(A) \longrightarrow N_2(X, v{=}0) + N_2(X, v{=}4)$	3.00×10^{-24}	124, 102
$N_2(X, v{=}5) + N_2(A) \longrightarrow N_2(X, v{=}0) + N_2(X, v{=}5)$	3.00×10^{-24}	124, 102
$N_2(X, v{=}6) + N_2(A) \longrightarrow N_2(X, v{=}0) + N_2(X, v{=}6)$	3.00×10^{-24}	124, 102
$N_2(A) + N_2(A) \longrightarrow N_2(X, v{=}0) + N_2(A)$	3.50×10^{-16}	102, 180
$N_2(X, v{=}0) + N(D) \longrightarrow N_2(X, v{=}0) + N(S)$	1.30×10^{-20}	219
$N_2(X, v{=}1) + N(D) \longrightarrow N_2(X, v{=}1) + N(S)$	1.30×10^{-20}	219
$N_2(X, v{=}2) + N(D) \longrightarrow N_2(X, v{=}2) + N(S)$	1.30×10^{-20}	219
$N_2(X, v{=}3) + N(D) \longrightarrow N_2(X, v{=}3) + N(S)$	1.30×10^{-20}	219
$N_2(X, v{=}4) + N(D) \longrightarrow N_2(X, v{=}4) + N(S)$	1.30×10^{-20}	219
$N_2(X, v{=}5) + N(D) \longrightarrow N_2(X, v{=}5) + N(S)$	1.30×10^{-20}	219
$N_2(X, v{=}6) + N(D) \longrightarrow N_2(X, v{=}6) + N(S)$	1.30×10^{-20}	219
$N_2(A) + N(D) \longrightarrow N_2(A) + N(S)$	1.30×10^{-20}	219
$N_2(X, v{=}0) + N(P) \longrightarrow N_2(X, v{=}0) + N(S)$	3.30×10^{-23}	219
$N_2(X, v{=}1) + N(P) \longrightarrow N_2(X, v{=}1) + N(S)$	3.30×10^{-23}	219
$N_2(X, v{=}2) + N(P) \longrightarrow N_2(X, v{=}2) + N(S)$	3.30×10^{-23}	219
$N_2(X, v{=}3) + N(P) \longrightarrow N_2(X, v{=}3) + N(S)$	3.30×10^{-23}	219
$N_2(X, v{=}4) + N(P) \longrightarrow N_2(X, v{=}4) + N(S)$	3.30×10^{-23}	219
$N_2(X, v{=}5) + N(P) \longrightarrow N_2(X, v{=}5) + N(S)$	3.30×10^{-23}	219
$N_2(X, v{=}6) + N(P) \longrightarrow N_2(X, v{=}6) + N(S)$	3.30×10^{-23}	219
$N_2(A) + N(P) \longrightarrow N_2(A) + N(S)$	3.30×10^{-23}	219
$N(S) + N(P) \longrightarrow N(S) + N(S)$	6.20×10^{-19}	246
$N(D) + N(P) \longrightarrow N(S) + N(D)$	6.20×10^{-19}	246
$N(P) + N(P) \longrightarrow N(S) + N(P)$	6.20×10^{-19}	246
$N_2(A) + N(S) \longrightarrow N_2(X, v{=}0) + N(P)$	4.00×10^{-17}	182
$N(D) + N(P) \longrightarrow N_2^+ + e$	1.00×10^{-18}	124
$N(P) + N(P) \longrightarrow N_2^+ + e$	1.00×10^{-18}	124
$N_2(A) + N_2(A) \longrightarrow N_4^+ + e$	1.00×10^{-19}	81
$N_2(A) + N_2^+ \longrightarrow N(S) + N_3^+$	5.50×10^{-17}	30
$N(S) + N_3^+ \longrightarrow N_2(A) + N_2^+$	6.60×10^{-17}	124
$N(D) + N_3^+ \longrightarrow N_2(A) + N_2^+$	6.60×10^{-17}	124

Table A.2: (continued)

Reaction	Rate coefficient [m^3/s]	Reference
$N(P) + N_3^+ \longrightarrow N_2(A) + N_2^+$	6.60×10^{-17}	124
$N(S) + N_4^+ \longrightarrow N_2(X, v{=}0) + N_2(X, v{=}0) + N^+$	1.00×10^{-17}	124
$N(D) + N_4^+ \longrightarrow N_2(X, v{=}4) + N_2(X, v{=}4) + N^+$	1.00×10^{-17}	124
$N(P) + N_4^+ \longrightarrow N_2(X, v{=}6) + N_2(X, v{=}6) + N^+$	1.00×10^{-17}	124
$N_2(X, v{=}0) + N_4^+ \longrightarrow N_2(X, v{=}0) + N_2(X, v{=}0) + N_2^+$	$8.67 \times 10^{-23}\ (300/T_g)^{-6.45} e^{900/T_g}$	81, 225
$N_2(X, v{=}1) + N_4^+ \longrightarrow N_2(X, v{=}0) + N_2(X, v{=}1) + N_2^+$	$8.67 \times 10^{-23}\ (300/T_g)^{-6.45} e^{900/T_g}$	81, 225
$N_2(X, v{=}2) + N_4^+ \longrightarrow N_2(X, v{=}0) + N_2(X, v{=}2) + N_2^+$	$8.67 \times 10^{-23}\ (300/T_g)^{-6.45} e^{900/T_g}$	81, 225
$N_2(X, v{=}3) + N_4^+ \longrightarrow N_2(X, v{=}0) + N_2(X, v{=}3) + N_2^+$	$8.67 \times 10^{-23}\ (300/T_g)^{-6.45} e^{900/T_g}$	81, 225
$N_2(X, v{=}4) + N_4^+ \longrightarrow N_2(X, v{=}0) + N_2(X, v{=}4) + N_2^+$	$8.67 \times 10^{-23}\ (300/T_g)^{-6.45} e^{900/T_g}$	81, 225
$N_2(X, v{=}5) + N_4^+ \longrightarrow N_2(X, v{=}0) + N_2(X, v{=}5) + N_2^+$	$8.67 \times 10^{-23}\ (300/T_g)^{-6.45} e^{900/T_g}$	81, 225
$N_2(X, v{=}6) + N_4^+ \longrightarrow N_2(X, v{=}0) + N_2(X, v{=}6) + N_2^+$	$8.67 \times 10^{-23}\ (300/T_g)^{-6.45} e^{900/T_g}$	81, 225
$N_2(A) + N_4^+ \longrightarrow N_2(X, v{=}0) + N_2(A) + N_2^+$	$8.67 \times 10^{-23}\ (300/T_g)^{-6.45} e^{900/T_g}$	81, 225
$N_2(X, v{=}0) + N_2(X, v{=}1) \longrightarrow N_2(X, v{=}0) + N_2(X, v{=}0)$	$5.19 \times 10^{-28}\ (300/T_g)^{-8.51}$	22
$N_2(X, v{=}1) + N_2(X, v{=}1) \longrightarrow N_2(X, v{=}0) + N_2(X, v{=}1)$	$5.19 \times 10^{-28}\ (300/T_g)^{-8.51}$	22
$N_2(X, v{=}1) + N_2(X, v{=}2) \longrightarrow N_2(X, v{=}0) + N_2(X, v{=}2)$	$5.19 \times 10^{-28}\ (300/T_g)^{-8.51}$	22
$N_2(X, v{=}1) + N_2(X, v{=}3) \longrightarrow N_2(X, v{=}0) + N_2(X, v{=}3)$	$5.19 \times 10^{-28}\ (300/T_g)^{-8.51}$	22
$N_2(X, v{=}1) + N_2(X, v{=}4) \longrightarrow N_2(X, v{=}0) + N_2(X, v{=}4)$	$5.19 \times 10^{-28}\ (300/T_g)^{-8.51}$	22
$N_2(X, v{=}1) + N_2(X, v{=}5) \longrightarrow N_2(X, v{=}0) + N_2(X, v{=}5)$	$5.19 \times 10^{-28}\ (300/T_g)^{-8.51}$	22
$N_2(X, v{=}1) + N_2(X, v{=}6) \longrightarrow N_2(X, v{=}0) + N_2(X, v{=}6)$	$5.19 \times 10^{-28}\ (300/T_g)^{-8.51}$	22
$N_2(X, v{=}0) + N_2(X, v{=}2) \longrightarrow N_2(X, v{=}0) + N_2(X, v{=}1)$	$1.15 \times 10^{-27}\ (300/T_g)^{-8.54}$	22
$N_2(X, v{=}1) + N_2(X, v{=}2) \longrightarrow N_2(X, v{=}1) + N_2(X, v{=}1)$	$1.15 \times 10^{-27}\ (300/T_g)^{-8.54}$	22
$N_2(X, v{=}2) + N_2(X, v{=}2) \longrightarrow N_2(X, v{=}1) + N_2(X, v{=}2)$	$1.15 \times 10^{-27}\ (300/T_g)^{-8.54}$	22
$N_2(X, v{=}2) + N_2(X, v{=}3) \longrightarrow N_2(X, v{=}1) + N_2(X, v{=}3)$	$1.15 \times 10^{-27}\ (300/T_g)^{-8.54}$	22
$N_2(X, v{=}2) + N_2(X, v{=}4) \longrightarrow N_2(X, v{=}1) + N_2(X, v{=}4)$	$1.15 \times 10^{-27}\ (300/T_g)^{-8.54}$	22
$N_2(X, v{=}2) + N_2(X, v{=}5) \longrightarrow N_2(X, v{=}1) + N_2(X, v{=}5)$	$1.15 \times 10^{-27}\ (300/T_g)^{-8.54}$	22
$N_2(X, v{=}2) + N_2(X, v{=}6) \longrightarrow N_2(X, v{=}1) + N_2(X, v{=}6)$	$1.15 \times 10^{-27}\ (300/T_g)^{-8.54}$	22
$N_2(X, v{=}0) + N_2(X, v{=}3) \longrightarrow N_2(X, v{=}0) + N_2(X, v{=}2)$	$2.18 \times 10^{-27}\ (300/T_g)^{-8.53}$	22
$N_2(X, v{=}1) + N_2(X, v{=}3) \longrightarrow N_2(X, v{=}1) + N_2(X, v{=}2)$	$2.18 \times 10^{-27}\ (300/T_g)^{-8.53}$	22
$N_2(X, v{=}2) + N_2(X, v{=}3) \longrightarrow N_2(X, v{=}2) + N_2(X, v{=}2)$	$2.18 \times 10^{-27}\ (300/T_g)^{-8.53}$	22
$N_2(X, v{=}3) + N_2(X, v{=}3) \longrightarrow N_2(X, v{=}2) + N_2(X, v{=}3)$	$2.18 \times 10^{-27}\ (300/T_g)^{-8.53}$	22
$N_2(X, v{=}3) + N_2(X, v{=}4) \longrightarrow N_2(X, v{=}2) + N_2(X, v{=}4)$	$2.18 \times 10^{-27}\ (300/T_g)^{-8.53}$	22
$N_2(X, v{=}3) + N_2(X, v{=}5) \longrightarrow N_2(X, v{=}2) + N_2(X, v{=}5)$	$2.18 \times 10^{-27}\ (300/T_g)^{-8.53}$	22
$N_2(X, v{=}3) + N_2(X, v{=}6) \longrightarrow N_2(X, v{=}2) + N_2(X, v{=}6)$	$2.18 \times 10^{-27}\ (300/T_g)^{-8.53}$	22
$N_2(X, v{=}0) + N_2(X, v{=}4) \longrightarrow N_2(X, v{=}0) + N_2(X, v{=}3)$	$4.32 \times 10^{-27}\ (300/T_g)^{-8.30}$	22
$N_2(X, v{=}1) + N_2(X, v{=}4) \longrightarrow N_2(X, v{=}1) + N_2(X, v{=}3)$	$4.32 \times 10^{-27}\ (300/T_g)^{-8.30}$	22
$N_2(X, v{=}2) + N_2(X, v{=}4) \longrightarrow N_2(X, v{=}2) + N_2(X, v{=}3)$	$4.32 \times 10^{-27}\ (300/T_g)^{-8.30}$	22
$N_2(X, v{=}3) + N_2(X, v{=}4) \longrightarrow N_2(X, v{=}3) + N_2(X, v{=}3)$	$4.32 \times 10^{-27}\ (300/T_g)^{-8.30}$	22
$N_2(X, v{=}4) + N_2(X, v{=}4) \longrightarrow N_2(X, v{=}3) + N_2(X, v{=}4)$	$4.32 \times 10^{-27}\ (300/T_g)^{-8.30}$	22
$N_2(X, v{=}4) + N_2(X, v{=}5) \longrightarrow N_2(X, v{=}3) + N_2(X, v{=}5)$	$4.32 \times 10^{-27}\ (300/T_g)^{-8.30}$	22
$N_2(X, v{=}4) + N_2(X, v{=}6) \longrightarrow N_2(X, v{=}3) + N_2(X, v{=}6)$	$4.32 \times 10^{-27}\ (300/T_g)^{-8.30}$	22
$N_2(X, v{=}0) + N_2(X, v{=}5) \longrightarrow N_2(X, v{=}0) + N_2(X, v{=}4)$	$6.87 \times 10^{-27}\ (300/T_g)^{-8.27}$	22
$N_2(X, v{=}1) + N_2(X, v{=}5) \longrightarrow N_2(X, v{=}1) + N_2(X, v{=}4)$	$6.87 \times 10^{-27}\ (300/T_g)^{-8.27}$	22
$N_2(X, v{=}2) + N_2(X, v{=}5) \longrightarrow N_2(X, v{=}2) + N_2(X, v{=}4)$	$6.87 \times 10^{-27}\ (300/T_g)^{-8.27}$	22
$N_2(X, v{=}3) + N_2(X, v{=}5) \longrightarrow N_2(X, v{=}3) + N_2(X, v{=}4)$	$6.87 \times 10^{-27}\ (300/T_g)^{-8.27}$	22
$N_2(X, v{=}4) + N_2(X, v{=}5) \longrightarrow N_2(X, v{=}4) + N_2(X, v{=}4)$	$6.87 \times 10^{-27}\ (300/T_g)^{-8.27}$	22
$N_2(X, v{=}5) + N_2(X, v{=}5) \longrightarrow N_2(X, v{=}4) + N_2(X, v{=}5)$	$6.87 \times 10^{-27}\ (300/T_g)^{-8.27}$	22
$N_2(X, v{=}5) + N_2(X, v{=}6) \longrightarrow N_2(X, v{=}4) + N_2(X, v{=}6)$	$6.87 \times 10^{-27}\ (300/T_g)^{-8.27}$	22
$N_2(X, v{=}0) + N_2(X, v{=}6) \longrightarrow N_2(X, v{=}0) + N_2(X, v{=}5)$	$1.10 \times 10^{-26}\ (300/T_g)^{-8.15}$	22
$N_2(X, v{=}1) + N_2(X, v{=}6) \longrightarrow N_2(X, v{=}1) + N_2(X, v{=}5)$	$1.10 \times 10^{-26}\ (300/T_g)^{-8.15}$	22
$N_2(X, v{=}2) + N_2(X, v{=}6) \longrightarrow N_2(X, v{=}2) + N_2(X, v{=}5)$	$1.10 \times 10^{-26}\ (300/T_g)^{-8.15}$	22
$N_2(X, v{=}3) + N_2(X, v{=}6) \longrightarrow N_2(X, v{=}3) + N_2(X, v{=}5)$	$1.10 \times 10^{-26}\ (300/T_g)^{-8.15}$	22
$N_2(X, v{=}4) + N_2(X, v{=}6) \longrightarrow N_2(X, v{=}4) + N_2(X, v{=}5)$	$1.10 \times 10^{-26}\ (300/T_g)^{-8.15}$	22
$N_2(X, v{=}5) + N_2(X, v{=}6) \longrightarrow N_2(X, v{=}5) + N_2(X, v{=}5)$	$1.10 \times 10^{-26}\ (300/T_g)^{-8.15}$	22
$N_2(X, v{=}6) + N_2(X, v{=}6) \longrightarrow N_2(X, v{=}5) + N_2(X, v{=}6)$	$1.10 \times 10^{-26}\ (300/T_g)^{-8.15}$	22

Table A.2: (continued)

Reaction	Rate coefficient [m^3/s]	Reference
$N_2(X, v{=}3) + N_2(A) \longrightarrow N_2(X, v{=}0) + N_2(A)$	$3.00 \times 10^{-17}\ e^{-3757/T_g}$	181
$N_2(X, v{=}4) + N_2(A) \longrightarrow N_2(X, v{=}0) + N_2(A)$	$3.00 \times 10^{-17}\ e^{-533/T_g}$	181
$N_2(X, v{=}5) + N_2(A) \longrightarrow N_2(X, v{=}0) + N_2(A)$	3.00×10^{-17}	181
$N_2(X, v{=}6) + N_2(A) \longrightarrow N_2(X, v{=}0) + N_2(A)$	3.00×10^{-17}	181
$N_2(X, v{=}1) + N_2(X, v{=}1) \longrightarrow N_2(X, v{=}0) + N_2(X, v{=}2)$	$1.73 \times 10^{-20}\ (300/T_g)^{-1.42}$	22
$N_2(X, v{=}1) + N_2(X, v{=}2) \longrightarrow N_2(X, v{=}0) + N_2(X, v{=}3)$	$2.18 \times 10^{-20}\ (300/T_g)^{-1.54}$	22
$N_2(X, v{=}1) + N_2(X, v{=}3) \longrightarrow N_2(X, v{=}0) + N_2(X, v{=}4)$	$2.60 \times 10^{-20}\ (300/T_g)^{-1.55}$	22
$N_2(X, v{=}1) + N_2(X, v{=}4) \longrightarrow N_2(X, v{=}0) + N_2(X, v{=}5)$	$2.80 \times 10^{-20}\ (300/T_g)^{-1.63}$	22
$N_2(X, v{=}1) + N_2(X, v{=}5) \longrightarrow N_2(X, v{=}0) + N_2(X, v{=}6)$	$3.09 \times 10^{-20}\ (300/T_g)^{-1.63}$	22
$N_2(X, v{=}0) + N_2(X, v{=}2) \longrightarrow N_2(X, v{=}1) + N_2(X, v{=}1)$	$1.73 \times 10^{-20}\ (300/T_g)^{-1.42} e^{-42/T_g}$	22
$N_2(X, v{=}2) + N_2(X, v{=}2) \longrightarrow N_2(X, v{=}1) + N_2(X, v{=}3)$	$5.20 \times 10^{-20}\ (300/T_g)^{-1.42}$	22‡
$N_2(X, v{=}2) + N_2(X, v{=}3) \longrightarrow N_2(X, v{=}1) + N_2(X, v{=}4)$	$5.82 \times 10^{-20}\ (300/T_g)^{-1.54}$	22‡
$N_2(X, v{=}2) + N_2(X, v{=}4) \longrightarrow N_2(X, v{=}1) + N_2(X, v{=}5)$	$6.51 \times 10^{-20}\ (300/T_g)^{-1.55}$	22‡
$N_2(X, v{=}2) + N_2(X, v{=}5) \longrightarrow N_2(X, v{=}1) + N_2(X, v{=}6)$	$6.72 \times 10^{-20}\ (300/T_g)^{-1.63}$	22‡
$N_2(X, v{=}0) + N_2(X, v{=}3) \longrightarrow N_2(X, v{=}1) + N_2(X, v{=}2)$	$2.18 \times 10^{-20}\ (300/T_g)^{-1.54} e^{-82/T_g}$	22
$N_2(X, v{=}1) + N_2(X, v{=}3) \longrightarrow N_2(X, v{=}2) + N_2(X, v{=}2)$	$5.20 \times 10^{-20}\ (300/T_g)^{-1.42} e^{-40/T_g}$	22‡
$N_2(X, v{=}3) + N_2(X, v{=}3) \longrightarrow N_2(X, v{=}2) + N_2(X, v{=}4)$	$1.04 \times 10^{-19}\ (300/T_g)^{-1.42}$	22‡
$N_2(X, v{=}3) + N_2(X, v{=}4) \longrightarrow N_2(X, v{=}2) + N_2(X, v{=}5)$	$1.09 \times 10^{-19}\ (300/T_g)^{-1.54}$	22‡
$N_2(X, v{=}3) + N_2(X, v{=}5) \longrightarrow N_2(X, v{=}2) + N_2(X, v{=}6)$	$1.17 \times 10^{-19}\ (300/T_g)^{-1.55}$	22‡
$N_2(X, v{=}0) + N_2(X, v{=}4) \longrightarrow N_2(X, v{=}1) + N_2(X, v{=}3)$	$2.60 \times 10^{-20}\ (300/T_g)^{-1.55} e^{-124/T_g}$	22
$N_2(X, v{=}1) + N_2(X, v{=}4) \longrightarrow N_2(X, v{=}2) + N_2(X, v{=}3)$	$5.82 \times 10^{-20}\ (300/T_g)^{-1.54} e^{-82/T_g}$	22‡
$N_2(X, v{=}2) + N_2(X, v{=}4) \longrightarrow N_2(X, v{=}3) + N_2(X, v{=}3)$	$1.04 \times 10^{-19}\ (300/T_g)^{-1.42} e^{-42/T_g}$	22‡
$N_2(X, v{=}4) + N_2(X, v{=}4) \longrightarrow N_2(X, v{=}3) + N_2(X, v{=}5)$	$1.73 \times 10^{-19}\ (300/T_g)^{-1.42}$	22‡
$N_2(X, v{=}4) + N_2(X, v{=}5) \longrightarrow N_2(X, v{=}3) + N_2(X, v{=}6)$	$1.75 \times 10^{-19}\ (300/T_g)^{-1.54}$	22‡
$N_2(X, v{=}0) + N_2(X, v{=}5) \longrightarrow N_2(X, v{=}1) + N_2(X, v{=}4)$	$2.80 \times 10^{-20}\ (300/T_g)^{-1.63} e^{-165/T_g}$	22
$N_2(X, v{=}1) + N_2(X, v{=}5) \longrightarrow N_2(X, v{=}2) + N_2(X, v{=}4)$	$6.51 \times 10^{-20}\ (300/T_g)^{-1.55} e^{-124/T_g}$	22‡
$N_2(X, v{=}2) + N_2(X, v{=}5) \longrightarrow N_2(X, v{=}3) + N_2(X, v{=}4)$	$1.09 \times 10^{-19}\ (300/T_g)^{-1.54} e^{-83/T_g}$	22‡
$N_2(X, v{=}3) + N_2(X, v{=}5) \longrightarrow N_2(X, v{=}4) + N_2(X, v{=}4)$	$1.73 \times 10^{-19}\ (300/T_g)^{-1.42} e^{-42/T_g}$	22‡
$N_2(X, v{=}5) + N_2(X, v{=}5) \longrightarrow N_2(X, v{=}4) + N_2(X, v{=}6)$	$2.60 \times 10^{-19}\ (300/T_g)^{-1.42}$	22‡
$N_2(X, v{=}0) + N_2(X, v{=}6) \longrightarrow N_2(X, v{=}1) + N_2(X, v{=}5)$	$3.09 \times 10^{-20}\ (300/T_g)^{-1.63} e^{-204/T_g}$	22
$N_2(X, v{=}1) + N_2(X, v{=}6) \longrightarrow N_2(X, v{=}2) + N_2(X, v{=}5)$	$6.72 \times 10^{-20}\ (300/T_g)^{-1.63} e^{-162/T_g}$	22‡
$N_2(X, v{=}2) + N_2(X, v{=}6) \longrightarrow N_2(X, v{=}3) + N_2(X, v{=}5)$	$1.17 \times 10^{-19}\ (300/T_g)^{-1.55} e^{-122/T_g}$	22‡
$N_2(X, v{=}3) + N_2(X, v{=}6) \longrightarrow N_2(X, v{=}4) + N_2(X, v{=}5)$	$1.75 \times 10^{-19}\ (300/T_g)^{-1.54} e^{-80/T_g}$	22‡
$N_2(X, v{=}4) + N_2(X, v{=}6) \longrightarrow N_2(X, v{=}5) + N_2(X, v{=}5)$	$2.60 \times 10^{-19}\ (300/T_g)^{-1.42} e^{-39/T_g}$	22‡

‡Magnitude of cross section changed (see text).

Table A.3: Rate coefficients for collisions of three gaseous species.

Reaction	Rate coefficient [m^6/s]	Reference
$N_2(X, v{=}0) + N(S) + N(S) \longrightarrow N_2(X, v{=}0) + N_2(X, v{=}0)$	$8.27 \times 10^{-46}\ e^{500/T_g}$	124, 81
$N_2(X, v{=}0) + N(S) + N(D) \longrightarrow N_2(X, v{=}0) + N_2(X, v{=}1)$	$8.27 \times 10^{-46}\ e^{500/T_g}$	124, 81
$N_2(X, v{=}0) + N(S) + N(P) \longrightarrow N_2(X, v{=}0) + N_2(X, v{=}3)$	$8.27 \times 10^{-46}\ e^{500/T_g}$	124, 81
$N_2(X, v{=}0) + N(D) + N(D) \longrightarrow N_2(X, v{=}0) + N_2(X, v{=}3)$	$8.27 \times 10^{-46}\ e^{500/T_g}$	124, 81
$N_2(X, v{=}0) + N(D) + N(P) \longrightarrow N_2(X, v{=}0) + N_2(X, v{=}6)$	$8.27 \times 10^{-46}\ e^{500/T_g}$	124, 81
$N_2(X, v{=}0) + N(P) + N(P) \longrightarrow N_2(X, v{=}0) + N_2(A)$	$8.27 \times 10^{-46}\ e^{500/T_g}$	124, 81
$N_2(X, v{=}1) + N(S) + N(S) \longrightarrow N_2(X, v{=}0) + N_2(X, v{=}1)$	$8.27 \times 10^{-46}\ e^{500/T_g}$	124, 81
$N_2(X, v{=}1) + N(S) + N(D) \longrightarrow N_2(X, v{=}1) + N_2(X, v{=}1)$	$8.27 \times 10^{-46}\ e^{500/T_g}$	124, 81
$N_2(X, v{=}1) + N(S) + N(P) \longrightarrow N_2(X, v{=}1) + N_2(X, v{=}3)$	$8.27 \times 10^{-46}\ e^{500/T_g}$	124, 81
$N_2(X, v{=}1) + N(D) + N(D) \longrightarrow N_2(X, v{=}1) + N_2(X, v{=}3)$	$8.27 \times 10^{-46}\ e^{500/T_g}$	124, 81

Table A.3: (continued)

Reaction	Rate coefficient [m^6/s]	Reference
$N_2(X, v{=}1) + N(D) + N(P) \longrightarrow N_2(X, v{=}1) + N_2(X, v{=}6)$	$8.27 \times 10^{-46}\ e^{500/T_g}$	124, 81
$N_2(X, v{=}1) + N(P) + N(P) \longrightarrow N_2(X, v{=}1) + N_2(A)$	$8.27 \times 10^{-46}\ e^{500/T_g}$	124, 81
$N_2(X, v{=}2) + N(S) + N(S) \longrightarrow N_2(X, v{=}0) + N_2(X, v{=}2)$	$8.27 \times 10^{-46}\ e^{500/T_g}$	124, 81
$N_2(X, v{=}2) + N(S) + N(D) \longrightarrow N_2(X, v{=}1) + N_2(X, v{=}2)$	$8.27 \times 10^{-46}\ e^{500/T_g}$	124, 81
$N_2(X, v{=}2) + N(S) + N(P) \longrightarrow N_2(X, v{=}2) + N_2(X, v{=}3)$	$8.27 \times 10^{-46}\ e^{500/T_g}$	124, 81
$N_2(X, v{=}2) + N(D) + N(D) \longrightarrow N_2(X, v{=}2) + N_2(X, v{=}3)$	$8.27 \times 10^{-46}\ e^{500/T_g}$	124, 81
$N_2(X, v{=}2) + N(D) + N(P) \longrightarrow N_2(X, v{=}2) + N_2(X, v{=}6)$	$8.27 \times 10^{-46}\ e^{500/T_g}$	124, 81
$N_2(X, v{=}2) + N(P) + N(P) \longrightarrow N_2(X, v{=}2) + N_2(A)$	$8.27 \times 10^{-46}\ e^{500/T_g}$	124, 81
$N_2(X, v{=}3) + N(S) + N(S) \longrightarrow N_2(X, v{=}0) + N_2(X, v{=}3)$	$8.27 \times 10^{-46}\ e^{500/T_g}$	124, 81
$N_2(X, v{=}3) + N(S) + N(D) \longrightarrow N_2(X, v{=}1) + N_2(X, v{=}3)$	$8.27 \times 10^{-46}\ e^{500/T_g}$	124, 81
$N_2(X, v{=}3) + N(S) + N(P) \longrightarrow N_2(X, v{=}3) + N_2(X, v{=}3)$	$8.27 \times 10^{-46}\ e^{500/T_g}$	124, 81
$N_2(X, v{=}3) + N(D) + N(D) \longrightarrow N_2(X, v{=}3) + N_2(X, v{=}3)$	$8.27 \times 10^{-46}\ e^{500/T_g}$	124, 81
$N_2(X, v{=}3) + N(D) + N(P) \longrightarrow N_2(X, v{=}3) + N_2(X, v{=}6)$	$8.27 \times 10^{-46}\ e^{500/T_g}$	124, 81
$N_2(X, v{=}3) + N(P) + N(P) \longrightarrow N_2(X, v{=}3) + N_2(A)$	$8.27 \times 10^{-46}\ e^{500/T_g}$	124, 81
$N_2(X, v{=}4) + N(S) + N(S) \longrightarrow N_2(X, v{=}0) + N_2(X, v{=}4)$	$8.27 \times 10^{-46}\ e^{500/T_g}$	124, 81
$N_2(X, v{=}4) + N(S) + N(D) \longrightarrow N_2(X, v{=}1) + N_2(X, v{=}4)$	$8.27 \times 10^{-46}\ e^{500/T_g}$	124, 81
$N_2(X, v{=}4) + N(S) + N(P) \longrightarrow N_2(X, v{=}3) + N_2(X, v{=}4)$	$8.27 \times 10^{-46}\ e^{500/T_g}$	124, 81
$N_2(X, v{=}4) + N(D) + N(D) \longrightarrow N_2(X, v{=}3) + N_2(X, v{=}4)$	$8.27 \times 10^{-46}\ e^{500/T_g}$	124, 81
$N_2(X, v{=}4) + N(D) + N(P) \longrightarrow N_2(X, v{=}4) + N_2(X, v{=}6)$	$8.27 \times 10^{-46}\ e^{500/T_g}$	124, 81
$N_2(X, v{=}4) + N(P) + N(P) \longrightarrow N_2(X, v{=}4) + N_2(A)$	$8.27 \times 10^{-46}\ e^{500/T_g}$	124, 81
$N_2(X, v{=}5) + N(S) + N(S) \longrightarrow N_2(X, v{=}0) + N_2(X, v{=}5)$	$8.27 \times 10^{-46}\ e^{500/T_g}$	124, 81
$N_2(X, v{=}5) + N(S) + N(D) \longrightarrow N_2(X, v{=}1) + N_2(X, v{=}5)$	$8.27 \times 10^{-46}\ e^{500/T_g}$	124, 81
$N_2(X, v{=}5) + N(S) + N(P) \longrightarrow N_2(X, v{=}3) + N_2(X, v{=}5)$	$8.27 \times 10^{-46}\ e^{500/T_g}$	124, 81
$N_2(X, v{=}5) + N(D) + N(D) \longrightarrow N_2(X, v{=}3) + N_2(X, v{=}5)$	$8.27 \times 10^{-46}\ e^{500/T_g}$	124, 81
$N_2(X, v{=}5) + N(D) + N(P) \longrightarrow N_2(X, v{=}5) + N_2(X, v{=}6)$	$8.27 \times 10^{-46}\ e^{500/T_g}$	124, 81
$N_2(X, v{=}5) + N(P) + N(P) \longrightarrow N_2(X, v{=}5) + N_2(A)$	$8.27 \times 10^{-46}\ e^{500/T_g}$	124, 81
$N_2(X, v{=}6) + N(S) + N(S) \longrightarrow N_2(X, v{=}0) + N_2(X, v{=}6)$	$8.27 \times 10^{-46}\ e^{500/T_g}$	124, 81
$N_2(X, v{=}6) + N(S) + N(D) \longrightarrow N_2(X, v{=}1) + N_2(X, v{=}6)$	$8.27 \times 10^{-46}\ e^{500/T_g}$	124, 81
$N_2(X, v{=}6) + N(S) + N(P) \longrightarrow N_2(X, v{=}3) + N_2(X, v{=}6)$	$8.27 \times 10^{-46}\ e^{500/T_g}$	124, 81
$N_2(X, v{=}6) + N(D) + N(D) \longrightarrow N_2(X, v{=}3) + N_2(X, v{=}6)$	$8.27 \times 10^{-46}\ e^{500/T_g}$	124, 81
$N_2(X, v{=}6) + N(D) + N(P) \longrightarrow N_2(X, v{=}6) + N_2(X, v{=}6)$	$8.27 \times 10^{-46}\ e^{500/T_g}$	124, 81
$N_2(X, v{=}6) + N(P) + N(P) \longrightarrow N_2(X, v{=}6) + N_2(A)$	$8.27 \times 10^{-46}\ e^{500/T_g}$	124, 81
$N_2(A) + N(S) + N(S) \longrightarrow N_2(X, v{=}0) + N_2(A)$	$8.27 \times 10^{-46}\ e^{500/T_g}$	124, 81
$N_2(A) + N(S) + N(D) \longrightarrow N_2(X, v{=}1) + N_2(A)$	$8.27 \times 10^{-46}\ e^{500/T_g}$	124, 81
$N_2(A) + N(S) + N(P) \longrightarrow N_2(X, v{=}3) + N_2(A)$	$8.27 \times 10^{-46}\ e^{500/T_g}$	124, 81
$N_2(A) + N(D) + N(D) \longrightarrow N_2(X, v{=}3) + N_2(A)$	$8.27 \times 10^{-46}\ e^{500/T_g}$	124, 81
$N_2(A) + N(D) + N(P) \longrightarrow N_2(X, v{=}6) + N_2(A)$	$8.27 \times 10^{-46}\ e^{500/T_g}$	124, 81
$N_2(A) + N(P) + N(P) \longrightarrow N_2(A) + N_2(A)$	$8.27 \times 10^{-46}\ e^{500/T_g}$	124, 81
$N(S) + N(S) + N(S) \longrightarrow N_2(X, v{=}0) + N(S)$	1.00×10^{-44}	81
$N(S) + N(S) + N(D) \longrightarrow N_2(X, v{=}1) + N(S)$	1.00×10^{-44}	81
$N(S) + N(S) + N(P) \longrightarrow N_2(X, v{=}3) + N(S)$	1.00×10^{-44}	81
$N(S) + N(D) + N(D) \longrightarrow N_2(X, v{=}3) + N(S)$	1.00×10^{-44}	81
$N(S) + N(D) + N(P) \longrightarrow N_2(X, v{=}6) + N(S)$	1.00×10^{-44}	81
$N(S) + N(P) + N(P) \longrightarrow N_2(A) + N(S)$	1.00×10^{-44}	81
$N(D) + N(D) + N(D) \longrightarrow N_2(X, v{=}3) + N(D)$	1.00×10^{-44}	81
$N(D) + N(D) + N(P) \longrightarrow N_2(X, v{=}6) + N(D)$	1.00×10^{-44}	81
$N(D) + N(P) + N(P) \longrightarrow N_2(A) + N(D)$	1.00×10^{-44}	81
$N(P) + N(P) + N(P) \longrightarrow N_2(A) + N(P)$	1.00×10^{-44}	81
$N_2(X, v{=}0) + N(S) + N^+ \longrightarrow N_2(X, v{=}0) + N_2^+$	1.00×10^{-41}	124
$N_2(X, v{=}1) + N(S) + N^+ \longrightarrow N_2(X, v{=}1) + N_2^+$	1.00×10^{-41}	124
$N_2(X, v{=}2) + N(S) + N^+ \longrightarrow N_2(X, v{=}2) + N_2^+$	1.00×10^{-41}	124
$N_2(X, v{=}3) + N(S) + N^+ \longrightarrow N_2(X, v{=}3) + N_2^+$	1.00×10^{-41}	124
$N_2(X, v{=}4) + N(S) + N^+ \longrightarrow N_2(X, v{=}4) + N_2^+$	1.00×10^{-41}	124
$N_2(X, v{=}5) + N(S) + N^+ \longrightarrow N_2(X, v{=}5) + N_2^+$	1.00×10^{-41}	124

Table A.3: (continued)

Reaction	Rate coefficient [m^6/s]	Reference
$N_2(X, v{=}6) + N(S) + N^+ \longrightarrow N_2(X, v{=}6) + N_2^+$	1.00×10^{-41}	124
$N_2(A) + N(S) + N^+ \longrightarrow N_2(A) + N_2^+$	1.00×10^{-41}	124
$N_2(X, v{=}0) + N(D) + N^+ \longrightarrow N_2(X, v{=}0) + N_2^+$	1.00×10^{-41}	124
$N_2(X, v{=}1) + N(D) + N^+ \longrightarrow N_2(X, v{=}1) + N_2^+$	1.00×10^{-41}	124
$N_2(X, v{=}2) + N(D) + N^+ \longrightarrow N_2(X, v{=}2) + N_2^+$	1.00×10^{-41}	124
$N_2(X, v{=}3) + N(D) + N^+ \longrightarrow N_2(X, v{=}3) + N_2^+$	1.00×10^{-41}	124
$N_2(X, v{=}4) + N(D) + N^+ \longrightarrow N_2(X, v{=}4) + N_2^+$	1.00×10^{-41}	124
$N_2(X, v{=}5) + N(D) + N^+ \longrightarrow N_2(X, v{=}5) + N_2^+$	1.00×10^{-41}	124
$N_2(X, v{=}6) + N(D) + N^+ \longrightarrow N_2(X, v{=}6) + N_2^+$	1.00×10^{-41}	124
$N_2(A) + N(D) + N^+ \longrightarrow N_2(A) + N_2^+$	1.00×10^{-41}	124
$N_2(X, v{=}0) + N(P) + N^+ \longrightarrow N_2(X, v{=}0) + N_2^+$	1.00×10^{-41}	124
$N_2(X, v{=}1) + N(P) + N^+ \longrightarrow N_2(X, v{=}1) + N_2^+$	1.00×10^{-41}	124
$N_2(X, v{=}2) + N(P) + N^+ \longrightarrow N_2(X, v{=}2) + N_2^+$	1.00×10^{-41}	124
$N_2(X, v{=}3) + N(P) + N^+ \longrightarrow N_2(X, v{=}3) + N_2^+$	1.00×10^{-41}	124
$N_2(X, v{=}4) + N(P) + N^+ \longrightarrow N_2(X, v{=}4) + N_2^+$	1.00×10^{-41}	124
$N_2(X, v{=}5) + N(P) + N^+ \longrightarrow N_2(X, v{=}5) + N_2^+$	1.00×10^{-41}	124
$N_2(X, v{=}6) + N(P) + N^+ \longrightarrow N_2(X, v{=}6) + N_2^+$	1.00×10^{-41}	124
$N_2(A) + N(P) + N^+ \longrightarrow N_2(A) + N_2^+$	1.00×10^{-41}	124
$N_2(X, v{=}0) + N_2(X, v{=}0) + N_2^+ \longrightarrow N_2(X, v{=}0) + N_4^+$	$5.20 \times 10^{-41}\ (300/T_g)^{2.20}$	96
$N_2(X, v{=}0) + N_2(X, v{=}1) + N_2^+ \longrightarrow N_2(X, v{=}0) + N_4^+$	$5.20 \times 10^{-41}\ (300/T_g)^{2.20}$	96
$N_2(X, v{=}0) + N_2(X, v{=}2) + N_2^+ \longrightarrow N_2(X, v{=}0) + N_4^+$	$5.20 \times 10^{-41}\ (300/T_g)^{2.20}$	96
$N_2(X, v{=}0) + N_2(X, v{=}3) + N_2^+ \longrightarrow N_2(X, v{=}0) + N_4^+$	$5.20 \times 10^{-41}\ (300/T_g)^{2.20}$	96
$N_2(X, v{=}0) + N_2(X, v{=}4) + N_2^+ \longrightarrow N_2(X, v{=}0) + N_4^+$	$5.20 \times 10^{-41}\ (300/T_g)^{2.20}$	96
$N_2(X, v{=}0) + N_2(X, v{=}5) + N_2^+ \longrightarrow N_2(X, v{=}0) + N_4^+$	$5.20 \times 10^{-41}\ (300/T_g)^{2.20}$	96
$N_2(X, v{=}0) + N_2(X, v{=}6) + N_2^+ \longrightarrow N_2(X, v{=}0) + N_4^+$	$5.20 \times 10^{-41}\ (300/T_g)^{2.20}$	96
$N_2(X, v{=}0) + N_2(A) + N_2^+ \longrightarrow N_2(X, v{=}0) + N_4^+$	$5.20 \times 10^{-41}\ (300/T_g)^{2.20}$	96
$N_2(X, v{=}1) + N_2(X, v{=}1) + N_2^+ \longrightarrow N_2(X, v{=}1) + N_4^+$	$5.20 \times 10^{-41}\ (300/T_g)^{2.20}$	96
$N_2(X, v{=}1) + N_2(X, v{=}2) + N_2^+ \longrightarrow N_2(X, v{=}1) + N_4^+$	$5.20 \times 10^{-41}\ (300/T_g)^{2.20}$	96
$N_2(X, v{=}1) + N_2(X, v{=}3) + N_2^+ \longrightarrow N_2(X, v{=}1) + N_4^+$	$5.20 \times 10^{-41}\ (300/T_g)^{2.20}$	96
$N_2(X, v{=}1) + N_2(X, v{=}4) + N_2^+ \longrightarrow N_2(X, v{=}1) + N_4^+$	$5.20 \times 10^{-41}\ (300/T_g)^{2.20}$	96
$N_2(X, v{=}1) + N_2(X, v{=}5) + N_2^+ \longrightarrow N_2(X, v{=}1) + N_4^+$	$5.20 \times 10^{-41}\ (300/T_g)^{2.20}$	96
$N_2(X, v{=}1) + N_2(X, v{=}6) + N_2^+ \longrightarrow N_2(X, v{=}1) + N_4^+$	$5.20 \times 10^{-41}\ (300/T_g)^{2.20}$	96
$N_2(X, v{=}1) + N_2(A) + N_2^+ \longrightarrow N_2(X, v{=}1) + N_4^+$	$5.20 \times 10^{-41}\ (300/T_g)^{2.20}$	96
$N_2(X, v{=}2) + N_2(X, v{=}2) + N_2^+ \longrightarrow N_2(X, v{=}2) + N_4^+$	$5.20 \times 10^{-41}\ (300/T_g)^{2.20}$	96
$N_2(X, v{=}2) + N_2(X, v{=}3) + N_2^+ \longrightarrow N_2(X, v{=}2) + N_4^+$	$5.20 \times 10^{-41}\ (300/T_g)^{2.20}$	96
$N_2(X, v{=}2) + N_2(X, v{=}4) + N_2^+ \longrightarrow N_2(X, v{=}2) + N_4^+$	$5.20 \times 10^{-41}\ (300/T_g)^{2.20}$	96
$N_2(X, v{=}2) + N_2(X, v{=}5) + N_2^+ \longrightarrow N_2(X, v{=}2) + N_4^+$	$5.20 \times 10^{-41}\ (300/T_g)^{2.20}$	96
$N_2(X, v{=}2) + N_2(X, v{=}6) + N_2^+ \longrightarrow N_2(X, v{=}2) + N_4^+$	$5.20 \times 10^{-41}\ (300/T_g)^{2.20}$	96
$N_2(X, v{=}2) + N_2(A) + N_2^+ \longrightarrow N_2(X, v{=}2) + N_4^+$	$5.20 \times 10^{-41}\ (300/T_g)^{2.20}$	96
$N_2(X, v{=}3) + N_2(X, v{=}3) + N_2^+ \longrightarrow N_2(X, v{=}3) + N_4^+$	$5.20 \times 10^{-41}\ (300/T_g)^{2.20}$	96
$N_2(X, v{=}3) + N_2(X, v{=}4) + N_2^+ \longrightarrow N_2(X, v{=}3) + N_4^+$	$5.20 \times 10^{-41}\ (300/T_g)^{2.20}$	96
$N_2(X, v{=}3) + N_2(X, v{=}5) + N_2^+ \longrightarrow N_2(X, v{=}3) + N_4^+$	$5.20 \times 10^{-41}\ (300/T_g)^{2.20}$	96
$N_2(X, v{=}3) + N_2(X, v{=}6) + N_2^+ \longrightarrow N_2(X, v{=}3) + N_4^+$	$5.20 \times 10^{-41}\ (300/T_g)^{2.20}$	96
$N_2(X, v{=}3) + N_2(A) + N_2^+ \longrightarrow N_2(X, v{=}3) + N_4^+$	$5.20 \times 10^{-41}\ (300/T_g)^{2.20}$	96
$N_2(X, v{=}4) + N_2(X, v{=}4) + N_2^+ \longrightarrow N_2(X, v{=}4) + N_4^+$	$5.20 \times 10^{-41}\ (300/T_g)^{2.20}$	96
$N_2(X, v{=}4) + N_2(X, v{=}5) + N_2^+ \longrightarrow N_2(X, v{=}4) + N_4^+$	$5.20 \times 10^{-41}\ (300/T_g)^{2.20}$	96
$N_2(X, v{=}4) + N_2(X, v{=}6) + N_2^+ \longrightarrow N_2(X, v{=}4) + N_4^+$	$5.20 \times 10^{-41}\ (300/T_g)^{2.20}$	96
$N_2(X, v{=}4) + N_2(A) + N_2^+ \longrightarrow N_2(X, v{=}4) + N_4^+$	$5.20 \times 10^{-41}\ (300/T_g)^{2.20}$	96
$N_2(X, v{=}5) + N_2(X, v{=}5) + N_2^+ \longrightarrow N_2(X, v{=}5) + N_4^+$	$5.20 \times 10^{-41}\ (300/T_g)^{2.20}$	96
$N_2(X, v{=}5) + N_2(X, v{=}6) + N_2^+ \longrightarrow N_2(X, v{=}5) + N_4^+$	$5.20 \times 10^{-41}\ (300/T_g)^{2.20}$	96
$N_2(X, v{=}5) + N_2(A) + N_2^+ \longrightarrow N_2(X, v{=}5) + N_4^+$	$5.20 \times 10^{-41}\ (300/T_g)^{2.20}$	96
$N_2(X, v{=}6) + N_2(X, v{=}6) + N_2^+ \longrightarrow N_2(X, v{=}6) + N_4^+$	$5.20 \times 10^{-41}\ (300/T_g)^{2.20}$	96
$N_2(X, v{=}6) + N_2(A) + N_2^+ \longrightarrow N_2(X, v{=}6) + N_4^+$	$5.20 \times 10^{-41}\ (300/T_g)^{2.20}$	96
$N_2(A) + N_2(A) + N_2^+ \longrightarrow N_2(A) + N_4^+$	$5.20 \times 10^{-41}\ (300/T_g)^{2.20}$	96

Table A.3: (continued)

Reaction	Rate coefficient [m^6/s]	Reference
$N_2(X, v{=}0) + N_2(X, v{=}0) + N^+ \longrightarrow N_2(X, v{=}0) + N_3^+$	$1.70 \times 10^{-41}\ (300/T_g)^{2.10}$	96
$N_2(X, v{=}0) + N_2(X, v{=}1) + N^+ \longrightarrow N_2(X, v{=}0) + N_3^+$	$1.70 \times 10^{-41}\ (300/T_g)^{2.10}$	96
$N_2(X, v{=}0) + N_2(X, v{=}2) + N^+ \longrightarrow N_2(X, v{=}0) + N_3^+$	$1.70 \times 10^{-41}\ (300/T_g)^{2.10}$	96
$N_2(X, v{=}0) + N_2(X, v{=}3) + N^+ \longrightarrow N_2(X, v{=}0) + N_3^+$	$1.70 \times 10^{-41}\ (300/T_g)^{2.10}$	96
$N_2(X, v{=}0) + N_2(X, v{=}4) + N^+ \longrightarrow N_2(X, v{=}0) + N_3^+$	$1.70 \times 10^{-41}\ (300/T_g)^{2.10}$	96
$N_2(X, v{=}0) + N_2(X, v{=}5) + N^+ \longrightarrow N_2(X, v{=}0) + N_3^+$	$1.70 \times 10^{-41}\ (300/T_g)^{2.10}$	96
$N_2(X, v{=}0) + N_2(X, v{=}6) + N^+ \longrightarrow N_2(X, v{=}0) + N_3^+$	$1.70 \times 10^{-41}\ (300/T_g)^{2.10}$	96
$N_2(X, v{=}0) + N_2(A) + N^+ \longrightarrow N_2(X, v{=}0) + N_3^+$	$1.70 \times 10^{-41}\ (300/T_g)^{2.10}$	96
$N_2(X, v{=}1) + N_2(X, v{=}1) + N^+ \longrightarrow N_2(X, v{=}1) + N_3^+$	$1.70 \times 10^{-41}\ (300/T_g)^{2.10}$	96
$N_2(X, v{=}1) + N_2(X, v{=}2) + N^+ \longrightarrow N_2(X, v{=}1) + N_3^+$	$1.70 \times 10^{-41}\ (300/T_g)^{2.10}$	96
$N_2(X, v{=}1) + N_2(X, v{=}3) + N^+ \longrightarrow N_2(X, v{=}1) + N_3^+$	$1.70 \times 10^{-41}\ (300/T_g)^{2.10}$	96
$N_2(X, v{=}1) + N_2(X, v{=}4) + N^+ \longrightarrow N_2(X, v{=}1) + N_3^+$	$1.70 \times 10^{-41}\ (300/T_g)^{2.10}$	96
$N_2(X, v{=}1) + N_2(X, v{=}5) + N^+ \longrightarrow N_2(X, v{=}1) + N_3^+$	$1.70 \times 10^{-41}\ (300/T_g)^{2.10}$	96
$N_2(X, v{=}1) + N_2(X, v{=}6) + N^+ \longrightarrow N_2(X, v{=}1) + N_3^+$	$1.70 \times 10^{-41}\ (300/T_g)^{2.10}$	96
$N_2(X, v{=}1) + N_2(A) + N^+ \longrightarrow N_2(X, v{=}1) + N_3^+$	$1.70 \times 10^{-41}\ (300/T_g)^{2.10}$	96
$N_2(X, v{=}2) + N_2(X, v{=}2) + N^+ \longrightarrow N_2(X, v{=}2) + N_3^+$	$1.70 \times 10^{-41}\ (300/T_g)^{2.10}$	96
$N_2(X, v{=}2) + N_2(X, v{=}3) + N^+ \longrightarrow N_2(X, v{=}2) + N_3^+$	$1.70 \times 10^{-41}\ (300/T_g)^{2.10}$	96
$N_2(X, v{=}2) + N_2(X, v{=}4) + N^+ \longrightarrow N_2(X, v{=}2) + N_3^+$	$1.70 \times 10^{-41}\ (300/T_g)^{2.10}$	96
$N_2(X, v{=}2) + N_2(X, v{=}5) + N^+ \longrightarrow N_2(X, v{=}2) + N_3^+$	$1.70 \times 10^{-41}\ (300/T_g)^{2.10}$	96
$N_2(X, v{=}2) + N_2(X, v{=}6) + N^+ \longrightarrow N_2(X, v{=}2) + N_3^+$	$1.70 \times 10^{-41}\ (300/T_g)^{2.10}$	96
$N_2(X, v{=}2) + N_2(A) + N^+ \longrightarrow N_2(X, v{=}2) + N_3^+$	$1.70 \times 10^{-41}\ (300/T_g)^{2.10}$	96
$N_2(X, v{=}3) + N_2(X, v{=}3) + N^+ \longrightarrow N_2(X, v{=}3) + N_3^+$	$1.70 \times 10^{-41}\ (300/T_g)^{2.10}$	96
$N_2(X, v{=}3) + N_2(X, v{=}4) + N^+ \longrightarrow N_2(X, v{=}3) + N_3^+$	$1.70 \times 10^{-41}\ (300/T_g)^{2.10}$	96
$N_2(X, v{=}3) + N_2(X, v{=}5) + N^+ \longrightarrow N_2(X, v{=}3) + N_3^+$	$1.70 \times 10^{-41}\ (300/T_g)^{2.10}$	96
$N_2(X, v{=}3) + N_2(X, v{=}6) + N^+ \longrightarrow N_2(X, v{=}3) + N_3^+$	$1.70 \times 10^{-41}\ (300/T_g)^{2.10}$	96
$N_2(X, v{=}3) + N_2(A) + N^+ \longrightarrow N_2(X, v{=}3) + N_3^+$	$1.70 \times 10^{-41}\ (300/T_g)^{2.10}$	96
$N_2(X, v{=}4) + N_2(X, v{=}4) + N^+ \longrightarrow N_2(X, v{=}4) + N_3^+$	$1.70 \times 10^{-41}\ (300/T_g)^{2.10}$	96
$N_2(X, v{=}4) + N_2(X, v{=}5) + N^+ \longrightarrow N_2(X, v{=}4) + N_3^+$	$1.70 \times 10^{-41}\ (300/T_g)^{2.10}$	96
$N_2(X, v{=}4) + N_2(X, v{=}6) + N^+ \longrightarrow N_2(X, v{=}4) + N_3^+$	$1.70 \times 10^{-41}\ (300/T_g)^{2.10}$	96
$N_2(X, v{=}4) + N_2(A) + N^+ \longrightarrow N_2(X, v{=}4) + N_3^+$	$1.70 \times 10^{-41}\ (300/T_g)^{2.10}$	96
$N_2(X, v{=}5) + N_2(X, v{=}5) + N^+ \longrightarrow N_2(X, v{=}5) + N_3^+$	$1.70 \times 10^{-41}\ (300/T_g)^{2.10}$	96
$N_2(X, v{=}5) + N_2(X, v{=}6) + N^+ \longrightarrow N_2(X, v{=}5) + N_3^+$	$1.70 \times 10^{-41}\ (300/T_g)^{2.10}$	96
$N_2(X, v{=}5) + N_2(A) + N^+ \longrightarrow N_2(X, v{=}5) + N_3^+$	$1.70 \times 10^{-41}\ (300/T_g)^{2.10}$	96
$N_2(X, v{=}6) + N_2(X, v{=}6) + N^+ \longrightarrow N_2(X, v{=}6) + N_3^+$	$1.70 \times 10^{-41}\ (300/T_g)^{2.10}$	96
$N_2(X, v{=}6) + N_2(A) + N^+ \longrightarrow N_2(X, v{=}6) + N_3^+$	$1.70 \times 10^{-41}\ (300/T_g)^{2.10}$	96
$N_2(A) + N_2(A) + N^+ \longrightarrow N_2(A) + N_3^+$	$1.70 \times 10^{-41}\ (300/T_g)^{2.10}$	96
$N_2(X, v{=}0) + N(S) + N_2^+ \longrightarrow N_2(X, v{=}0) + N_3^+$	$9.00 \times 10^{-42}\ e^{400/T_g}$	124
$N_2(X, v{=}1) + N(S) + N_2^+ \longrightarrow N_2(X, v{=}1) + N_3^+$	$9.00 \times 10^{-42}\ e^{400/T_g}$	124
$N_2(X, v{=}2) + N(S) + N_2^+ \longrightarrow N_2(X, v{=}2) + N_3^+$	$9.00 \times 10^{-42}\ e^{400/T_g}$	124
$N_2(X, v{=}3) + N(S) + N_2^+ \longrightarrow N_2(X, v{=}3) + N_3^+$	$9.00 \times 10^{-42}\ e^{400/T_g}$	124
$N_2(X, v{=}4) + N(S) + N_2^+ \longrightarrow N_2(X, v{=}4) + N_3^+$	$9.00 \times 10^{-42}\ e^{400/T_g}$	124
$N_2(X, v{=}5) + N(S) + N_2^+ \longrightarrow N_2(X, v{=}5) + N_3^+$	$9.00 \times 10^{-42}\ e^{400/T_g}$	124
$N_2(X, v{=}6) + N(S) + N_2^+ \longrightarrow N_2(X, v{=}6) + N_3^+$	$9.00 \times 10^{-42}\ e^{400/T_g}$	124
$N_2(A) + N(S) + N_2^+ \longrightarrow N_2(A) + N_3^+$	$9.00 \times 10^{-42}\ e^{400/T_g}$	124
$N_2(X, v{=}0) + N(D) + N_2^+ \longrightarrow N_2(X, v{=}0) + N_3^+$	$9.00 \times 10^{-42}\ e^{400/T_g}$	124
$N_2(X, v{=}1) + N(D) + N_2^+ \longrightarrow N_2(X, v{=}1) + N_3^+$	$9.00 \times 10^{-42}\ e^{400/T_g}$	124
$N_2(X, v{=}2) + N(D) + N_2^+ \longrightarrow N_2(X, v{=}2) + N_3^+$	$9.00 \times 10^{-42}\ e^{400/T_g}$	124
$N_2(X, v{=}3) + N(D) + N_2^+ \longrightarrow N_2(X, v{=}3) + N_3^+$	$9.00 \times 10^{-42}\ e^{400/T_g}$	124
$N_2(X, v{=}4) + N(D) + N_2^+ \longrightarrow N_2(X, v{=}4) + N_3^+$	$9.00 \times 10^{-42}\ e^{400/T_g}$	124
$N_2(X, v{=}5) + N(D) + N_2^+ \longrightarrow N_2(X, v{=}5) + N_3^+$	$9.00 \times 10^{-42}\ e^{400/T_g}$	124
$N_2(X, v{=}6) + N(D) + N_2^+ \longrightarrow N_2(X, v{=}6) + N_3^+$	$9.00 \times 10^{-42}\ e^{400/T_g}$	124
$N_2(A) + N(D) + N_2^+ \longrightarrow N_2(A) + N_3^+$	$9.00 \times 10^{-42}\ e^{400/T_g}$	124
$N_2(X, v{=}0) + N(P) + N_2^+ \longrightarrow N_2(X, v{=}0) + N_3^+$	$9.00 \times 10^{-42}\ e^{400/T_g}$	124
$N_2(X, v{=}1) + N(P) + N_2^+ \longrightarrow N_2(X, v{=}1) + N_3^+$	$9.00 \times 10^{-42}\ e^{400/T_g}$	124

Table A.3: (continued)

Reaction	Rate coefficient [m^6/s]	Reference
$N_2(X, v{=}2) + N(P) + N_2^+ \longrightarrow N_2(X, v{=}2) + N_3^+$	$9.00 \times 10^{-42}\ e^{400/T_g}$	124
$N_2(X, v{=}3) + N(P) + N_2^+ \longrightarrow N_2(X, v{=}3) + N_3^+$	$9.00 \times 10^{-42}\ e^{400/T_g}$	124
$N_2(X, v{=}4) + N(P) + N_2^+ \longrightarrow N_2(X, v{=}4) + N_3^+$	$9.00 \times 10^{-42}\ e^{400/T_g}$	124
$N_2(X, v{=}5) + N(P) + N_2^+ \longrightarrow N_2(X, v{=}5) + N_3^+$	$9.00 \times 10^{-42}\ e^{400/T_g}$	124
$N_2(X, v{=}6) + N(P) + N_2^+ \longrightarrow N_2(X, v{=}6) + N_3^+$	$9.00 \times 10^{-42}\ e^{400/T_g}$	124
$N_2(A) + N(P) + N_2^+ \longrightarrow N_2(A) + N_3^+$	$9.00 \times 10^{-42}\ e^{400/T_g}$	124

Table A.4: Wall interactions.

Reaction	Rate coefficient [1/s]	γ
$N_2(X, v=1) + \text{wall} \longrightarrow N_2(X, v=0)$	$\left[\frac{\Lambda_0^2}{D_{N_2(v=1)}} + \frac{2V(2-\gamma_{Q,N_2(v=1)})}{A\overline{v}_{N_2(v=1)}\gamma_{Q,N_2(v=1)}}\right]^{-1}$	1
$N_2(X, v=2) + \text{wall} \longrightarrow N_2(X, v=1)$	$\left[\frac{\Lambda_0^2}{D_{N_2(v=2)}} + \frac{2V(2-\gamma_{Q,N_2(v=2)})}{A\overline{v}_{N_2(v=2)}\gamma_{Q,N_2(v=2)}}\right]^{-1}$	1
$N_2(X, v=3) + \text{wall} \longrightarrow N_2(X, v=2)$	$\left[\frac{\Lambda_0^2}{D_{N_2(v=3)}} + \frac{2V(2-\gamma_{Q,N_2(v=3)})}{A\overline{v}_{N_2(v=3)}\gamma_{Q,N_2(v=3)}}\right]^{-1}$	1
$N_2(X, v=4) + \text{wall} \longrightarrow N_2(X, v=3)$	$\left[\frac{\Lambda_0^2}{D_{N_2(v=4)}} + \frac{2V(2-\gamma_{Q,N_2(v=4)})}{A\overline{v}_{N_2(v=4)}\gamma_{Q,N_2(v=4)}}\right]^{-1}$	1
$N_2(X, v=5) + \text{wall} \longrightarrow N_2(X, v=4)$	$\left[\frac{\Lambda_0^2}{D_{N_2(v=5)}} + \frac{2V(2-\gamma_{Q,N_2(v=5)})}{A\overline{v}_{N_2(v=5)}\gamma_{Q,N_2(v=5)}}\right]^{-1}$	1
$N_2(X, v=6) + \text{wall} \longrightarrow N_2(X, v=5)$	$\left[\frac{\Lambda_0^2}{D_{N_2(v=6)}} + \frac{2V(2-\gamma_{Q,N_2(v=6)})}{A\overline{v}_{N_2(v=6)}\gamma_{Q,N_2(v=6)}}\right]^{-1}$	1
$N_2(A) + \text{wall} \longrightarrow N_2(X, v=0)$	$\left[\frac{\Lambda_0^2}{D_{N_2(A)}} + \frac{2V(2-\gamma_{Q,N_2(A)})}{A\overline{v}_{N_2(A)}\gamma_{Q,N_2(A)}}\right]^{-1}$	1
$N(D) + \text{wall} \longrightarrow N(S)$	$\left[\frac{\Lambda_0^2}{D_{N(D)}} + \frac{2V(2-\gamma_{Q,N(D)})}{A\overline{v}_{N(D)}\gamma_{Q,N(D)}}\right]^{-1}$	0.93
$N(P) + \text{wall} \longrightarrow N(S)$	$\left[\frac{\Lambda_0^2}{D_{N(P)}} + \frac{2V(2-\gamma_{Q,N(P)})}{A\overline{v}_{N(P)}\gamma_{Q,N(P)}}\right]^{-1}$	0.93
$N(S) + \text{wall} \longrightarrow 0.5N_2(X, v=0)$	$\left[\frac{\Lambda_0^2}{D_{N(S)}} + \frac{2V(2-\gamma_{rec,N(S)})}{A\overline{v}_{N(S)}\gamma_{rec,N(S)}}\right]^{-1}$	0.07
$N(D) + \text{wall} \longrightarrow 0.5N_2(X, v=0)$	$\left[\frac{\Lambda_0^2}{D_{N(D)}} + \frac{2V(2-\gamma_{rec,N(D)})}{A\overline{v}_{N(D)}\gamma_{rec,N(D)}}\right]^{-1}$	0.07
$N(P) + \text{wall} \longrightarrow 0.5N_2(X, v=0)$	$\left[\frac{\Lambda_0^2}{D_{N(P)}} + \frac{2V(2-\gamma_{rec,N(P)})}{A\overline{v}_{N(P)}\gamma_{rec,N(P)}}\right]^{-1}$	0.07
$N_2^+ + \text{wall} \longrightarrow N_2(X, v=0)$	$2u_{B,N_2^+}(R^2h_L + RLh_R)/R^2L$	
$N^+ + \text{wall} \longrightarrow N(S)$	$2u_{B,N^+}(R^2h_L + RLh_R)/R^2L$	
$N_3^+ + \text{wall} \longrightarrow N_2(X, v=0) + N(S)$	$2u_{B,N_3^+}(R^2h_L + RLh_R)/R^2L$	
$N_4^+ + \text{wall} \longrightarrow N_2(X, v=0) + N_2(X, v=0)$	$2u_{B,N_4^+}(R^2h_L + RLh_R)/R^2L$	

Table A.5: Spontaneous emission of excited species.

Reaction	Rate coefficient [1/s]	Reference
$N_2(A) \longrightarrow N_2(X, v = 0) + \hbar\omega$	4.22×10^{-1}	184
$N(P) \longrightarrow N(S) + \hbar\omega$	5.40×10^{-3}	185
$N(P) \longrightarrow N(D) + \hbar\omega$	5.30×10^{-2}	241
$N(D) \longrightarrow N(S) + \hbar\omega$	1.90×10^{-5}	241

Table A.6: Pumping of species in and out of the chamber.

Reaction	Rate coefficient [1/s]
[Pump In] $\longrightarrow N_2(X, v = 0)$	$Q_{N_2(X)}/V$
$N_2(X, v = 0) \longrightarrow$ [Pump Out]	Q_{in}/pV
$N_2(X, v = 1) \longrightarrow$ [Pump Out]	Q_{in}/pV
$N_2(X, v = 2) \longrightarrow$ [Pump Out]	Q_{in}/pV
$N_2(X, v = 3) \longrightarrow$ [Pump Out]	Q_{in}/pV
$N_2(X, v = 4) \longrightarrow$ [Pump Out]	Q_{in}/pV
$N_2(X, v = 5) \longrightarrow$ [Pump Out]	Q_{in}/pV
$N_2(X, v = 6) \longrightarrow$ [Pump Out]	Q_{in}/pV
$N_2(A) \longrightarrow$ [Pump Out]	Q_{in}/pV
$N(S) \longrightarrow$ [Pump Out]	Q_{in}/pV
$N(D) \longrightarrow$ [Pump Out]	Q_{in}/pV
$N(P) \longrightarrow$ [Pump Out]	Q_{in}/pV
$N_2^+ \longrightarrow$ [Pump Out]	Q_{in}/pV
$N^+ \longrightarrow$ [Pump Out]	Q_{in}/pV
$N_3^+ \longrightarrow$ [Pump Out]	Q_{in}/pV
$N_4^+ \longrightarrow$ [Pump Out]	Q_{in}/pV

Table A.7: Electron energy loss by the nitrogen molecule, $N_2(X^1\Sigma_g^+, v = 0)$.

Final state	Threshold [eV]	Rate coefficient [m^3/s]	Reference
N_2^+	15.6	$1.04 \times 10^{-14}\ T_e^{0.76}\ e^{-17.76/T_e}$	231
$X\,^1\Sigma_g^+(v = 0)$	$3m_e/m_{N_2(X)}\,T_e$	$1.09 \times 10^{-13}\ T_e^{0.34}\ e^{-0.21/T_e}$	69, 108
$X\,^1\Sigma_g^+(v = 0, j = 2)$	0.00148	$1.16 \times 10^{-13}\ T_e^{-1.45}\ e^{-2.21/T_e}$	177, 34
$X\,^1\Sigma_g^+(v = 1)$	0.289	$7.85 \times 10^{-14}\ T_e^{-1.45}\ e^{-2.44/T_e}$	194
$X\,^1\Sigma_g^+(v = 2)$	0.574	$4.00 \times 10^{-14}\ T_e^{-1.46}\ e^{-2.38/T_e}$	194
$X\,^1\Sigma_g^+(v = 3)$	0.856	$2.22 \times 10^{-14}\ T_e^{-1.47}\ e^{-2.38/T_e}$	194
$X\,^1\Sigma_g^+(v = 4)$	1.13	$1.33 \times 10^{-14}\ T_e^{-1.47}\ e^{-2.42/T_e}$	194
$X\,^1\Sigma_g^+(v = 5)$	1.41	$9.23 \times 10^{-15}\ T_e^{-1.48}\ e^{-2.53/T_e}$	194
$X\,^1\Sigma_g^+(v = 6)$	1.68	$5.87 \times 10^{-15}\ T_e^{-1.48}\ e^{-2.68/T_e}$	194
$A\,^3\Sigma_u^+$	6.17	$1.53 \times 10^{-14}\ T_e^{-0.49}\ e^{-8.68/T_e}$	108
$B\,^3\Pi_g$	7.35	$3.76 \times 10^{-14}\ T_e^{-0.73}\ e^{-9.82/T_e}$	108
$W\,^3\Delta_u$	7.36	$2.05 \times 10^{-14}\ T_e^{-0.50}\ e^{-10.61/T_e}$	108
$B'\,^3\Sigma_u^-$	8.16	$2.29 \times 10^{-14}\ T_e^{-0.82}\ e^{-12.42/T_e}$	108
$a'\,^1\Sigma_u^-$	8.4	$1.18 \times 10^{-14}\ T_e^{-0.78}\ e^{-10.90/T_e}$	108
$a\,^1\Pi_g$	8.55	$2.51 \times 10^{-14}\ T_e^{-0.30}\ e^{-10.24/T_e}$	108
$w\,^1\Delta_u$	8.89	$1.26 \times 10^{-14}\ T_e^{-0.78}\ e^{-10.59/T_e}$	108
$C\,^3\Pi_u$	11	$7.43 \times 10^{-14}\ T_e^{-0.86}\ e^{-12.66/T_e}$	108

Table A.7: (continued)

Final state	Threshold [eV]	Rate coefficient [m^3/s]	Reference
$E\,^3\Sigma_g^+$	11.9	$2.57 \times 10^{-15}\ T_e^{-0.74}\ e^{-10.93/T_e}$	108
$a''\,^1\Sigma_g^+$	12.3	$5.40 \times 10^{-15}\ T_e^{-0.41}\ e^{-13.83/T_e}$	108

Table A.8: Electron energy loss by the nitrogen atom, $N(^4S)$.

Final state	Threshold [eV]	Rate coefficient [m^3/s]	Reference
N^+	14.5	$4.99 \times 10^{-15}\ T_e^{0.77}\ e^{-15.24/T_e}$	119
^4S	$3m_e/m_{N(S)}\ T_e$	$4.26 \times 10^{-13}\ T_e^{-0.98}\ e^{-1.60/T_e}$	189, 162
^2D	2.38	$2.74 \times 10^{-14}\ T_e^{-0.40}\ e^{-3.35/T_e}$	228
^2P	3.58	$9.11 \times 10^{-15}\ T_e^{-0.45}\ e^{-4.80/T_e}$	228
$3s\,^4P$	10.3	$7.37 \times 10^{-15}\ T_e^{0.37}\ e^{-9.06/T_e}$	228
$2s2p^4\,^4P$	10.9	$9.67 \times 10^{-15}\ T_e^{0.13}\ e^{-11.47/T_e}$	228
$4s\,^4P$	12.9	$2.37 \times 10^{-15}\ T_e^{-0.16}\ e^{-13.45/T_e}$	228
$3d\,^4P$	13	$1.92 \times 10^{-15}\ T_e^{0.12}\ e^{-13.66/T_e}$	228

Bibliography

1 Abramzon, N., Siegel, R. B., and Becker, K. (1999). Absolute cross section for the formation of $N_2^+(X^2\Sigma_g^+)$ ions produced by electron impact on N_2. *Journal of Physics B: Atomic, Molecular and Optical Physics*, 32(10):L247–L254.

2 Adamovich, I. (2001). Three-dimensional analytic model of vibrational energy transfer in molecule-molecule collisions. *AIAA Journal*, 39(10):1916–1925.

3 Adamovich, I., Macheret, S., Rich, J., and Treanor, C. (1998). Vibrational energy transfer rates using a forced harmonic oscillator model. *Journal of Thermophysics and Heat Transfer*, 12(1):57–65.

4 Adams, S. F. and Miller, T. A. (2000). Surface and volume loss of atomic nitrogen in a parallel plate rf discharge reactor. *Plasma Sources Science and Technology*, 9(3):248–255.

5 Agarwal, S., Hoex, B., van de Sanden, M. C. M., Maroudas, D., and Aydil, E. S. (2003). Absolute densities of N and excited N_2 in a N_2 plasma. *Applied Physics Letters*, 83(24):4918–4920.

6 Ahn, T., Adamovich, I., and Lempert, W. (2004). Determination of nitrogen V–V transfer rates by stimulated Raman pumping. *Chemical Physics*, 298(1–3):233–240.

7 Albritton, D. L. (1978). Ion-neutral reaction-rate constants measured in flow reactors through 1977. *Atomic Data and Nuclear Data Tables*, 22(1):1–101.

8 Allan, M. (1985). Excitation of vibrational levels up to $v = 17$ in N_2 by electron impact in the 0–5 eV region. *Journal of Physics B: Atomic, Molecular and Optical Physics*, 18(22):4511–4517.

9 Allan, M. (2005). Measurement of the elastic and $v = 0 \rightarrow 1$ differential electron-N_2 cross sections over a wide angular range. *Journal of Physics B: Atomic, Molecular and Optical Physics*, 38(20):3655–3672.

10 Amemiya, H. (1997). Sheath formation criterion and ion flux for non-Maxwellian plasma. *Journal of the Physical Society of Japan*, 66(5):1335–1338.

11 Armentrout, P. B., Tarr, S. M., Dori, A., and Freund, R. S. (1981). Electron impact ionization cross section of metastable $N_2(A^3\Sigma_u^+)$. *Journal of Chemical Physics*, 75(6):2786–2794.

12 Ashida, S., Lee, C., and Lieberman, M. A. (1995). Spatially averaged (global) model of time modulated high density argon plasma. *Journal of Vacuum Science and Technology A*, 13(5):2498–2507.

13 Ashida, S. and Lieberman, M. A. (1997). Spatially averaged (global) model of time modulated high density chlorine plasmas. *Japanese Journal of Applied Physics*, 36(2):854–861.

14 Aydil, E. S. (2003). Personal communication.

15 Bacri, J. and Medani, A. (1982). Electron diatomic molecule weighted total cross section calculation: III. Main inelastic processes for N_2 and N_2^+. *Physica B & C*, 112(3):101–118.

16 Bahati, E. M., Jureta, J. J., Belic, D. S., Cherkani-Hassani, H., Abdellahi, M. O., and Defrance, P. (2001). Electron impact dissociation and ionization of N_2^+. *Journal of Physics B: Atomic, Molecular and Optical Physics*, 34(15):2963–2973.

17 Bakowski, B., Hancock, G., Peverall, R., Ritchie, G. A. D., and Thornton, L. J. (2004). Characterization of an inductively coupled N_2 plasma using sensitive diode laser spectroscopy. *Journal of Physics D: Applied Physics*, 37(15):2064–2072.

18 Bates, D. R. (1989). Temperature dependence of termolecular association of diatomic ions with diatomic molecules. *Journal of Chemical Physics*, 90(1):87.

19 Belmonte, T., Bockel, S., Bordot, C., Ablitzer, D., and Michel, H. (1998). Measurement of the loss probability of nitrogen atoms at 823 K on iron nitride ϵ-Fe_2N_{1-x}. *Applied Surface Science*, 135(1–4):259–268.

20 Belmonte, T., Lefevre, L., Czerwiec, T., Michel, H., and Ricard, A. (1999). Measurements of the loss probability of nitrogen atoms versus temperature on various surfaces. *Thin Solid Films*, 341(1–2):27–30.

21 Berrington, K. A., Burke, P. G., and Robb, W. D. (1975). The scattering of electrons by atomic nitrogen. *Journal of Physics B: Atomic, Molecular and Optical Physics*, 8(15):2500–2511.

22 Billing, G. and Fisher, E. (1979). VV-rate and VT-rate coefficients in N_2 by a quantum-classical model. *Chemical Physics*, 43(3):395–401.

23 Biloiu, C., Scime, E. E., Biloiu, I. A., and Sun, X. (2007a). Nitrogen dissociation degree in the diffusion region of a helicon plasma source obtained by atomic lines to molecular band intensities ratio. *Journal of Applied Physics*, 102(5):053303.

24 Biloiu, C., Sun, X., Harvey, Z., and Scime, E. (2007b). An alternative method for gas temperature determination in nitrogen plasmas: Fits of the bands of the first positive system ($B^3\Pi_g \rightarrow A^3\Sigma_u^+$). *Journal of Applied Physics*, 101(7):073303.

25 Black, G., Wise, H., Schechter, S., and Sharpless, R. L. (1974). Measurements of vibrationally excited molecules by Raman scattering. II. Surface deactivation of vibrationally excited N_2. *Journal of Chemical Physics*, 60(9):3526–3536.

26 Bohm, D. (1949). Minimum ionic kinetic energy for a stable sheath. In Guthrie, A. and Wakerling, R. K., editors, *The characteristics of electrical discharges in magnetic fields*, number I, volume 5 in National nuclear energy series – Manhattan project technical section, chapter 3, pages 77–86. McGraw-Hill, New York.

27 Bol'shakov, A., Cruden, B., and Sharma, S. (2004). Determination of gas temperature and thermometric species in inductively coupled plasmas by emission and diode laser absorption. *Plasma Sources Science and Technology*, 13(4):691–700.

28 Booth, J. P. and Sadeghi, N. (1991). Oxygen and fluorine kinetics in electron cyclotron resonance plasmas by time-resolved actinometry. *Journal of Applied Physics*, 70(2):611–620.

29 Borst, W. L. (1972). Excitation of several important metastable states of N_2 by electron impact. *Physical Review A*, 5(2):648–656.

30 Bowers, M. T., Kemper, P. R., and Laudenslager, J. B. (1974). Reactions of ions in excited electronic states: $(N_2^+\cdot)^* + N_2 \rightarrow N_3^+ + N$. *Journal of Chemical Physics*, 61(11):4394–4399.

31 Bray, K. N. C. (1968). Vibrational relaxation of anharmonic oscillator molecules: Relaxation under isothermal conditions. *Journal of Physics B: Atomic, Molecular and Optical Physics*, 1(4):705–717.

32 Britun, N., Gaillard, M., Ricard, A., Kim, Y. M., Kim, K. S., and Han, J. G. (2007). Determination of the vibrational, rotational and electron temperatures in N_2 and Ar/N_2 rf discharge. *Journal of Physics D: Applied Physics*, 40(4):1022–1029.

33 Brook, E., Harrison, M. F. A., and Smith, A. C. H. (1978). Measurements of the electron impact ionisation cross sections of He, C, O and N atoms. *Journal of Physics B: Atomic, Molecular and Optical Physics*, 11(17):3115–3132.

34 Brunger, M., Buckman, S., and Elford, M. (2003). Excitation cross sections. In Itikawa, Y., editor, *Interactions of Photons and Electrons with Molecules*, volume 17C of *Landolt-Börnstein - Group I: Elementary Particles, Nuclei and Atoms*, chapter 6.4, pages 6118–6201. Springer-Verlag, New York.

35 Brunger, M. J. and Buckman, S. J. (2002). Electron-molecule scattering cross-sections. I. Experimental techniques and data for diatomic molecules. *Physics Reports*, 357(3–5):215–458.

36 Buckman, S., Brunger, M., and Elford, M. (2003). *Integral elastic cross sections*, volume 17C of *Landolt-Börnstein - Group I: Elementary Particles, Nuclei and Atoms*, chapter 6.2, pages 6052–6084. Springer-Verlag, New York.

37 Burke, P. G., Berrington, K. A., LeDourneuf, M., and Lan, V. K. (1974). The $^3P^e$ resonance in the low-energy scattering of electrons by atomic nitrogen. *Journal of Physics B: Atomic, Molecular and Optical Physics*, 7(18):L531–L535.

38 Cacciatore, M., Capitelli, M., and Gorse, C. (1982). Non-equilibrium dissociation and ionization of nitrogen in electrical discharges: The role of electronic collisions from vibrationally excited molecules. *Chemical Physics*, 66(1–2):141–151.

39 Cacciatore, M., Kurnosov, A., and Napartovich, A. (2005). Vibrational energy transfer in N_2 - N_2 collisions: A new semiclassical study. *Journal of Chemical Physics*, 123(17):174315.

40 Campbell, L., Brunger, M. J., Cartwright, D. C., and Teubner, P. J. O. (2004). Production of vibrationally excited N_2 by electron impact. *Planetary and Space Science*, 52(9):815–822.

41 Campbell, L., Brunger, M. J., Nolan, A. M., Kelly, L. J., Wedding, A. B., Harrison, J., Teubner, P. J. O., Cartwright, D. C., and McLaughlin, B. (2001). Integral cross sections for electron impact excitation of electronic states of N_2. *Journal of Physics B: Atomic, Molecular and Optical Physics*, 34(7):1185–1199.

42 Canosa, A., Gomet, J. C., Rowe, B. R., and Queffelec, J. L. (1991). Flowing afterglow Langmuir probe measurement of the $N_2^+(v = 0)$ dissociative recombination rate coefficient. *Journal of Chemical Physics*, 94(11):7159–7163.

43 Cao, Y. S. and Johnsen, R. (1991). Recombination of N_4^+ ions with electrons. *Journal of Chemical Physics*, 95(10):7356–7359.

44 Capitelli, M., Armenise, I., Bruno, D., Cacciatore, M., Celiberto, R., Colonna, G., De Pascale, O., Diomede, P., Esposito, F., Gorse, C., Hassouni, K., Laricchiuta, A., Longo, S., Pagano, D., Pietanza, D., and Rutigliano, M. (2007). Non-equilibrium plasma kinetics: a state-to-state approach. *Plasma Sources Science and Technology*, 16(1):S30–S44.

45 Cartwright, D. C., Trajmar, S., Chutjian, A., and Williams, W. (1977). Electron impact excitation of the electronic states of N_2. II. Integral cross sections at incident energies from 10 to 50 eV. *Physical Review A*, 16(3):1041–1051.

46 Cenian, A. and Chernukho, A. (2003). MC simulations of nitrogen swarm parameters: comparison of cross-section sets. *Radiation Physics and Chemistry*, 68(1–2):103–107.

47 Chantry, P. J. (1987). A simple formula for diffusion calculations involving wall reflection and low density. *Journal of Applied Physics*, 62(4):1141–1148.

48 Chen, J. C. Y. (1964). Theory of subexcitation electron scattering by molecules. II. Excitation and de-excitation of molecular vibration. *Journal of Chemical Physics*, 40(12):3513–3520.

[49] Cho, J., Han, S., Lee, Y., Kim, O. K., Kim, G.-H., Kim, Y.-W., Lim, H., and Suh, M. (2001). The measurement of nitrogen ion species ratio in inductively coupled plasma source ion implantation. *Surface and Coatings Technology*, 136(1-3):106–110.

[50] Clark, W. G. and Setser, D. W. (1980). Energy transfer reactions of $N_2(A^3\Sigma_u^+)$. 5. Quenching by hydrogen halides, methyl halides, and other molecules. *Journal of Physical Chemistry*, 84(18):2225–2233.

[51] Conrad, J., Radtke, J., Dodd, R., F.J., W., and Tran, N. (1987). Plasma source ion-implantation technique for surface modification of materials. *Journal of Applied Physics*, 52(11):4591–4596.

[52] Cook, C. J. and Peterson, J. R. (1962). Direct and dissociative ionization cross sections for electrons in N_2. *Physical Review Letters*, 9(4):164–166.

[53] Cosby, P. C. (1993). Electron-impact dissociation of nitrogen. *Journal of Chemical Physics*, 98(12):9544–9553.

[54] Crowe, A. and McConkey, J. W. (1973). Dissociative ionization by electron impact. II. N^+ and N^{++} from N_2. *Journal of Physics B: Atomic, Molecular and Optical Physics*, 6(10):2108–2117.

[55] Cunningham, A. J. and Hobson, R. M. (1972). Dissociative recombination at elevated temperatures. IV. N_2^+ dominated afterglows. *Journal of Physics B: Atomic, Molecular and Optical Physics*, 5(12):2328–2331.

[56] Czerwiec, T., Greer, F., and Graves, D. B. (2005). Nitrogen dissociation in a low pressure cylindrical ICP discharge studied by actinometry and mass spectrometry. *Journal of Physics D: Applied Physics*, 38(24):4278–4289.

[57] da Costa, R. F. and Lima, M. A. P. (2007). Electron-impact electronic excitation of molecular nitrogen using the Schwinger multichannel variational method. *Physical Review A*, 75(2):022705.

[58] da Silva, M. L., Guerra, V., Loureiro, J., and Sá, P. A. (2008). Vibrational distributions in N_2 with an improved calculation of energy levels using the RKR method. *Chemical Physics*, 348(1–3):187–194.

[59] Daly, N. R. and Powell, R. E. (1966). Electron collisions in nitrogen. *Proceedings of the Physical Society*, 89(2):273–280.

60 Darracht, M., Wang, S., Woolsey, J. M., and McConkey, J. W. (1993). Spectroscopic diagnosis of vibrationally-hot N_2. *Plasma Sources Science and Technology*, 2(4):258–260.

61 Deutsch, H., Becker, K., Defrance, P., Onthong, U., Parajuli, R., Probst, M., Matt, S., and Märk, T. D. (2002). Calculated absolute cross section for the electron-impact ionization of CO_2^+ and N_2^+. *Journal of Physics B: Atomic, Molecular and Optical Physics*, 35(3):L65–L69.

62 Dilecce, G., Ambrico, P., and De Benedictis, S. (2007). On $N_2(C^3\Pi_u, v = 0)$ state lifetime and collisional deactivation rate by N_2. *Chemical Physics Letters*, 444(1-3):39–43.

63 Donnelly, V. M. and Malyshev, M. V. (2000). Diagnostics of inductively coupled chlorine plasmas: Measurements of the neutral gas temperature. *Applied Physics Letters*, 77(16):2467–2469.

64 Dubé, L. and Herzenberg, A. (1979). Absolute cross sections from the "boomerang model" for resonant electron-molecule scattering. *Physical Review A*, 20(1):194–213.

65 DuBois, R. D. and Rudd, M. E. (1976). Differential cross sections for elastic scattering of electrons from argon, neon, nitrogen and carbon monoxide. *Journal of Physics B: Atomic, Molecular and Optical Physics*, 9(15):2657–2667.

66 Egorov, V. I., Gershenzon, Y. M., Rozenshtein, V. B., and Umanskii, S. Y. (1973). On the mechanism of heterogeneous relaxation of vibrationally excited nitrogen molecules. *Chemical Physics Letters*, 20(1):77–80.

67 Esposito, F., Armenise, I., and Capitelli, M. (2006). N-N_2 state to state vibrational-relaxation and dissociation rates based on quasiclassical calculations. *Chemical Physics*, 331(1):1–8.

68 Esposito, F. and Capitelli, M. (2006). QCT calculations for the process $N_2(v)$+N $\rightarrow$ $N_2(v')$+N in the whole vibrational range. *Chemical Physics Letters*, 418(4–6):581–585.

69 Feng, H., Sun, W., and Morrison, M. A. (2003). Parameter-free nonadiabatic correlation-polarization potential for vibrational excitation in electron-molecule scattering: Application to e-N_2 collisions. *Physical Review A*, 68(6):062709.

70 Fisher, E. (1997). Calculations of the effect of nitrogen vibrational kinetics on laminar flame temperature profiles. *Combustion and Flame*, 108(1–2):127–138.

71 Fitaire, M., Pointu, A. M., Stathopoulos, D., and Vialle, M. (1984). Measurement of N_4^+ recombination rate vs electron temperature in a proton beam created plasma. *Journal of Chemical Physics*, 81(4):1753–1758.

72 Florescu-Mitchell, A. I. and Mitchell, J. B. A. (2006). Dissociative recombination. *Physics Reports*, 430(5-6):277–374.

73 Freund, R. S., Wetzel, R. C., and Shul, R. J. (1990). Measurements of electron-impact-ionization cross sections of N_2, CO, CO_2, CS, S_2, CS_2, and metastable N_2. *Physical Review A*, 41(11):5861–5868.

74 Frost, R. M., Awakowicz, P., Summers, H. P., and Badnell, N. R. (1998). Calculated cross sections and measured rate coefficients for electron-impact excitation of neutral and singly ionized nitrogen. *Journal of Applied Physics*, 84(6):2989–3003.

75 Geoghegan, M., Adams, N. G., and Smith, D. (1991). Determination of the electron-ion dissociative recombination coefficients for several molecular ions at 300 K. *Journal of Physics B: Atomic, Molecular and Optical Physics*, 24(10):2589–2599.

76 Gillan, C. J., Noble, C. J., and Burke, P. G. (1988). Electron-scattering by nitrogen molecules including polarized pseudostates. *Journal of Physics B: Atomic, Molecular and Optical Physics*, 21(3):L53–L59.

77 Gillan, C. J., Tennyson, J., McLaughlin, B. M., and Burke, P. G. (1996). Low-energy electron impact excitation of the nitrogen molecule: optically forbidden transitions. *Journal of Physics B: Atomic, Molecular and Optical Physics*, 29(8):1531–1547.

78 Godefroid, M. and Fischer, C. F. (1984). MCHF-BP fine-structure splittings and transition rates for the ground configuration in the nitrogen sequence. *Journal of Physics B: Atomic, Molecular and Optical Physics*, 17(5):681–692.

79 Godyak, V. A. (1986). *Soviet Radio Frequency Discharge Research*. Delphic Associates, Falls Church, V.A.

80 Godyak, V. A., Piejak, R. B., and Alexandrovich, B. M. (1993). Probe diagnostics of non-Maxwellian plasmas. *Journal of Applied Physics*, 73(8):3657–3663.

81 Gordiets, B., Ferreira, C., Guerra, V., Loureiro, J., Nahorny, J., Pagnon, D., Touzeau, M., and Vialle, M. (1995). Kinetic model of a low-pressure N_2-O_2 flowing glow discharge. *IEEE Transactions on Plasma Science*, 23(4):750–768.

82 Gordiets, B. F., Ferreira, C. M., Nahorny, J., Pagnon, D., Touzeau, M., and Vialle, M. (1996). Surface kinetics of N and O atoms in N_2-O_2 discharges. *Journal of Physics D: Applied Physics*, 29(4):1021–1031.

83 Gote, M. and Ehrhardt, H. (1995). Rotational excitation of diatomic molecules at intermediate energies: Absolute differential state-to-state transition cross sections for electron scattering from N_2, Cl_2, CO and HCl. *Journal of Physics B: Atomic, Molecular and Optical Physics*, 28(17):3957–3986.

84 Guberman, S. L. (1991). Dissociative recombination of the ground state of N_2^+. *Geophysical Research Letters*, 18(6):1051–1054.

85 Gudmundsson, J. T. (2001). On the effect of the electron energy distribution on the plasma parameters of argon discharge: A global (volume averaged) model study. *Plasma Sources Science and Technology*, 10(1):76–81.

86 Gudmundsson, J. T., Kimura, T., and Lieberman, M. A. (1999). Experimental studies of O_2/Ar plasma in a planar inductive discharge. *Plasma Sources Science and Technology*, 8(1):22–30.

87 Gudmundsson, J. T., Kouznetsov, I. G., Patel, K. K., and Lieberman, M. A. (2001). Electronegativity of low-pressure high-density oxygen discharges. *Journal of Physics D: Applied Physics*, 34(7):1100–1109.

88 Gudmundsson, J. T. and Lieberman, M. A. (1998). Model and measurements for a planar inductive oxygen discharge. *Plasma Sources Science and Technology*, 7(1):1–12.

89 Gudmundsson, J. T., Marakhtanov, A. M., Patel, K. K., Gopinath, V. P., and Lieberman, M. A. (2000). On the plasma parameters of a planar inductive oxygen discharge. *Journal of Physics D: Applied Physics*, 33(11):1323–1331.

90 Gudmundsson, J. T. and Thorsteinsson, E. G. (2007b). Oxygen discharges diluted with argon: dissociation processes. *Plasma Sources Science and Technology*, 16(2):399–412.

91 Gudmundsson, J. T. and Thorsteinsson, E. G. (July 15 - 20, 2007a). On the role of argon reactions in a low pressure Ar/O_2 discharge. In Schmidt, J., Šimek, M., Pekárek, S., and Prukner, V., editors, *Proceedings of the XXVIII International Conference on Phenomena in Ionized Gases*, pages 79 – 82, Prague, Czech Republic. Institute of Plasma Physics AS CR, v.v.i.

92 Guerra, V. and Loureiro, J. (1995). Non-equilibrium coupled kinetics in stationary N_2-O_2 discharges. *Journal of Physics D: Applied Physics*, 28(9):1903–1918.

93 Guerra, V. and Loureiro, J. (1997). Electron and heavy particle kinetics in a low-pressure nitrogen glow discharge. *Plasma Sources Science and Technology*, 6(3):361–372.

94 Guerra, V., Sá, P. A., and Loureiro, J. (2004). Kinetic modeling of low-pressure nitrogen discharges and post-discharges. *The European Physical Journal: Applied Physics*, 28(2):125–152.

95 Guerra, V., Tatarova, E., Dias, F. M., and Ferreira, C. M. (2002). On the self-consistent modeling of a traveling wave sustained nitrogen discharge. *Journal of Applied Physics*, 91(5):2648–2661.

96 Guthrie, J. A., Chaney, R. C., and Cunningham, A. J. (1991). Temperature dependencies of ternary ion–molecule association reactions yielding N_3^+, N_4^+, and $(CO)_2^+$. *Journal of Chemical Physics*, 95(2):930–936.

97 Halas, S. and Adamczyk, B. (1972). Cross sections for the production of N_2^+, N^+ and N_2^{2+} from nitrogen by electrons in the energy range 16-600 eV. *International Journal of Mass Spectrometry and Ion Physics*, 10(2):157–160.

98 Hancock, G., Peverall, R., Ritchie, G. A. D., and Thornton, L. J. (2006). Absolute number densities of vibrationally excited $N_2(A^3\Sigma_u^+)$ produced in a low pressure rf plasma. *Journal of Physics D: Applied Physics*, 39(9):1846–1852.

99 Hays, G. N. and Oskam, H. J. (1973). Reaction rate constant for $2N_2(A^3\Sigma_u^+) \rightarrow N_2(C^3\Pi_u) + N_2(X^1\Sigma_g^+, \nu' > 0)$. *Journal of Chemical Physics*, 59(11):6088–6091.

100 Hays, G. N., Tracy, C. J., and Oskam, H. J. (1974). Surface catalytic efficiency of a sputtered molybdenum layer on quartz and Pyrex for the recombination of nitrogen atoms. *Journal of Chemical Physics*, 60(5):2027–2034.

101 Henry, R. J. W., Burke, P. G., and Sinfailam, A.-L. (1969). Scattering of electrons by C, N, O, N^+, O^+, and O^{++}. *Physical Review*, 178(1):218–224.

102 Herron, J. T. (1999). Evaluated chemical kinetics data for reactions of $N(^2D)$, $N(^2P)$, and $N_2(A^3\Sigma_u^+)$ in the gas phase. *Journal of Physical and Chemical Reference Data*, 28(5):1453–1483.

103 Herron, J. T., Franklin, J. L., Bradt, P., and Dibeler, V. H. (1959). Kinetics of nitrogen atom recombination. *Journal of Chemical Physics*, 30(4):879–885.

104 Hopwood, J. (1994). Planar RF induction plasma coupling efficiency. *Plasma Sources Science and Technology*, 3(4):460 – 464.

105 Hudson, J., Hamilton, M., Vallance, C., and Harland, P. (2003). Absolute electron impact ionization cross-sections for the C_1 to C_4 alcohols. *Physical Chemistry Chemical Physics*, 5(15):3162–3168.

106 Huo, W. M., Gibson, T. L., Lima, M. A. P., and McKoy, V. (1987). Schwinger multichannel study of the $^2\Pi_g$ shape resonance in N_2. *Physical Review A*, 36(4):1632–1641.

107 Ishikawa, K., Yamaoka, Y., Nakamura, M., Yamazaki, Y., Yamasaki, S., Ishikawa, Y., and Samukawa, S. (2006). Surface reactions during etching of organic low-k films by plasmas of N_2 and H_2. *Journal of Applied Physics*, 99(8):083305.

108 Itikawa, Y. (2006). Cross sections for electron collisions with nitrogen molecules. *Journal of Physical and Chemical Reference Data*, 35(1):31–53.

109 Itikawa, Y., Hayashi, M., Ichimura, A., Onda, K., Sakimoto, K., Takayanagi, K., Nakamura, M., Nishimura, H., and Takayanagi, T. (1986). Cross-sections for collisions of electrons and photons with nitrogen molecules. *Journal of Physical and Chemical Reference Data*, 15(3):985–1010.

110 Jaffe, S., Karpas, Z., and Klein, F. S. (1973). Ion cyclotron mass spectrometric study of the reaction $N_2^+ + N_2 \rightarrow N_3^+ + N$. *Journal of Chemical Physics*, 58(5):2190–2191.

111 John, T. L. and Williams, R. J. (1977). Elastic-scattering of low-energy electrons by atomic nitrogen. *Journal of Physics B: Atomic, Molecular and Optical Physics*, 10(14):L531–L533.

112 Johnson, P. V., Malone, C. P., Kanik, I., Tran, K., and Khakoo, M. A. (2005). Integral cross sections for the direct excitation of the $A^3\Sigma_u^+$, $B^3\Pi_g$, $W^3\Delta_u$, $B'^3\Sigma_u^-$, $a'^1\Sigma_u^-$, $a^1\Pi_g$, $w^1\Delta_u$, and $C^3\Pi_u$ electronic states in N_2 by electron impact. *Journal of Geophysical Research*, 110:A11311.

113 Kaplan, J. (1932). Products of dissociation in nitrogen. *Physical Review*, 42(1):97–100.

114 Kasner, W. H. (1967). Study of the temperature dependence of electron-ion recombination in nitrogen. *Physical Review*, 164(1):194–200.

115 Kato, T. (1994). Electron impact excitation of notrogen and nitrogen-like ions: A review of available data and recommendations. *Atomic Data and Nuclear Data Tables*, 57(1–2):181–214.

116 Keck, J. and Carrier, G. (1965). Diffusion theory of nonequilibrium dissociation and recombination. *Journal of Chemical Physics*, 43(7):2284–2298.

117 Kella, D., Johnson, P. J., Pedersen, H. B., Vejby-Christensen, L., and Andersen, L. H. (1996). Branching ratios for dissociative recombination of $^{15}N^{14}N^+$. *Physical Review Letters*, 77(12):2432–2435.

118 Kim, S., Lieberman, M. A., Lichtenberg, A. J., and Gudmundsson, J. T. (2006). Improved volume-averaged model for steady and pulsed-power electronegative discharges. *Journal of Vacuum Science and Technology A*, 24(6):2025–2040.

119 Kim, Y.-K. and Desclaux, J.-P. (2002). Ionization of carbon, nitrogen, and oxygen by electron impact. *Physical Review A*, 66(1):012708.

120 Kim, Y.-K., Irikura, K., and Ali, M. (2000). Electron-impact total ionization cross sections of molecular ions. *Journal of Research of the National Institute of Standards and Technology*, 105(2):285–291.

121 Kimura, T. and Ohe, K. (2001). Global model of inductively coupled Ar plasmas using two-temperature approximation. *Journal of Applied Physics*, 89(8):4240–4246.

122 Kitajima, T., Nakano, T., Samukawa, S., and Makabe, T. (2008). Diagnostics of N_2 dissociation in RF plasmas by vacuum ultraviolet emission and absorption spectroscopy. *Plasma Sources Science and Technology*, 17(2):024018.

123 Kossyi, I. and Silakov, V. (2005). Step photoionization as a mechanism responsible for the Raether paradox. *Plasma Sources Science and Technology*, 14(3):594–598.

124 Kossyi, I. A., Kostinsky, A. Y., Matveyev, A. A., and Silakov, V. P. (1992). Kinetic scheme of the non-equilibrium discharge in nitrogen-oxygen mixtures. *Plasma Sources Science and Technology*, 1(3):207–220.

125 Kozlov, S. N., Aleksandrov, E. N., Zhestkov, B. E., and Kislyuk, M. U. (1987a). Study of nitrogen and oxygen atom recombination on a quartz surface using resonance fluorescence spectroscopy. *Russian Chemical Bulletin*, 36(11):2272–2276.

126 Kozlov, S. N., Zhestkov, B. E., and Aleksandrov, E. N. (1987b). Rate of heterogeneous quenching of nitrogen and hydrogen atoms on gold. *Russian Chemical Bulletin*, 36(1):43–46.

127 Krishnakumar, E. and Srivastava, S. K. (1990). Cross sections for the production of N_2^+, $N^+ + N_2^{2+}$ and N^{2+} by electron impact on N_2. *Journal of Physics B: Atomic, Molecular and Optical Physics*, 23(11):1893–1903.

128 Kutasi, K. and Loureiro, J. (2007). Role of the wall reactor material on the species density distributions in an N_2-O_2 post-discharge for plasma sterilization. *Journal of Physics D: Applied Physics*, 40(18):5612–5623.

129 Kutz, H. and Meyer, H.-D. (1995). Rotational excitation of N_2 and Cl_2 molecules by electron impact in the energy range 0.01–1000 eV: Investigation of excitation mechanisms. *Physical Review A*, 51(5):3819–3830.

130 Lee, C., Graves, D. B., Lieberman, M. A., and Hess, D. W. (1994). Global model of plasma chemistry in a high density oxygen discharge. *Journal of the Electrochemical Society*, 141(6):1546–1555.

131 Lee, C. and Lieberman, M. A. (1995). Global model of Ar, O_2, Cl_2 and Ar/O_2 high-density plasma discharges. *Journal of Vacuum Science and Technology A*, 13(2):368–380.

132 Lefèvre, L., Belmonte, T., Czerwiec, T., Ricard, A., and Michel, H. (1999). Measurements of nitrogen atom loss probability versus temperature on iron surfaces. *Surface and Coatings Technology*, 116–119:1244–1248.

133 Lefèvre, L., Belmonte, T., and Michel, H. (2000). Modeling of nitrogen atom recombination on Pyrex: Influence of the vibrationally excited N_2 molecules on the loss probability of N. *Journal of Applied Physics*, 87(10):7497–7507.

134 Li, H. (2006). Measurements of electron energy distribution function and neutral gas temperature in an inductively coupled plasma. Master's thesis, University of Saskatchewan, Saskatoon, Saskatchewan, Canada.

135 Lias, S. G. (2005). Ionization energy evaluation. In Linstrom, P. J. and Mallard, W. G., editors, *NIST chemistry WebBook, NIST Standard Reference Database*, number 69. National Institude of Standards and Technology, Gaithersburg MD.

136 Lieberman, M. A. and Gottscho, R. A. (1994). Design of high-density plasma sources for materials processing. In Francombe, M. and Vossen, J., editors, *Physics of Thin Films, vol. 18*, pages 1–119. Academic Press, New York.

137 Lieberman, M. A. and Lichtenberg, A. J. (2005). *Principles of Plasma Discharges and Materials Processing*. John Wiley & Sons, New York, 2nd edition.

138 Lin, C. L. and Kaufman, F. (1971). Reactions of metastable nitrogen atoms. *Journal of Chemical Physics*, 55(8):3760–3770.

139 Lindsay, B. and Mangan, M. (2003). Ionization. In Itikawa, Y., editor, *Interactions of Photons and Electrons with Molecules*, volume 17C of *Landolt-Börnstein - Group I: Elementary Particles, Nuclei and Atoms*, chapter 5.1, pages 5001–5077. Springer-Verlag, New York.

140 Linss, V., Kupfer, H., Peter, S., and Richter, F. (2005). Determination of the neutral gas temperature of nitrogen-containing low-pressure plasmas using a two-temperature model. *Surface and Coatings Technology*, 200(5–6):1696–1701.

141 Lofthus, A. and Krupenie, P. H. (1977). Spectrum of molecular nitrogen. *Journal of Physical and Chemical Reference Data*, 6(1):113–307.

142 Ma, J. and Pu, Y.-K. (2003). Tuning effect on the electron energy distribution function of an inert gas mixture in nitrogen inductively coupled plasma discharges. *Chinese Physics Letters*, 20(9):1527–1529.

143 Märk, T. D. (1975). Cross section for single and double ionization of N_2 and O_2 molecules by electron impact from threshold up to 170 eV. *Journal of Chemical Physics*, 63(9):3731–3736.

144 Marković, V., Petrović, Z., and Pejović, M. (1994). Surface recombination of atoms in a nitrogen afterglow. *Journal of Chemical Physics*, 100(11):8514–8521.

145 McGuire, E. J. (1971). Inelastic scattering of electrons and protons by the elements He to Na. *Physical Review A*, 3(1):267–279.

146 Mehr, F. J. and Biondi, M. A. (1969). Electron temperature dependence of recombination of O_2^+ and N_2^+ ions with electrons. *Physical Review*, 181(1):264–271.

147 Meyer, J. A., Klosterboer, D. H., and Setser, D. W. (1971). Energy transfer reactions of $N_2(A^3\Sigma_u^+)$. IV. Measurement of the radiative lifetime and study of the interaction with olefins and other molecules. *Journal of Chemical Physics*, 55(5):2084–2091.

148 Meyer, J. A., Setser, D. W., and Stedman, D. H. (1970). Energy transfer reactions of $N_2(A^3\Sigma_u^+)$. II. Quenching and emission by oxygen and nitrogen atoms. *Journal of Physical Chemistry*, 74(10):2238–2240.

149 Mi, L. and Bonham, R. A. (1998). Electron–ion coincidence measurements: The neutral dissociation plus excitation cross section for N_2. *Journal of Chemical Physics*, 108(5):1904–1909.

150 Mihajlov, A., Stojanović, V., and Petrović, Z. (1999). Resonant vibrational excitation/de-excitation of $N_2(v)$ by electrons. *Journal of Physics D: Applied Physics*, 32(20):2620–2629.

151 Miller, T. M., Aubrey, B. B., Eisner, P. N., and Bederson, B. (1970). Relative cross section measurements for electron scattering by atomic nitrogen (0.2 – 3 eV). *Bulletin Of The American Physical Society*, 15(3):416.

152 Morgan, J. E. and Schiff, H. I. (1963). The study of vibrationally excited N_2 molecules with the aid of an isothermal calorimeter. *Canadian Journal of Chemistry*, 41(4):903–912.

153 Morgan, L. A. (1986). Resonant vibrational excitation of N_2 by low-energy electron impact. *Journal of Physics B: Atomic, Molecular and Optical Physics*, 19(11):L439–L445.

154 Morrison, M. A., Saha, B. C., and Gibson, T. L. (1987). Electron-N_2 scattering calculations with a parameter-free model polarization potential. *Physical Review A*, 36(8):3682–3698.

155 Morrison, M. A., Sun, W., Isaacs, W. A., and Trail, W. K. (1997). Ultrasimple calculation of very-low-energy momentum-transferand rotational-excitation cross sections: e–N_2 scattering. *Physical Review A*, 55(4):2786–2798.

156 Moustakas, T. D., Lei, T., and Molnar, R. J. (1993). Growth of GaN by ECR-assisted MBE. *Physica B*, 185(1–4):36–49.

157 Mowat, J. R., Danared, H., Sundström, G., Carlson, M., Andersen, L. H., Vejby-Christensen, L., af Ugglas, M., and Larsson, M. (1995). High-resolution, low-energy dissociative recombination spectrum of $^3HeH^+$. *Physical Review Letters*, 74(1):50–53.

158 Mul, P. M. and McGowan, J. W. (1979). Merged electron-ion beam experiments. iii - temperature dependence of dissociative recombination for atmospheric ions NO^+, O_2^+, and N_2^+. *Journal of Physics B: Atomic, Molecular and Optical Physics*, 12(9):1591–1601.

159 Mulliken, R. S. (1932). The interpretation of band spectra. Part III. Electron quantum numbers and states of molecules and their atoms. *Reviews of Modern Physics*, 4(1):1–86.

160 Nagpal, R. and Ghosh, P. K. (1990). Electron energy distribution functions and vibrational population densities of excited electronic states in DC discharges through nitrogen. *Journal of Physics D: Applied Physics*, 23(12):1663–1670.

161 Nakano, T., Kumagai, S., and Samukawa, S. (2002). Estimation of dissociation degree of N_2 in an inductively coupled plasma by vacuum ultraviolet emission spectroscopy. *Journal of Applied Physics*, 92(6):2990–2995.

162 Neynaber, R. H., Marino, L. L., Rothe, E. W., and Trujillo, S. M. (1963). Low-energy electron scattering from atomic nitrogen. *Physical Review*, 129(5):2069–2071.

163 Nickel, J. C., Mott, C., Kanik, I., and McCollum, D. C. (1988). Absolute elastic differential electron scattering cross sections for carbon monoxide and molecular nitrogen in the intermediate energy region. *Journal of Physics B: Atomic, Molecular and Optical Physics*, 21(10):1867–1877.

164 Niimi, H. and Lucovsky, G. (1999). Monolayer-level controlled incorporation of nitrogen in ultrathin gate dielectrics using remote plasma processing: Formation of stacked 'N-O-N' gate dielectrics. *Journal of Vacuum Science and Technology B*, 17(6):2610–2621.

165 Noren, C., Yousif, F. B., and Mitchell, J. (1989). Dissociative recombination and excitation of N_2^+. *Journal of the Chemical Society, Faraday Transactions 2: Molecular and Chemical Physics*, 85(10):1697–1703.

166 Oddone, S., Sheldon, J. W., Hardy, K. A., and Peterson, J. R. (1997). Dissociative recombination of the $A^2\Pi_u$ and the $X^2\Sigma_g$ states of N_2^+ in a glow discharge. *Physical Review A*, 56(6):4737–4741.

167 Ohmori, Y., Shimozuma, M., and Tagashira, H. (1988). Boltzmann equation analysis of electron swarm behaviour in nitrogen. *Journal of Physics D: Applied Physics*, 21(5):724–729.

168 Omidvar, K., Kyle, H. L., and Sullivan, E. C. (1972). Ionization of multielectron atoms by fast charged particles. *Physical Review A*, 5(3):1174–1187.

169 Ono, S. and Teii, S. (1983). Vibrational temperature in a weakly ionized steady-state nitrogen discharge plasma. *Journal of Physics D: Applied Physics*, 16(2):163–170.

170 Ormonde, S., Smith, K., Torres, B. W., and Davies, A. R. (1973). Configuration-interaction effects in the scattering of electrons by atoms and ions of nitrogen and oxygen. *Physical Review A*, 8(1):262–295.

171 Patel, C. K. N. (1964). Selective excitation through vibrational energy transfer and optical maser action in N_2–CO_2. *Physical Review Letters*, 13(21):617–619.

172 Patel, K. K. (1998). Volume averaged modeling of high density discharges. Master's thesis, University of California at Berkeley.

173 Peach, G. (1970). Ionization of neutral atoms with outer 2p, 3s and 3p electrons by electron and proton impact. *Journal of Physics B: Atomic, Molecular and Optical Physics*, 3(3):328–349.

174 Peach, G. (1971). Ionization of atoms and positive ions by electron and proton impact. *Journal of Physics B: Atomic, Molecular and Optical Physics*, 4(12):1670–1677.

175 Peterson, J. R., Le Padellec, A., Danared, H., Dunn, G. H., Larsson, M., Larson, A., Peverall, R., Strömholm, C., Rosén, S., af Ugglas, M., and van der Zande, W. J. (1998). Dissociative recombination and excitation of N_2^+: Cross sections and product branching ratios. *Journal of Chemical Physics*, 108(5):1978–1988.

176 Phelps, A. V. (1991). Cross-sections and swarm coefficients for nitrogen-ions and neutrals in N_2 and argon ions and neutrals in Ar for energies from 0.1 eV to 10 keV. *Journal of Physical and Chemical Reference Data*, 20(3):557–573.

177 Phelps, A. V. (2008). Compilation of electron cross sections. http://jilawww.colorado.edu/~avp/collision_data/electronneutral/ELECTRON.TXT.

178 Phelps, A. V. and Pitchford, L. C. (1985). Anisotropic scattering of electrons by N_2 and its effect on electron transport. *Physical Review A*, 31(5):2932–2949.

179 Phillips, L. F. (1990). Collision-theory treatment of three-body reactions forming N_4^+, O_4^+, $N_2O_2^+$, and N_2NO^+. *Journal of Chemical Physics*, 92(11):6523–6526.

180 Piper, L. G. (1988). State-to-state $N_2(A^3\Sigma_u^+)$ energy-pooling reactions. I. The formation of $N_2(C^3\Pi_u)$ and the Herman infrared system. *Journal of Chemical Physics*, 88(1):231–239.

181 Piper, L. G. (1989a). The excitation of $N_2(B^3\Pi_g, v = 1 - 12)$ in the reaction between $N_2(A^3\Sigma_u^+)$ and $N_2(X, v \geq 5)$. *Journal of Chemical Physics*, 91(2):864–873.

182 Piper, L. G. (1989b). The excitation of $N(^2P)$ by $N_2(A^3\Sigma_u^+, v' = 0, 1)$. *Journal of Chemical Physics*, 90(12):7087–7095.

183 Piper, L. G. (1989c). The rate coefficient for quenching $N(^2D)$ by $O(^3P)$. *Journal of Chemical Physics*, 91(6):3516–3524.

184 Piper, L. G. (1993). Reevaluation of the transition-moment function and Einstein coefficients for the $N_2(A^3\Sigma_u^+ - X^1\Sigma_g^+)$ transition. *Journal of Chemical Physics*, 99(5):3174–3181.

185 Piper, L. G. (1998). Experimental determination of the Einstein coefficient for the N(^{2}P-^{4}S) transition. *Chemical Physics Letters*, 296(3–4):397–402.

186 Piper, L. G., Holtzclaw, K. W., Green, B. D., and Blumberg, W. A. M. (1989). Experimental determination of the Einstein coefficients for the $N_2(B - A)$ transition. *Journal of Chemical Physics*, 90(10):5337–5345.

187 Porter, R. A. and Harshbarger, W. R. (1979). Gas rotational temperature in an RF plasma. *Journal of The Electrochemical Society*, 126(3):460–464.

188 Ralchenko, Y., Kramida, A., Reader, J., and NIST ASD Team (2008). NIST atomic spectra database (version 3.1.5). http://physics.nist.gov/asd3.

189 Ramsbottom, C. A. and Bell, K. L. (1994). Low-energy electron scattering by atomic nitrogen. *Physica Scripta*, 50(6):666–671.

190 Randell, J., Lund, S. L., Mrotzek, G., Ziesel, J.-P., and Field, D. (1994). Low energy electron scattering in H_2, N_2 and O_2. *Journal of Physics B: Atomic, Molecular and Optical Physics*, 27(11):2369–2382.

191 Rapp, D. and Englander-Golden, P. (1965). Total cross sections for ionization and attachment in gases by electron impact. I. Positive ionization. *Journal of Chemical Physics*, 43(5):1464–1479.

192 Rapp, D., Englander-Golden, P., and Briglia, D. D. (1965). Cross sections for dissociative ionization of molecules by electron impact. *Journal of Chemical Physics*, 42(12):4081–4085.

193 Ren, W., Sun, W., Hou, S., and Feng, H. (2005). Accurate studies on the full vibrational energy spectra and molecular dissociation energies for some electronic states of N_2 molecule. *Science in China Series G – Physics, Mechanics & Astronomy*, 48(4):385–398.

194 Ristić, M., Poparić, G. B., and Belić, D. S. (2007). Rate coefficients for resonant vibrational excitation of N_2. *Chemical Physics*, 331(2):410–416.

195 Robertson, A. G., Elford, M. T., Crompton, R. W., Morrison, M. M., Sun, W., and Trail, W. K. (1997). Rotational and vibrational excitation of nitrogen by electron impact. *Australian Journal of Physics*, 50(3):441–472.

196 Robinson, L. B. (1957). Elastic scattering of low-energy electrons by atomic nitrogen and atomic oxygen. *Physical Review*, 105(3):922–927.

197 Sancier, K. M., Fredericks, W. J., Hatchett, J. L., and Wise, H. (1962). Luminescence of solids excited by surface recombination of atoms. II. Recombination coefficients. *Journal of Chemical Physics*, 37(4):860–864.

198 Sarma, M., Adhikari, S., and Mishra, M. K. (2007). Simple systematization of vibrational excitation cross-section calculations for resonant electron-molecule scattering in the boomerang and impulse models. *Journal of Chemical Physics*, 126(4):044309.

199 Sarrette, J., Rouffet, B., and Ricard, A. (2006). Determination of nitrogen atoms loss probabilities on copper, aluminium, alumina, brass and nylon surfaces. *Plasma Processes and Polymers*, 3(2):120–126.

200 Schofield, K. (1973). Evaluated chemical kinetic rate constants for various gas phase reactions. *Journal of Physical and Chemical Reference Data*, 2(1):25–84.

201 Schofield, K. (1979). Critically evaluated rate constants for gaseous reactions of several electronically excited states. *Journal of Physical and Chemical Reference Data*, 8(3):723–798.

202 Schulz, G. J. (1964). Vibrational excitation of N_2, CO, and H_2 by electron impact. *Physical Review*, 135(4):A988–A994.

203 Schwartz, R. N. and Herzfeld, K. F. (1954). Vibrational relaxation times in gases (three-dimensional treatment). *Journal of Chemical Physics*, 22(5):767–773.

204 Schwartz, R. N., Slawsky, Z. I., and Herzfeld, K. F. (1952). Calculation of vibrational relaxation times in gases. *Journal of Chemical Physics*, 20(10):1591–1599.

205 Seaton, M. J. (1959). Electron impact ionization of Ne, O, and N. *Physical Review*, 113(3):814–814.

206 Shah, M. S., Salem, M., Ahmad, R., Zakaullah, M., Qayyum, A., and Murtaza, G. (2008). Langmuir probe characterization of nitrogen plasma for surface nitriding of AISI-4140 steel. *Journal of Materials Processing Technology*, 199(1–3):363–368.

207 Sheehan, C. H. and St.-Maurice, J.-P. (2004). Dissociative recombination of N_2^+, O_2^+, and NO^+: Rate coefficients for ground state and vibrationally excited ions. *Journal of Geophysical Research*, 109:A03302.

208 Shemansky, D. E. and Carleton, N. P. (1969). Lifetime of the N_2 Vegard–Kaplan system. *Journal of Chemical Physics*, 51(2):682–688.

209 Shimada, M., Tynan, G. R., and Cattolica, R. (2006). Rotational and translational temperature equilibrium in an inductively coupled plasma. *Journal of Vacuum Science and Technology A*, 24(5):1878–1883.

210 Shin, Y. M., Kim, E. Y., and Chung, T. H. (2008). Measurement of the degree of dissociation in inductively coupled nitrogen discharges by using optical emission actinometry and mass spectrometry. *Journal of the Korean Physical Society*, 53(2):617–623.

211 Shyn, T. W. and Carignan, G. R. (1980). Angular distribution of electrons elastically scattered from gases: 1.5–400 eV on N_2. II. *Physical Review A*, 22(3):923–929.

212 Singh, H., Coburn, J. W., and Graves, D. B. (2000). Recombination coefficients of O and N radicals on stainless steel. *Journal of Applied Physics*, 88(6):3748–3755.

213 Singh, H. and Graves, D. B. (2000a). Measurements of the electron energy distribution function in molecular gases in a shielded inductively coupled plasma. *Journal of Applied Physics*, 88(7):3889–3898.

214 Singh, H. and Graves, D. B. (2000b). Measurements of the electron energy distribution function in molecular gases in an inductively coupled plasma. *Journal of Applied Physics*, 87(9):4098–4106.

215 Smith, A. C., Caplinger, E., Neynaber, R. H., Rothe, E. W., and Trujillo, S. M. (1962). Electron impact ionization of atomic nitrogen. *Physical Review*, 127(5):1647–1649.

216 Smith, K., Henry, R. J. W., and Burke, P. G. (1967). Calculations on the scattering of electrons by atomic systems with configurations $2p^q$. *Physical Review*, 157(1):51–68.

217 Stallcop, J. R., Partridge, H., and Levin, E. (1991). Resonance charge transfer, transport cross sections, and collision integrals for $N^+(^3P)$–$N(^4S_0)$ and $O^+(^4S_0)$–$O(^3P)$ interactions. *Journal of Chemical Physics*, 95(9):6429–6439.

218 Straub, H. C., Renault, P., Lindsay, B. G., Smith, K. A., and Stebbings, R. F. (1996). Absolute partial cross sections for electron-impact ionization of H_2, N_2, and O_2 from threshold to 1000 eV. *Physical Review A*, 54(3):2146–2153.

219 Sugawara, K., Ishikawa, Y., and Sato, S. (1980). The rate constants of the reactions of the metastable nitrogen-atoms, ^2D and ^2P, and the reactions of $N(^4S) + NO^- \rightarrow N_2 + O(^3P)$ and $O(^3P) + NO + M \rightarrow NO_2 + M$. *Bulletin of the Chemical Society of Japan*, 53(11):3159–3164.

220 Sun, W., Morrison, M. A., Isaacs, W. A., Trail, W. K., Alle, D. T., Gulley, R. J., Brennan, M. J., and Buckman, S. J. (1995). Detailed theoretical and experimental analysis of low-energy electron-N_2 scattering. *Physical Review A*, 52(2):1229–1256.

221 Szmytkowski, C., Maciag, K., and Karwasz, G. (1996). Absolute electron-scattering total cross section measurements for noble gas atoms and diatomic molecules. *Physica Scripta*, 54(3):271–280.

222 Tabata, T., Shirai, T., Sataka, M., and Kubo, H. (2006). Analytic cross sections for electron impact collisions with nitrogen molecules. *Atomic Data and Nuclear Data Tables*, 92(3):375–406.

223 Tao, K., Mao, D., and Hopwood, J. (2002). Ionized physical vapor deposition of titanium nitride: A global plasma model. *Journal of Applied Physics*, 91(7):4040–4048.

224 Tashiro, M. and Morokuma, K. (2007). R-matrix calculation of integral and differential cross sections for low-energy electron-impact excitations of the N_2 molecule. *Physical Review A*, 75(1):012720.

225 Tatarova, E., Dias, F. M., Gordiets, B., and Ferreira, C. M. (2005). Molecular dissociation in N_2–H_2 microwave discharges. *Plasma Sources Science and Technology*, 14(1):19–31.

226 Tayal, S. S. (2000). Effective collision strengths for electron impact excitation of N. I. *Atomic Data and Nuclear Data Tables*, 76(2):191–212.

227 Tayal, S. S. and Beatty, C. A. (1999). Oscillator strengths and electron-excitation cross sections for atomic nitrogen. *Physical Review A*, 59(5):3622–3631.

228 Tayal, S. S. and Zatsarinny, O. (2005). B-spline R-matrix with pseudostates approach for electron impact excitation of atomic nitrogen. *Journal of Physics B: Atomic, Molecular and Optical Physics*, 38(20):3631–3645.

229 Thomas, L. D. and Nesbet, R. K. (1975). Low-energy electron scattering by atomic nitrogen. *Physical Review A*, 12(6):2369–2377.

230 Thompson, D. G. (1971). Elastic scattering of electrons by nitrogen, neon, phosphorus and argon atoms. *Journal of Physics B: Atomic, Molecular and Optical Physics*, 4(4):468–482.

231 Tian, C. and Vidal, C. R. (1998). Electron impact ionization of N_2 and O_2: contributions from different dissociation channels of multiply ionized molecules. *Journal of Physics B: Atomic, Molecular and Optical Physics*, 31(24):5369–5381.

232 Tunis Wentink, J., Sullivan, J. O., and Wray, K. L. (1958). Nitrogen atomic recombination at room temperature. *Journal of Chemical Physics*, 29(1):231–232.

233 Tuszewski, M. (2006). Ion and gas temperatures of 0.46 MHz inductive plasma discharges. *Journal of Applied Physics*, 100(5):053301.

234 Van Zyl, B. and Dunn, G. H. (1967). Dissociation of N_2^+ and O_2^+ by electron impact. *Physical Review*, 163(1):43–45.

235 Vicic, M., Poparic, G., and Belic, D. S. (1996). Large vibrational excitation of N_2 by low-energy electrons. *Journal of Physics B: Atomic, Molecular and Optical Physics*, 29(6):1273–1281.

236 Walter, C. W., Cosby, P. C., and Helm, H. (1993). $N(^4S^0)$, $N(^2D^0)$, $N(^2P^0)$ yields in predissociation of excited singlet states of N_2. *Journal of Chemical Physics*, 99(5):3553–3561.

237 Wang, L., Ji, S., and Sun, J. (2006). Effect of nitriding time on the nitrided layer of AISI 304 austenitic stainless steel. *Surface and Coatings Technology*, 200(16-17):5067–5070.

238 Weber, M. and Deutsch, T. (1966). 4B2–pulsed and steady-state infrared emission studies of CO_2 laser systems. *IEEE Journal of Quantum Electronics*, 2(9):369–375.

239 Whitaker, M., Biondi, M. A., and Johnsen, R. (1981). Electron-temperature dependence of dissociative recombination of electrons with $N_2^+ \cdot N_2$ dimer ions. *Physical Review A*, 24(2):743–745.

240 White, M. and Ross, K. (1976). Vibrational ground-state population distributions of an N_2 flowing afterglow deduced from electron energy-loss spectra. *Journal of Physics B: Atomic, Molecular and Optical Physics*, 9(12):2147–2151.

241 Wiese, W. L., Fuhr, J. R., and Deters, T. M. (1996). Atomic transition probabilities of carbon, nitrogen, and oxygen - a critical data compilation. *Journal of Physical and Chemical Reference Data*, 25(Supplement 7):1–522.

242 Winters, H. F. (1966). Ionic adsorption and dissociation cross section for nitrogen. *The Journal of Chemical Physics*, 44(4):1472–1476.

243 Yamashita, T. (1979). Rate of recombination of nitrogen atoms. *Journal of Chemical Physics*, 70(9):4248–4253.

244 Yang, J. and Doering, J. P. (1996). Absolute differential and integral electron excitation cross sections for atomic nitrogen. 3. The $^4S^0 \rightarrow {}^2D$ (λ 5200 Å) transition from 5 to 30 eV. *Journal of Geophysical Research*, 101(A10):21765–21768.

245 Young, R. A. (1961). Pressure dependence of the absolute catalytic efficiency of surfaces for removal of atomic nitrogen. *Journal of Chemical Physics*, 34(4):1292–1294.

246 Young, R. A. and Dunn, O. J. (1975). The excitation and quenching of $N(^2P)$. *Journal of Chemical Physics*, 63(3):1150–1153.

247 Yu, R.-M., Zhou, Y.-J., Wang, Y., and Jiao, L.-G. (2006). Electron impact ionization cross section of nitrogen atoms. *Chinese Physics Letters*, 23(12):3256–3258.

248 Zhaunerchyk, V., Geppert, W. D., Vigren, E., Hamberg, M., Danielsson, M., Larsson, M., Thomas, R. D., Kaminska, M., and Österdahl, F. (2007). Dissociative recombination study of N_3^+: Cross section and branching fraction measurements. *Journal of Chemical Physics*, 127(1):014305.

249 Zhu, X.-M. and Pu, Y.-K. (2008). Using OES to determine electron temperature and density in low-pressure nitrogen and argon plasmas. *Plasma Sources Science and Technology*, 17(2):024002.

250 Zipf, E. C. (1980). The dissociative recombination of vibrationally excited N_2^+ ions. *Geophysical Research Letters*, 7(9):645–648.

251 Zipf, E. C. and Mclaughlin, R. W. (1978). On the dissociation of nitrogen by electron impact and by E. U. V. photo-absorption. *Planetary and Space Science*, 26(5):449–462.